Application of optically pure chiral anionic complexes in the construction of molecular conductors

by

Nikola Paul Chmel

A thesis submitted in partial fulfilment of the requirements of the degree of

Doctor of Philosophy in Chemistry

Department of Chemistry, University of Warwick

October 2010

Table of Contents

List of Figures

List of Schemes

List of Tables

Acknowledgements

First, I would like to thank my supervisors Prof. Peter Scott and Dr. Scott Turner for allowing me to work on this project as well for all the guidance, knowledge and heroic patience during these last few years.

I would like to also thank the other members of the Department and the University for without their help this project would be impossible to complete: Dr. Guy Clarkson for all the crystallography; Dr. Adam Clarke and Dr. Ivan Prokes for help with NMR spectrometry; Dr. Lijang Song for the mass spectrometry and ICP; Prof. Alison Rodger and her group for allowing me to use their facilities and all the help with CD spectrometry; Prof. Pat Unwin and his group for allowing me to use their equipment and all the help with electrochemistry; Prof. Richard Walton for allowing me use his powder diffractometers and being a “good cop” on my advisory panel; Dr. Martin Lees from Physics, for allowing me to use the SQuID facilities and other equipment, and all the help with the interpretation of magnetic data, Jack Sleigh and Prof. Alessandro Troisi for the DFT calculations and Dr. Andrew Edmonds from Diamond group for help with EPR spectroscopy. Finally I would like to give thanks to Prof. Mike Shipman for being on my advisory panel and asking the difficult questions.

I would also like to thank Dr. Martin Grossel from the University of Southampton and his group, and the National Crystallographic Service for their help with crystallography.

Special thanks goes to all of the Scottgroup members, past and present, in particular to Giles, Suzanne and Laura, for all of their help and involvement in my project.

Finally, I would like to thank the members of the Weight Training Club for helping to keep me sane during these trying times, and Lucy and Nic for the genuine British Christmas experience each year and trying to get me drunk every time I visit.

Publications

The following publications have arisen from the work described in this thesis:

Chapter 3

TTF salts of optically pure cobalt pyridine amidates; detection of soluble assemblies with stoichiometry corresponding to the solid state, Nikola Paul Chmel, Laura E. N. Allan, Jan M. Becker, Guy J. Clarkson, Scott S. Turner and Peter Scott, *Dalton Trans.*, **2010**, doi: 10.1039/C103DT01184C.

Chapter 4

Organic-soluble optically pure anionic metal complexes; PPh_4[M(*S*,*S*-EDDS)]·$2H_2O$ (M = Fe, Co, Cr), Nikola Paul Chmel, Suzanne E. Howson, Laura E. N. Allan, James Barker, Guy J. Clarkson, Scott S. Turner and Peter Scott, *Dalton Trans.*, **2010**, (39), 2919 – 2927.

Chapter 5

Helical Semiconductor Phases; the optically pure $D_3[M^{III}(S,S\text{-EDDS})]_2$ (D = TTF, TSF) family, Nikola Paul Chmel, Guy J. Clarskon, Alessandro Troisi, Scott S. Turner and Peter Scott, *Inorg. Chem.*, **2010**, *submitted.*

Other

Self-Assembling Optically Pure Fe(A-B)$_3$ Chelates, Suzanne E. Howson, Laura E. N. Allan, Nikola P. Chmel, Guy J. Clarkson, Remy van Gorkum and Peter Scott, *Chem. Commun.*, **2009**, 1727

Declaration

The work performed in this thesis was carried out in the Department of Chemistry, University of Warwick between July 2007 and October 2010. Unless otherwise stated, it is the work of the author and has not been submitted in whole or in part for any degree at this or any other university.

Summary

Chapter 1 introduces the phenomenon of Magnetic Chiral Anisotropy in chiral conductors and reviews the current literature on chiral charge transfer molecular conductors and synthetic routes towards them. The second part of the chapter focuses on examples of chiral anionic species reported in the literature.

Chapter 2 describes the synthesis and improvements to the literature procedures for organic donor molecules: tetrathiafulvalene, tetraselenafulvalene and bis(ethylenedithio)tetraselenafulvalene. The synthesis and characterisation of new chiral TTF imine systems are also reported. A stable TTF imine derivative of chiral biphenyl amine was used in the synthesis of a homochiral bimetallic helicate with copper(I). Unusual structural and magnetic properties of this compound are reported.

Chapter 3 focuses on the synthesis and properties of optically pure anionic complexes, $[M^{III}(L^n)_2]^-$(M = Co, Fe), of chiral pyridinecarboxamide ligands (L^n). The complexes show interesting extended structures ranging from 0D discrete units through 1D zigzag chains to 2D honeycomb layers. The complex anions were used in the synthesis of radical cation salts with tetrathiafulvalene (TTF). The salts (TTF)$[Co^{III}(R,R\text{-}L^1)_2]$ and (TTF)$[Co^{III}(S,S\text{-}L^2)_2]$·EtOAc were characterised by single crystal X-ray diffraction and conductivity measurements. Solution spectroscopic and cyclic voltammetric evidence points to the formation of soluble assemblies between TTF^+ and the counterion which correspond to the stoichiometry observed by crystallography and other methods in the solid state.

Chapter 4 describes the synthesis of the first diastereomerically pure, organic-soluble salts of cobalt, iron and chromium complexes of optically pure chelate: H_4EDDS. A number of synthetic approaches were attempted, but finally the

$PPh_4[M^{III}(EDDS)]\cdot 2H_2O$ series emerged providing readily accessible compounds in reasonable yields *via* the silver salts. The species are very soluble in methanol, acetonitrile and even THF and isolation of highly crystalline solids is possible upon addition of water. The structures of the three compounds are isomorphous and comprise of H_2O-bridged extended hydrogen bonded structures with large channels occupied by the counterion molecules. The magnetic properties and circular dichroism spectra are reported. The diastereomeric purity in the paramagnetic systems is assessed through powder XRD.

Chapter 5 focuses on the use of organic-soluble EDDS complexes in the resolution of optically active cations and as a chiral NMR shift agent. The initial results of the resolution of (±)-$[Ru^{II}(bpy)_3]^{2+}$ are reported along with the crystal structure of the $\{\Lambda\text{-}[Ru^{II}(bpy)_3]\}\{\Lambda\text{-}[Fe^{III}(S,S\text{-EDDS})]\}Cl\cdot H_2O$ adduct. The result of testing of the diamagnetic $PPh_4[Co^{III}(S,S\text{-EDDS})]$ salt as a ^1H NMR shift agent for chiral complex cations: $[ML_3]^{2+}$, (M = Co, Ru, Fe; L = bpy, phen, en) and small organic molecules are also reported.

Chapter 6 describes the electrochemical synthesis of a new family of conductive optically pure tetrathiafulvalenium and tetraselenafulvalenium salts $D_3[M^{III}(S,S\text{-EDDS})]_2\cdot nH_2O$ (where D = TTF, TSF; M = Co, Fe, Cr). The compounds are characterised by single crystal X-ray diffraction, conductivity measurements and elemental microanalysis and exhibit well-behaved semiconductor behaviour with conductivities up to $2.8\cdot 10^{-4}$ $S\cdot cm^{-1}$ (E_a *ca* 0.1 eV). Computational work indicates that it is feasible to generate metallic conductors with similar structures. Initial results for an ET analogue showing metallic conductivity are also reported.

Chapter 7 details the experimental procedures used to carry out the work in this thesis.

Symbols and abbreviations

Most of the abbreviations and symbols used in this thesis are in common use within the scientific community. Non-standard abbreviations and symbols used in this work are given below:

BEDT-TTF	Bis(ethylenedithio)tetrathiafulvalene
BETS	Bis(ethylenedithio)tetraselenafulvalene
CD	Circular Dichroism
ET	BEDT-TTF
H_4EDDS	Ethylenediaminedisuccinic acid
LC	Liquid Chromatography
LDA	Lithium diisopropylamide
MCA	Magnetic Chiral Anisotropy
SCE	Saturated Calomel Electrode
TIP	Temperature Independent Paramagnetism
TSF	Tetraselenafulvalene
TTF	Tetrathiafulvalene

Chapter 1

Introduction

Chiral TTF based conducting phases

The history of organic charge transfer compounds starts in the 1950s with the discovery of the perylene bromine complex, (per)Br_n (n ≈ 3-4), the first organic compound showing high conductivity.[1] The discovery of tetrathiafulvalene (TTF) in 1970 by Wudl *et al.*[2] initiated more intensive research into the field. Today, the family of molecular conductors based on TTF and its derivatives consists of thousands of known compounds.[3]

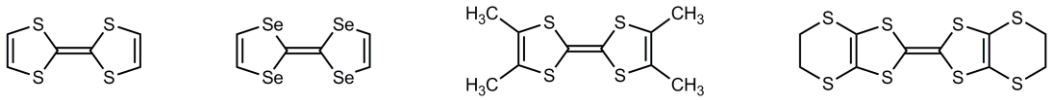

Figure 1.1. Examples of common donor molecules: tetrathiafulvalene (TTF), tetraselenafulvalne (TSF), tetramethyltetraselenafulvalene (TM-TTF) and bis(ethylenedithio)tetrathiafulvalene (BEDT-TTF, ET).

Organic charge transfer molecular conductors usually consist of two components: a planar, electron rich donor molecule, and a counterion. Most of the known assemblies comprise of a donor molecule structurally related to TTF (Fig. 1.1) and one of a variety of counterions, from simple inorganic or organic anions to complex supramolecular structures.[3] Counterions are often selected

in order to introduce an additional functionality to the assembly, *e.g*. magnetic or optical properties.[4]

While the first chiral conductive material was reported in 1986[5] the interest in these types of materials and their properties has been marginal until recently. In 2001, Rikken predicted that "electrical resistance of any chiral conductor should depend linearly both on the external magnetic field and the current through the conductor and on its handedness".[6] As a result, electrical resistance in a chiral medium depends on both the direction of the spin polarisation as well as on its magnitude. This new unique property called Magnetic Chiral Anisotropy (MCA) was indeed observed in metallic bismuth helices and chiral carbon nanotubes.[7] Since these properties would allow chiral conductive materials to be used as molecular switches and in the field of spintronics,[7] the interest in these types of species has risen significantly.

In the reported conductive assemblies the chirality element is introduced either through the use of chiral building blocks (chiral counterion or donor molecule) or the induction of a chiral space group (guest molecules, chiral symmetry breaking).[4,8,9] A more general approach to the synthesis of chiral molecular conductors however, has not yet been developed.

Conductive materials based on chiral donor molecules

Syntheses of several different chiral donor molecules have been reported in the literature,[10,11] Chapter 2 will focus further on this topic. Only two of these species: tetramethyl(ethyleneditio)tetrathiafulvalene (Me_4ET, TM-ET, TM-BEDT-TTF) and dimethyl(ethylenedithio)tetrathiafulvalene (Me_2ET), however, yielded any conductive materials.

The synthesis of optically pure (*S*,*S*,*S*,*S*)-tetramethylbis(ethyleneditio)tetrathiafulvalene and its semiconducting salt, [(*S*,*S*,*S*,*S*)-$Me_4ET]_2PF_6$ was first reported by Wallis *et al*. in 1986.[5]

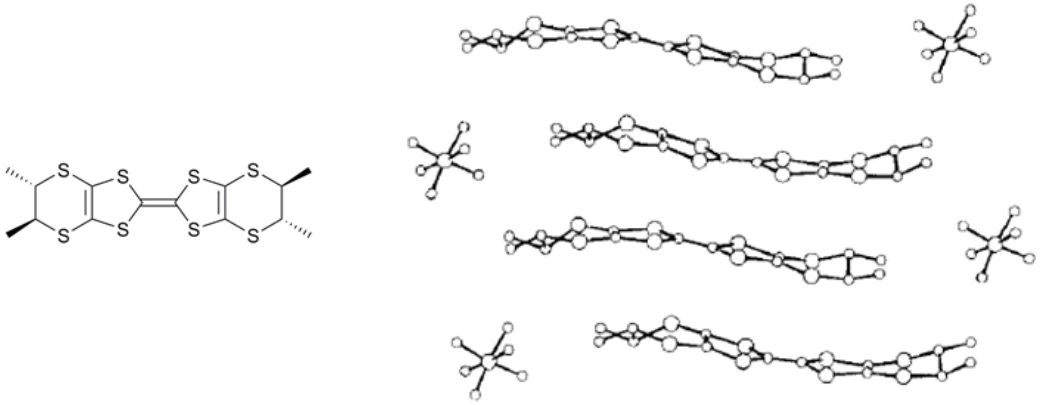

Figure1.2. Structure of (*S*,*S*,*S*,*S*)-Me_4ET donor and a view of molecular stack in the crystal structure of [(*S*,*S*,*S*,*S*)-$Me_4ET]_2PF_6$.[5]

Further research by Wallis *et al*. focused on extending this family through the synthesis of salts with different octahedral (PF_6^-, AsF_6^-, SbF_6^-) and tetrahedral (BF_4^-, ClO_4^-, ReO_4^-) anions.[12] Two general structural types have been identified: 2:1 stoichiometric salts with octahedral anions and semiconductive properties, and 3:2 stoichoiometric salts with tetrahedral anions. Both types have similar cell parameters and structures within each group. All of the structures comprise of stacks of donor molecules with anions bound by methyl groups within the channels between the stacks. For smaller, tetrahedral ions the width of the channels allows for alternative locations and occupations of the anions, and solvent molecules. The conductivity of the salts of tetrahedral ions is strongly dependant on the solvent used and changes from semiconductive (trichlorobenzene/nitrobenzene) to metallic (1,1,1-trichloroethane/nitro-benzene). Interestingly the salt of linear triiodide forms a similar structure to

these of octahedral anions, with a stoichiometry, however, close to 3:2 and a weakly metallic conductivity resembling salts with the tetrahedral anions.

Recently a synthesis of [(*S*,*S*,*S*,*S*)-$Me_4ET]_x[MnCr(ox)_3]\cdot CH_2Cl_2$, the first molecular material with coexistence of ferromagnetism, metallic conductivity and chirality has been reported by Galán-Mascarós *et al*.[13] The compound shows β-type packing[14] with stacks of donor molecules along [100] direction. The structure of the ferromagnetic anionic part cannot be determined, its presence however is demonstrated by magnetic measurements. The compound shows temperature independent paramagnetism (TIP) down to 150 K, where ferromagnetic interactions become apparent. Curie temperature of 5.5 K typical of honeycomb $[MnCr(ox)_3]^-$ networks was determined from AC measurements. The compound shows metallic conductivity down to 190 K where charge localisation occurs. On continued cooling the compound re-enters the metallic regime below 10 K. Near 5 K resistivity increases rapidly coinciding with the ferromagnetic ordering of the anionic layer. Magnetoresistance measurements show weak Shubnikov-de Haas oscillations.[15] No evidence of magnetic chiral anisotropy was observed.

Another thoroughly investigated family of chiral conductors are species based on (*S*,*S*)-*trans*-dimethylbis(ethylenedithio)tetrathiafulvalene. Synthesis of the donor and its salt [(*S*,*S*)-$Me_2ET]_2ClO_4$ was first reported by Zambounis *et al*. in 1992.[16] The salt grown electrochemically forms a κ-phase,[14] which on cooling to 2 K under pressure undergoes transition into possibly superconductive state.

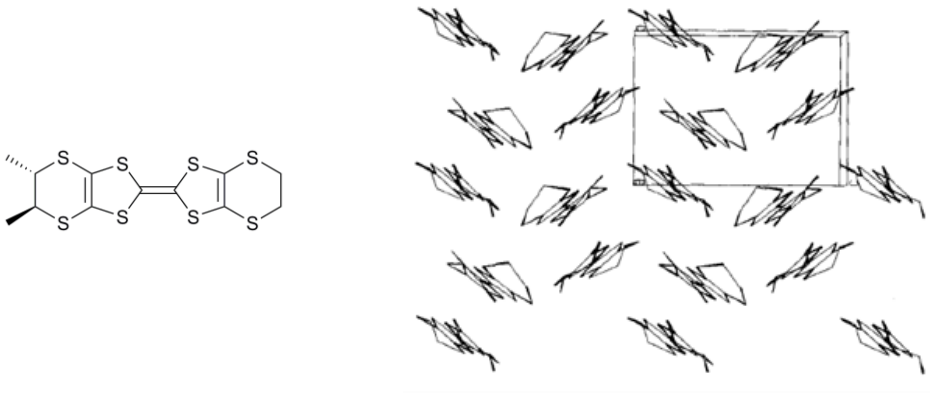

Figure 1.3. Structure of (*S*,*S*)-Me_2ET donor and a view of κ-phase packing in the crystal structure of $[(S,S)\text{-}Me_2ET]_2ClO_4$.[16]

Further research by Matsumiya *et al*.[17] focused on salts of both chiral (*R*,*R*)- and racemic (±)-Me_2TTF with PF_6^-, ClO_4^- and ReO_4^-, $(Me_2ET)_2X$ salts were prepared electrochemically and their crystal structures and conductive properties were investigated. Structurally, the compounds show similar features: the donor molecules are stacked head-to-tail in columns with an additional twist (*ca* 30°) in order to reduce steric repulsion caused by the methyl groups. Crystal packing of the racemic salt differs from the optically pure ones in the symmetry relation between the neighbouring stacks (inversion instead of 2-fold symmetry). Disorder in counterions position is also observed. Despite differences in the counterion size, all of the structures show an analogous arrangement of the donor molecules, which suggests that packing is largely determined by the steric properties of the donor. All of the salts show similar semiconductive properties with room temperature conductivity of ~0.2 $S{\cdot}cm^{-1}$.

Other semiconductive and metallic salts with this donor molecule and linear counterions I_3^-, $[Ag(CN)_2]^-$ and $[AuI_2]^-$ have also been reported in brief.[18]

A family of corresponding pyrazine fused donor with linear $[AuI_2]^-$, $[AuBr_2]^-$ and $[Ag(CN)_2]^-$ has been reported by Papavassiliou *et al.*[19,20] The salts form metallic τ-phases of stoichiometry 2:1.7 containing alternating layers of donor molecules and anions (in 2:1 ratio), and additional disordered anions. The properties of these compounds were studied and phenomena like large negative magnetoresistance and giant Shubnikov-de Haas oscillations have been reported.[11]

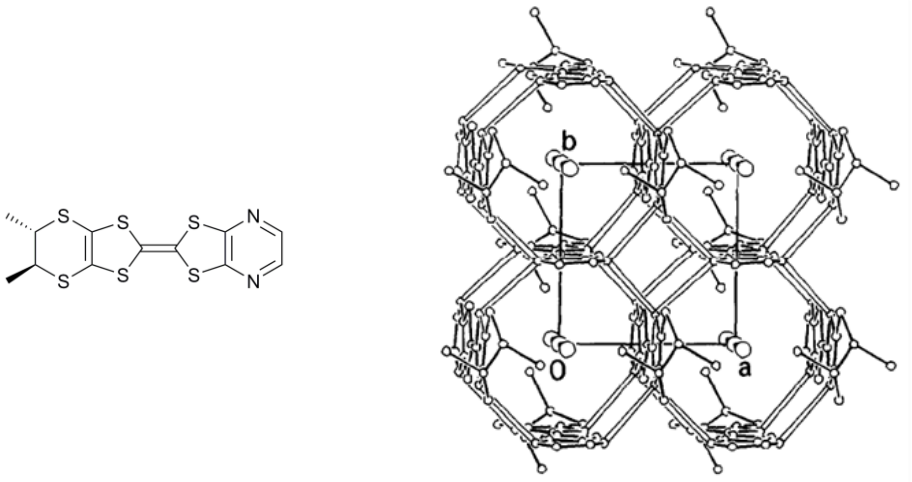

Figure 1.4. Structure of pyrazino-(*S*,*S*)-dimethyl(ethylenedithio)tetrathiafulvalene P-(*S*,*S*)-DMEDT-TTF donor and a view packing in the crystal structure of [P-(*S*,*S*)-DMEDT-TTF]$_2$[AuBr$_2$]$_1$[AuBr$_2$]$_{\sim 0.75}$.[21]

Another family of chiral donor molecules based on racemic and optically pure TTF oxazolines have been introduced by Rethore *et al.*[22,23] A series of conductive salts with the methyl substituted oxazoline (Fig 1.5) have been reported. Electrocrystallisation of (*R*)-, (*S*)- and (±)-EDT-TTF-Meox in the presence of AsF_6^- counterion yields mixed valence salts of 2:1 stoichiometry. All three salts crystallise in a triclinic system with the same unit cell parameters.

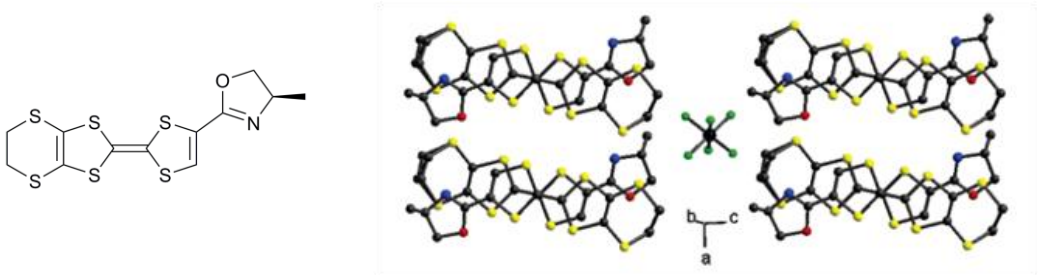

Figure 1.5. Structure of (ethylenedithio)tetrathiafulvalene-methyloxazoline (*R*)-EDT-TTF-Meox donor and a view packing in the crystal structure of $[(R)\text{-EDT-TTF-ox}]_2AsF_6$.[23]

The asymmetric parts of the unit cells of the optically pure salts contain two independent molecules, representing two lowest energy conformations of the donor molecule. In case of the racemic compound both conformations are located at the same crystallographic site introducing a structural disorder. All of the salts show metallic conductivity down to 230 K followed by a localised regime with the room temperature conductivity. The conductivity of optically pure salts is one order of magnitude higher than that of the racemic one, which is contributed to the structural disorder in the latter.

Conductive materials based on achiral donor molecule and chiral anions

Another approach towards the synthesis of chiral conductive materials is the use of achiral donor molecules, *e.g*. TTF, ET with chiral counterions. The first reported successful use of this strategy is one by Olejniczak *et al*.[24,25] Salts of bis(ethylenedithio)tetrathiafulvalene (ET) with racemic perfluorinated sulfonic acids, $(ET)_2SF_5CHFSO_3$ and $(ET)_2SF_5CHFCF_2SO_3$, have been prepared electrochemically and their properties were compared to those of achiral $(ET)_2SF_5CH_2CF_2SO_3$. All of the compounds crystallise in β-phase[14] and form a metallic, metal-insulator and superconducting (T_c ~ 5.2 K) materials

respectively. The effects of a disorder resulting from the introduction of chiral groups on the conductive properties of the assembly have also been discussed.

Another example of a material prepared using this methodology is $(ET)_3[Sb_2(L\text{-tart})_2]\cdot CH_3CN$, synthesised by Coronado *et al.*[26] An electrocrystallisation of ET in the presence of optically pure antimony L-tartrate results in the formation of a layered structure with α-type packing[14]. The compound shows small ambient temperature conductivity and a semiconductive behaviour.

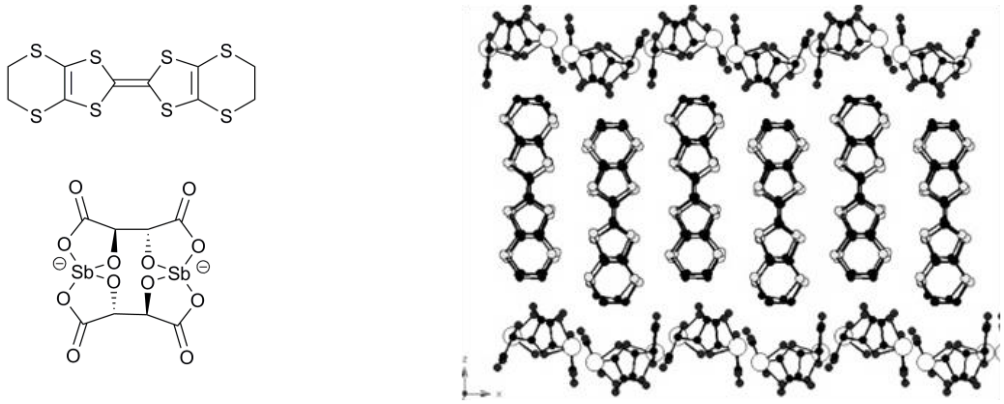

Figure 1.6. Structures of ET and antimony L-tartrate anion and a view of solid state packing in the crystal structure of $(ET)_3[Sb_2(L\text{-tart})_2]\cdot CH_3CN$.[26]

Recent work by Coronado *et al*. resulted in a synthesis of chiral phases based on a chiral polyoxometalate $[H_4Co_2Mo_{10}O_{98}]^{6-}$ with either ET or polypyrrole.[27] Crystals of $(ET)_9[(\pm)\text{-}H_4Co_2Mo_{10}O_{98}]\cdot H_2O$, obtained electrochemically, form a layered structure with alternating stacks of donor molecules along the crystallographic b axis and counterions. The compound is a semiconductor with ambient temperature conductivity of 9 $S\cdot cm^{-1}$.

Several conductive ET salts were prepared with racemic *tris* ligand anionic complexes (Fig. 1.7) e.g. $[M(ox)_3]^{3-}$ (M = Fe^{3+}, Cr^{3+}, Ga^{3+}),[4,28,29]

$[Fe(croconate)_3]^{3-}$,[30] $[Cr(2,2'\text{-bpy})(ox)_2]^-$ [31] or TRISPHAT.[32] All of these are prepared from racemic mixtures and no effects of chirality on the compound properties were observed. The compounds are generally semiconducting with some metals and superconductors in the oxalato systems.

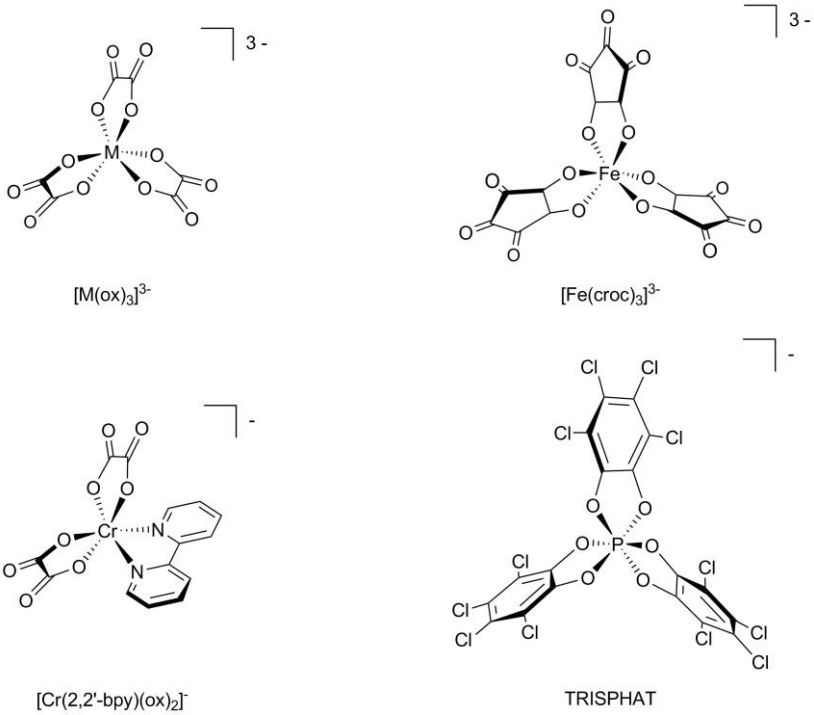

Figure 1.7. Chiral anions used in their racemic form in the synthesis of conductive salts with ET.

Further work on oxalato systems resulted in a synthesis of two new phases, $(ET)_4(NH_4)[Fe(ox)_3]\cdot solv.$ (where *solv*. = (±)-, (*S*)-*sec*-phenylethanol).[8] Both structures contain racemic $[Fe(ox)_3]^{3-}$ anions and were crystallised from either racemic or optically pure solvent. The structure of the optically pure compound is closely similar to that of racemic one. Both compounds are semiconductors, with only small differences in metal-insulating properties due to enantiomeric disorder in the racemic salt.

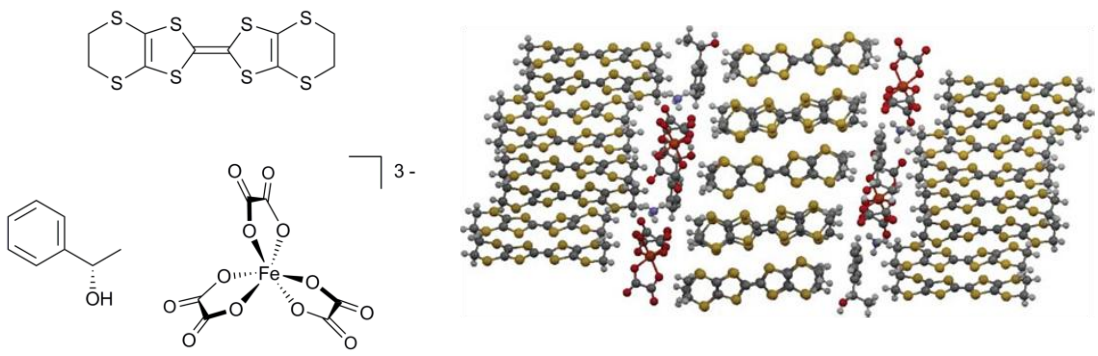

Figure 1.8. Structures of ET, (*S*)-1-phenylethanol and tris(oxalato)ferrate (left) and the solid state packing of $(ET)_4(NH_4)[Fe(ox)_3]\cdot solv$.[8]

Crystallisation of ET in the presence of $Na[Cr(ox)_3]$ and (*R*)-carvone as a chiral auxiliary resulted in a formation of two polymorphs of $(ET)_3Na[Cr(ox)_3]\cdot CH_3NO_2$.[33] Both phases are composed of alternating layers of donor molecules and layers of $[Cr(ox)_3]^{3-}$, Na^+ and nitromethane. The polymorphs show similar solid state structures, their enantiomeric composition is, however, different. One of the polymorphs is a racemic twin, with the other showing preference towards Δ configuration (64:36). Both assemblies exhibit semiconductive properties.

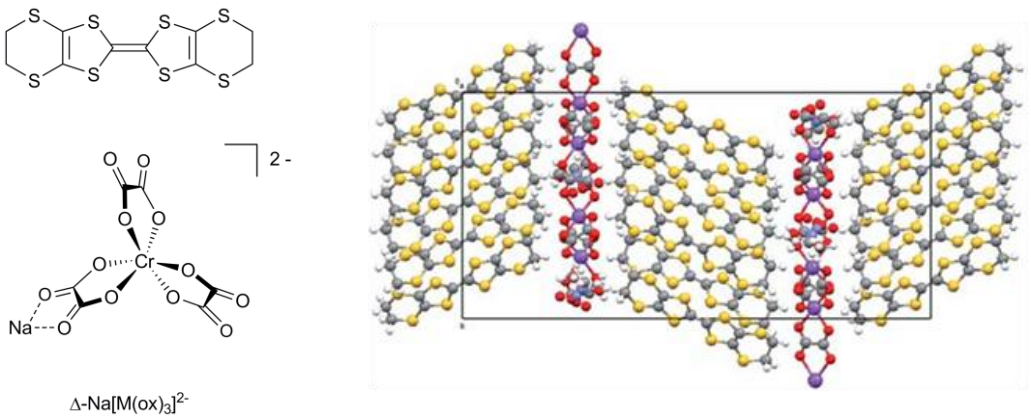

Figure 1.9. Structure of ET and sodium (Δ)-tris(oxalato)chromate (left) and the solid state packing of $(ET)_3Na[Cr(ox)_3]\cdot CH_3NO_2$.[33]

A very recent publication by Brezgunova *et al*. reported the synthesis of a chiral optically pure salt of an unsymmetrical donor diiodo(ethylenedithio)tetrathiafulvalene (EDT-TTF-I_2) with D-camphoro-sulfonate.[34] The compound, (EDT-TTF-I_2)$_2$(D-camphorophosphonate)·H_2O crystallises in a triclinic system and exhibits layered structure, with strong halogen bonding interactions between the layers. The compound displays an elevated room temperature conductivity (3-5 S·cm^{-1}) and metallic behaviour above 200 K.

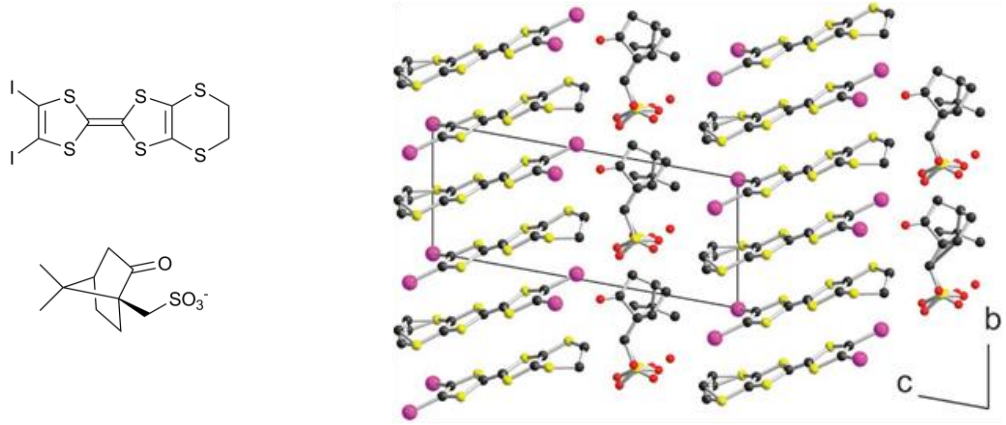

Figure 1.10. Structure of EDT-TTF-I_2 and D-camphorsulfonate (left) and the solid state packing of (EDT-TTF-I_2)$_2$(D-camphorophosphonate)·H_2O.[34]

Supramolecular chirality

A unique approach to the introduction of chirality into the conductive assembly was used by Kobayashi and Inabe.[35,36] Electrochemical oxidation of TTF in the presence of mellitic acid resulted in the formation of an exceptional helical hydrogen bonded structure. In the solid state mellitate anions form a hydrogen bonded double helix, which through further hydrogen bonding affects the TTF stack in its centre. Thus formed TTF columns adapt helical arrangement, with a period of repeat after six molecules (Fig. 1.11). No conductivity measurements

were reported, magnetic measurements and structural analysis however show that the TTF molecules in the stack are dimerised, with only 1-2% of the radical cation remaining unpaired.

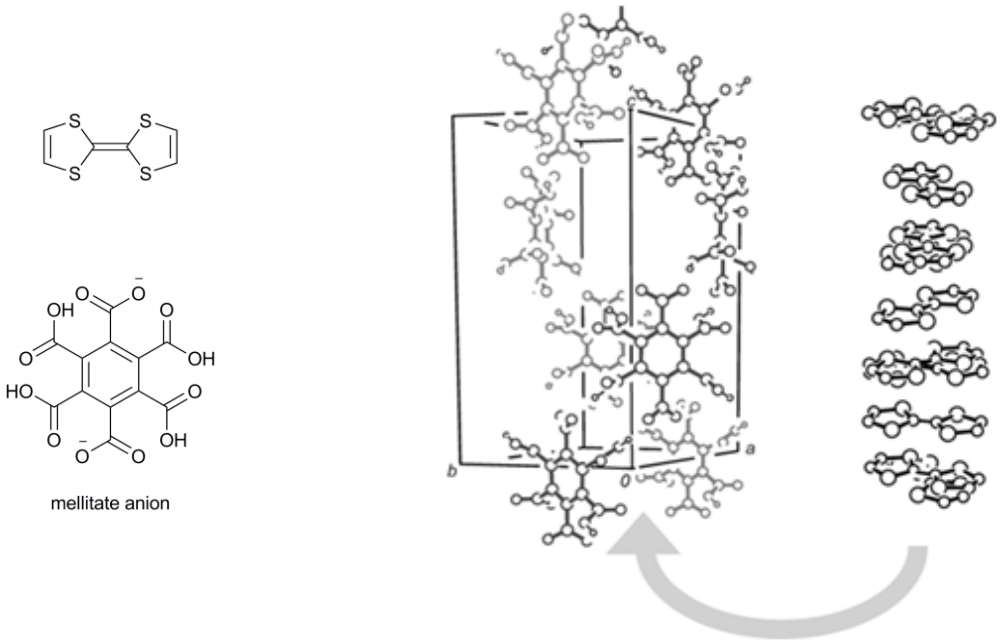

Figure 1.11. Structure of TTF and mellitate (left) and the solid state packing of $(TTF)_2[C_6(COO)_6H_4]$.[35]

Other reported assemblies employing supramolecular approaches to introduce chirality include the use of an electroactive helical polymer with built in TTF units and chiral conductive nanocoils built from chiral derivatives of hexabenzocoronene.[37,38]

Summary

It is apparent that the synthesis of chiral organic charge transfer conductive species is a challenging field, in which much is yet to be achieved. Several groups working in this field over period of 20 years have produced only a handful of conductive species and these with mainly semiconductive properties.

Only in one case was the magneto-transport phenomena researched and this produced a negative result.[13]

Significant efforts have been put into the synthesis of chiral donor molecules. From a variety of reported species only two however have been found to form conductive assemblies. It is therefore evident that an approach towards the synthesis of these materials through the use of achiral donor molecules and chiral counterions may be potentially more productive.

Optically pure anions

Coordination chemistry and inorganic chemistry in general is a chemistry of cations. Despite their ubiquity, anions are often overlooked, treated only as gegenions, with no significant involvement in the concerned processes. Few families of complex organic or inorganic anions are known. The situation is even more apparent in the case of chiral anions, and while optically pure cations play an important role in catalysis, biochemistry, material sciences *etc.*, anionic species are largely unknown. Recently however, with the development of ionic liquids[39-42] and recognition of the importance of ion pairing in inorganic and organometallic chemistry,[43,44] the interest in chiral anionic species has risen. Many new species have been developed recently, as well as several known compounds which have been adapted for new applications. A number of comprehensive review articles have been published on the anion mediated chemistry[45-47] and on chiral anionic species.[48-51] Hence, this chapter will only shortly summarise the main families of chiral anionic species reported in the literature.

Following a recent review by Lacour *et al*., at least four well established families of chiral anionic species can be distinguished.[51] These are: organic carboxylates and sulfonates, borates, phosphates, and hexacoordinate phosphorus compounds. Other chiral anionic species include chiral-at-metal *bis* and *tris* ligand complexes, complexes with chiral ligands, supramolecular anions, *etc*. Another well recognized family of anions, not mentioned in the review, are octahedral complexes of hexadentate chelates *e.g*. EDTA.

Organic carboxylates and sulfonates

Conjugated bases of chiral carboxylic and sulfonic acids are possibly the most ubiquitous type of chiral anions.[52] These compounds are generally hydrophilic and are usually widely available in large quantities and in their optically pure forms. Derivatisation often grants an easy access to other anionic species *e.g*. cyclic polyacids.[53] Coordination to metal ions provides more rigid anionic complexes *e.g*. antimonyl tartrate. These compounds have been used in a number of different applications and especially in optical resolution. [54-56]

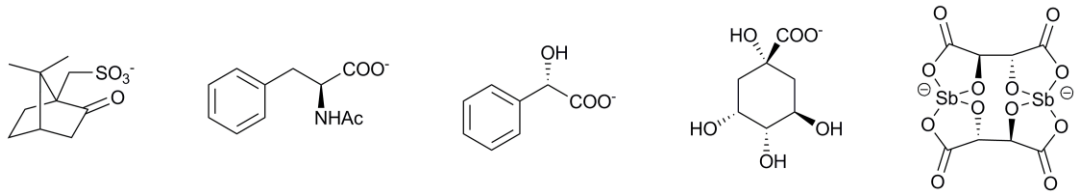

Figure 1.12. Examples of common chiral carboxylates and sulfonates: (from the left) 10-camphorosulfonate, *N*-phenylalaninate, mandelate, quinate, antimononyl tartrate.[50,52]

Borates

Boron gives access to readily available trivalent tetrahedral compounds. Coordination with two unsymmetrical ligands leads to the formation of a chiral

centre. This was frst recognised in 1925 (Fig. 1.13a).[57] Initially however, lability of the boron centre and resulting racemisation was a significant problem. Since then several configurationally stable assemblies of this type were synthesised. Two general approaches are used in the synthesis of chiral borates: the use of achiral ligands followed by resolution using traditional methods (Fig. 1.13b),[58,59] or the coordination of a boron centre by chiral ligands, usually derived from binaphthol (Fig. 1.13c).[60,61]

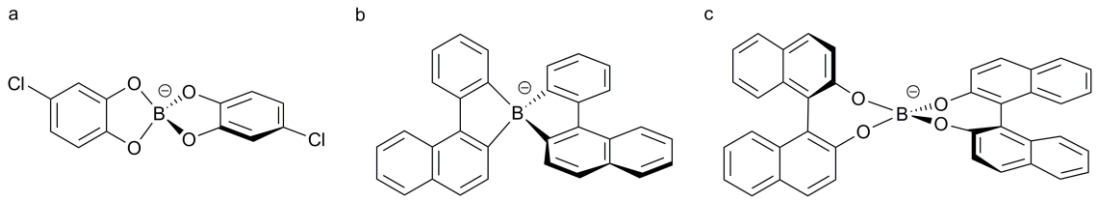

Figure 1.13. Examples of chiral borate anions.[50,57,58,60]

Excellent solubility in low-polarity solvents, large ionic radius and low nucleophilicity make these anions a valuable tool in ion mediated asymmetric chemistry.[62]

Phosphates

Similar to the case of conjugated bases of carboxylic and sulfonic acids, phosphonic acids are also a useful source of chiral anions. For many years, the only compound of this type was binaphthyl-2,2'-diyl phosphate (Fig. 1.14).[63] Recently however, more species based on different binaphthol derivatives have emerged.[64-68] These type of species find wide use in asymmetric chemistry *e.g.* in catalysis[69] and chiral recognition.[70]

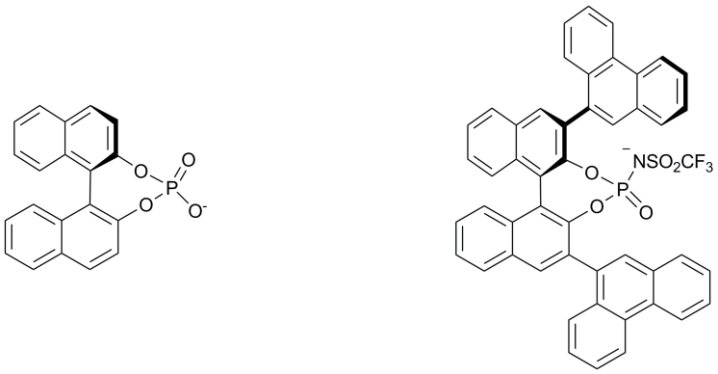

Figure 1.14. Examples of chiral phosphate anions. [63,68]

Hexacoordinated phosphorus and arsenic anions

Octahedral *tris* ligand compounds of pentavalent phosphorus and arsenic are intrinsically chiral due to the formation of a new chiral centre at the central atom. This was recognised by Hellwinkel in 1965 (Fig. 1.15a).[71] Synthetically easily accessible tris(benzenediolato)arsenate(V)[72] and phosphate(V)[73] followed soon after (Fig. 1.15b). The latter unfortunately is configurationally labile in the solution and the former is derived from highly toxic arsenic acid, which limits their practical applications. Introduction of electron withdrawing chlorine substituents into the ligands allowed for the synthesis of a stable non-racemising derivative, tris(tetrachlorobenzenediolato)phosphate(V)[74] (TRISPHAT, Fig. 1.15c), which since found wide use in e.g. optical resolution and as an NMR shift agent (see chapter 5).[49,75,76] In order to improve the enantioselectivity of TRISPHAT synthesis and remove the necessity of optical resolution, several C_2 symmetric derivatives with chiral ligands were synthesised.[77,78]

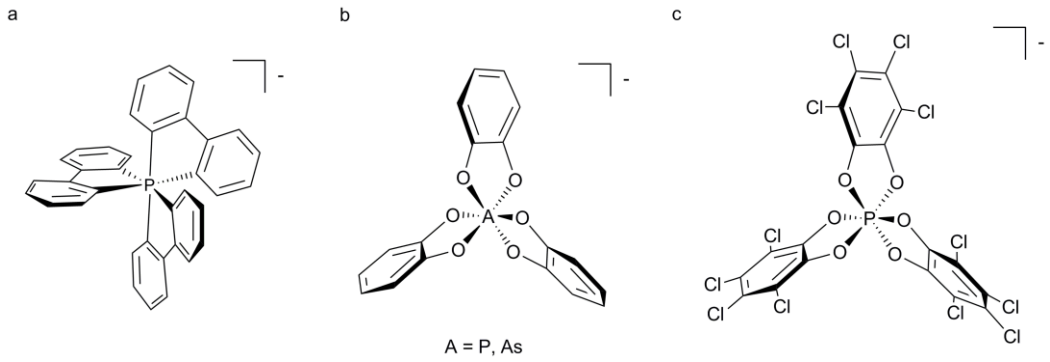

Figure 1.15. Examples of chiral hexacoordinate phosphate and arsenate anions.[71-73]

Intrinsically chiral metal complexes

This group of compounds includes several families of different metal complexes, with the simplest example being *tris* bidentate ligand complexes. Tris(oxalato) chromium(III) and cobalt(III) complexes are prime example of this category. They can be easily prepared in their racemic form and their optical resolution has been reported.[79,80] Several magnetic[81] and conductive (*vide supra*) phases with racemic and partially resolved $[M(ox)_3]^-$ complexes have been reported.

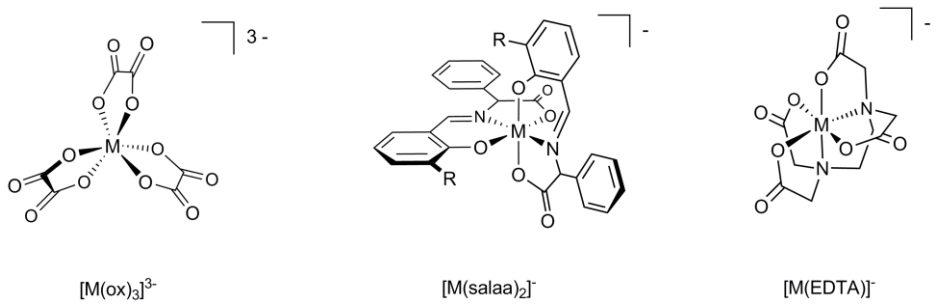

Figure 1.16. Examples of chiral-at-metal anionic complexes.

Another family of compounds are *bis* complexes of unsymmetrical salicylaldimine tridentate ligands, $[M(salaa)_2]^-$. This family, developed primarily by Belokon' has been thoroughly studied and several compounds of this type

have been synthesised and resolved as well as applied in asymmetric catalysis (also see chapter 3).[82-84]

Common examples of chiral species are octahedral complexes of hexadentate ligands *e.g*. EDTA. Complexes of this type have been known since the 1930s,[85,86] their intrinsic chiral properties are however, often overlooked. Due to lability at the metal centre, optical resolution of this type of complex is challenging; chemically inert cobalt(III)[87-89] and rhodium(III)[90] complexes have been successfully resolved, however racemisation in solution can be observed at elevated temperatures.[91] In order to alleviate this problem several optically active analogues of EDTA have been obtained (see Chapter 4).

Other anionic compounds

Other chiral anionic compounds include complexes of chiral ligands *e.g*. lanthanide complexes with camphor derivatives, $[Eu(tfc)_4]^-$, (tfc = 3-(trifluoro-methylhydroxymethylene)camphorate), commonly used as NMR shift agents (Fig. 1.17a).[92] Another are conjugated bases of sulphonamide derivatives (Fig. 1.17b,c).[93,94] Interesting chiral supramolecular anionic species have been recently reported by Jacobsen,[95-97] and Pan and List.[98] These species consist of hydrogen bonded complexes of a chiral thiourea derivative with chloride or cyanide (Fig. 1.17d,e).

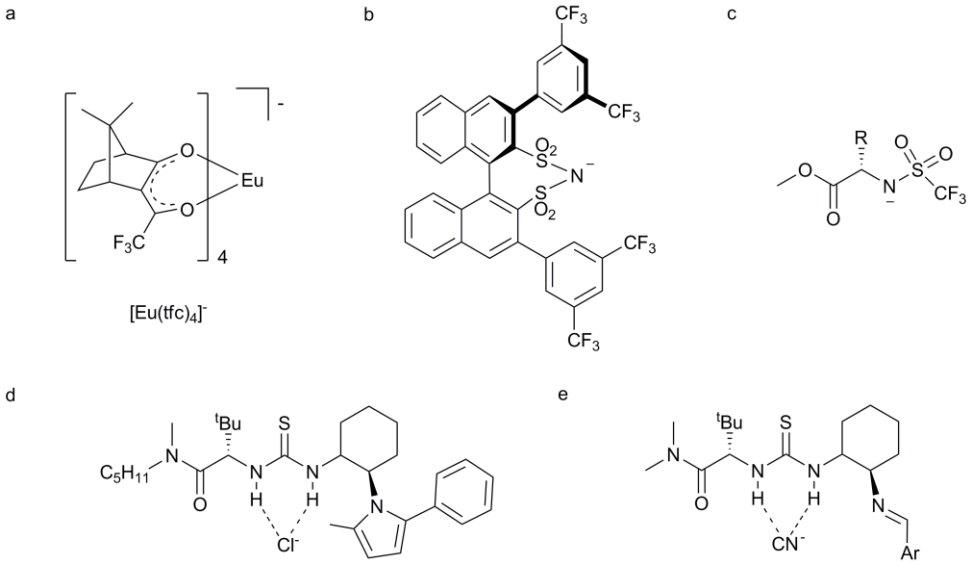

Figure 1.17. Examples of chiral anionic species.[92-95,98]

Conclusions

It is apparent that despite the ubiquity of anionic species, only a limited number of chiral optically pure systems are available. Several of the reported species are synthetically challenging and often require complex resolution procedures. To avoid these issues the main focus of this thesis is on diastereoselective synthesis of hexacoordinate octahedral anionic metal complexes using well defined chiral tridentate and hexadentate ligands (Chapters 3 and 4) and the utilisation of these in the construction of conductive materials (Chapters 3 and 6) and other applications (Chapter 5).

References

1. H. Akamatu, H. Inokuchi and Y. Matsunaga, *Nature*, 1954, **173**, 168-169.
2. F. Wudl, G. M. Smith and E. J. Hufnagel, *J. Chem. Soc. D Chem. Comm.*, 1970, 1453-1454.
3. G. Saito and Y. Yoshida, *Bull. Chem. Soc. Jpn.*, 2007, **80**, 1-137.
4. E. Coronado and J. R. Galan-Mascaros, *J. Mater. Chem.*, 2005, **15**, 66-74.
5. J. D. Wallis, A. Karrer and J. D. Dunitz, *Helv. Chim. Acta*, 1986, **69**, 69-70.
6. G. L. J. A. Rikken, J. Folling and P. Wyder, *Phys. Rev. Lett.*, 2001, **87**, 236602.
7. V. Krstic and G. L. J. A. Rikken, *Chem. Phys. Lett.*, 2002, **364**, 51-56.
8. L. Martin, P. Day, H. Akutsu, J.-i. Yamada, S. i. Nakatsuji, W. Clegg, R. W. Harrington, P. N. Horton, M. B. Hursthouse, P. McMillan and S. Firth, *CrystEngComm*, 2007, **9**, 865-867.
9. X. Ribas, M. Mas-Torrent, A. Perez-Benitez, J. C. Dias, H. Alves, E. B. Lopes, R. T. Henriques, E. Molins, I. C. Santos, K. Wurst, P. Foury-Leylekian, M. Almeida, J. Veciana and C. Rovira, *Adv. Funct. Mater.*, 2005, **15**, 1023-1035.
10. J. P. Griffiths, H. Nie, R. J. Brown, P. Day and J. D. Wallis, *Org. Biomol. Chem.*, 2005, **3**, 2155-2166.
11. N. Avarvari and J. D. Wallis, *J. Mater. Chem.*, 2009, **19**, 4061-4076.
12. A. Karrer, J. D. Wallis, J. D. Dunitz, B. Hilti, C. W. Mayer, M. Bürkle and J. Pfeiffer, *Helv. Chim. Acta*, 1987, **70**, 942-953.
13. J. R. Galán-Mascarós, E. Coronado, P. A. Goddard, J. Singleton, A. I. Coldea, J. D. Wallis, S. J. Coles and A. Alberola, *J. Am. Chem. Soc.*, 2010, **132**, 9271-9273.
14. N. Toyota, M. Lang and J. Müller, *Low-dimensional molecular metals*, Springer, Berlin ; [London], 2007.
15. B. M. Askerov, *Electron transport phenomena in semiconductors*, World Scientific, Singapore, 1994.
16. J. S. Zambounis, C. W. Mayer, K. Hauenstein, B. Hilti, W. Hofherr, J. Pfeiffer, M. Bürkle and G. Rihs, *Adv. Mater.*, 1992, **4**, 33-35.
17. S. Matsumiya, A. Izuoka, T. Sugawara, T. Taruishi, Y. Kawada and M. Tokumoto, *Bull. Chem. Soc. Jpn.*, 1993, **66**, 1949-1954.
18. J. S. Zambounis, C. W. Mayer, K. Hauenstein, B. Hilti, W. Hofherr, J. Pfeiffer, M. Buerkle and G. Rihs, *Mater. Res. Soc. Symp. Proc.*, 1992, **247**, 509-513.
19. I. Olejniczak, W. Pukacki and G. C. Papavassiliou, *Adv. Mater. Opt. Electron.*, 1996, **6**, 288-292.
20. G. C. Papavassiliou, D. J. Lagouvardos, A. Terzis, C. P. Raptopoulou, P. Delhaes, K. Murata, N. A. Fortune, N. Shirakawa, B. Hilti, W. Hofherr, J. S. Zambounis, G. Rihs and J. Pfeiffer, *Synth. Met.*, 1995, **70**, 787-788.
21. J. S. Zambounis, J. Pfeiffer, G. C. Papavassiliou, D. J. Lagouvardos, A. Terzis, C. P. Raptopoulou, P. Delhaès, L. Ducasse, N. A. Fortune and K. Murata, *Solid State Commun.*, 1995, **95**, 211-215.

22. C. Rethore, M. Fourmigue and N. Avarvari, *Chem Commun*, 2004, 1384-1385.
23. C. Réthoré, N. Avarvari, E. Canadell, P. Auban-Senzier and M. Fourmigué, *J. Am. Chem. Soc.*, 2005, **127**, 5748-5749.
24. A. D. Garlach, J. L. Musfeldt, J. M. Pigos, B. R. Jones, I. Olejniczak, A. Graja, M. H. Whangbo, J. A. Schlueter, U. Geiser, Winter and Gard, *Chem. Mater.*, 2002, **14**, 2969-2976.
25. I. Olejniczak, B. R. Jones, Z. Zhu, J. Dong, J. L. Musfeldt, J. A. Schlueter, E. Morales, U. Geiser, P. G. Nixon, R. W. Winter and G. L. Gard, *Chem. Mater.*, 1999, **11**, 3160-3165.
26. E. Coronado, J. R. Galan-Mascaros, C. J. Gomez-Garcia, A. Murcia-Martinez and E. Canadell, *Inorg. Chem.*, 2004, **43**, 8072-8077.
27. E. Coronado, S. Curreli, C. Giménez-Saiz, C. J. Gómez-García and J. Roth, *Synth. Met.*, 2005, **154**, 241-244.
28. P. Day and M. Kurmoo, *J. Mater. Chem.*, 1997, **7**, 1291-1295.
29. E. Coronado and P. Day, *Chem. Rev.*, 2004, **104**, 5419-5448.
30. C. J. Gomez-Garcia, E. Coronado, S. Curreli, C. Gimenez-Saiz, P. Deplano, M. L. Mercuri, L. Pilia, A. Serpe, C. Faulmann and E. Canadell, *Chem Commun*, 2006, 4931-4933.
31. A. M. Madalan, E. Canadell, P. Auban-Senzier, D. Branzea, N. Avarvari and M. Andruh, *New J. Chem.*, 2008, **32**, 333-339.
32. M. Clemente-León, E. Coronado, C. J. Gómez-García, A. Soriano-Portillo, S. Constant, R. Frantz and J. Lacour, *Inorg. Chim. Acta*, 2007, **360**, 955-960.
33. L. Martin, P. Day, P. Horton, S. Nakatsuji, J. Yamada and H. Akutsu, *J. Mater. Chem.*, 2010, **20**, 2738-2742.
34. M. Brezgunova, K.-S. Shin, P. Auban-Senzier, O. Jeannin and M. Fourmigue, *Chem Commun*, 2010, **46**, 3926-3928.
35. N. Kobayashi, T. Naito and T. Inabe, *Adv. Mater.*, 2004, **16**, 1803-1806.
36. T. Inabe, *J. Mater. Chem.*, 2005, **15**, 1317-1328.
37. E. Gomar-Nadal, J. Veciana, C. Rovira and D. Amabilino, *Adv. Mater.*, 2005, **17**, 2095-2098.
38. T. Yamamoto, T. Fukushima, A. Kosaka, W. Jin, Y. Yamamoto, N. Ishii and T. Aida, *Angew. Chem. Int. Ed.*, 2008, **47**, 1672-1675.
39. T. Welton, *Coord. Chem. Rev.*, 2004, **248**, 2459-2477.
40. T. Welton, *Chem. Rev.*, 1999, **99**, 2071-2084.
41. P. Wasserscheid and W. Keim, *Angew. Chem. Int. Ed.*, 2000, **39**, 3772-3789.
42. R. Sheldon, *Chem Commun*, 2001, 2399-2407.
43. Y. Marcus and G. Hefter, *Chem. Rev.*, 2006, **106**, 4585-4621.
44. A. Macchioni, *Chem. Rev.*, 2005, **105**, 2039-2074.
45. *Supramolecular Chemistry of Anions*, Wiley-VCH, Weinheim, 1997.
46. M. T. Pope and A. Müller, *Angew. Chem. Int. Ed.*, 1991, **30**, 34-48.
47. R. Lescouëzec, L. M. Toma, J. Vaissermann, M. Verdaguer, F. S. Delgado, C. Ruiz-Pérez, F. Lloret and M. Julve, *Coord. Chem. Rev.*, 2005, **249**, 2691-2729.
48. J. Lacour, *Chimia*, 2002, **56**, 672-675.
49. J. Lacour and R. Frantz, *Org. Biomol. Chem.*, 2005, **3**, 15-19.
50. J. Lacour and V. Hebbe-Viton, *Chem. Soc. Rev.*, 2003, **32**, 373-382.
51. J. Lacour and D. Moraleda, *Chem Commun*, 2009, 7073-7089.

52. H. U. Blaser, *Chem. Rev.*, 1992, **92**, 935-952.
53. J. M. Girodeau, J. M. Lehn and J. P. Sauvage, *Angew. Chem. Int. Ed.*, 1975, **14**, 764-764.
54. J. Jacques, A. Collet and S. H. Wilen, *Enantiomers, Racemates and Resolutions*, Krieger, Melbourne, USA, 1994.
55. E. L. Eliel, S. H. Wilen and L. N. Mander, *Stereochemistry of Organic Compounds*, Wiley, New York, 1994.
56. D. Berthier, T. Buffeteau, J.-M. Léger, R. Oda and I. Huc, *J. Am. Chem. Soc.*, 2002, **124**, 13486-13494.
57. J. Böeseken and J. A. Mijs, *Recueil des Travaux Chimiques des Pays-Bas et de la Belgique*, 1925, **44**, 758-762.
58. K. Torssell, *Acta Chem. Scand.*, 1962, **16**, 87-93.
59. D. J. Owen, D. VanDerveer and G. B. Schuster, *J. Am. Chem. Soc.*, 1998, **120**, 1705-1717.
60. K. Ishihara, M. Miyata, K. Hattori, T. Tada and H. Yamamoto, *J. Am. Chem. Soc.*, 1994, **116**, 10520-10524.
61. M. Periasamy, L. Venkatraman, S. Sivakumar, N. Sampathkumar and C. R. Ramanathan, *J. Org. Chem.*, 1999, **64**, 7643-7645.
62. D. B. Llewellyn and B. A. Arndtsen, *Tetrahedron: Asymmetry*, 2005, **16**, 1789-1799.
63. J. Jacques and C. Fouquey, *Org. Synth.*, 1989, **67**, 1-12.
64. S. Hoffmann, A. M. Seayad and B. List, *Angew. Chem. Int. Ed.*, 2005, **44**, 7424-7427.
65. D. Uraguchi and M. Terada, *J. Am. Chem. Soc.*, 2004, **126**, 5356-5357.
66. T. Akiyama, J. Itoh, K. Yokota and K. Fuchibe, *Angew. Chem. Int. Ed.*, 2004, **43**, 1566-1568.
67. G. Adair, S. Mukherjee and B. List, *Aldrichimica Acta*, 2008, **41**, 31–39.
68. M. Rueping, B. Nachtsheim, S. Moreth and M. Bolte, *Angew. Chem. Int. Ed.*, 2008, **47**, 593-596.
69. M. Terada, *Chem Commun*, 2008, 4097-4112.
70. J. Reeder, P. P. Castro, C. B. Knobler, E. Martinborough, L. Owens and F. Diederich, *J. Org. Chem.*, 1994, **59**, 3151-3160.
71. D. Hellwinkel, *Angew. Chem.*, 1965, **77**, 378-379.
72. J. Mason and S. F. Mason, *Tetrahedron*, 1967, **23**, 1919-1927.
73. J. Cavezzan, G. Etemad-Moghadam, M. Koenig and A. Klaebe, *Tetrahedron Lett.*, 1979, **20**, 795-798.
74. J. Lacour, C. Ginglinger, C. Grivet and G. Bernardinelli, *Angew. Chem. Int. Ed.*, 1997, **36**, 608-610.
75. J. Lacour, C. Ginglinger, F. Favarger and S. TorcheHaldimann, *Chem Commun*, 1997, 2285-2286.
76. G. Bruylants, C. Bresson, A. Boisdenghien, F. Pierard, A. K.-D. Mesmaeker, J. Lacour and K. Bartik, *New J. Chem.*, 2003, **27**, 748-751.
77. J. Lacour, A. Londez, C. Goujon-Ginglinger, V. Buss and G. Bernardinelli, *Org. Lett.*, 2000, **2**, 4185-4188.
78. J. Lacour, A. Londez, D. H. Tran, V. Desvergnes-Breuil, S. Constant and G. Bernardinelli, *Helv. Chim. Acta*, 2002, **85**, 1364-1381.
79. R. Andrés, M. Brissard, M. Gruselle, C. Train, J. Vaissermann, B. Malézieux, J.-P. Jamet and M. Verdaguer, *Inorg. Chem.*, 2001, **40**, 4633-4640.

80. M. Brissard, H. Amouri, M. Gruselle and R. Thouvenot, *C. R. Chimie*, 2002, **5**, 53-58.
81. R. Andrés, M. Brissard, M. Gruselle, C. Train, J. Vaissermann, B. Malézieux, J.-P. Jamet and M. Verdaguer, *Inorganic Chemistry*, 2001, **40**, 4633-4640.
82. R. C. Burrows and J. C. Bailar, *J. Am. Chem. Soc.*, 1966, **88**, 4150-4156.
83. Yu. N. Belokon, V. I. Maleev, I. L. Mal'fanov, T. F. Savel'eva, N. S. Ikonnikov, A. G. Bulychev, D. L. Usanov, D. A. Kataev and M. North, *Russ. Chem. Bull.*, 2006, **55**, 821-827.
84. Y. N. Belokon, V. I. Maleev, D. A. Kataev, I. L. Mal'fanov, A. G. Bulychev, M. A. Moskalenko, T. y. F. Saveleva, T. y. V. Skrupskaya, K. A. Lyssenko, I. A. Godovikov and M. North, *Tetrahedron: Asymmetry*, 2008, **19**, 822-831.
85. *Germany Pat.,* DE718981, 1942.
86. *US Pat.,* US2130505, 1938.
87. D. H. Busch and J. C. Bailar, *J. Am. Chem. Soc.*, 1953, **75**, 4574-4575.
88. R. D. Gillard, P. R. Mitchell and C. F. Weick, *J. Chem. Soc., Dalton Trans.*, 1974, 1635-1636.
89. F. P. Dwyer, F. L. Garvan and S. Kirschner, *Resolution of the Ethylenediamine-Tetraacetatocobaltate(III) Ion*, John Wiley & Sons, Inc., 2007.
90. K. Yamasaki and K. Sugiura, *Naturwissenschaften*, 1961, **48**, 552-553.
91. F. P. Dwyer, E. C. Gyarfas and D. P. Mellor, *J. Phys. Chem.*, 1955, **59**, 296-297.
92. T. J. Wenzel and J. Zaia, *Anal. Chem.* , 1987, **59**, 562-567.
93. P. García-García, F. Lay, C. Rabalakos and B. List, *Angew. Chem.*, 2009, **48**, 4363-4366.
94. K. Fukumoto and H. Ohno, *Chem Commun*, 2006, 3081-3083.
95. I. T. Raheem, P. S. Thiara, E. A. Peterson and E. N. Jacobsen, *J. Am. Chem. Soc.*, 2007, **129**, 13404-13405.
96. I. T. Raheem, P. S. Thiara and E. N. Jacobsen, *Org. Lett.*, 2008, **10**, 1577-1580.
97. S. E. Reisman, A. G. Doyle and E. N. Jacobsen, *J. Am. Chem. Soc.*, 2008, **130**, 7198-7199.
98. S. Pan and B. List, *Chem. Asian J.*, 2008, **3**, 430-437.

Chapter 2

Syntheses of organic donor molecules and some chiral derivatives

This chapter focuses on the synthesis of organic donor molecules, including improvements to the literature procedures, as well as on the synthesis of new chiral systems.

Introduction

Since the discovery of tetrathiafulvalene by Wudl *et al*.,[1] the research into electron rich heterocyclic olefins has been very intensive, hundreds of TTF derivatives have been synthesised and used not only in the construction of charge transfer solids but also in other molecular devices.[2-6] Several of the available procedures however, are published only in an outline and omit the details necessary to reproduce them. Quite often therefore, an effort has to be made into the redevelopment and improvement of the incomplete procedures.

The discovery of Magnetic Chiral Anisotropy (MCA, see Chapter 1)[7] raised a substantial interest in chiral donor molecules and many examples of these type of species were synthesised.[8-12] These efforts however, mainly focus on the introduction of a chirality element into the backbone of the molecule,

close to the electrochemically active core. Examples of this type of compound are given in Fig. 2.1.

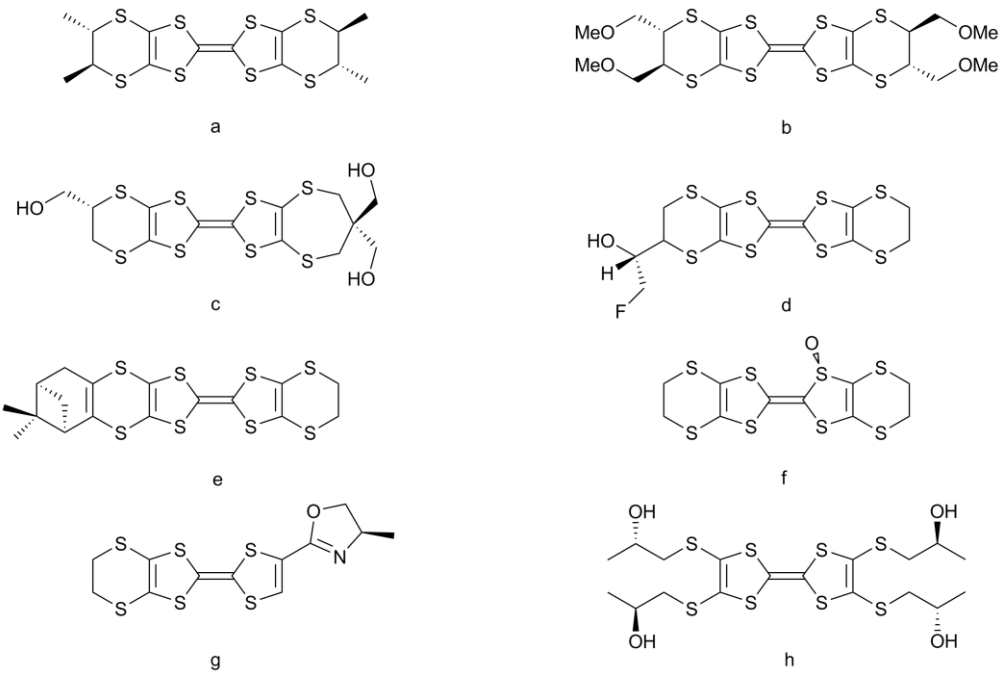

Figure 2.1. Examples of chiral TTFs in the literature: (a) Wallis *et al.*,[13] (b) Gomar-Nadal *et al.*,[8] (c) Ozturk *et al.*,[10] (d) Ozturk *et al.*,[14] (e) Yang *et al.*,[15] (f) Chas *et al.*,[16] (g) Réthoré *et al.*[17] and (h) Yang *et al.*[18]

This approach usually leads to distortion from planarity due to the introduction of an sp^3 carbon. At the same time the introduction of a chiral centre usually adds extra steric bulk further discouraging stacking behaviour. Only two species of this type, both containing methyl groups (Fig. 2.1a) yielded any conductive materials (see Chapter 1).

This work focuses on an alternative approach towards the synthesis of chiral donor molecules. The introduction of the chiral functionality further away from the molecule core should prevent the distortion from planarity and simultaneously, it should allow for easier accommodation of the extra steric

bulk introduced, potentially leading to materials with higher conductivity. This approach is based on working hypothesis that the expression of chirality near the elctroactive core of the molecule is not necessary and that the presence of a chiral element anywhere in the structure would suffice in order to ensure crystallisation of the product in a chiral space group.

This chapter focuses on the synthesis of the donor molecules: tetrathiafulvalene (TTF), bisethylenedithiotetraselenafulvalene (BEDT-TSF, BETS) and tetraselenafulvalene (TSF) as well as on further functionalisation of the TTF molecule towards the synthesis of chiral electroactive materials.

Results and discussion

Tetrathiafulvalene

Since the discovery of tetratiafulvalene[1] several different synthetic procedures towards this class of compounds were employed,[2,19-21] many of them however use carbon disulfide which is highly flammable and toxic. A relatively simple six step multigram scale synthesis which also circumvents the problem of CS_2 was developed by Melby *et al*.[22]

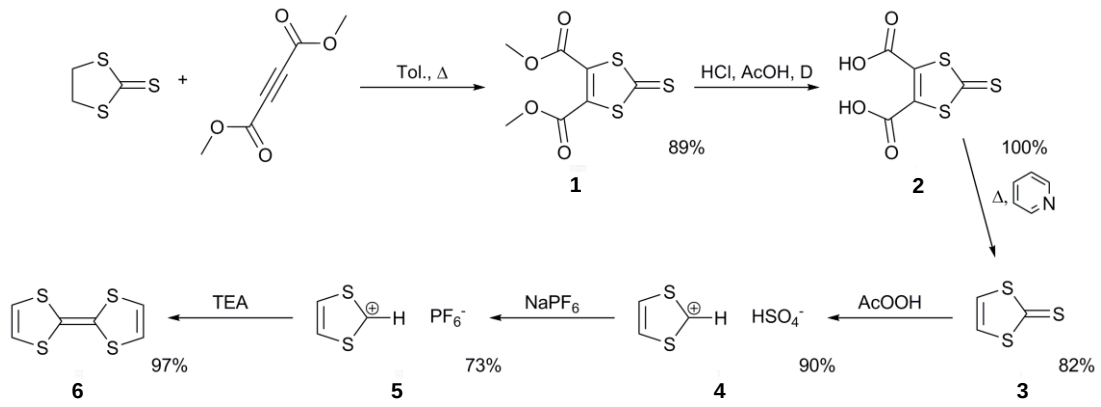

Scheme 2.1. Synthesis of tetrathiafulvalene.

Condensation of readily available dimethyl acetylenedicarboxylate and ethylene trithiocarbonate in toluene under reflux conditions gave dimethyl 1,3-dithiole-2-thione-4,5-dicarboxylate (**1**) in high yield (89%, reported 85%).[22] Subsequent hydrolysis with HCl and glacial acetic acid yielded the 1,3-dithiole-2-thione-4,5-dicarboxylic acid (**2**) upon heating in quantitative yield. Decarboxylation in pyridine under reflux condition yielded a thick black oil. Repeated extraction with hot hexane gave pure yellow solid 1,3-dithiole-2-thione (**3**) in 82% yield (92% reported)[22]. Oxidation of **3** with peracetic acid in acetone yielded air-sensitive 1,3-dithiolium hydrogen sulphate (**4**) (90% yield, reported 87%).[22] The reaction with peracid is highly exothermic and the temperature control during the process is crucial, as the product can undergo a thermal decomposition at higher temperatures. The product was collected by suction filtration under a constant stream of dinitrogen and used immediately in the subsequent reaction to avoid decomposition. Salt metathesis with sodium hexafluorophosphate in deaerated water yielded the stable salt, 1,3-dithiolium hexafluorophosphate (**5**) in 73% yield (reported 90%).[22] This salt can be easily purified and stored over extended periods of time without decomposition. The final coupling of **5** in dry MeCN under argon in the presence of dry TEA gave TTF (**6**). Slow cannula addition of deaerated water to the reaction mixture resulted in a separation of fibrous crystals of the product. Suction filtration under a stream of dinitrogen yielded **6** of purity adequate for most synthetic applications in 97% yield (reported 91%).[22] The product was used in the subsequent synthesis of chiral donor molecules (*vide infra*) and conductive materials (see Chapters 3 and 6).

Tetraselenafulvalene

In comparison with TTF, the higher polarisability and larger size of selenium atoms in tetraselenafulvalene increase electronic interactions and reduce the coulombic repulsion,[23] while not substantially changing the overall geometry of the molecule. This makes it feasible to obtain isostructural compounds of both TTF and TSF.

To our knowledge, only three synthetic routes to TSF have been established. The original procedure, developed by Engeler *et al.*[23] involves a two step synthesis starting from sodium acetylide. Unfortunately it requires the use of carbon diselenide which is not widely available and is highly toxic (Scheme 2.2). Another procedure, developed by Jackson *et al.*[24] utilises acetaldehyde semicarbazone and selenium dioxide to form the intermediate, 1,2,3-selenadiazole, which decomposes in the presence of potassium *tert*-butoxide forming 2-methylene-1,3-diselenole (**7**). This, upon addition of iodine in the presence of an amine, forms TSF (**8**). The mechanism of this last step is unknown and the reported yields are generally poor (<30%).[24]

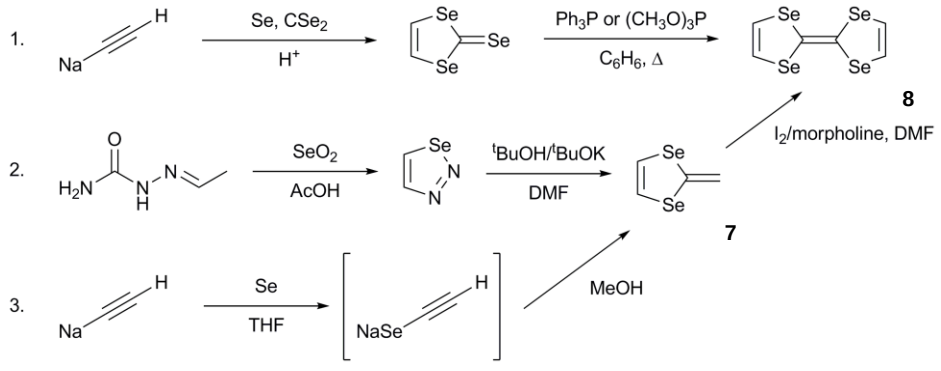

Scheme 2.2. The published synthetic routes towards tetraselenafulvalene. (1) Engeler et al.,[23] (2) Jackson *et al.*,[24] (3) Takimiya *et al.*[25]

Modification by Takimiya *et al*. simplifies this procedure, starting from sodium acetylide and relatively low toxicity selenium powder, forming **7** in one step.[25]

Tetraselenafulvalene was synthesised using the method by Takimiya *et al*., due to its apparent simplicity and availability of the starting materials. Sodium acetylide suspension in xylene:mineral oil was washed with pentane and diethyl ether and stored in the glove box. Reaction with a suspension of selenium powder in dry THF under argon yielded an orange suspension of the intermediate, sodium ethyneselenolate, which was subsequently hydrolysed with dry methanol. This was quenched with water and extracted with pentane. The product, 2-methylene-1,3-diselenole (**7**), was obtained after removal of the solvent *in vacuo*. The extraction was found to be a crucial step in this procedure, highly affecting the final yield. The product obtained is light sensitive and decomposes quickly at ambient temperature. Therefore, all of the extractions and subsequent solvent removal were performed in the dark with additional cooling. Even with these precautions yields obtained were still lower than reported (69% reported, max. 25% obtained). When necessary the compound was stored under dinitrogen in the dark at -30°C for a short period of time.

The coupling step was performed under argon using dry DMF and dry morpholine. A solution of iodine and morpholine in DMF was added to a solution of selenole **7** in dry DMF with cooling. An extraction and purification by column chromatography on silica using DCM:hexane (1:2) as eluent gave **8**, which was additionally recrystallised from boiling hexane. This procedure was repeated several times, but no yields higher than 9% were recorded (lit. ~30%). The product was used in the synthesis of conducting materials (see Chapter 6).

Bis(ethylenedithio)tetraselenafulvalene

Bis(ethylenedithio)tetraselenafulvalene (BETS) is a mixed selenium sulphur donor molecule similar to the more commonly used bis(ethylenedithio)-tetrathiafulvalene (BEDT-TTF, ET). Introduction of selenium into the structure generally improves charge transfer properties of the molecule.[26] Several compounds of BETS exhibit metallic conductivity and superconductivity.[27] BETS was first prepared by Schumaker *et al*. in 1983.[28] The synthetic procedure was however published only in an outline. The procedure was later simplified by Kato *et al*.,[26] again without disclosing all of the details of the procedure. The synthesis of 2,3-dihydro-1,4-dithiin (**9**) was further improved by Courcet *et al*.[29] This final procedure was used in this work and was optimised with help of Prof. Hiroki Akutsu from the University of Hyogo, Japan (Scheme 2.3).

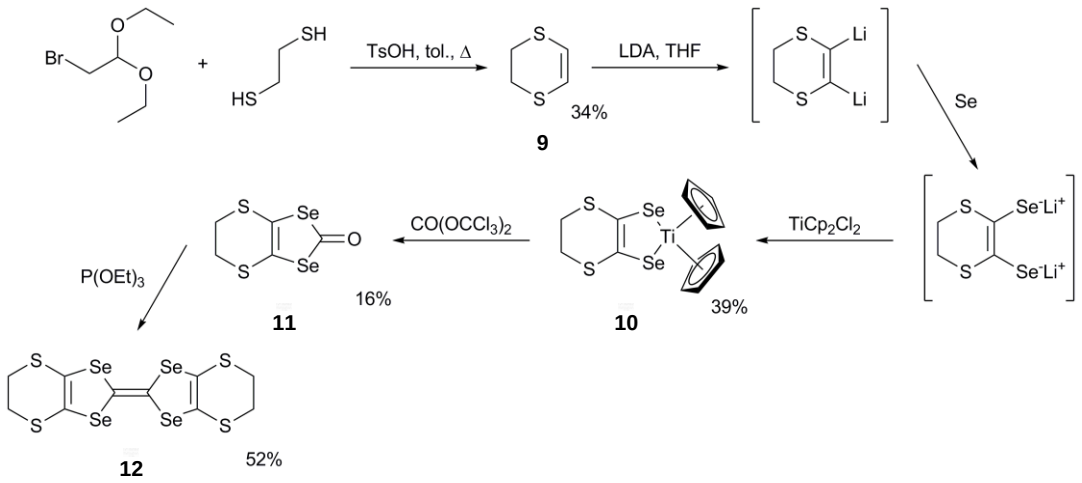

Scheme 2.3. Synthesis of bis(ethylenedithio)tetraselenafulvalene (BETS).

A one step condensation of 1,2-ethylenedithiol and 2-bromo-1,1-diethoxyethane in toluene in the presence of *p*-toluenesulphonic acid under reflux yielded 2,3-dihydro-1,4-dithiin (**9**) in 35% yield. A lithiation of **9** in THF followed by a reaction with selenium powder resulted in lithium 5,6-dihydro-

1,4-dithiine-2,3-bis(selenolate) which was treated using titanocene dichloride to bis(η^5-cyclopentadienyl)(5,6-dihydro-1,4-dithiine-2,3-diselenolato-κ^{2}Se,Se')-titanium(IV) (**10**). A chalcogen transfer[30,31] to triphosgene in THF under argon gave 4,5-ethylenedithio-1,3-diselenol-2-one (**11**). A cross-coupling of **11** under standard conditions[32] yielded BETS (**12**) as a microcrystalline solid in 52% yield. The obtained product was recrystallised from hot carbon disulphide and used in the subsequent syntheses of conductive materials (see Chapter 6).

Chiral TTF derivatives

Several different methods have been used in the synthesis of chiral substituted tetrathiafulvalenes.[12] Our approach focused on a direct substitution of the TTF molecule as the most suitable method for our purposes. A lithiation of TTF under mild conditions enables a route towards several different TTF derivatives.[33,34]

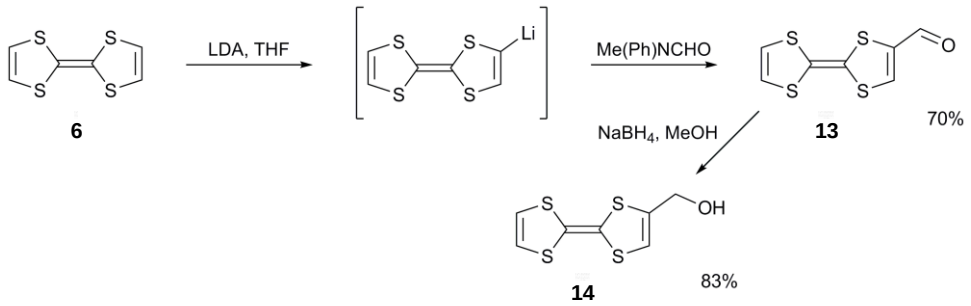

Scheme 2.4. Synthesis of 4-formyltetrathiafulvalene and 4-(hydroxymethyl)tetrathiafulvalene.

Our efforts focused on the synthesis of TTF imines and ethers using a simple imine condensation and the Williamson reaction respectively. The intermediates needed for those reactions, 4-formyltetrathiafulvalene (**13**) and 4-(hydroxymethyl)tetrathiafulvalene (**14**) were synthesised following a procedure by Garin *et al.*[34]. Reaction of TTF in THF with a slight excess of LDA

yielded monolithiated product which was treated further with *N*-methyl-*N*-phenylformamide to give **13** in good yields. A reduction of **13** using sodium borohydride in methanol gave **14** in 83% yield.

Several examples of simple aliphatic TTF ethers have been reported in the literature.[34-42] All of these compounds were prepared using Williamson reaction, starting from 4-(hydroxymethyl)tetrathiafulvalene and an aliphatic halogenate or tosylate/mesylate in the presence of sodium hydride in THF or toluene.[34-52] To our knowledge no compounds with amine substituents have been synthesised this way.

Several attempts to synthesise TTF ethers using this method with different derivatives of (*R*)-phenylglycinol and (*S*)-alaninol (Fig. 2.2) were made. Initial reactions with **16** and **21** in THF in the presence of excess of NaH resulted in unreacted starting materials. In order to investigate this further, a number of derivatives with different leaving groups (methanesulfonate, iodine) and amine protecting groups (di-*tert*-butyldicarbonate, phthalic anhydride) as well as ones with no protecting group were synthesised. All of the obtained derivatives were treated with **14** in THF in the presence of NaH. Reaction with derivative **19** was also repeated using toluene as a solvent. All of the reactions resulted in unreacted starting materials.

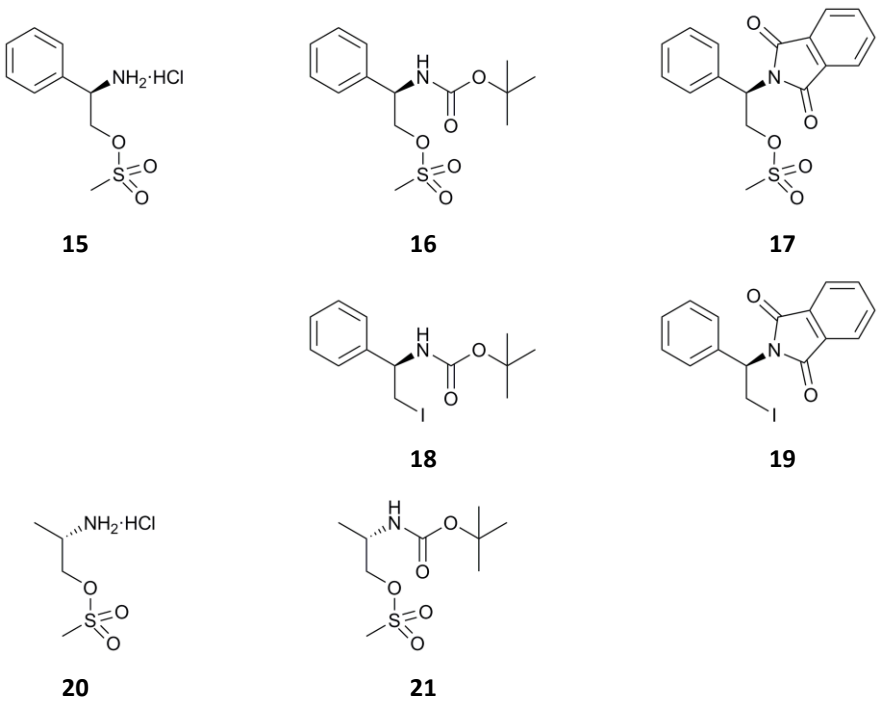

Figure 2.2. Derivatives of (*R*)-phenylglycinol and (*S*)-alaninol used in attempted syntheses of TTF ethers; (*R*)-2-amino-2-phenylethyl methanesulfonate hydrochloride (**15**), (*R*)-2-(tert-butoxycarbonylamino)-2-phenylethyl methanesulfonate (**16**), (*R*)-2-(1,3-dioxoisoindolin-2-yl)-2-phenylethyl methanesulfonate (**17**),(*R*)-tert-butyl 2-iodo-1-phenylethylcarbamate (**18**), (*R*)-2-(2-iodo-1-phenylethyl)isoindoline-1,3-dione (**19**), (*S*)-2-aminopropyl methanesulfonate hydrochloride (**20**), (*S*)-2-(tert-butoxycarbonylamino)propyl methanesulfonate (**21**).

In order to open an alternative route toward TTF ethers, an attempt was also made to obtain 4-(*halogeno*methyl)tetrathiafulvalene. Unfortunately, due to the inherent instability of this class of compounds[53] the product could not be isolated and this approach was abandoned.

4-Formyltetrathiafulvalene (**13**) was used to synthesise imines with (*R*)-phenylglycinol and (*R*)-α-methylbenzylamine (Scheme 2.5). The resulting alkylimino compounds were detected in the post reaction mixtures using ^{1}H NMR. They were however found to be air/water sensitive and difficult to purify. The compounds decomposed on silica and the attempts to distill or sublime

under high vacuum also resulted in decomposition. Further work on these types of imines was therefore abandoned.

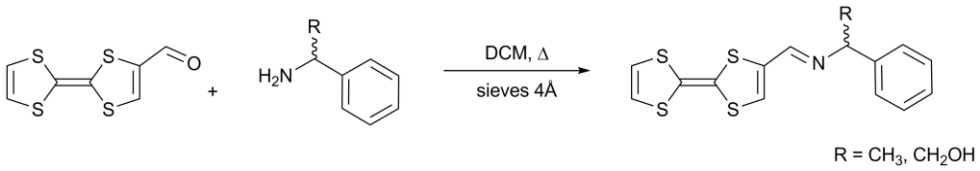

Scheme 2.5. Synthesis of aliphatic TTF imines.

6,6'-Dimethyl-N^2,$N^{2'}$-bis(tetrathiafulvalen-2-ylmethylene)biphenyl-2,2'-diamine

Following the discovery that aliphatic imine derivatives of 4-formyltetrathiafulvalene (**13**) were insufficiently stable, our efforts focused on the synthesis of Schiff bases. A reflux of **13** with 6,6'-dimethylbiphenyl-2,2'-diamine in dry THF in the presence of titanium(IV) chloride and TEA[54] under inert atmosphere resulted in the synthesis of a stable arylimino compound **22**. Attempts to synthesise this compound under milder conditions resulted only in unreacted starting materials. The compound was synthesised in both optically pure and racemic form.

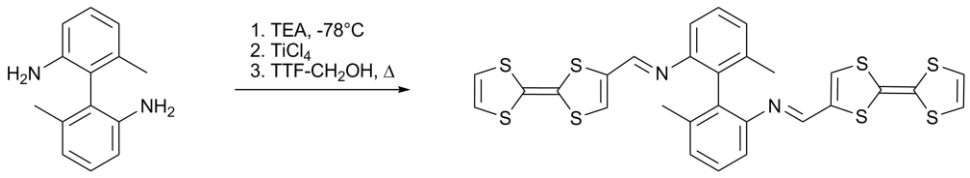

Scheme 2.6. Synthesis of biphTTF (**22**).

Cyclic voltammetry measurements of **22** show two quasi-reversible oxidation waves, similar to other TTF derivatives. The formal redox potentials,

0.412 and 0.803 V, recorded against SCE, are shifted towards higher values compared to the unsubsituted TTF molecule by ~0.10 V. No additional redox waves were observed, which suggests that there is no electronic interaction between the two linked TTF units.

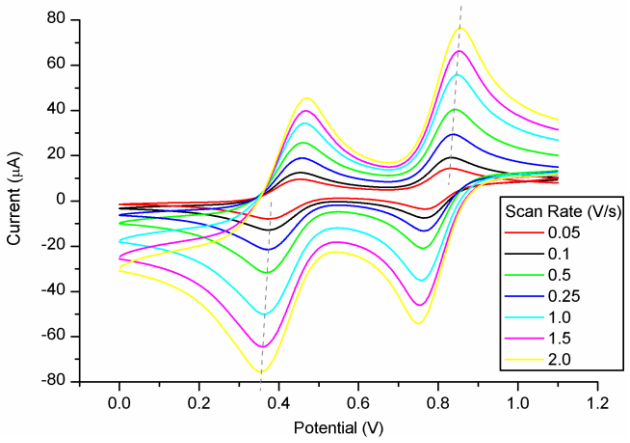

Figure 2.3. Cyclic voltammogram of **22** (0.1 mM solution in 0.1 M $NaPF_6$ in MeCN)

The UV-Vis spectrum of neutral **22** recorded in acetonitrile strongly resembles that of TTF, with an intense π→π* band at 300 nm, characteristic of the neutral TTF species. The additional bands at 450 nm and below 250 nm originate from the biphenyl core of the molecule.

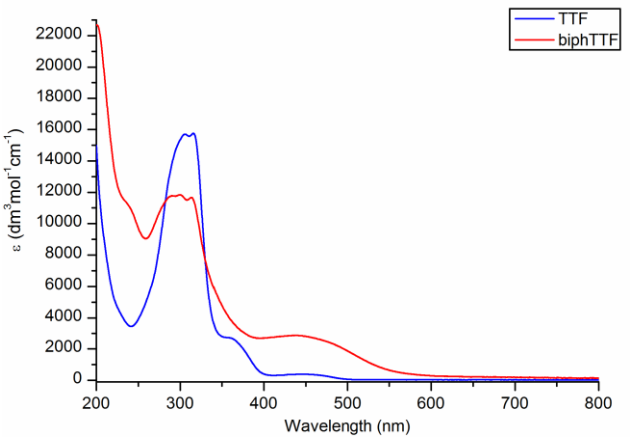

Figure 2.4. Absorption spectrum of 22 (red) and tetrathiafulvalene (blue) in acetonitrile.

The solution of neutral **22** was titrated with approximately stoichiometric portions of hydrogen peroxide/HCl solution and the UV-Vis spectra of the resulting mixtures were recorded. Upon addition of one equivalent of H_2O_2/HCl a new broad band at 390 nm appears (Fig. 2.5, red line). The intensity of this band increases on addition of a second equivalent. Upon further addition, an emergence of a second band at 430 nm (Fig. 2.5, blue line) was observed. This is consistent with the two step oxidation of the TTF units in the molecule: biph$(TTF^0)_2$ → biph$(TTF^+)_2$ → biph$(TTF^{2+})_2$, concluded from the CV measurements.

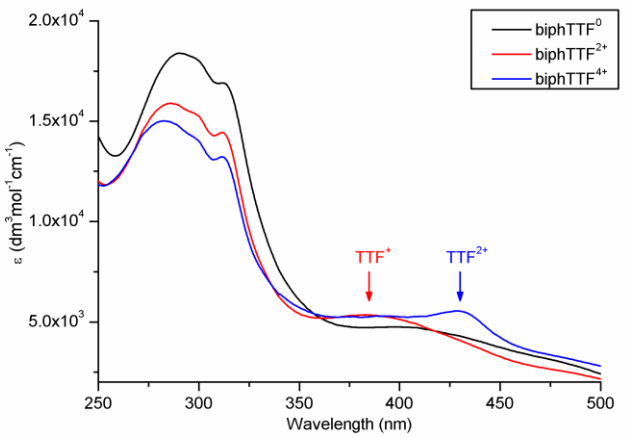

Figure 2.5. Absorption spectra of different oxidation states of 22.

The CD spectrum of optically pure **22** was also recorded. Several bands of various intensities can be observed (Fig. 2.6). Strong negative bands at ~300 and 320 nm can be most likely assigned to the π→π* transitions in the TTF groups and the remaining peaks to the phenyl backbone of the molecule.

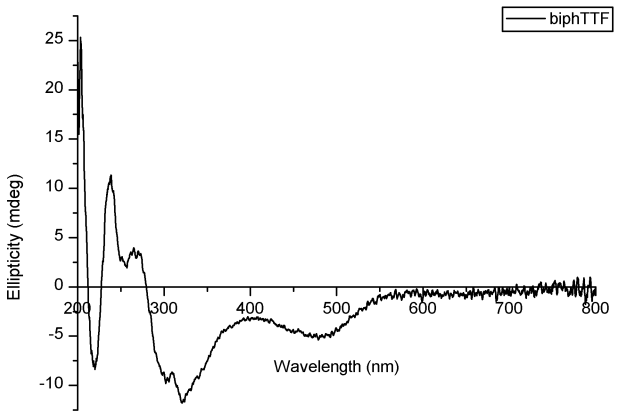

Figure 2.6. CD spectrum of 22 in acetonitrile (0.1 mM solution, 1 cm pathlength).

$[Cu_2(biphTTF)_2](BF_4)_2$

A reaction of racemic **22** with an anhydrous copper(I) tetrafluoroborate in dry DCM under argon resulted in a precipitatation of an interesting homochiral helical bimetallic structure $[Cu_2(biphTTF)_2](BF_4)_2$ (**23**), similar to other biphenyl imine complexes obtained previously in the group.[55]

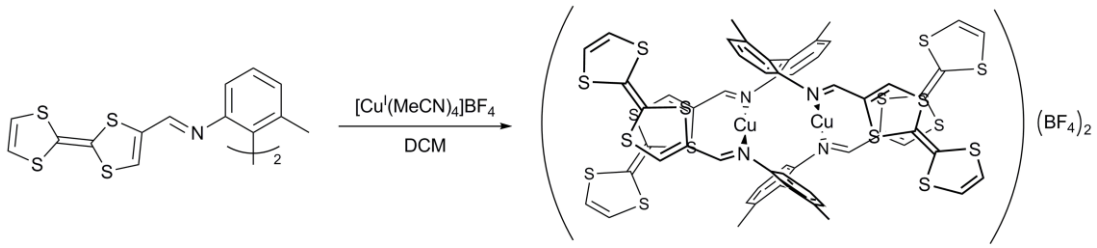

Scheme 2.7. Synthesis of **23**.

The compound was found to decompose in solution at ambient temperature even under inert atmosphere conditions. The solid compound is however stable, and was characterised using single crystal X-ray diffraction, magnetic measurements and EPR spectroscopy.

A single crystal of the compound was obtained from the filtrate after several weeks at -30°C. The compound crystallises in an achiral triclinic space group $P\bar{1}$. The asymmetric unit contains one complex, two BF_4^- counterions and a molecule of DCM and water, with the unit cell containing two of these. Both of the ligands of each complex are of the same hand, with the other complex in the unit cell being the opposite enantiomer.

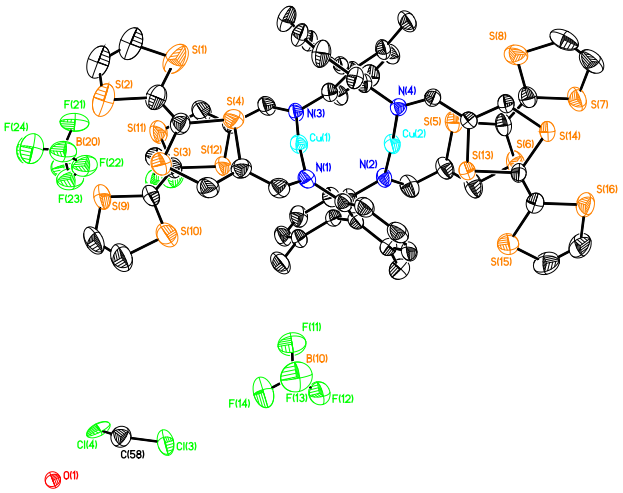

Figure 2.7. Asymmetric unit of $[Cu_2(biphTTF)_2](BF_4)_2{\cdot}CH_2Cl_2{\cdot}H_2O$ with the thermal ellipsoids at 50% probability. Hydrogen atoms were omitted for clarity.

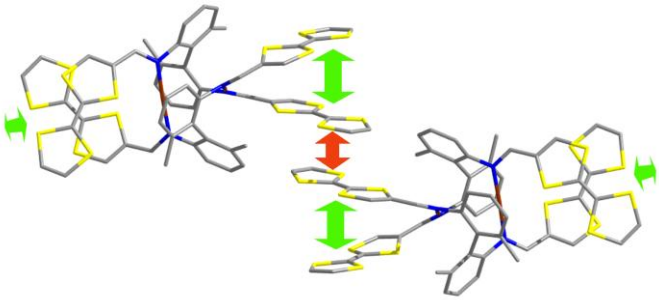

Figure 2.8. Packing diagram of **23** showing the intermolecular (red) and intramolecular (green) TTF stacking, hydrogen atoms, counterions and solvent molecules were removed for clarity.

The compound shows both intramolecular and intermolecular π-π stacking within the crystal structure (Fig. 2.8). The nature of the intermolecular

stacking interaction is conventional, with the TTF units in the stack parallel to each other and orientated along the same main axis. The distance between the planes of TTF units is 3.7 Å.

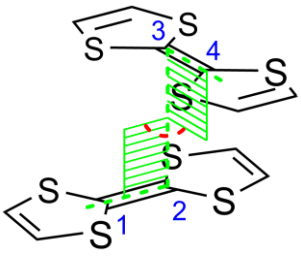

Figure 2.9. Dihedral angle (red) between the TTF molecules in the stack, atoms 1, 2, 3 and 4 are chosen this way so the distance between 2 and 3 is the shortest.

The intramolecular stacks are however of a different nature, due to the constraints of the molecular geometry (Fig. 2.9). The crossover angle between the TTF units was defined as a dihedral angle between carbon atoms of the middle double bonds of the molecules, with the axis going through the two closest carbon atoms. Two different interactions of this type can be distinguished in each molecule. The crossover angles of these stacks are equal to 114.69° and 74.14°, the distances between the TTF molecules in each stack are approximately 3.6 Å and the angles between planes of sulphur atoms of the TTF units are 3.42° and 9.37° respectively.

Analysis of the C-S bond distances in the four TTF units in the solid state structure shows some interesting differences. Bond lengths in two of the TTFs are consistent with partial oxidation (~0.2+), whereas in the two remaining ones, they are consistent with a neutral molecule (see Chapter 3). This suggests a weak charge transfer between the Cu^{I} centres and the TTF units. To further investigate this, the UV-Vis spectrum in methanol was recorded (Fig. 2.10). Due

to the limited stability of the species in solution, the spectrum was recorded immediately after sample preparation to avoid decomposition.

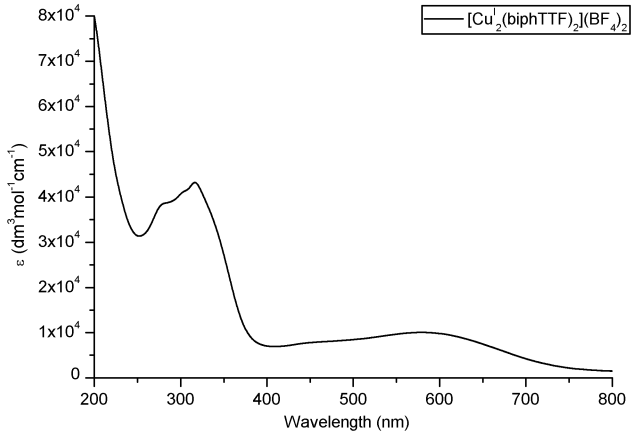

Figure 2.10. UV-Vis spectrum of 23 in methanol.

The spectrum shows features similar to those of the ligand with an additional broad absorption at ~600 nm originating from LMCT transitions to copper centres. The strong CT band at 317 nm (ε = 43200 $dm^3mol^{-1}cm^{-1}$) shows a small shift towards higher wavelengths compared with the isolated ligand, as well as much higher intensity (ligand ε = 11600 $dm^3mol^{-1}cm^{-1}$). This is consistent with a possible partial charge transfer between the TTF units and copper centres.

EPR spectra of the solid and DCM, DCM/methanol solutions of the compound were recorded in order to investigate the extent of the phenomena. The obtained spectrum of the solid sample gave a single signal with a peak-to-peak linewidth of 15 G. The position of the peak in the magnetic field, corrected for the offset of the used system, gives $g \approx 2.008$, a value consistent with TTF and other organic radicals. Given the width of the resonance line and the lack of hyperfine detail no interpretation of the data is feasible.

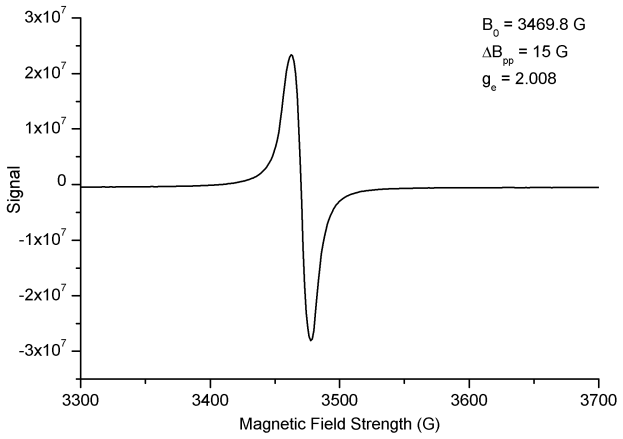

Figure 2.11 EPR spectrum of a solid sample of **23** (293 K)

Attempts to record a spectrum in DCM or DCM/methanol mixtures did not result in a significant improvement of the resolution of the spectrum and the limited solubility of the compound resulted in a reduction of the signal-to-noise ratio. No additional data were obtained this way.

Magnetic measurements show that the compound is a diamagnet with a weak paramagnetic contribution (Fig. 2.12).

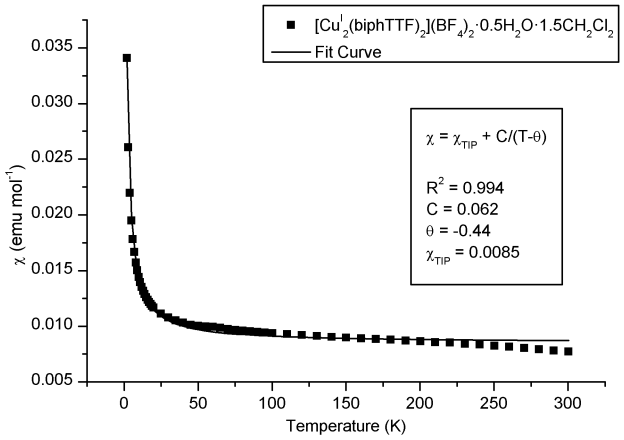

Figure 2.12. Magnetic data and Curie-Weiss law fit for **23**.

Application of the Curie-Weiss law corrected for temperature independent paramagnetism (χ_{TIP}) gives a reasonable fit.

$$\chi = \frac{C}{T - \theta} + \chi_{TIP}$$

The Curie constant value obtained allows for estimation of magnetic moment using the equation:

$$C = \frac{N_A \mu_{eff}^2 \mu_B^2}{3k} \quad \Rightarrow \quad \mu_{eff} = \sqrt{\frac{3kC}{N_A \mu_B^2}} \approx 2.828\, C^{1/2}\ (\mu_B, \text{c.g.s.units})$$

The effective magnetic moment calculated is 0.70 μ_B, which is consistent with a partial charge transfer (~0.1) to the copper centres (2.45 μ_B expected for a full charge transfer on both centres).

In order to investigate the possibility of a formation of a complex with mono-oxidised TTF species, a reaction of the neutral ligand **22** with copper(II) trifluoromethanesulfonate was conducted. No product was obtained this way; the reaction mixture was however investigated using UV-Vis spectrometry. The obtained spectrum was found to be consistent with that of a ligand with mono-oxidised TTF units (Fig. 2.5, red line).

Conclusions

Syntheses of three different donor molecules, tetrathiafulvalene (TTF), tetraselenafulvalene (TSF) and bis(ethylenedithio)tetraselenafulvalene (BETS) were successfully reproduced and conducted on a scale allowing for their subsequent use in electrochemical syntheses of conductive materials.

Different routes toward chiral functionalisation of the TTF molecule, starting from 4-formyltetrathiafulvalene and 4-(hydroxymethyl)tetrathia-fulvalene were explored. Williamson reaction was found to be an unsuitable

route towards TTF ethers. The condensation of 4-formyltetrathiafulvalene with chiral amines yielded unstable aliphatic imines, characterised by ^{1}H NMR. Stable Schiff bases were obtained from reactions with both racemic and optically pure 6,6'-dimethylbiphenyl-2,2'-diamine. The compounds were found to have electrochemical properties similar to the TTF molecule. Chiral species also shows optical activity by circular dichroism.

A novel homochiral bimetallic helicate was obtained by the complexation of Cu^{I} with the racemic biphenyl TTF imine. The compound exhibits a partial charge transfer between the Cu^{I} centres and TTF units of the ligand. An analysis of the magnetic measurements and the crystal structure allows for the estimation of the extent of the phenomena to 10-20%.

References

1. F. Wudl, G. M. Smith and E. J. Hufnagel, *J. Chem. Soc. D Chem. Comm.*, 1970, 1453-1454.
2. A. E.-W. A. O. Sarhan, *Tetrahedron*, 2005, **61**, 3889-3932.
3. T. Otsubo and K. Takimiya, *Bull. Chem. Soc. Jpn.*, 2004, **77**, 43-58.
4. J. L. Segura and N. Martín, *Angew. Chem. Int. Ed.*, 2001, **40**, 1372-1409.
5. M. R. Bryce, *J. Mater. Chem.*, 2000, **10**, 589-598.
6. in *Multifunctional Conducting Molecular Materials*, eds. G. Saito, F. Wudl, R. C. Haddon, K. Tanigaki, T. Enoki and H. E. Katz, The Royal Society of Chemistry, Cambridge, 2006.
7. G. L. J. A. Rikken, J. Folling and P. Wyder, *Phys. Rev. Lett.*, 2001, **87**, 236602.
8. E. Gomar-Nadal, C. Rovira and D. B. Amabilino, *Tetrahedron*, 2006, **62**, 3370-3379.
9. J. P. Griffiths, H. Nie, R. J. Brown, P. Day and J. D. Wallis, *Org. Biomol. Chem.*, 2005, **3**, 2155-2166.
10. T. Ozturk, N. Saygili, S. Ozkara, M. Pilkington, C. R. Rice, D. A. Tranter, F. Turksoy and J. D. Wallis, *J. Chem. Soc., Perkin Trans. 1*, 2001, 407-414.
11. G. A. Horley, T. Ozturk, F. Turksoy and J. D. Wallis, *J. Chem. Soc., Perkin Trans. 1*, 1998, 3225-3231.
12. N. Avarvari and J. D. Wallis, *J. Mater. Chem.*, 2009, **19**, 4061-4076.
13. J. D. Wallis, A. Karrer and J. D. Dunitz, *Helv. Chim. Acta*, 1986, **69**, 69-70.
14. T. Ozturk, C. R. Rice and J. D. Wallis, *J. Mater. Chem.*, 1995, **5**, 1553-1556.
15. S. Yang, A. C. Brooks, P. Day, M. Pilkington and J. D. Wallis, unpublished work.
16. M. Chas, F. Riobé, R. Sancho, C. Minguíllon and N. Avarvari, *Chirality*, 2009, **21**, 818-825.
17. C. Rethore, M. Fourmigue and N. Avarvari, *Chem Commun*, 2004, 1384-1385.
18. S. Yang, A. C. Brooks and J. D. Wallis, unpublished work.
19. R. L. Meline and R. L. Elsenbaumer, *J. Chem. Soc., Perkin Trans. 1*, 1998, 2467-2469.
20. M. Narita and C. U. Pittman Jr, *Synthesis*, 1976, **1976**, 489-514.
21. A. Krief, *Tetrahedron*, 1986, **42**, 1204-1252.
22. L. R. Melby, H. D. Hartzler and W. A. Sheppard, *J. Org. Chem.*, 1974, **39**, 2456-2458.
23. E. M. Engler and V. V. Patel, *J. Am. Chem. Soc.*, 1974, **96**, 7376-7378.
24. Y. A. Jackson, C. L. White, M. V. Lakshmikantham and M. P. Cava, *Tetrahedron Lett.*, 1987, **28**, 5635-5636.
25. K. Takimiya, H. J. Jeon and T. Otsubo, *Synthesis*, 2005, **2005**, 2810-2813.
26. R. Kato, H. Kobayashi and A. Kobayashi, *Synth. Met.*, 1991, **42**, 2093-2096.
27. H. Kobayashi, H. Cui and A. Kobayashi, *Chem. Rev.*, 2004, **104**, 5265-5288.
28. R. R. Schumaker, V. Y. Lee and E. M. Engler, *Journal De Physique*, 1983, **44**, 1139-1145.
29. T. Courcet, I. Malfant, K. Pokhodnia and P. Cassoux, *New J. Chem.*, 1998, **22**, 585-589.

30. C. M. Bolinger and T. B. Rauchfuss, *Inorg. Chem.*, 1982, **21**, 3947-3954.
31. M. Schmidt, B. Block, H. D. Block, H. Köpf and E. Wilhelm, *Angew. Chem. Int. Ed.*, 1968, **7**, 632-633.
32. T. Imakubo, M. Kibune, H. Yoshino, T. Shirahata and K. Yoza, *J. Mater. Chem.*, 2006, **16**, 4110-4116.
33. D. C. Green, *J. Org. Chem.*, 1979, **44**, 1476-1479.
34. J. Garin, J. Orduna, S. Uriel, A. J. Moore, M. R. Bryce, S. Wegener, D. S. Yufit and J. A. K. Howard, *Synthesis*, 1994, 489-493.
35. C. Thobie-Gautier, A. Gorgues, M. Jubault and J. Roncali, *Macromolecules*, 1993, **26**, 4094-4099.
36. M. A. Blower, M. R. Bryce and W. Devonport, *Adv. Mater.*, 1996, **8**, 63-65.
37. M. Á. Herranz, L. Yu, N. Martín and L. Echegoyen, *J. Org. Chem.*, 2003, **68**, 8379-8385.
38. A. Kanibolotsky, S. Roquet, M. Cariou, P. Leriche, C.-O. Turrin, R. de Bettignies, A.-M. Caminade, J.-P. Majoral, V. Khodorkovsky and A. Gorgues, *Org. Lett.*, 2004, **6**, 2109-2112.
39. T. Kitamura, S. Nakaso, N. Mizoshita, Y. Tochigi, T. Shimomura, M. Moriyama, K. Ito and T. Kato, *J. Am. Chem. Soc.*, 2005, **127**, 14769-14775.
40. T. Yamaguchi, S. Tashiro, M. Tominaga, M. Kawano, T. Ozeki and M. Fujita, *Chem. Asian J.*, 2007, **2**, 468-476.
41. A. Y. Ziganshina, Y. H. Ko, W. S. Jeon and K. Kim, *Chem Commun*, 2004, 806-807.
42. L. M. Goldenberg, R. Andreu, M. Saviron, A. J. Moore, J. Garin, M. R. Bryce and M. C. Petty, *J. Mater. Chem.*, 1995, **5**, 1593-1599.
43. J. C. Goeltz and C. P. Kubiak, *J. Phys. Chem. C*, 2008, **112**, 8114-8116.
44. L. M. Goldenberg, R. Andreu, M. Saviron, A. J. Moore, J. Garin, M. R. Bryce and M. C. Petty, *J. Mater. Chem.*, 1995, **5**, 1593-1599.
45. M. Á. Herranz, N. Martín, S. Campidelli, M. Prato, G. Brehm and D. M. Guldi, *Angew. Chem. Int. Ed.*, 2006, **45**, 4478-4482.
46. L. Huchet, S. Akoudad, E. Levillain, J. Roncali, A. Emge and P. Bauerle, *J. Phys. Chem. B*, 1998, **102**, 7776-7781.
47. L. Huchet, S. Akoudad and J. Roncali, *Adv. Mater.*, 1998, **10**, 541-545.
48. L. Huchet and J. Roncali, *J. Chim. Phys.*, 1998, **95**, 1270-1273.
49. I. Hwang, A. Y. Ziganshina, Y. H. Ko, G. Yun and K. Kim, *Chem Commun*, 2009, 416-418.
50. B. Patro, M. C. Merrett, S. D. Makin, J. A. Murphy and K. E. B. Parkes, *Tetrahedron Lett.*, 2000, **41**, 421-424.
51. G. Zotti, S. Zecchin, G. Schiavon, A. Berlin, L. Huchet and J. Roncali, *J. Electroanal. Chem.*, 2001, **504**, 64-70.
52. *United States Pat.,* 20060208220, 2006.
53. P. Hudhomme, S. Le Moustarder, C. Durand, N. Gallego-Planas, N. Mercier, P. Blanchard, E. Levillain, M. Allain, A. Gorgues and A. Riou, *Chemistry-a European Journal*, 2001, **7**, 5070-5083.
54. R. Carlson, U. Larsson and L. Hansson, *Acta Chem. Scand.*, 1992, **46**, 1211-1214.
55. C. J. Sanders, PhD, University of Warwick, 2000.

Chapter 3

Tetrathiafulvalenium salts of optically pure pyridine amidates (TTF)[$Co^{III}(L^n)_2$]

Introduction

In the search for viable building blocks for the construction of optically pure conducting materials few families of anionic octahedral complexes with tridentate chiral ligands were found. Initially the complexes of salicyladimine derivatives of chiral aminoacids (Fig. 3.1) were investigated, following work by Belokon *et al*.[1] These asymmetric tridentate ligands usually coordinate metal ions in a meridional fashion,[1,2] and form an additional stereogenic centre at the metal ion.

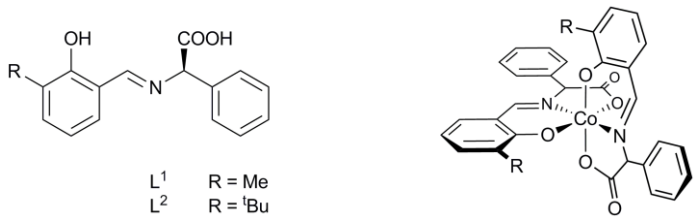

Figure 3.1. Structure of salycilaldimine derivative of (*R*)-2-phenylglycine and a model of its complex.

The control of the configuration of this new centre poses a significant challenge since diastereoselection in this class of compounds is known to be poor.[2] It was

postulated that the introduction of a bulky substituent in the R position, *e.g.* ^{t}Bu group, would enhance the diastereoselectivity by making one of the diastereoisomers sterically unfeasible, which was confirmed in preliminary experiments as follows. The ^{1}H NMR spectrum of the $[Co^{III}(L^{1})_2]^-$ complex (Me substituent) shows a mixture of isomers, comparable with literature reports of similar compounds.[1] In the case of $[Co^{III}(L^{2})_2]^-$ (R = ^{t}Bu) a single diastereoisomer was observed. These complexes have, however, proven to be very difficult to purify and crystallise.[1] The preliminary attempts to obtain tertrathiafulvalenium salts of these anions have yielded no products. Thus, the work with this class of compounds was abandoned. C_2 symmetric tridentate ligands were selected for further work, since these would preclude the formation of the additional chiral centre in the coordination complex and simplify the process by removal of the diastereoselectivity problem.

Over the last decade a new family of C_2 symmetric tridentate pyridinecarboxyamide ligands have been developed.[3-6] These ligands have shown ability to stabilise the trivalent oxidation state of the transition metals, due to the presence of deprotonated organic amide groups.[7] Recently, ligands from this family have been shown to form bimetallic complexes tested for their catalytic activity.[8]

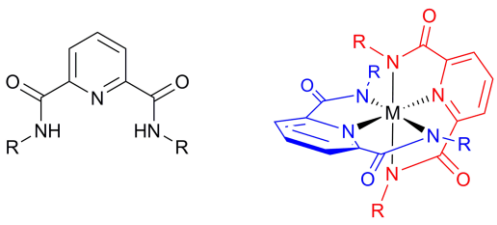

Figure 3.2. Structure of the pyridinecarboxyamide ligand (left) and its metal complex.

The family of pyridine amidate $[M^{III}(L^n)_2]^-$ (M = Co, Fe) complexes has been chosen due to its relatively easy accessibility and the wide range of modifications possible. The synthetic routes towards these type of complexes and their application in the construction of molecular solids have been previously investigated in the group.[9] This chapter focuses on the synthesis of such anions and their charge transfer salts with organic donors *e.g*. tetrathiafulvalene (TTF), as well as on determination of the relations between the electro- and spectrochemical properties of the solution, to the stoichiometry and properties of the solid state material.

Results and discussion

Ligands and complex anions synthesis

A synthetic procedure to *N*^{2},*N*^{6}-bis((*R*)-α-methylbenzyl)pyridine-2,6-dicaroxyamide, H_2(*R*,*R*-L^3) (Scheme 3.1) was developed previously in the group (J. Becker & C. Hart).[9,10] It is formed in a good yield in the reaction of the (*R*)-α-methylbenzylamine with pyridine-2,6-dicabonyl dichloride in DCM in the presence of TEA. The chloride is usually synthesised *in situ* by a reflux of pyridine-2,6-dicarboxylic acid with thionyl chloride in DCM. It was, however, observed that higher yields are obtained if the chloride was isolated and purified by distillation under high vacuum. The purified compound can be stored for a period of a few weeks without decomposition. Several commercially available chiral amines and their derivatives were used in the search for suitable ligands, focusing mainly on the natural and synthetic amino acids and their derivatives. The commercially available compounds used were:

R-(+)-α-methybenzylamine H_2(*R*,*R*-L^3), *S*-(+)-1-methoxy-2-propylamine H_2(*S*,*S*-L^4), (*R*)-2-phenylglycine H_2(*R*,*R*-L^5) L-Valine H_2(*S*,*S*-L^6) and (*R*)-2-phenylglycine methyl ester hydrochloride H_2(*R*,*R*-L^7). The synthesised derivatives: (*R*)-2-phenylglycinol[11] H_2(*R*,*R*-L^8) and (*R*)-2-phenylglycinol methyl ether[12] H_2(*R*,*R*-L^9) were obtained following the literature procedures. Only one enantiomer of each of the ligands was synthesised, thus in the further text the chirality descriptors will be omitted (i.e. H_2(*R*,*R*-L^3) ≡ H_2L^3).

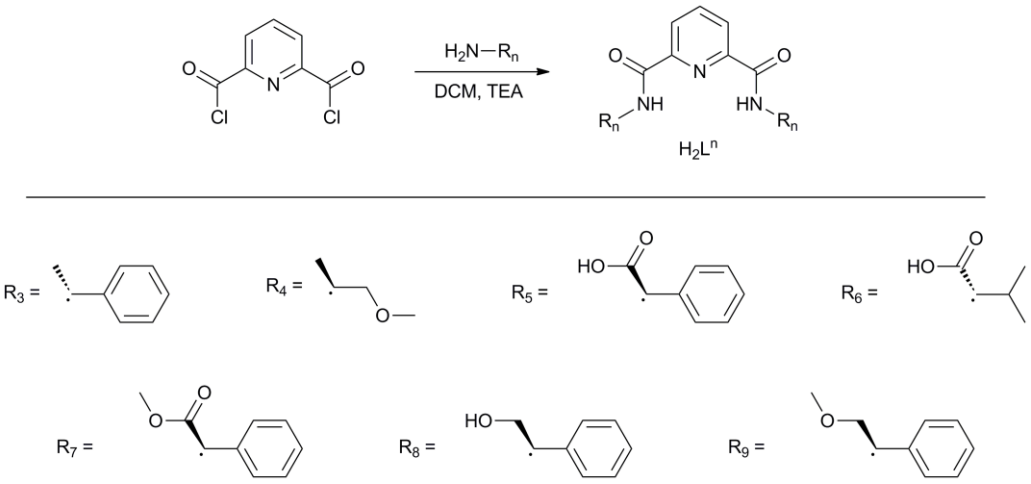

Scheme 3.1. Reaction scheme of synthesis of pyridinecarboxyamide ligands.

Proligands H_2L^5 – H_2L^9 were found not to form stable complexes with cobalt(III). With iron(III) only a small amount of desired complex $[Fe^{III}(L^n)_2]^-$ was formed along with the main product $[Fe^{III}(L^n)]^+$ (ESI). Further work on these compounds was abandoned.

The metal complexes were obtained using the synthetic strategy adapted from the literature.[7] Deprotonation of the ligand (H_2L^3) with potassium hydride in dry THF gave the potassium salt K_2L^3 which in the reaction with anhydrous cobalt(II) or iron(II) chloride under Schlenk conditions yielded the dianionic metal(II) complexes. *In situ* oxidation in air gave the desired complexes

(Scheme 3.2). The use of 18-crown-6 improves the solubility of the complexes in organic solvents. Resulting (18-crown-6)K[$Co^{III}(L^3)_2$] (**24**) and (18-crown-6)K[$Fe^{III}(L^3)_2$] (**25**) are readily crystallised and were fully characterised (**25** was reported previously in the group[9,10]). The crystal structure of the complex K[$Co^{III}(L^3)_2$] without the crown ether was also obtained.

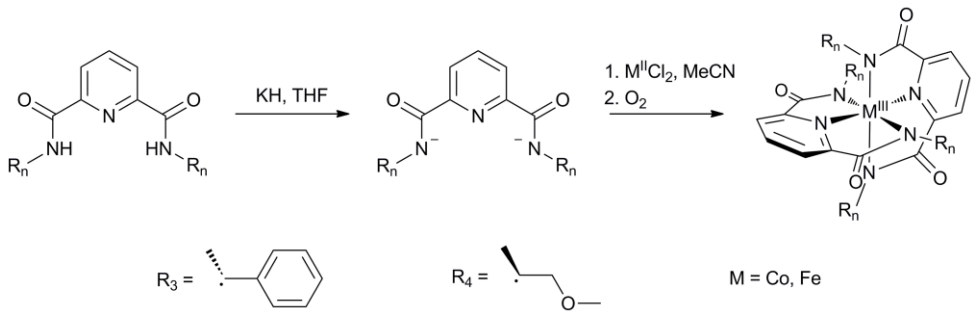

Scheme 3.2. Reaction scheme for the synthesis of the pyramid complexes.

Analogous treatment of ligand H_2L^4 gave K[$Co^{III}(L^4)_2$]·$3H_2O$ (**26**). The use of crown ether was not necessary, as the complex exhibits excellent solubility in acetonitrile and other organic solvents. The compound was characterised by NMR, mass spectrometry, microanalysis and single crystal X-ray diffractometry.

Crystal structures of $[Co^{III}(L^n)_2]^-$ anionic complexes

K[$Co^{III}(L^3)_2$]·MeOH

Single crystals of the complex were grown by slow diffusion of diethyl ether into the solution of the complex without the crown ether in acetonitrile. The compound crystallises in a monoclinic chiral $P2_1$ space group. The asymmetric unit consists of the cobalt complex, a potassium counter ion and a coordinated methanol. Large thermal parameters of the methanol molecule are most likely due to the thermal vibrations at ambient temperature. The angle between the

ligand planes is 88.8°. Selected bond lengths and angles can be found in Appendix B and the details of the crystal solution and refinement in Table A.2 in Appendix A.

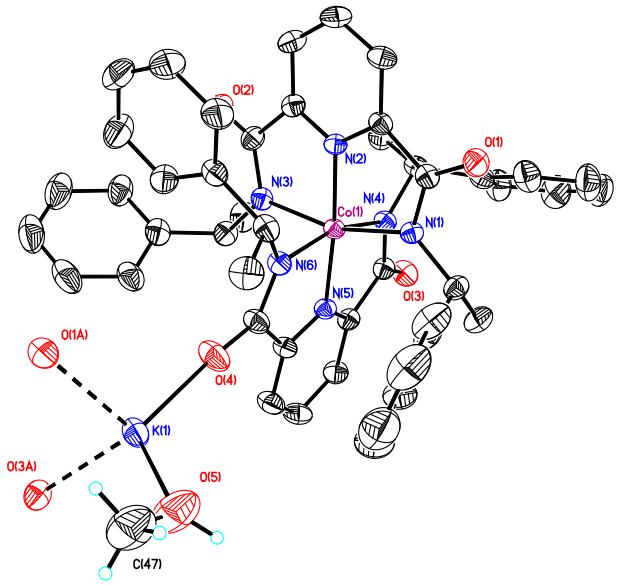

Figure 3.3. Solid state structure of $K[Co^{III}(L^3)_2]$ with thermal ellipsoids at 35% probability. Hydrogen atoms were removed on the major complex for clarity.

Coordination of the potassium ion by the carbonyl groups of the three adjacent complex anions results in formation of extended 2D honeycomb type layers in the crystal structure. (Fig. 3.4). Each of the potassium ions is coordinated to three carbonyl groups and one methanol molecule forming a distorted tetrahedron (Fig. 3.4a). The O···K distances are in 2.50-2.64 Å range. Each of the complex anions can also be described as a distorted tetrahedron with the metal atom in the centre and the carbonyl groups of the ligands pointing in the directions of the apices (Fig. 3.4a). Three of the corners of each tetrahedron participate in the formation of the extended network, resulting in a formation of a 2D extended structure.

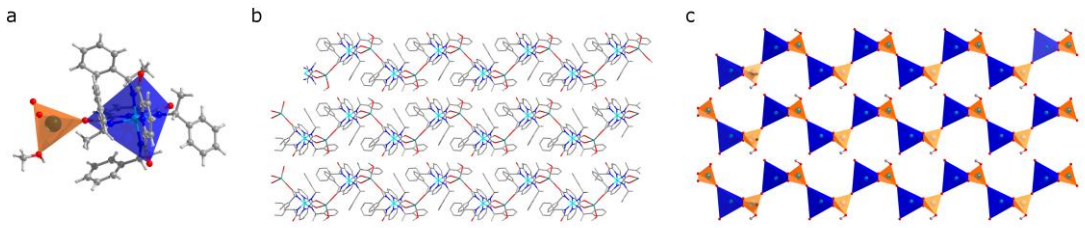

Figure 3.4. (a) Polyhedral model of the molecule, indicating tetrahedral orientation of the carbonyl groups. (b)The layered structure of $K[Co^{III}(L^3)_2]$ viewed from [100] direction with hydrogen atoms omitted for clarity, and (c) a simplified polyhedral model.

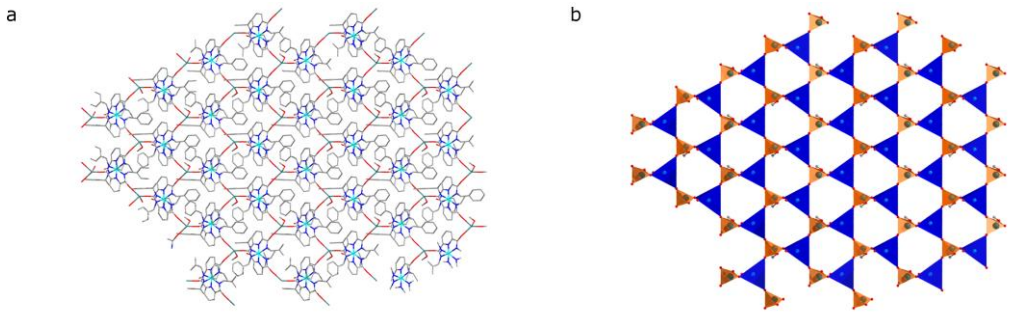

Figure 3.5. (a) Hexagonal sheet of $K[Co^{III}(L^3)_2]$ viewed from [001] direction with hydrogen atoms omitted for clarity and (b) a simplified polyhedral model.

Our analysis of the crystal structures of previously reported achiral compounds of this type shows, in several cases, similar extended structures with different topologies; 1D chains[6,13] and ribbons[14], 2D layers[14] and 0D clusters/pairs[13]. This is however the first example where chirality of the system results in formation of a chiral extended structure.

(18-crown-6)K[$Co^{III}(L^3)_2$]·H_2O·MeCN (24·H_2O·MeCN)

Single crystals of the complex **24** have been obtained by slow diffusion of diethyl ether into a solution of the complex in acetonitrile. The compound crystallises in a chiral monoclinic space group $P2_1$. The unit cell contains the complex anion, potassium counterion coordinated by 18-crown-6 and one water molecule. There is also one molecule of acetonitrile. The potassium ion is

additionally coordinated to the complex anion by the oxygen atom of one of the carbonyl groups forming discrete units of [(18-crown-6)(H_2O)K]·[$Co^{III}(L^3)_2$].

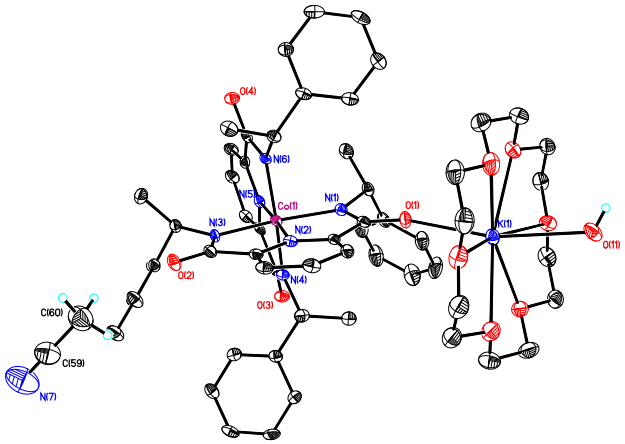

Figure 3.6. Solid state structure of (18-crown-6)K[$Co^{III}(L^3)_2$]·H_2O·MeCN with thermal ellipsoids at 50% probability. Hydrogen atoms have been omitted from the metal complex and the crown for clarity.

No extended coordination structure is formed, unlike in the case of K[$Co^{III}(L^3)_2$] due to the 18-crown-6 chelation of the potassium ion. Hydrogen bonding between a hydrogen atom of the water molecule coordinated to the potassium ion and the carbonyl group of an adjacent anion leads to the formation of a helical chain along the [010] direction (Fig. 3.7).

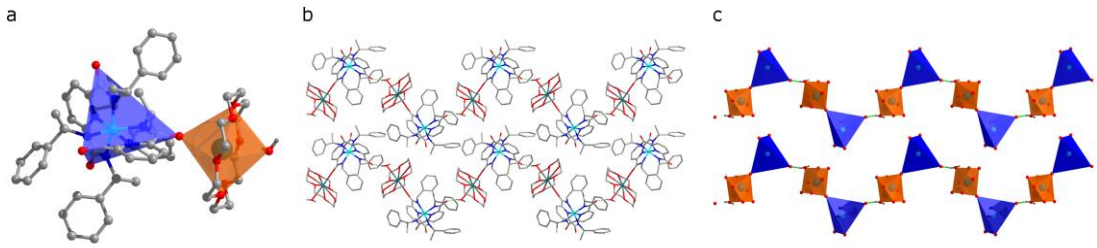

Figure 3.7. (a) Polyhedral model of (18-crown-6)K[$Co^{III}(L^3)_2$]·H_2O·MeCN, indicating tetrahedral orientation of the carbonyl groups. (b) helical chains viewed along the [100] direction with hydrogen atoms omitted for clarity, and (c) a simplified polyhedral model.

K[Co^{III}(L^4)$_2$]·3H$_2$O (26)

Crystals of **26** have been obtained by slow addition of diethyl ether into the solution of the complex in acetonitrile in the presence of a few drops of water. The compound crystallises in a chiral space group $P2_1$. The asymmetric unit consists of one complex anion, a potassium counterion and three water molecules coordinated to potassium. The relevant bond lengths can be found in Table B.4 in Appendix B and the detail of the crystal solution and refinement in Table A.2 in Appendix A.

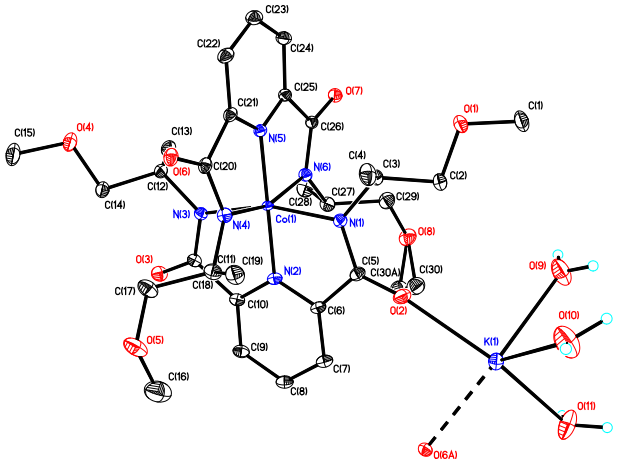

Figure 3.8. Solid state structure of K[Co^{III}(L^4)$_2$]·3H$_2$O with atomic numbering showing the potassium and coordinated waters and symmetry related carbonyl O6A

Analogous to the previous structures the geometry of the compound is octahedral with meridional arrangement of the ligands. The angle between the planes is θ = 87.7°. Through the coordination of the potassium counterion with the oxygen atoms of the carbonyl groups the compound forms 1D extended zig-zag chains in the solid state (Fig. 3.9). Each of the potassium ions is coordinated by three water molecules and two carbonyl groups of the adjacent anions forming a distorted square pyramid. The O···K distances are in 2.65-2.81 Å range.

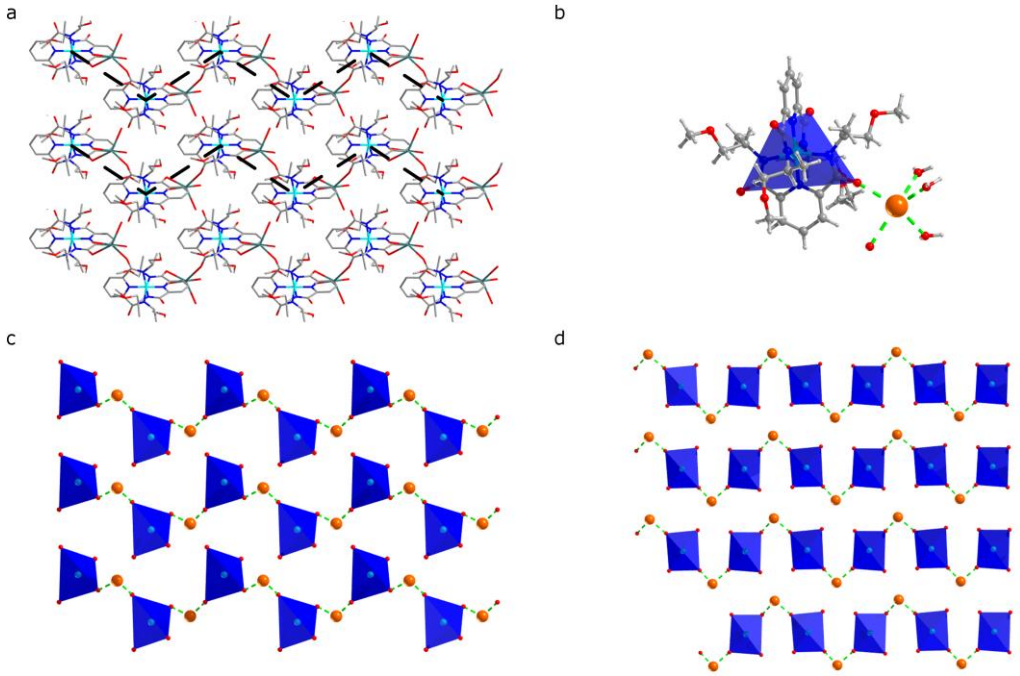

Figure 3.9. Extended 1D zig-zag chain structure of $K[Co^{III}(L^4)_2]\cdot 3H_2O$. (a) view from [001] direction (hydrogen atoms were removed for clarity), (b) polyhedral model of the molecule, indicating the tetrahedral orientation of the carbonyl groups, (c) simplified view from the [001] and (c) [100] direction.

When considering the extended structure of the compound, the complex anion can be also described as a distorted tetrahedron, with the metal atom in the centre and the coordination capable oxygen atoms of the carbonyl groups of the ligands in the corners (Fig. 3.9b). Only two of the corners of each tetrahedron participate in the formation of the extended structure, compared with three in the case of **24**. This results in formation of extended chains (1D) instead of layers (2D) (Fig. 3.9c,d).

Synthesis of the charge transfer materials

The obtained compounds, **24**, **25** and **26** were used in subsequent syntheses of the charge transfer molecular materials.

The two main techniques used in the synthesis of the charge transfer materials are electrocrystallisation and salt metathesis. The former depends on the electrochemical oxidation of the donor molecules (*e.g*. tetrathiafulvalene) in the presence of the desired counterion, resulting in a crystal growth. The process was conducted in an H-shaped cell with the cathode and anode chambers separated by a grass frit. Platinum wires were used as electrodes (Fig. 3.10). The cell was filled with a solution of the neutral donor (anode chamber) and the counterion (cathode chamber) in a suitable organic solvent or mix of solvents. To slow the crystal growth, the donor molecule was often placed in the anode chamber in a solid form. Additionally, by varying the composition of the solvent mixture, concentrations and the current density, the crystal growth rate can be modified in order to obtain suitably sized crystals. A typical procedure involved an initial set of electrocrystallisations of the compound with TTF and ET, in a range of solvents (MeCN, THF, DCM, PhCN, and MeOH) and their 20:1 mixtures with water under 1μA constant current conditions (20 cells). After the possible solvents/solvent mixtures were identified an additional set of cells was prepared in order to find the optimal solvent ratios, substrate concentrations and current conditions.

Although electrocrystallisation is considered to be a self-purifying process, it usually requires the use of very clean glassware and electrodes as well as ultra-pure substrates and solvents.[15] All of the used solvents were distilled and degassed before use, the substrates have been recrystallised at least twice and the cells were prepared under inert atmosphere.

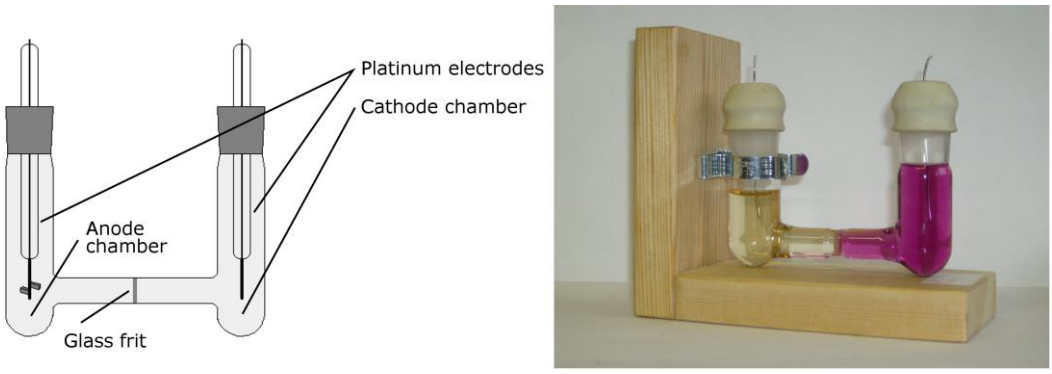

Figure 3.10. Electrocrystallisation cell schematic and a picture of an actual cell.

(TTF)[$Co^{III}(L^3)_2$] (27)

Electrocrystallisation of **24** with TTF in dry THF under constant current conditions (1 μA) gave black crystals of (TTF)[$Co^{III}(L^3)_2$] (**27**) suitable for X-ray diffraction and conductivity measurements. The crystal structure of the compound was determined.

The compound crystallises in a chiral monoclinic C_2 space group. The asymmetric unit contains one ligand, half of a cobalt ion and half of an oxidized TTF molecule. There are two complete complex anions and two TTF molecules in the unit cell. The cobalt complex lies on a twofold axis through the cobalt as does the middle of the C=C bond of the oxidised TTF. The complex is C_2 symmetric with the central metal ion lying on the axis and the two ligands equivalent by symmetry. The bond lengths of the TTF molecule are consistent with the values expected for the TTF^+ (Table B.5, Appendix B).[16]

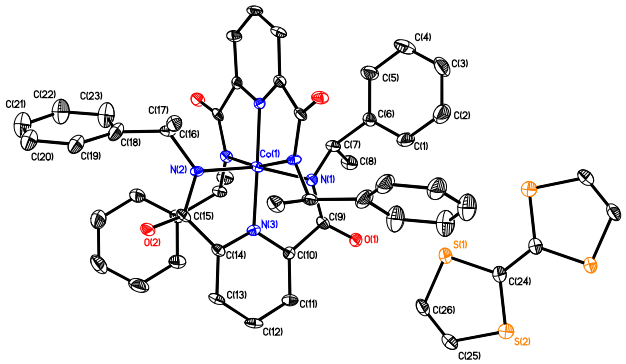

Figure 3.11. Molecular structure of (TTF)[Co^{III}(*R*,*R*-L^3)$_2$]. Hydrogen atoms were removed to aid clarity.

There is no significant difference between the bond lengths within the complex anion compared to **24**. Interestingly the ligands' orientation changes slightly, demonstrating much more symmetrical arrangement compared to the parent compound, presumably due to the lack of a coordinated potassium ion in **27**.

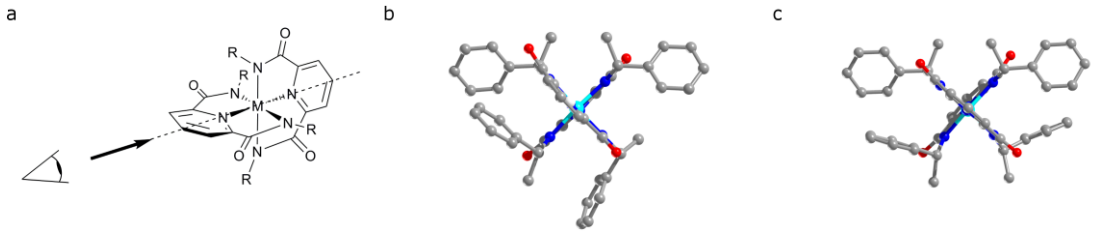

Figure 3.12. Comparision of the orientation of the phenyl groups of the ligand in (b) the parent compound **24** and (c) its TTF salt **27**. (a) View along the main axis of the molecule.

In the parent compound, K[Co^{III}(L^3)$_2$], the orientation of the two ligands is not identical, the phenyl group of one of the ligands points above and below the plane of the ligand, whereas the analogous groups on the other ligand both point in the same direction (Fig. 3.12b). In the TTF salt **27** the ligand orientation is C_2 symmetric, with both ligands being symmetrically equivalent (Fig. 3.12c).

The crystal packing of the compound is different from the usual stacked arrangement, common for this type of compound. The full oxidation of the TTF molecule and the resulting electrostatic interaction with the complex results in the formation of ionic pairs $[TTF]^{+}\cdot[Co^{III}(L^{3})_2]^{-}$ instead of typical layers of TTF stacks. The distance between the neighbouring TTF molecules in the structure is 9.53 Å, which is too great to result in electrical conductivity, which was confirmed by the conductivity measurements.

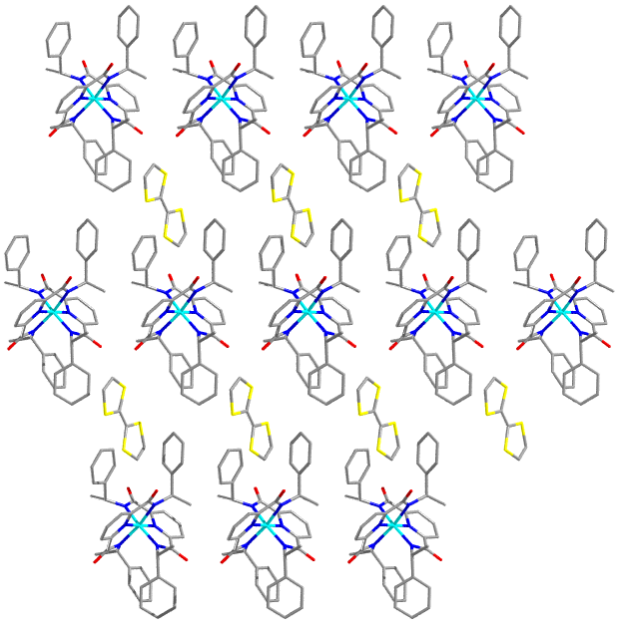

Figure 3.13. Extended structure of $(TTF)[Co^{III}(L^{3})_2]$. Hydrogen atoms were removed for clarity.

The analysis of the extended structure of the compound shows alternating layers of the complex anions and TTF molecules. The phenyl rings of the anion penetrate the cationic layer, potentially disrupting closer stacking between the TTF molecules (Fig. 3.13).

$(TTF)[Co^{III}(L^{4})_2]\cdot EtOAc$ (28)

To overcome these issues, a new ligand (*S*,*S*-H_2L^4) was designed (Scheme 3.1). It was expected that the removal of the phenyl rings would eliminate the

disruption of the stacking of the donor molecules, as well as reduce the overall size of the anion, thus, allowing for closer packing and enhancing the conductivity. Attempts to electrocrystallise the modified complex with TTF however, have proven fruitless, most likely due to the high solubility of the resulting material preventing crystallisation. Therefore, a different approach to the synthesis was used, namely the salt metathesis, using the pre-oxidised TTF salt: $(TTF)_3(BF_4)_2$. This compound was prepared previously in the group (C. Hart)[10] by the oxidation of TTF with hydrogen peroxide in the presence of borofluoric acid in acetonitrile, following the procedure by Wudl *et al*.[17]

$(TTF)[Co^{III}(L^4)_2]\cdot EtOAc$ (**28**) was obtained by an addition of the acetonitrile solution of $(TTF)_3(BF_4)_2$ to the solution of $K[Co^{III}(L^4)_2]\cdot 3H_2O$ (**26**) in acetonitrile. Single crystals of the product were obtained by slow diffusion of EtOAc into the solution. The compound was characterised using single crystal X-ray diffraction, conductivity measurements, CD and UV spectrometry and cyclic voltammetry.

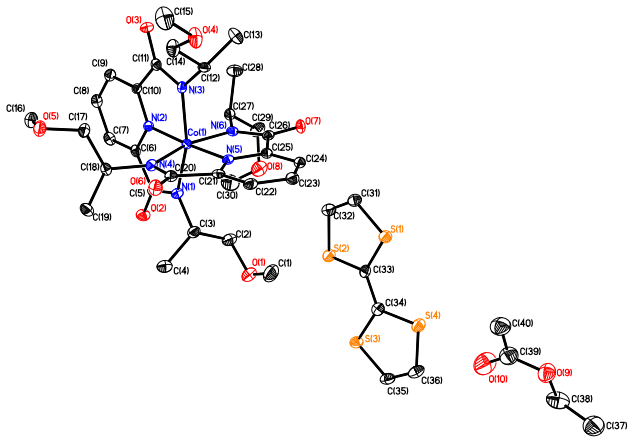

Figure 3.14. Crystal structure of $(TTF)[Co^{III}(L^4)_2]\cdot EtOAc$, the hydrogen atoms were removed for clarity.

(TTF)[$Co^{III}(L^4)_2$]·EtOAc crystallises in a monoclinic chiral $P2_1$ space group. The asymmetric unit contains the complex anion, one TTF molecule and one molecule of ethyl acetate.

The bond lengths of the TTF molecule are consistent with the expected values for TTF^+ (*vide supra*).[16] There are no significant changes in bond length within the complex anion compared to **26**. Similarly to **27** however, the ligand orientation in this structure is much more symmetrical compared to the parent compound (Fig. 3.15).

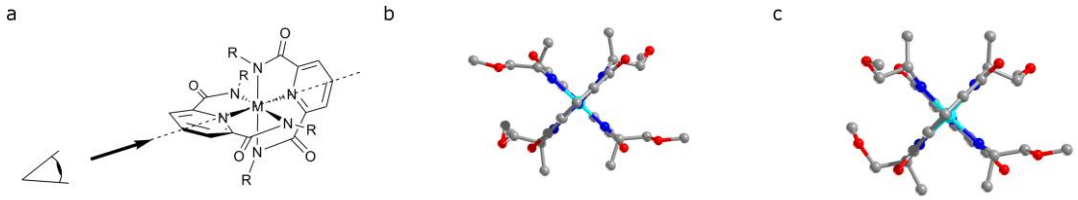

Figure 3.15. Comparision of the orientation of the phenyl groups of (b) the ligand in the parent compound **26** and (c) its TTF salt **28**. (a) View along the main axis of the molecule.

As in the case of **24**, the arrangement of the two ligands in the parent compound is not identical. The methoxy groups of the one ligand point outward from the octahedron, whereas the corresponding groups of the second ligand are pointing inwards. The complex anion in the TTF salt **28** displays a more symmetrical configuration with one of the groups pointing outwards and one inwards in both ligands. Unlike the L^3 analogue however, the complex does not display C_2 symmetry.

The extended structure of the compound, similar to **27**, does not exhibit TTF stacking. The compound is composed of alternating anionic and cationic

layers. The cationic layer consists of TTF units and ethyl acetate molecules in an alternating arrangement (Fig. 3.16).

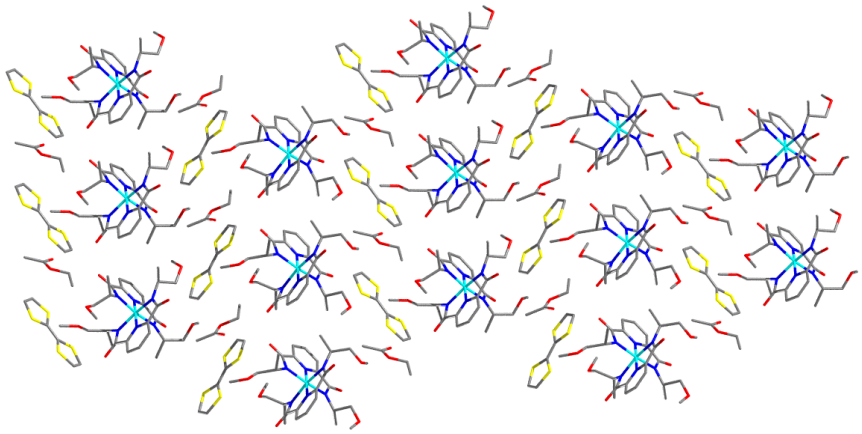

Figure 3.16. Extended structure of **28**, hydrogen atoms were removed for clarity.

Similar to the structure of **27**, methoxy groups that were used to replace the phenyl ring penetrate into the cationic layer. Unlike the previous structure however, the molecule of non-solvent is incorporated into the cationic layer further disrupting the stacking. This opens a possibilty of post-synthetic modifications by crystallisation using different non-solvents. The attempts to recrystallise the compound from acetonitrile/diethyl ether mixture yielded microcrystalline solids. However, no single crystals of quality suitable for X-ray diffraction or conductivity measurements were obtained.

Other attempts

Electrocrystallisation and salt metathesis of (18-crown-6)K[$Fe^{III}(L^3)_2$] (**25**) to obtain its TTF salt yielded insoluble microcrystalline solids. No single crystals suitable for X-ray diffraction or conductivity measurements were obtained.

Attempts to obtain ET salts of either (18-crown-6)K[$Co^{III}(L^3)_2$] (**24**) or K[$Co^{III}(L^3)_2$]·$3H_2O$ (**26**) by electrocrystallisation yielded no products.

Oxidation state of the donor molecule

Analysis of the molecular structures of the TTF based charge transfer compounds reveals an interesting correlation between the average bond distances in the TTF molecule and its average charge (oxidation state). Clemente *et al*. through analysis of several crystal structures concluded that this relation can be best observed using C=C or C-S distances and follows a simple linear trend.[16]

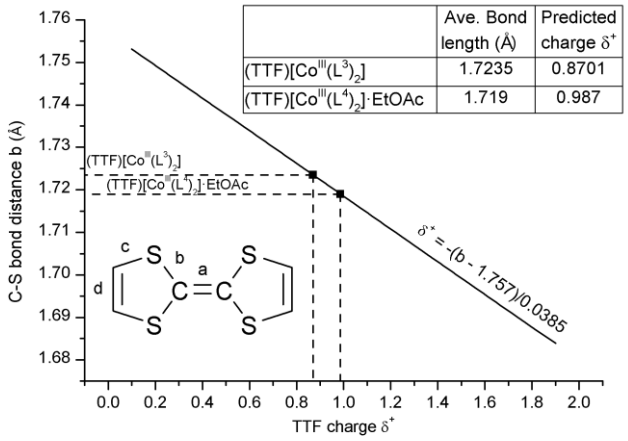

Figure 3.17. Analysis of the average C-S bond distance in the TTF molecule and its average charge for (TTF)[$Co^{III}(L^3)_2$] (**27**) and (TTF)[$Co^{III}(L^4)_2$·EtOAc (**28**).

The analysis of the average C-S (b) bond distances in the TTF molecules of both synthesised compounds confirms the oxidation state close to +1, consistent with the formulae (Fig. 3.17).

Conductivity measurements

All of the conductivity measurements were performed using a typical 4 probe setup at ambient temperature. The method used involves attaching 4 gold wires

(25 μm) to one of the crystal surfaces using conductive carbon cement. The prepared crystal was then mounted in a DIL socket, the contacts between the socket and gold wires were made using conductive carbon cement. The schematic of the conductivity measurement and picture of the mounted crystal can be seen below (Fig. 3.18). The process of mounting the electrodes is fraught with difficulty and requires considerable patience. In order to try to eliminate random errors, measurements were made on at least 3 different crystals.

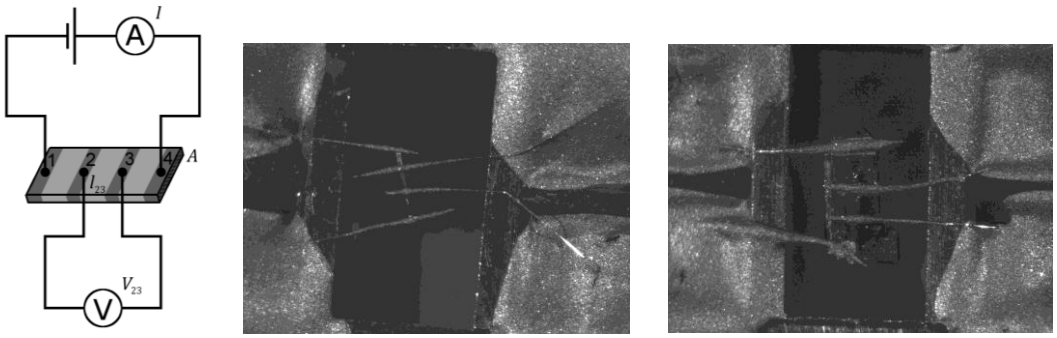

Figure 3.18. Scheme of the conductivity measurement and pictures of the actual setup.

A constant current (I) is applied to the sample through the contacts 1 and 4. The resistance of the sample causes a drop in potential as the current flows along the sample. The voltage drop between is measured between the probes 2 and 3 (V_{23}). The resistance of the sample between probes 2 and 3 (R_{23}) is therefore the ratio of the voltage recorded to the value of the applied current (I).

$$R_{23} = \frac{V_{23}}{I}$$

The distance between the probes 2 and 3 (l_{23}) and the cross-section area (A) are measured and the resistivity of the sample (ρ) can be calculated.

$$\rho = R_{23}\frac{A}{l_{23}}$$

Conductivity (σ) is an inverse of the calculated resistivity.

$$\sigma = \frac{1}{\rho} = \frac{l_{23}I}{V_{23}A}$$

To eliminate the inaccuracies due to the measurement errors, all of the quoted values are an average of measurements on at least three different crystals.

UV-Vis and CD spectrometry

UV-Vis absorption and CD spectra of the synthesised protonated ligands and their complexes were recorded in acetonitrile. UV-Vis spectra of both proligands (H_2L^3 and H_2L^4) show a strong absorption in the 200-300 nm region due to π*←π bands originating from the pyridine backbone (Fig. 3.19 and 3.20 blue lines). The absorption coefficients are significantly larger for H_2L^3 due to the presence of the additional phenyl groups.

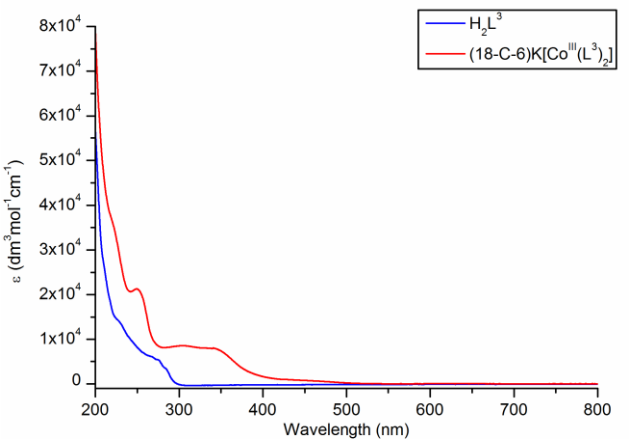

Figure 3.19. UV-Vis spectra of the H_2L^3 proligand and its complex (18-crown-6)K[$Co^{III}(L^3)_2$].

A comparison of the spectra of proligands and their complexes show several additional CT bands in spectra of the latter (Fig. 3.19 and 3.20 red lines) in the region 200-400 nm. The spectrum of (TTF)[$Co^{III}(L^4)_2$]·EtOAc (**28**) shows similar features to the parent complex with the exception of additional bands in the

250-350 nm region, originating from the TTF^+ moiety (Fig. 3.20 green line). A spectrum of the TTF^+ species was obtained by a subtraction of the spectrum of $K[Co^{III}(L^4)_2]$ from the spectrum of **28** (Fig. 3.20 inset).

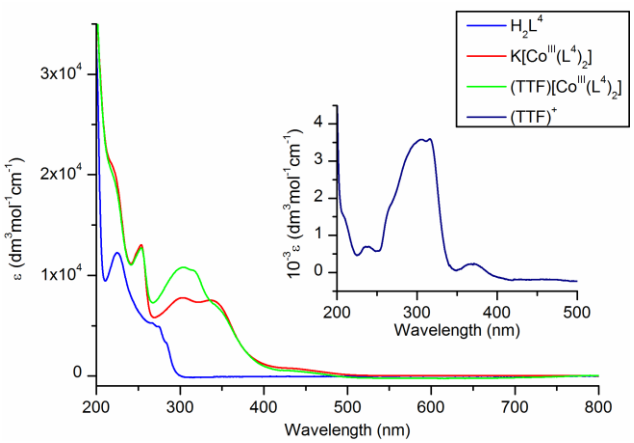

Figure 3.20. UV-Vis spectra of the H_2L^4 proligand, its complex $K[Co^{III}(L^4)_2]$, the charge transfer salt $(TTF)[Co^{III}(L^4)_2]\cdot EtOAc$ and $(TTF)^+$ (inset).

In 'free' TTF^+ a strong absorption is expected at 430 nm, a strong hypsochromic shift (1.2-1.5 eV) is therefore apparent into the region usually associated neutral TTF.[18,19] We propose that this arises from a strong interaction between the cationic donor molecule and the anion in the solution. Incidentally, no bands characteristic for the $(TTF^+)_2$ dimers are observed. Strong shifts in UV-Vis spectra of TTF species were previously observed for species trapped inside zeolites.[20]

The CD spectra of the H_2L^3 proligand and its complexes are insignificant and were previously reported.[9] The only interesting feature is the apparent inversion of the spectrum while comparing spectra of the proligand and the complex (Fig. 3.21).[9]

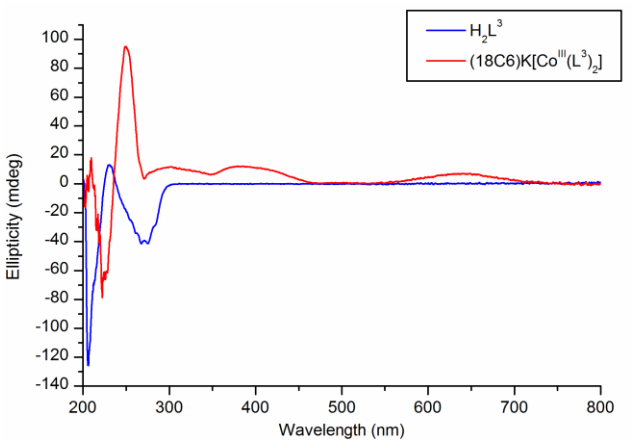

Figure 3.21. CD spectra of the protonated ligand H_2L^3 and its complex (18-crown-6)$K[Co^{III}(L^3)_2]$ (0.1 mM solutions in MeCN).

The spectrum of the methoxy derivative (H_2L^4) shows almost no features in the measured spectral range, only a weak band can be observed at 250-300 nm (Fig. 3.22 blue line). This is most likely due to the absence of strongly absorbing functional groups near the stereogenic centres of the molecule. CD spectra of complexes **24** and **26** show broad, weak features in the 550-750 nm region, originating from the *d-d* transitions. The low intensity (ellipticity) of these bands can be explained by a weak expression of chirality at the metal centre (the complexes are not chiral-at-metal). Several strong CT bands can be observed in the 200-500 nm region, with the strongest bands between 200 and 300 nm.

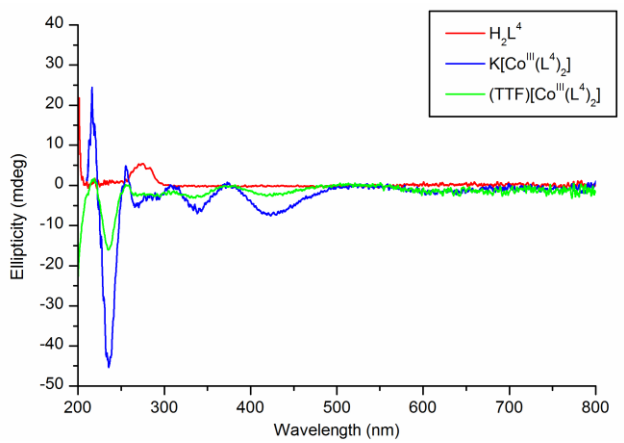

Figure 3.22. CD spectra of the H_2L^4 proligand, its complex $K[Co^{III}(L^4)_2]\cdot 3H_2O$ and the charge transfer salt $(TTF)[Co^{III}(L^4)_2]\cdot EtOAc$ (0.1 mM solutions in MeCN).

Similar to the H_2L^3 case, the spectrum of the complex seems to be reversed vertically compared to the spectrum of its proligand.

The CD spectrum of the TTF salt **28** shows analogous features to the spectrum of the parent complex **26** (Fig. 3.22 green line). No measurable effects originating from TTF^+ ion were observed.

Cyclic voltammetry

The synthesised complexes display an apparent affinity to crystallise as TTF^+ salts, instead of the more common, partially oxidised $TTF^{\sim 0.7+}$ form. To further investigate this phenomenon, cyclic voltammograms of the parent complexes and $(TTF)[Co^{III}(L^4)_2]\cdot EtOAc$ were collected. The voltammograms were recorded without supporting electrolyte in order to observe only the interactions between the non-innocent species in the solution, and this results in broadness due to ohmic effects.[21] The scans were started at positive potentials and are reported relative to the Ag/AgCl (3M KCl) reference electrode.

Voltammograms of (18-crown-6)K[$Co^{III}(L^3)_2$] (**24**) and K[$Co^{III}(L^4)_2$]·$3H_2O$ (**26**) show analogous features (Fig. 3.23). Both compounds show wide voltammograms characteristic of irreversible/quasi-reversible processes.[21] Weak peaks for at least two steps can be observed. The strongest one, in the range 0.75-2.0 V, is most likely associated with Co^{III}/Co^{IV} redox couple, given that the Co^{2+} ion is readily oxidised by oxygen and this ligand environment is known to stabilise the higher oxidation states (*vide supra*). The formal redox potentials can be estimated at ~1.28 V for **24** and ~1.41 V for **26**.

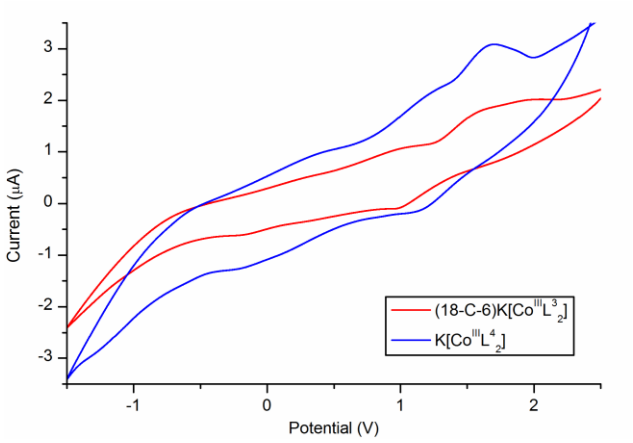

Figure 3.23. Cyclic voltammograms of (18-crown-6)K[$Co^{III}(L^3)_2$] (**24**) and K[$Co^{III}(L^4)_2$]·EtOAc (**26**) in acetonitrile (0.1 mM solutions).

The recorded curve for the TTF salt **28** (Fig. 3.24) shows features originating from both the TTF moiety (0 to 1.3 V) and the complex anion (-1 to 1.75 V). The peaks associated with TTF (0.38 V and 0.87 V) are shifted towards slightly higher potentials compared to the isolated TTF molecule in the presence of the same concentration of PF_6^- (0.34 V and 0.79 V) (Fig. 3.24 inset). The Co^{III}/Co^{IV} wave in the 0.75-2.0 V range is more pronounced compared to the curve of the isolated complex, giving a formal redox potential of 1.25 V, significantly lower than the value for the parent compound **26** (1.42 V). Upon

changing the scan speeds in the range 25-2000 mV/s all of the observed peaks shift demonstrating typical irreversible/quasi-reversible behaviour.[21]

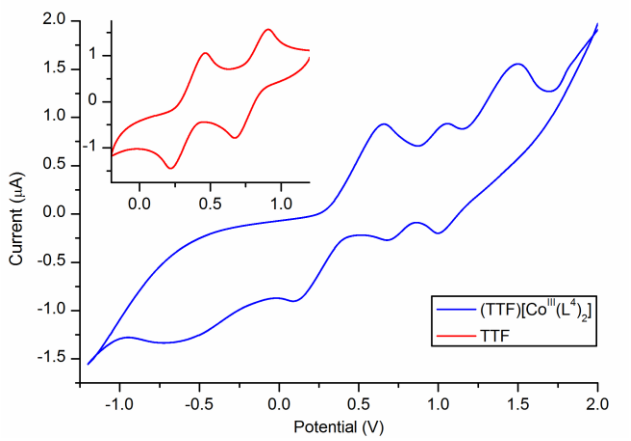

Figure 3.24. Cyclic voltammogram of (TTF)[$Co^{III}(L^4)_2$]·EtOAc (**28**) in acetonitrile (0.1 mM solution) and TTF (inset) (0.1 mM $NaPF_6$ solution in acetonitrile).

Interestingly the peak currents associated with first redox step (TTF/TTF^+) increase significantly compared with the second (TTF^+/TTF^{2+}) and the curve for isolated TTF molecule. This is consistent with a Chemical-Electrochemical (CE) process in which the TTF^+ undergoes a chemical process – association with the anion, to form a soluble assembly – which reduces its concentration in the region of the electrode. Formation of such assemblies has been observed in TTF compounds[22-24] as well as in several other types of materials and there is a growing body of evidence that the formation of such assemblies is a key step in crystallisation processes.[25]

Conclusions

Pyridinecarboxaldehydes are a versatile and easily accessible family of ligands. Several chiral optically pure members of this family and their complexes were

synthesised and characterised. The obtained compounds: (18-crown-6)K[$Co^{III}(L^3)_2$] (**24**), K[$Co^{III}(L^3)_2$]·MeOH and K[$Co^{III}(L^4)_2$]·$3H_2O$ (**26**) show interesting extended structures, from 0D discrete units, through 1D zig-zag chains, to 2D honeycomb layers, formed by coordination of the potassium counterion by carbonyl oxygen atoms of the ligands.

The compounds were tested for their application in the synthesis of charge transfer materials with tetrathiafulvalene. The obtained compounds (TTF)[$Co^{III}(L^3)_2$] (**27**) and (TTF)[$Co^{III}(L^4)_2$]·EtOAc (**28**) were characterised by a single crystal X-ray diffraction and conductivity measurements. Both compounds exhibit similar layered structures with no TTF stacking, which results in a non-conductive behaviour. Interestingly, the crystal structure of the former contains molecules of the non-solvent, which opens a possibility of post-synthetic modifications of the compound at the crystallisation stage.

Cyclic voltammetry and spectroscopic evidence points to the formation of $[TTF]^{+}\cdot[Co^{III}(L^n)_2]^{-}$ assemblies in the solution and this mirrors the solid state structure in which stoichiometric $[TTF]^{+}\cdot[Co^{III}(L^n)_2]^{-}$ rather than electrically conductive non-stoichiometric phases are observed.

References

1. Y. Belokon', V. Maleev, I. Mal'fanov, T. Savel'eva, N. Ikonnikov, A. Bulychev, D. Usanov, D. Kataev and M. North, *Russ. Chem. Bull.*, 2006, **55**, 821-827.
2. R. C. Burrows and J. C. Bailar, *J. Am. Chem. Soc.*, 1966, **88**, 4150-4156.
3. M. Nonoyama, *Inorg. Chim. Acta*, 1974, **10**, 59-63.
4. F. A. Chavez, M. M. Olmstead and P. K. Mascharak, *Inorg. Chem.*, 1996, **35**, 1410-1412.
5. F. A. Chavez, C. V. Nguyen, M. M. Olmstead and P. K. Mascharak, *Inorg. Chem.*, 1996, **35**, 6282-6291.
6. A. N. Dwyer, M. C. Grossel and P. N. Horton, *Supramol. Chem.*, 2004, **16**, 405 - 410.
7. M. Ray, D. Ghosh, Z. Shirin and R. Mukherjee, *Inorg. Chem.*, 1997, **36**, 3568-3572.
8. A. Mishra, A. Ali, S. Upreti, M. S. Whittingham and R. Gupta, *Inorg. Chem.*, 2009, **48**, 5234-5243.
9. J. M. Becker, PhD, University of Warwick, 2009.
10. C. Hart, *Unpublished work*, University of Warwick, 2007.
11. M. J. McKennon, A. I. Meyers, K. Drauz and M. Schwarm, *J. Org. Chem.*, 1993, **58**, 3568-3571.
12. R. N. Bream, S. V. Ley, B. McDermott and P. A. Procopiou, *J. Chem. Soc., Perkin Trans. 1*, 2002, 2237-2242.
13. J. L. Bricks, G. Reck, K. Rurack, B. Schulz and M. Spieles, *Supramol. Chem.*, 2003, **15**, 189 - 197.
14. D. S. Marlin, M. M. Olmstead and P. K. Mascharak, *Inorg. Chem.*, 1999, **38**, 3258-3260.
15. N. Toyota, M. Lang and J. Müller, *Low-dimensional molecular metals*, Springer, Berlin ; [London], 2007.
16. D. A. Clemente and A. Marzotto, *J. Mater. Chem.*, 1996, **6**, 941-946.
17. F. Wudl, *J. Am. Chem. Soc.*, 1975, **97**, 1962-1963.
18. F. Wudl, G. M. Smith and E. J. Hufnagel, *J. Chem. Soc. D Chem. Comm.*, 1970, 1453-1454.
19. J. B. Torrance, B. A. Scott, B. Welber, F. B. Kaufman and P. E. Seiden, *Phys. Rev. B*, 1979, **19**, 730.
20. T. Imakubo, M. Kibune, H. Yoshino, T. Shirahata and K. Yoza, *J. Mater. Chem.*, 2006, **16**, 4110-4116.
21. J. Wang, in *Analytical Electrochemistry (Third Edition)*, Wiley-VCH, Hoboken, 2006, pp. 29-66.
22. R. Carlier, A. Tallec, P. Frere, M. Salle, M. Jubault, A. Gorgues and J. Cousseau, *Synth. Met.*, 1993, **56**, 2359-2363.
23. Y. Tatewaki, T. Hatanaka, R. Tsunashima, T. Nakamura, M. Kimura and H. Shirai, *Chem. Asian J.*, 2009, **4**, 1474-1479.
24. M. Iyoda, M. Hasegawa and H. Enozawa, *Chem. Lett.*, 2007, **36**, 1402-1407.

25. C. E. Hughes, S. Hamad, K. D. M. Harris, C. R. A. Catlow and P. C. Griffiths, *Faraday Discuss.*, 2007, **136**, 71-89.

Chapter 4

Organic soluble EDDS complexes; $PPh_4[M^{III}(S,S\text{-}EDDS)]\cdot 2H_2O$

Introduction

In the search for viable anionic building blocks for the construction of molecular conductors, we came across ethylenediaminedisuccinic acid (H_4EDDS, Fig. 4.1) complexes.[1] The diastereomeric purity and stability of these complexes and the commercial availability of the optically pure ligand have aroused our interest.

A key structural difference between EDDS and the widely used chelating agent ethylenediaminetetraacetic acid (H_4EDTA) is the presence of two stereogenic carbon atoms in the former. As a result, three possible isomers exist: *S*,*S*-, *R*,*R*- and *meso R*,*S*-EDDS. Similarly to EDTA, upon complexation EDDS usually forms hexacoordinate octahedral complexes (Fig. 4.1). In EDTA complexes, all four N,O chelate rings are five-membered while EDDS forms two six-membered and two five-membered rings. The six-membered rings always take an equatorial position due to the additional strain energy associated with having the five-membered rings in these locations.[1,2]

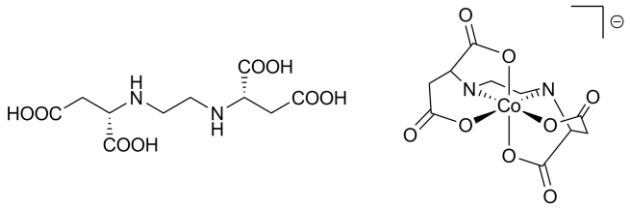

Figure 4.1. The structure of (*S*,*S*)-H_4EDDS and a model of EDDS complex.

Thus, for homochiral (*S*,*S*)- or (*R*,*R*)-EDDS only one diastereomer (Λ or Δ respectively) has ever been observed.[1] This well defined and predictable structural behaviour, the long-term chemical and optical stability, and favourable circular dichroism (CD) spectra has allowed the use of optically and diastereomerically pure homochiral $Na[Co^{III}(S,S\text{-EDDS})]\cdot H_2O$ complexes as a standard in CD spectroscopy.[3] EDDS is also a commercial alternative to EDTA in *e.g*. microelement fertilisers and detergents, photographic processing or as molluscicide.[4-9] Critically, while anthropogenic EDTA is ubiquitous in waste waters,[10] *S*,*S*-EDDS is readily biodegradable.[11,12]

These attractive properties of EDDS and its complexes, along with the presence of four carbonyl groups and two NH units capable of coordination and hydrogen bonding,[13,14] indicate potential for further uses in supramolecular and materials chemistry. The architectural chirality and capacity for introduction of various metal ions may produce interesting magnetic[15,16] and optical properties.[17,18] The utility of EDDS complexes[1,2,13,14,19-26] in this regard is however, limited by the fact that they are soluble only in water. This chapter focuses on the synthesis, structural characterisation, UV-Vis and CD spectra and magnetic properties of a range of new organic-soluble, optically and diastereomerically pure EDDS complexes of Co, Fe and Cr.

Results and Discussion

A range of methods for the isolation of organic-soluble EDDS complexes was investigated.

Synthesis of $[Co^{III}(S,S\text{-EDDS})]^-$ salts

$Na[Co^{III}(S,S\text{-EDDS})]\cdot 2H_2O$ (**29**) can be synthesised by the reaction of *S*,*S*-H_4EDDS with freshly prepared $Na_3[Co^{III}(CO_3)_3]\cdot 3H_2O$ following Neal *et al.*[1] In order to more readily access salts of other cations, an alternative method was required. Accordingly, the reaction of cobalt(II) acetate with *S*,*S*-H_4EDDS in the presence of NaOH, followed by oxidation with hydrogen peroxide was developed in our group, by S. Howson,[27] giving **29** in satisfactory yield (Scheme 4.1). The amount of water present in the solid was established from elemental and thermogravimetric (TGA) analyses and was found to be different to that previously reported.[1,3] TGA (Fig. 4.2) shows one molecule of water is lost on heating to 80°C, with one further molecule lost at higher temperatures, in disagreement with the earlier formulations of this compound as a monohydrate.[1,3]

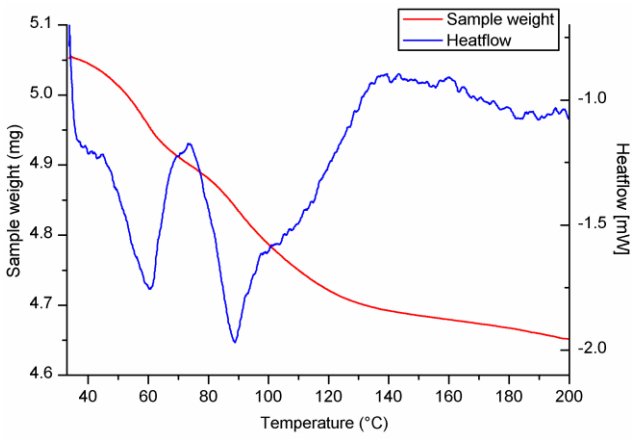

Figure 4.2. TGA of a sample of $Na[Co^{III}(S,S\text{-EDDS})]\cdot 2H_2O$ (**29**).

The potassium salt K[Co^{III}(*S*,*S*-EDDS)]·*x*H$_2$O·*y*MeOH (**30**) can also be made by this method, but unfortunately with various amounts of water, methanol or other solvents of crystallisation.[27]

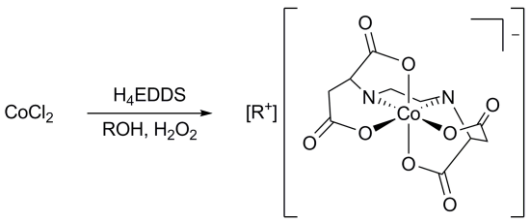

R	No.
Na	29
K	30
NBu_4	31
NEt_4	32

Scheme 4.1. General synthesis of cobalt(III) EDDS complexes.

Previous attempts to solubilise thus obtained complexes by the use of the crown ethers (15-crown-5 for the sodium salt and 18-crown-6 for potassium) have proven unsuccessful;[27] it seems that *e.g.* **29** is much less soluble in water than [Na(18-crown-6)][Co^{III}(*S*,*S*-EDDS)] and thus at equilibrium the crown ether remains in solution. The metal salts did not extract into non-aqueous solvents on addition of the appropriate crown ether.

NBu_4[Co^{III}(*S*,*S*-EDDS)]·*x*H$_2$O (**31**) was synthesised in an analogous manner to the potassium and sodium salts using tetrabutylammonium hydroxide as a base. The product was found to be extremely hygroscopic, forming a viscous oil on exposure to air, and was thus difficult to purify and fully characterise. Nevertheless the anion/cation ratio was established from a ^{1}H NMR spectrum. Notably this oil was very soluble in many organic solvents. The tetraethylammonium salt, NEt_4[Co^{III}(S,S-EDDS)] (**32**) behaved in a similar manner.

Access to PPh_4[Co^{III}(*S*,*S*-EDDS)]·2H$_2$O (**33**) was achieved *via* salt metathesis. First, treatment of **29** with silver nitrate gave light-sensitive Ag[Co^{III}(*S*,*S*-EDDS)] which was treated immediately with PPh_4Br (Scheme 4.2).

The AgBr precipitate was removed by filtration and the filtrate was evaporated to dryness under reduced pressure. Attempted recrystallisation of the obtained residue by concentration of the solutions in pure acetonitrile gave only oily products, but addition of a few drops of water to the acetonitrile solution gave excellent purple crystals of **33**.

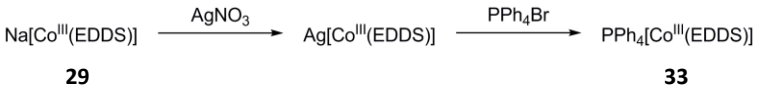

Scheme 4.2. Synthesis of PPh4[Co^{III}(*S*,*S*-EDDS)].

Due to the high solubility of both **29** and **33** in water, isolation of the tetraphenylphosphonium salt from a solution containing both PPh_4^+ and Na^+ cations is implausible, thus exchange through the silver salt is necessary.

Compound **33** shows solubility in water as well as in organic solvents: methanol, ethanol, DMSO, acetonitrile (>1 g/l) and noticeable solubility in tetrahydrofuran.

Synthesis of [Fe^{III}(S,S-EDDS)]$^-$ salts

First, NH_4[Fe^{III}(*S*,*S*-EDDS)] (**34**) was synthesised from iron(III) hydroxide and *S*,*S*-H_4EDDS in the presence of ammonia and iron powder (Scheme 4.3).[6,28]

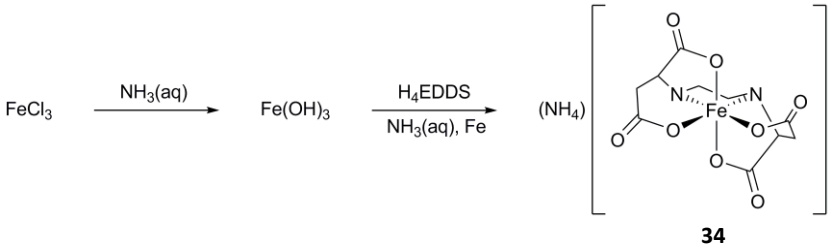

Scheme 4.3. Synthesis of NH_4[Fe^{III}(*S*,*S*-EDDS)].

Attempts to synthesise $NBu_4[Fe^{III}(S,S\text{-EDDS})]$ by methods analogous to those used above for **31** led to a low yield of hygroscopic product, and work on this compound was abandoned.

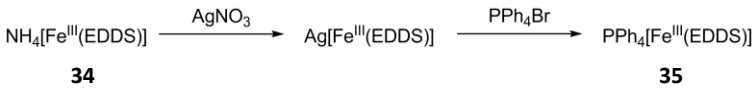

Scheme 4.4. Synthesis of $PPh_4[Fe^{III}(S,S\text{-EDDS})]\cdot 2H_2O$.

$PPh_4[Fe^{III}(S,S\text{-EDDS})]\cdot 2H_2O$ (**35**) was obtained by an analogous route to **33**, through cation exchange, starting from **34** through the intermediate silver salt (Scheme 4.4). Salt **35** was found to be highly crystalline and easily to purify by recrystallisation from an acetonitrile/water mixture. **35** shows similar solubilities to **33**.

Synthesis of $[Cr^{III}(S,S\text{-EDDS})]^-$ salts

The synthesis of $Ag[Cr^{III}(S,S\text{-EDDS})]\cdot 1.5H_2O$ (**36**) has been previously reported by treatment of $CrCl_3$ with *S*,*S*-H_4EDDS in the presence of KOH, followed by addition of excess of $AgClO_4$ to remove solid AgCl and $KClO_4$. [29] The product was then obtained by ion exchange chromatography of the resulting filtrate. To remove the necessity of the ion exchange chromatography a simplified method was developed. We found that **36** could be prepared readily *via* the reaction in water of chromium(III) sulphate with *S*,*S*-H_4EDDS in the presence of barium hydroxide. During the reaction Ba^{2+} cations are removed from the solution by precipitation of $BaSO_4$ and thus presumably $[H_3O][Cr^{III}(S,S\text{-EDDS})]$ remains in solution.

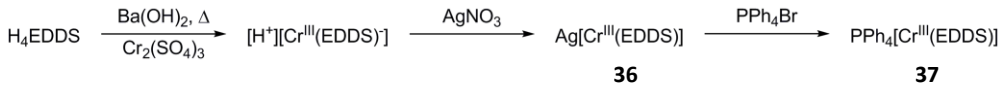

Scheme 4.5. Synthesis of $PPh_4[Cr^{III}(S,S\text{-EDDS})]\cdot 2H_2O$.

The crystalline silver salt **36** was obtained by the addition of $AgNO_3$ followed by a slow addition of methanol. A solution of $PPh_4[Cr^{III}(S,S\text{-EDDS})]$ was obtained subsequently by the addition of PPh_4Br to an aqueous solution of **36** and removal of the AgBr precipitate (Scheme 4.5). Evaporation to dryness and recrystallisation from methanol/ethyl acetate, again in the presence of a few drops of water, gave crystalline $PPh_4[Cr^{III}(S,S\text{-EDDS})]\cdot 2H_2O$ (**37**). **37** shows similar solubilities in water and organic solvents to **33** and **35**.

Single crystal X-ray Diffraction

Compounds **33**, **35** and **37** have been characterised by single crystal X-ray diffraction. Crystal structure of the intermediate $Ag[Co^{III}(S,S\text{-EDDS})]$ salt has been also obtained. Details of the structure solutions and refinement are summarised in Table A.1 (Appendix A).

$Ag[Co^{III}(S,S\text{-EDDS})]\cdot 2H_2O\cdot 2AgNO_3$

Single crystals of $Ag[Co^{III}(S,S\text{-EDDS})]\cdot 2H_2O\cdot 2AgNO_3$ were obtained by a slow evaporation of the filtrate containing $Ag[Co^{III}(S,S\text{-EDDS})]$ and an excess of $AgNO_3$ over period of few weeks. The compound crystallises in a chiral orthorhombic space group $P2_12_12_1$ with two EDDS complex anions, six silver ions, four nitrate ions and four water molecules in the asymmetric unit of the cell. The silver ions are coordinated by the oxygen atom of carbonyl groups of adjacent complex anions and nitrate ions. There are also several short Ag-Ag

contacts (~3 Å) within the cell. Figure 4.3 demonstrates the extensive coordination of silver ions in the structure.

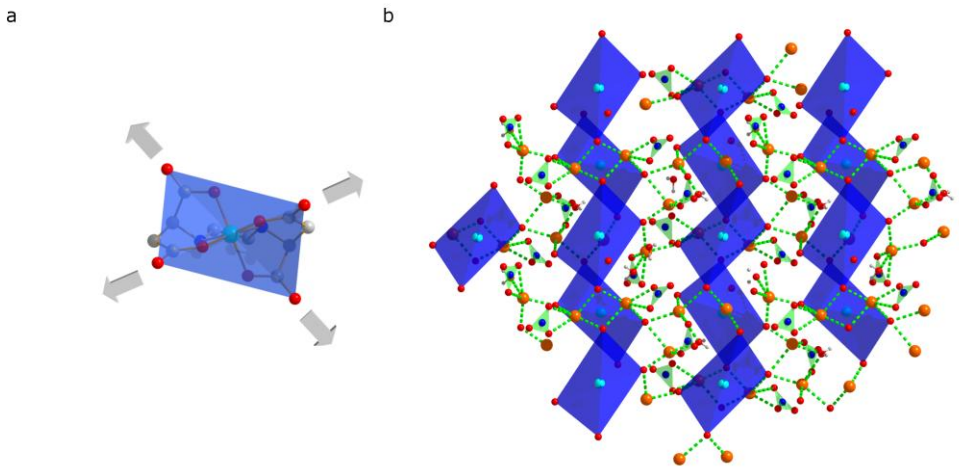

Figure 4.3. (a) A simplified polyhedral model of the $[Co^{III}(S,S\text{-EDDS})]^-$ ion and (b) the extended coordination structure of $Ag[Co^{III}(S,S\text{-EDDS})]\cdot 2H_2O\cdot 2AgNO_3$.

$PPh_4[M^{III}(S,S\text{-EDDS})]\cdot 2H_2O$

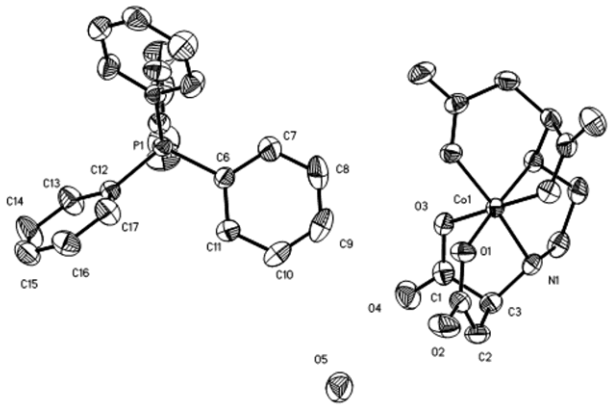

Figure 4.4. Molecular structure of **33**. Hydrogen atoms have been removed for clarity.

The complex anionic components of complexes **33**, **35** and **37** are all of a conventional nature with the *S*,*S*-EDDS ligands giving the Λ helicity at metal as expected. Selected bond lengths and angles are summarised in the table 4.1. The

M-N and M-O (trans) distances increase in the order Co^{III} < Cr^{III} < Fe^{III}, concurring with the increase of ionic radii. Similarly the O-M-O (cis) angle increases in the same fashion. As could be anticipated, elongation of M-O and M-N bonds causes decrease of the N-M-N and O-M-O angles due to the additional restraint of the chelate rings.

Table 4.1. Selected angles and bond lengths in the solid state structures of $PPh_4[M^{III}(S,S\text{-EDDS})]\cdot 2H_2O$.

Complex	**33** (M = Co^{III})	**35** (M = Fe^{III})	**37** (M = Cr^{III})
M-N	1.9125(10)	2.1467(17)	2.0426(15)
M-O (trans)	1.9027(9)	2.0043(14)	1.9771(12)
M-O (cis)	1.9140(8)	1.9442(14)	1.9610(12)
N-M-N	88.44(6)	81.60(9)	85.63(9)
O-M-O (trans)	177.40(6)	168.87(9)	173.71(8)
O-M-O (cis)	87.21(5)	103.33(9)	94.83(7)

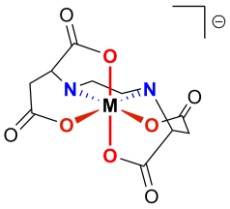

The compounds, **33**, **35** and **37** are isostructural, crystallising in the orthorhombic chiral space group $P2_12_12$, with an asymmetric unit consisting of half of the formula unit, with the central metal ion and phosphorus atoms lying in special positions on 2-fold axes (Fig. 4.4).

The compounds show interesting hydrogen-bonded extended structure in the solid state. The four carbonyl groups of the $[M(S,S\text{-EDDS})]^-$ anion are pointing in the directions of the four corners of a distorted tetrahedron (Fig. 4.5a). Each carbonyl group is hydrogen bonded through the water molecule to the adjacent anion, forming infinite double layers closely packed together into a three dimensional structure (Fig. 4.5b).

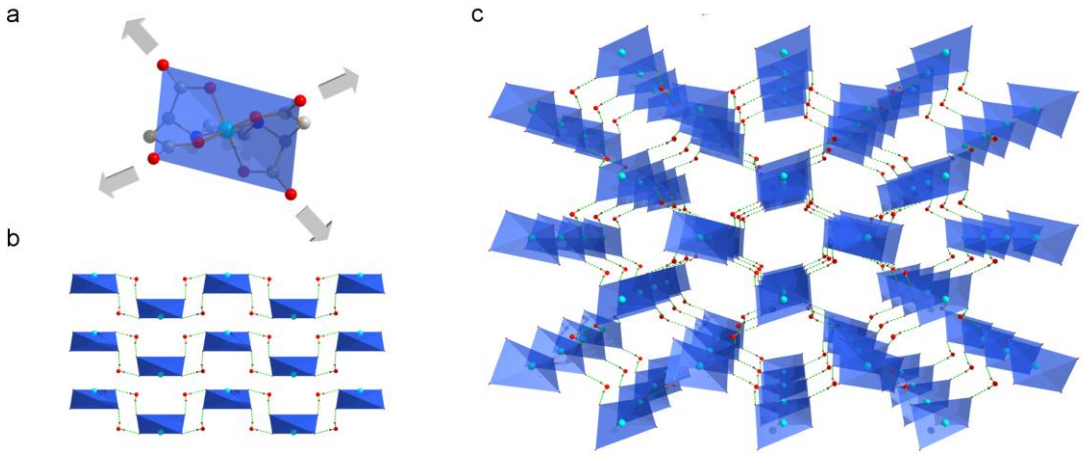

Figure 4.5. Extended structure of **33**, counterions were omitted for clarity. (a) Polyhedral model of [M^{III}(*S*,*S*-EDDS)]$^-$ anion indicating tetrahedral arrangement of carbonyl groups, (b) view from [010] direction and (c) [001] direction.

Large channels in the structure (>9 Å) (Fig. 4.5c) are occupied by the counterion molecules (omitted for clarity).

Diastereomeric Purity

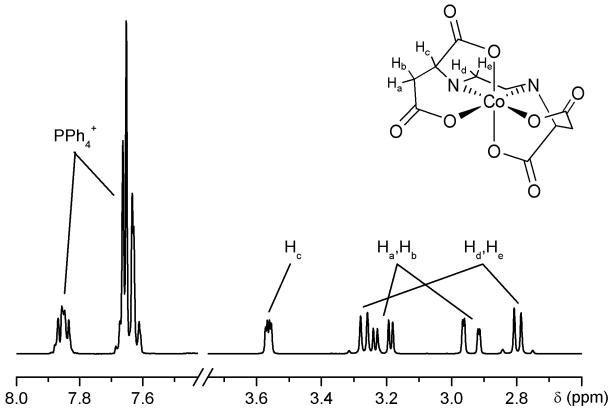

Figure 4.6. ^{1}H NMR of **33** in D_2O.

The diastereomeric purity of diamagnetic Na[Co^{III}(*S*,*S*-EDDS)]·2H_2O (**29**) and PPh_4[Co^{III}(*S*,*S*-EDDS)]·2H_2O (**33**) were confirmed by ^{1}H NMR spectroscopy (Fig. 4.6). Both compounds show only one set of peaks, relating to a single diastereomer.

The diastereomeric purity of paramagnetic $PPh_4[Fe^{III}(S,S\text{-EDDS})]\cdot 2H_2O$ (**35**) and $PPh_4[Cr^{III}(S,S\text{-EDDS})]\cdot 2H_2O$ (**37**) were assessed by comparison of the measured powder diffraction patterns with patterns calculated from the single crystal structures.

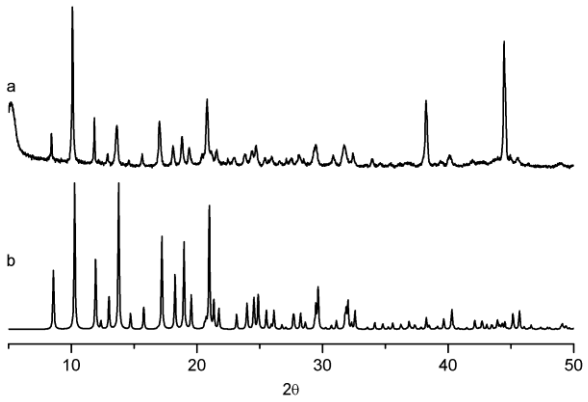

Figure 4.7. Comparison of the (a) measured and (b) calculated powder diffraction patterns of **35**.

The positions of the reflections in powder patterns of **35** and **37** show excellent agreement (δ_θ < 0.2°) with their respective calculated patterns (Fig. 4.7 and 4.8). This indicates that the single phase present in the bulk sample corresponds to that of the single crystal, and that the bulk sample is therefore diastereomerically pure to the level detectable by powder XRD.[30] Minor discrepancies in the relative intensities of the peaks are most probably a result of preferred orientation due to the very high crystallinity of the samples. The intense reflections above 35° absent in the simulated diffractograms come from the aluminium sample holder.

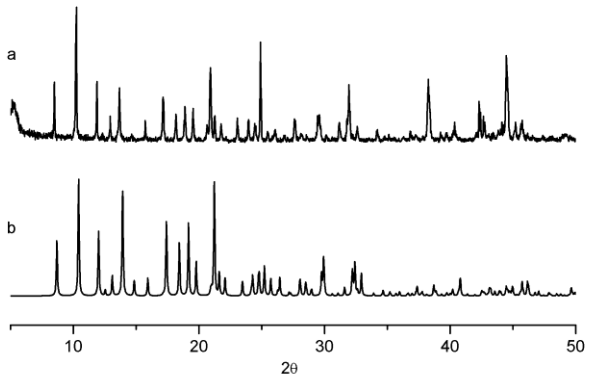

Figure 4.8. Comparison of the (a) measured and (b) calculated powder diffraction patterns of **37**.

Magnetic data

Magnetisation measurements were conducted in the range 300 – 2 K for $PPh_4[Fe^{III}(S,S\text{-EDDS})]\cdot 2H_2O$ (**35**) and $PPh_4[Cr^{III}(S,S\text{-EDDS})]\cdot 2H_2O$ (**37**). As could be expected, similarly to previously reported $NH_4[Fe(S,S\text{-EDDS})]$,[27] compound **35** persists in the high spin state over the measured temperature range and displays paramagnetic behaviour (Fig. 4.9).

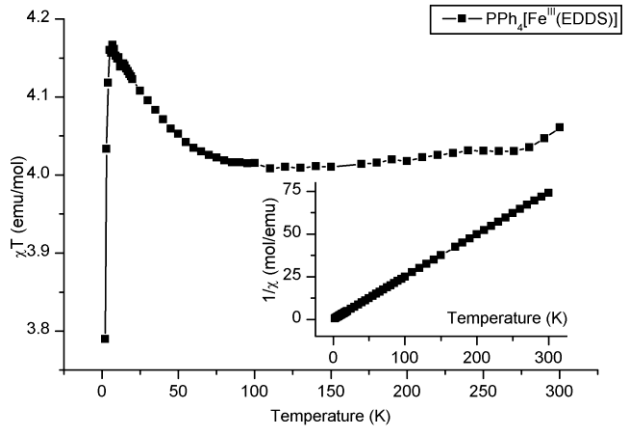

Figure 4.9. Curves of χT vs T and $1/\chi$ vs T (inset) for **35**. χ is the molar magnetic susceptibility and T is the temperature.

The plot of $1/\chi$ *vs*. T, where χ is the molar magnetic susceptibility and T is the temperature, gives straight line modelled by the Curie-Weiss law. The Weiss constant calculated for compound **35** was -0.64 K, which suggested negligible interactions between the metal centres. Paramagnetic behaviour is shown by the essentially constant value of χT except at the lowest temperatures where the value rapidly decreases, almost certainly due to zero field splitting of the $^6A_{1g}$ manifold. At 300 K the compound has a magnetic moment of 5.6 μ_B, that approaches that of the spin only value of 5.92 μ_B, when S=5/2 and g = 2.

Similar to the Fe(III) compound, the Cr(III) compound **37** also shows paramagnetic behaviour with a small Weiss constant of θ = -0.77 K (Fig. 4.10), suggesting negligible short range anti-ferromagnetic interactions. In this case the magnetic moment at 300 K is close to 3.9 μ_B, which is very close to the spin only value for S=3/2 when g =2 of 3.87 μ_B.

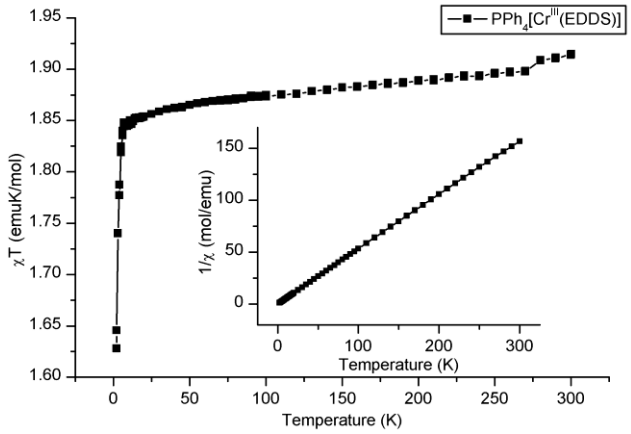

Figure 4.10. Plots of χT vs T and $1/\chi$ vs T (inset) for **37**. χ is the molar magnetic susceptibility and T is the temperature.

UV-Vis and Circular Dichroism Spectroscopy

UV-Vis and CD spectra were collected for all of the new compounds (**33**, **35** and **37**) in a selection of organic solvents, as well as in water, to allow for direct comparison with the water-only-soluble precursor compounds (**29**, **34** and **36**). Both UV-Vis and CD spectra of Na[Co^{III}(*S*,*S*-EDDS)]·2H$_2$O (**29**) are identical to those previously published[1,3]. The spectra of PPh$_4$[Co^{III}(*S*,*S*-EDDS)]·2H$_2$O (**33**) recorded in water are very similar to the spectra of the precursor, except that peaks below 230 nm are not visible due to the strong absorption of the phenyl groups. In the region 230 – 800 nm both compounds show several peaks with appropriate intensity for *d*-*d* transitions (Fig. 4.11). The corresponding peaks across the range of the CD spectrum have allowed Na[Co^{III}(*S*,*S*-EDDS)]·2H$_2$O to be used as a standard in aqueous CD spectroscopy.[3]

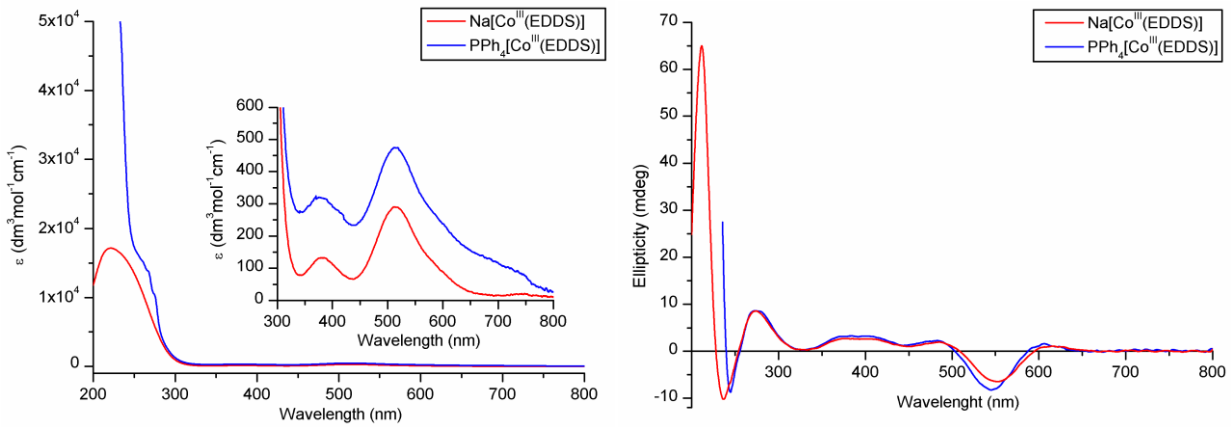

Figure 4.11. UV-Vis and CD spectra of **29** and **33** (0.1 mM solutions in water, 1 cm pathlenths).

The minor differences between the CD spectra of **29** and the tetraphenylphosphonium salt **33**, particularly in the 550 nm region are presumably due to counter-ion effects in water.

Some interesting differences were observed by comparison of the UV-Vis and CD spectra of the tetraphenylphosphonium salt recorded in various solvents (water, methanol, ethanol, dimethyl sulfoxide and acetonitrile).

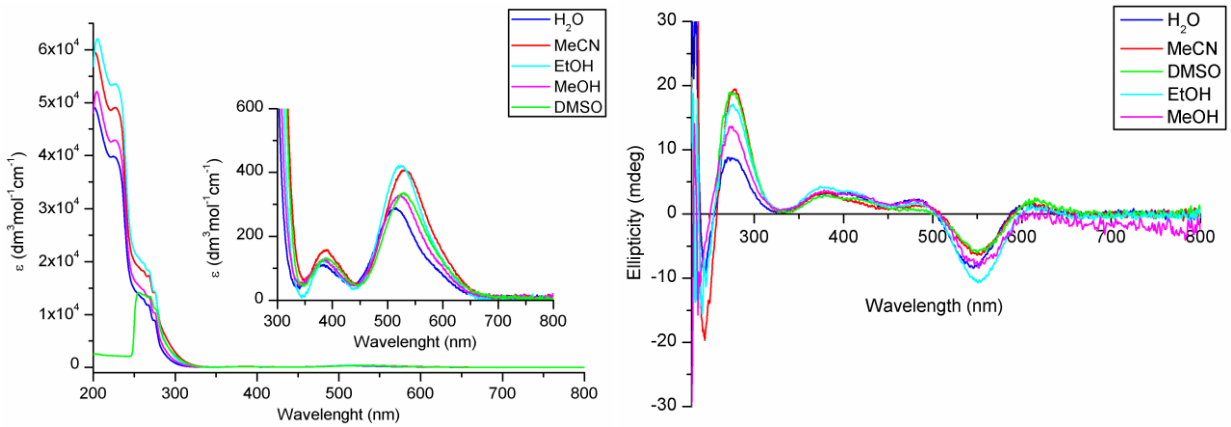

Figure 4.12. Comparison of the UV-Vis and CD spectra of **33** recorded in water, methanol, ethanol, acetonitrile and dimethyl sulfoxide (0.1 mM solutions).

The change of the solvent affects both intensities and peak positions on both UV-Vis and CD spectra. Maxima of the *d-d* transition bands (350-700 nm) on the UV-Vis spectra shift significantly (Fig. 4.12 top). This effect can be correlated linearly to the acceptor number (AN)[31,32] of the solvent, the λ_{max} shifts towards lower wavelengths (higher energy) with the increase of solvent electrophilicity (higher AN) (Fig. 4.13). A similar effect was previously found in the case of K[Co(EDTA)].[33] The effect was explained by an additional stabilisation of the excited state by strongly solvating and hydrogen bonding water, methanol and ethanol, compared to dipolar aprotic DMSO and acetonitrile.

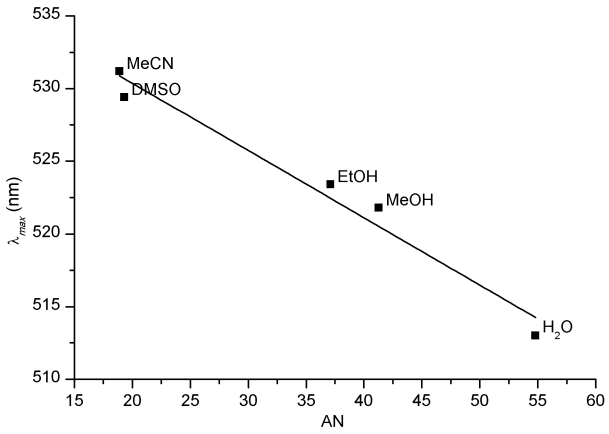

Figure 4.13. Linear correlation of absorption maxima (λ_{max}) of one of the *d-d* transition band of **33** to the acceptor number of the solvent used (AN).

The changes in the λ_{max} of the LMCT transition bands can be also correlated to another simple solvent property, namely proton affinity (PA) (Fig. 4.14). With the rising basicity of the solvent (higher PA) the maxima of the LMCT bands at ~277, 268 and 260 nm shift towards lower energies (higher λ_{max}). The effect might be explained by the preference of the more basic solvents towards the state with less charge separation (ground state), thus destabilising the excited state.

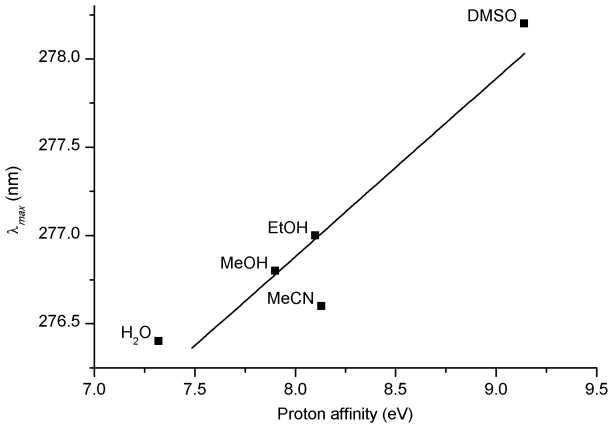

Figure 4.14. Correlation of the absorption maxima (λ_{max}) of one of the LMCT bands of **33** to the proton affinity of the solvent used.

The changes of intensity and peak maxima in the CD spectra do not correlate to the changes observed in the UV-Vis spectra. This could be expected because of anisotropy of the CD transitions, with the orientation of the polarisation vector of the transition towards the dipole moment of the whole molecule being an additional factor affecting the spectrum, not present in the case of simple UV-Vis spectroscopy. The interpretation of these changes is more challenging and we were unable to find reported treatments of this kind in the literature, most likely due to previous lack of such versatile, optically pure and readily soluble complexes as $PPh_4[M^{III}(S,S\text{-EDDS})]$.

An interesting correlation was found between the ellipticities of the LMCT transition bands and the acceptor number of the solvent. The intensities decrease with the rising value of the solvent acceptor number (Fig. 4.15). No similar dependence was found in the UV-Vis spectrum. This means that the specific interaction between solvent and the anion responsible for this spectral phenomenon must be anisotropic. In other words the first solvation sphere must be chiral.

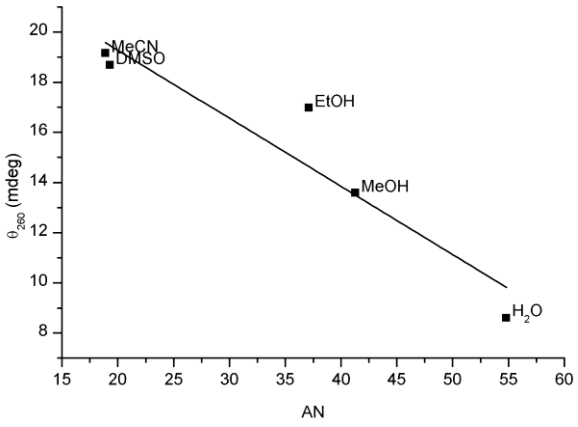

Figure 4.15. Correlation of the intensity of the CD peak at 260 nm of **33** (θ_{260}), to the acceptor number of the solvent (AN).

The changes in the intensities of the *d-d* bands are more complex and not correlated to the changes observed for the LMCT peaks. Most likely the changes in intensity are an effect of hydrogen bonding (lower intensities for MeCN and DMSO) and other electronic effects.

The UV-Vis spectra of $NH_4[Fe^{III}(S,S\text{-EDDS})]$ (**34**) and $PPh_4[Fe^{III}(S,S\text{-EDDS})]\cdot 2H_2O$ (**35**), recorded in water, show LMCT features in the range 200 – 400 nm (Fig. 4.16 top). As expected for a high-spin iron(III) complex with a weak field ligand ($^6A_1$ ground state), *d-d* transitions are absent. In the case of **35** strong absorbance is recorded below 230 nm due to the presence of phenyl groups.

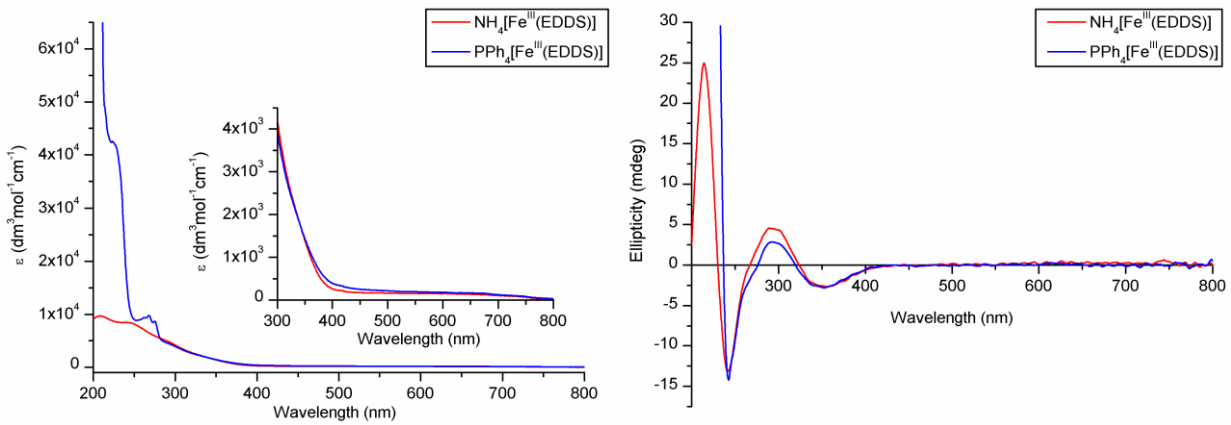

Figure 4.16. UV-Vis and CD spectra of **34** and **35** (0.1 mM solutions in water).

The CD spectra of these Fe complexes are correspondingly less interesting (Fig. 4.16 bottom), but the absence of bands in the visible region is of some practical value, which will be further exploited in Chapter 5.

A comparison of the spectra of **35** recorded in water and organic solvents shows significant changes, especially in the case of CD spectra (Fig. 4.17). Each of the transition bands in the LMCT region change its intensity

independently leading to significant modifications of the spectrum upon the change of the solvent.

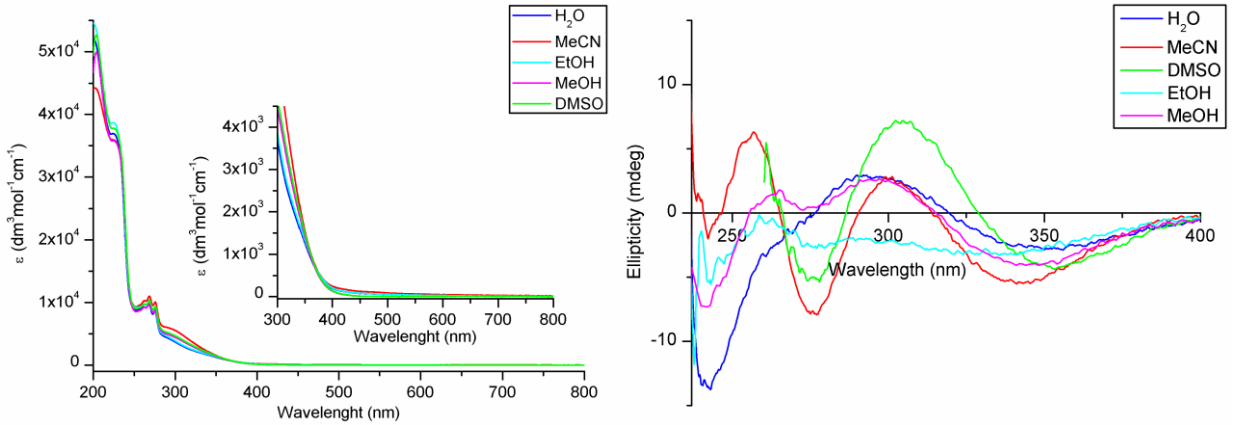

Figure 4.17. Comparison of the UV-Vis and CD spectra of **35** in water and acetonitrile (0.1 mM solutions).

Interpretation of these changes is not trivial but some trends can be extracted. Similar to the case of the cobalt complex, the ellipticity of the LMCT band at ~240 nm changes linearly with the rising acceptor number of the solvent. CD spectra recorded in highly polar and hydrogen bonding water and methanol show analogous features. Likewise the spectra recorded in non-hydrogen bonding DMSO and acetonitrile are comparable. This suggests that, similar to the cobalt complex, hydrogen bonding and polarity play an important role in the stabilisation/destabilisation of the excited states. Furthermore, some of these interactions are inherently chiral in nature.

The CD spectra of the chromium(III) complexes, **36** and **37** recorded in water are shown in Fig. 4.18 and show the expected features. Interestingly, the CD features arising from the *d-d* transitions are rather low in intensity compared to those of Co(III) complexes, despite the fact that the corresponding bands in the UV-Vis spectra are of similar intensity ($\varepsilon \approx 350$ dm^{3}mol^{-1}cm^{-1}).

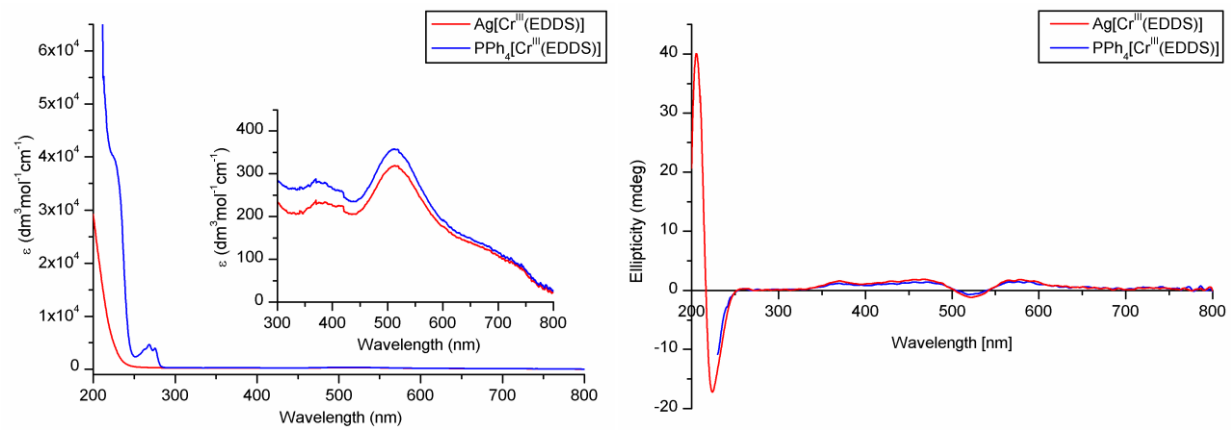

Figure 4.18. UV-Vis and CD spectra of **37** and Ag[Cr^{III}(*S*,*S*-EDDS)] (0.1 mM solutions).

The comparison of the CD spectra recorded in different solvents shows significant intensity change of the *d*-*d* transition bands with the change to the less polar solvents, whereas the intensities of the same bands in the UV-Vis spectrum remain almost unchanged (Fig. 4.19). CD spectra recorded in ethanol and DMSO show features identical to those recorded in acetonitrile with only minor differences in the peak ellipticity.

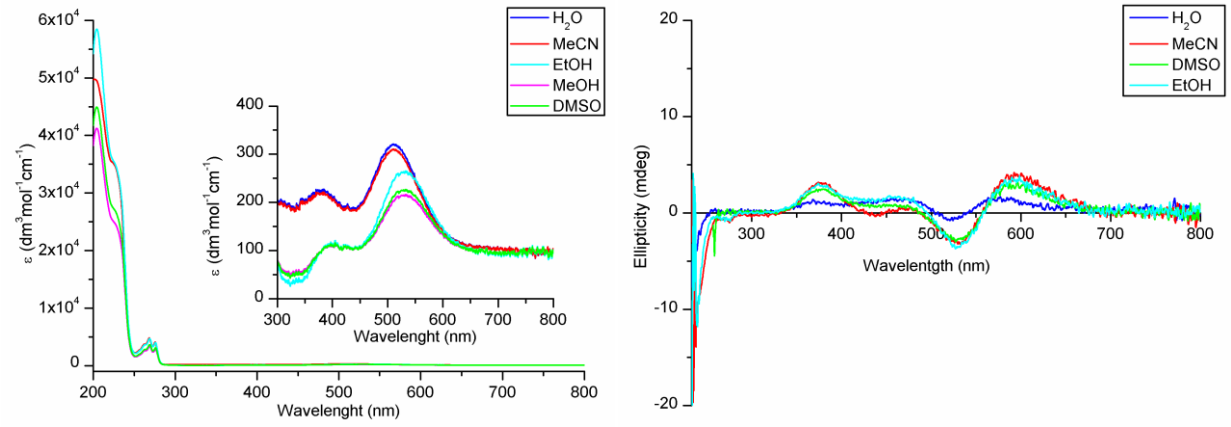

Figure 4.19. UV-Vis and CD spectra of **37** recorded in water, acetonitrile, ethanol and dimethyl sulfoxide (0.1 mM solutions).

The difference in the intensity of the CD spectrum recorded in water compared to the spectra recorded in organic solvents is intriguing, as it does not seem to

depend on the solvent polarity (EtOH, MeCN) and hydrogen bonding (EtOH) or coordinating abilities (DMSO, MeCN).

The comparison of the CD and UV-Vis spectra of the $[M^{III}(S,S\text{-EDDS})]^-$ complexes show a multitude of different electronic phenomena which differ significantly with the change of the central metal atom, despite the seemingly identical molecular structure of the complexes. Unfortunately, published literature on solvent effects on CD spectra was found to be scarce and no examples were found for direct comparison with the obtained data. Further explanation of the observed effects was found to be beyond the scope of this work.

Conclusions

The PPh_4^+ counter-ion provides ready access to organic-soluble EDDS complexes of trivalent Cr, Fe and Co in high yield *via* the silver salts without recourse to ion-exchange chromatography. Crystallinity was dramatically enhanced by addition of water, and the origin of this behaviour is readily apparent from the H_2O-bridged H-bonded networks in the crystal structures of all compounds $PPh_4[M^{III}(S,S\text{-EDDS})]\cdot 2H_2O$.

The issue of assessment of diastereomeric purity is addressed by use of ^1H NMR spectrometry in case of the diamagnetic $PPh_4[Co^{III}(S,S\text{-EDDS})]\cdot 2H_2O$ (**33**), and powder XRD in the paramagnetic systems: $PPh_4[Fe^{III}(S,S\text{-EDDS})]\cdot 2H_2O$ (**35**) and $PPh_4[Cr^{III}(S,S\text{-EDDS})]\cdot 2H_2O$ (**37**). While there are limitations imposed by crystal orientation effects, the apparent phase purity of the systems

indicated by a comparison of measured and calculated patterns indicates that single diastereomers are present.

UV-Vis and CD spectra of the obtained complexes were recorded in several solvents and compared with the water-only soluble precursor compounds. Analysis of the results shows a multitude of solvent effects strongly affecting both CD and UV-Vis spectra.

The application of these complexes in supramolecular and materials chemistry will be explored in Chapter 6. Additional applications in the fields of optical resolution and as ^{1}H NMR shift agents are reported in Chapter 5.

References

1. J. A. Neal and N. J. Rose, *Inorg. Chem.*, 1968, **7**, 2405-2412.
2. J. A. Neal and N. J. Rose, *Inorg. Chem.*, 1973, **12**, 1226-1232.
3. A. Damianoglou, E. J. Crust, M. R. Hicks, S. E. Howson, A. E. Knight, J. Ravi, P. Scott and A. Rodger, *Chirality*, 2008, **20**, 1029-1038.
4. M. Borowiec, P. Polańska and J. Hoffmann, *Pol. J. Chem. Tech*, 2007, **9**, 38-41.
5. J. S. Jaworska, D. Schowanek and T. C. J. Feijtel, *Chemosphere*, 1999, **38**, 3597-3625.
6. *United States Pat.,* 6472548, 2002.
7. *United States Pat.,* 5679817, 1997.
8. *United States Pat.,* 5763634, 1998.
9. *United States Pat.,* 6352706, 2002.
10. J. Majer, V. Springer and B. Kopecka, *Chem. Zvesti*, 1966, **20**, 414-422.
11. D. Schowanek, T. C. J. Feijtel, C. M. Perkins, F. A. Hartman, T. W. Federle and R. J. Larson, *Chemosphere*, 1997, **34**, 2375-2391.
12. R. Takahashi, N. Fujimoto, M. Suzuki and T. Endo, *Biosci. Biotechnol., Biochem.*, 1997, **61**, 1957-1959.
13. F. Pavelcik and V. Kettmann, *Collect. Czech. Chem. Commun.*, 1983, **48**, 1376-1389.
14. F. Pavelcik, V. Kettmann and J. Majer, *Collect. Czech. Chem. Commun.*, 1979, **44**, 1070-1079.
15. L. D. Barron, *Nat. Mater.*, 2008, **7**, 691-692.
16. M. Murrie and D. J. Price, *Annu. Rep. Prog. Chem. Sect. A: Inorg. Chem.*, 2007, **103**, 20-38.
17. M. Kauranen, T. Verbiest and A. Persoons, *J. Nonlinear Opt. Phys. Mater.*, 1999, **8**, 171-189.
18. P. Fischer and F. Hache, *Chirality*, 2005, **17**, 421-437.
19. J. Soldanova, F. Pavelcik, J. Majer and J. Garaj, *Chem. Zvesti*, 1984, **38**, 321-330.
20. T. N. Polynova, E. B. Chuklanova and M. A. Poraikoshits, *Dokl. Akad. Nauk*, 1985, **283**, 673-677.
21. F. Pavelcik and J. Majer, *Z. Naturforsch., B: Chem. Sci.*, 1977, **32**, 1089-1090.
22. F. Pavelcik, J. Garaj and J. Majer, *Acta Crystallogr B*, 1980, **36**, 2152-2154.
23. F. Pavelcik, J. Soldanova and J. Majer, *Collect. Czech. Chem. Commun.*, 1980, **45**, 1766-1774.
24. E. Horn, M. R. Snow and E. R. T. Tiekink, *Z. Kristallogr.*, 1993, **205**, 140-142.
25. K. Kanamori, K. Ino, H. Maeda, K. Miyazaki, M. Fukagawa, J. Kumada, T. Eguchi and K. Okamoto, *Inorg. Chem.*, 1994, **33**, 5547-5554.
26. F. Pavelcik and J. Majer, *Acta Crystallogr B*, 1978, **34**, 3582-3585.
27. S. Howson, MChem, University of Warwick, 2007.
28. J. Barker, C. Blundell and N. W. Alcock, *Unpublished results*.
29. D. J. Radanovic and B. E. Douglas, *J. Coord. Chem.*, 1975, **4**, 191-198.
30. J. M. Becker, PhD, University of Warwick, 2009.

31. U. Mayer, V. Gutmann and W. Gerger, *Monatsh. Chem.*, 1975, **106**, 1235-1257.
32. V. Gutmann, *Coord. Chem. Rev.*, 1976, **18**, 225-255.
33. T. Taura, *Chem. Lett.*, 1984, 2011-2012.

Chapter 5

Application of EDDS complexes in optical resolution and ^{1}H NMR spectrometry

Introduction

During the work with EDDS compounds it became apparent that stability, diastereomeric purity and availability of these complexes might also find applications in other fields. Recently the tris(tetrachlorobenzenediolato)phosphate(V) (TRISPHAT) anion[1,2] has emerged as a versatile tool in NMR spectroscopy[3-6] and molecular recognition.[5,7-12] This species can be synthesised on a practical scale by the reaction of tetrachlorocatechol with PCl_5 under inert atmosphere conditions. The optical resolution can be achieved by the use of cinchonidine, followed by further purification by recrystallisation (Δ enantiomer), and chromatography followed by recrystallisation (Λ enantiomer). The optical purity is determined by ^{31}P NMR in the presence of (-)-bis((*S*)-1-phenylethyl)amine hydrochloride.[1,13] An attractive feature of TRISPHAT is that the chirality of the system is very well expressed in the shape of the system *via* the helicity (Δ/Λ) *i.e.* the configuration at the central atom. Analogous transition metal systems, such as D_3 tris(oxalato) complexes generally suffer from lability at the metal, leading to racemisation and limiting their applications.[14-17] In comparison, EDDS complexes are stable in solution and do not show any

changes in their CD spectrum even after extended periods of time.[18] Additionally their diastereomeric purity and ease of synthetic preparation is a clear advantage over laborious procedure required for synthesis and resolution of other stable chiral anionic species (*e.g*. TRISPHAT).

The family of complexes, $PPh_4[M^{III}(S,S\text{-EDDS})]\cdot 2H_2O$, exhibit unique properties which may allow for their application to problems in a number of areas. The paramagnetic properties of Fe^{III} and Cr^{III} complexes might be interesting when incorporated into molecular materials. Diamagnetism of $PPh_4[Co^{III}(S,S\text{-EDDS})]\cdot 2H_2O$ (**33**) allows for an easy assessment of its purity by magnetic resonance techniques and its potential use as chiral ^1H NMR shift agent is explored in this chapter. Another interesting property of EDDS complexes is the absence of the CD bands over a wide spectral range in the spectrum of $PPh_4[Fe^{III}(S,S\text{-EDDS})]\cdot 2H_2O$ (**35**). This allows for its use as a chiral auxiliary without changing the CD spectrum of the parent compound in a significant way.

This chapter focuses on the use of $PPh_4[Co^{III}(S,S\text{-EDDS})]\cdot 2H_2O$ (**33**) as a chiral shift agent in ^1H NMR spectroscopy for cationic metal complexes and simple organic molecules, as well as on the use of $PPh_4[Fe^{III}(S,S\text{-EDDS})]\cdot 2H_2O$ (**35**) in the optical resolution of (±)-$[Ru^{II}(bpy)_3]Cl_2$.

Results and Discussion

Resolution of (±)-$[Ru^{II}(bpy)_3]Cl_2$

Preliminary experiments have been conducted in the application of EDDS complexes as new and readily available optical resolving agents. The addition of

acetonitrile solution of $PPh_4[Fe^{III}(S,S\text{-EDDS})\cdot 2H_2O$ (**35**) to one molar equivalent of (±)-$[Ru^{II}(bpy)_3]Cl_2$ in acetonitrile resulted in the precipitation of {Λ-$[Ru^{II}(bpy)_3]$}{Λ-$[Fe^{II}(S,S\text{-EDDS})]$}Cl adduct in good yield.

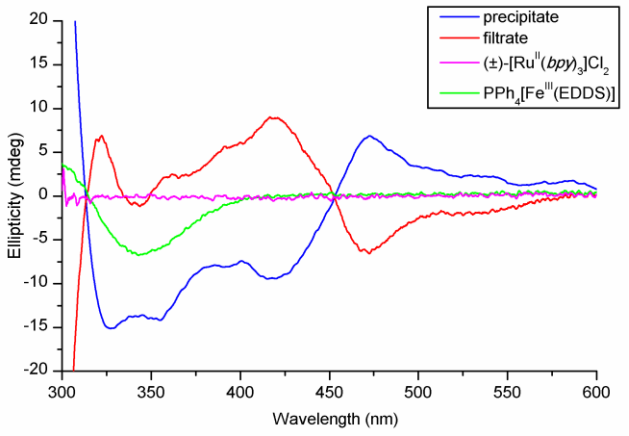

Figure 5.1. CD spectra of unresolved $[Ru^{II}(bpy)_3]Cl_2$ (pink), PPh_4{Λ-$[Fe^{III}(S,S\text{-EDDS})]$} (**35**) (green) and their adducts: precipitate (blue) and filtrate (red) (approx. 0.05 mM MeOH solutions).

The CD spectrum of this precipitate (Fig 5.1, blue line) has the characteristic features of Λ-$[Ru(bpy)_3]^{2+}$ ion, in the region 400-525 nm. The spectrum of the material isolated from the filtrate (Fig. 5.1, red line) is consistent with the published spectrum of Δ-$[Ru(bpy)_3]^{2+}$.[19,20]

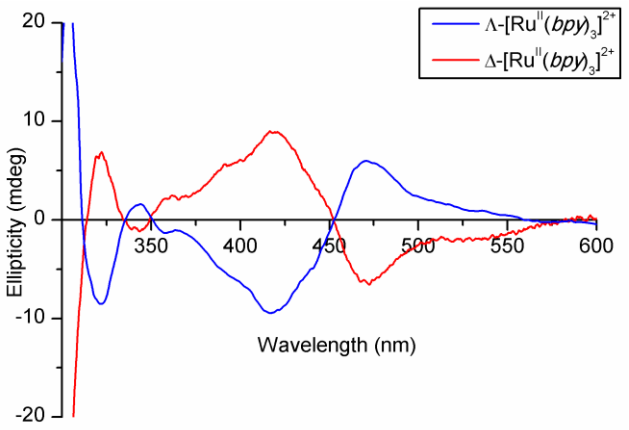

Figure 5.2. CD spectrum of resolved $[Ru^{II}(bpy)_3]Cl_2$ (approx. 0.5 mM solutions).

Figure 5.2 compares the spectra of the precipitate (blue line) following subtraction of the spectrum of [Fe(*S*,*S*-EDDS)]$^-$ (*vide supra*), and that of the unprocessed spectrum of the filtrate (red line).

Recrystallisation of the precipitate from methanol/ethyl acetate in the presence of few drops of water gave crystals of {Λ-[Ru^{II}(bpy)$_3$]}{Λ-[Fe^{III}(*S*,*S*-EDDS)]}Cl·H_2O, suitable for X-ray diffraction.

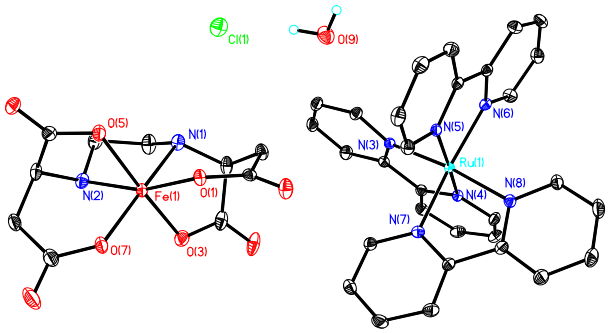

Figure 5.3. Crystal structure of {Λ-[Ru^{II}(bpy)$_3$]}{Λ-[Fe^{II}(*S*,*S*-EDDS)]}Cl·H_2O adduct, hydrogen atoms on both complex ions have been removed for clarity

The compound crystallises in an orthorhombic chiral space group $P2_12_12_1$. The asymmetric unit contains one tris(2,2'-bipyridyl)ruthenium(II) ion, one [Fe^{III}(*S*,*S*-EDDS)]$^-$ counterion, one chloride anion and a molecule of water. The details of the solution and refinement, and selected bond lengths and angles can be found in Table A.4 in Appendix A and Table B.7 in Appendix B respectively. The crystal structure confirms the absolute configuration assigned from the CD spectrum, {Λ-{Ru^{II}(bpy)$_3$]}{Λ-[Fe^{II}(*S*,*S*-EDDS)]}Cl. The extended structure of the compound is insignificant, the 'spacefill' view however, shows the possible origin of the diastereoselection. Figure 5.4a shows the interaction between the [Fe^{II}(*S*,*S*-EDDS)]$^-$ ion and the chiral ridge on the 'top' of the [Ru^{II}(bpy)$_3$]$^+$.

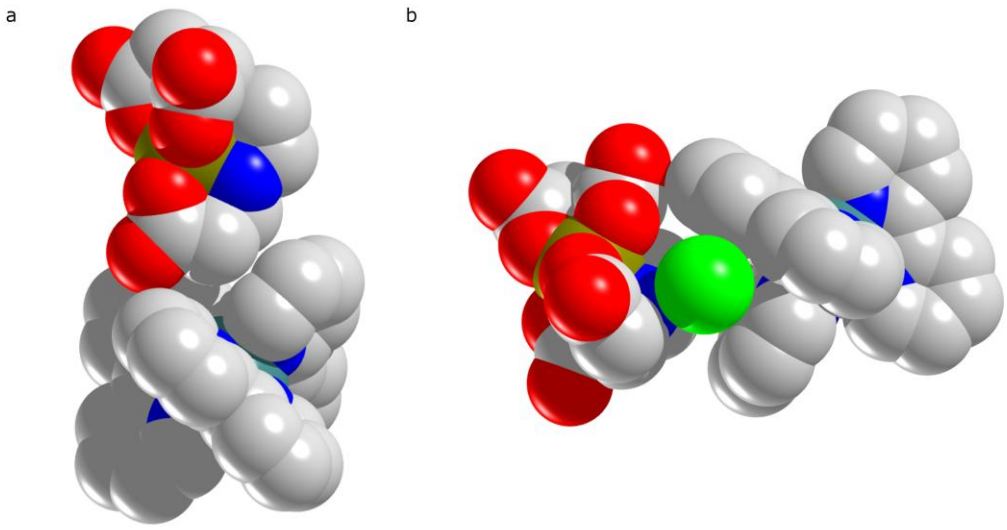

Figure 5.4. The 'spacefill' view of the {Λ-[$Ru^{II}(bpy)_3$]}{Λ-[Fe^{II}(*S*,*S*-EDDS)]}Cl adduct, hydrogen atoms have been removed for clarity

Figure 5.4b presents a different interaction between [Fe^{II}(*S*,*S*-EDDS)]$^-$ and [$Ru^{II}(bpy)_3$]$^+$ with the chlorine anion filling the cavity between the two. The importance of the presence of a small auxiliary anion in the diastereoselection process was further confirmed by the ^{1}H NMR study (*vide infra*).

To assess the optical purity of the resolved salts, samples were submitted for chiral LC analysis. The precipitate of {Λ-[$Ru^{II}(bpy)_3$]}{Λ-[Fe^{II}(*S*,*S*-EDDS)]}Cl was dissolved in methanol and the chloride and iron(III) EDDS counterions were removed through the addition of an excess of solid $AgNO_3$. The insoluble Ag[Fe^{III}(*S*,*S*-EDDS)] and AgCl were removed by filtration and the solvents were removed under reduced pressure. The obtained residue was then recrystallised from acetonitrile on addition of diethyl ether, to obtain Λ-[$Ru^{II}(bpy)_3$]NO_3.

The residue obtained from the filtrate (Δ-$[Ru^{II}(bpy)_3]Cl_2$) was treated in analogous manner to obtain Δ-$[Ru^{II}(bpy)_3]NO_3$. Samples of both enantiomers were submitted for LC analysis on a chiral IA column, using 0.1 M $NaPF_6$(aq):MeCN (1:1) as eluent and monitoring at 290 nm. The enantiomeric excess (ee) calculated from the peak integrations were 33% for the Δ-$[Ru^{II}(bpy)_3]NO_3$ and 16% for the Λ enantiomer.

These initial results show some promise taking into consideration that the process was not optimised towards high yields and *ee*. The optimisation of this process is being continued as a separate project.

$PPh_4[Co^{III}(S,S\text{-EDDS})]\cdot 2H_2O$ as a ^{1}H NMR chiral shift agent

Several experiments have been conducted in the application of the diamagnetic $PPh_4[Co^{III}(S,S\text{-EDDS})]\cdot 2H_2O$ (**33**) as an chiral ^{1}H NMR shift reagent for the determination of optical purity of chiral-at-metal cationic complexes and small chiral organic molecules.

Chiral-at-metal complex cations

A number of chiral-at-metal transition metal complexes were used as test substances; optically pure and racemic $[Ru^{II}(phen)_3](PF_6)_2$, $[Co^{II}(phen)_3](ClO_4)$, $[Fe^{II}(phen)_3](ClO_4)_2$, $[Cr^{II}(phen)_3](ClO_4)_2$, $[Co^{III}(en)_3]I_3$ and $[Ru^{II}(bpy)_3]X_2$ (X = Cl, Br). The phen and en complexes were kindly contributed by Prof. Alison Rodger. The (±)-$[Ru^{II}(bpy)_3]Cl_2$ was synthesised following the literature method,[21] from $RuCl_3$ and 2,2'-bipyridyl in the presence of NaH_2PO_2.

$[Ru^{II}(bpy)_3]X_2$

A series of samples of the (±)-$[Ru^{II}(bpy)_3]Cl_2$ with different stoichiometric amounts of **33** in *d*4-methanol were prepared and their ^1H NMR spectra were recorded to assess the scope of the effect and determine the optimal ratio of the substrates (Fig. 5.5).

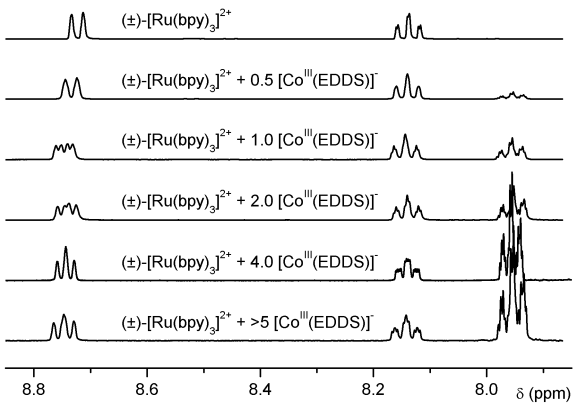

Figure 5.5. ^1H NMR spectra of $[Ru^{II}(bpy)_3]Cl_2$ with different stoichiometric amounts of **33**.

The addition of $[Co^{III}(S,S\text{-EDDS})]^-$ to the solution of $[Ru^{II}(bpy)_3]^{2+}$ causes splitting of all of the signals originating from the ruthenium salt to varying extents. The effect was observed to be the strongest in a doublet at 8.75 ppm, this peak therefore was chosen for all the further experiments. The optimal molar ratio of $[Ru^{II}(bpy)_3]^{2+}$: $[Co^{III}(S,S\text{-EDDS})]^-$, resulting in relatively clear splitting of the peaks, was found to be 1:4 (Fig. 5.5 bottom), no further changes to the spectrum were observed on increasing $[Co^{III}(S,S\text{-EDDS})]^-$ concentration. This ratio was therefore used in all of the subsequent experiments.

To test the possibility of application of **33** in the determination of enantiomeric excess (ee), a series of ^1H NMR experiments with partially resolved Λ- and Δ-$[Ru^{II}(bpy)_3]Br_2$ enantiomers were performed. The (±)-

$[Ru(bpy)_3]Cl_2$ was resolved by a formation of diastereomeric salts with (+)-antimonyl tartrate and subsequent recrystallisation, following the procedure by Joshi *et al*.[22] Only a partial resolution was achieved following this method (Δ-enantiomer 60% ee; Λ-enantiomer 30% *ee*; HPLC).

^{1}H NMR spectra of the samples of resolved Λ- and Δ-$[Ru^{II}(bpy)_3]Br_2$ were recorded in the presence of excess (1:4) of **33** in d^4-methanol and compared with the spectrum of racemic (±)-$[Ru(bpy)_3]Cl_2$. The integration of the peripheral peaks of the double doublet at 8.75 ppm gave the enantiomeric ratios (Fig. 2.6).

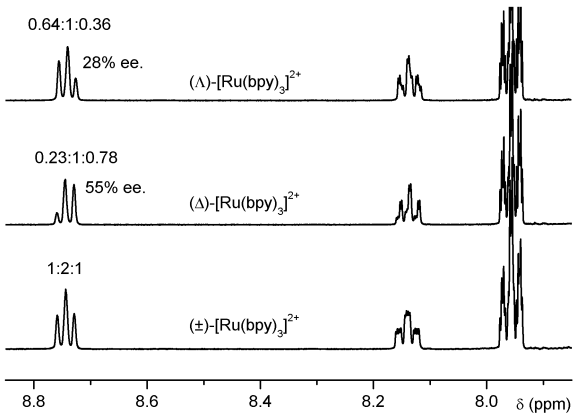

Figure 5.6. ^{1}H NMR spectra of (±)-, Λ- and Δ-$[Ru^{II}(bpy)_3]^{2+}$ in the presence of **33** (1:4 mol ratio).

The % ee values calculated from the integrals: 55 % for the Δ enantiomer and 28% for the Λ-$[Ru^{II}(bpy)_3]^{2+}$, were found to be in good agreement with the data obtained from chiral HPLC.

$[Co^{III}(en)_3]I_3$

Samples were prepared by co-dissolution of $[Co^{III}(en)_3]I_3$ and $PPh_4[Co^{III}$(*S*,*S*-EDDS)]·$2H_2O$ (1:4 ratio) in d^6-DMSO. It was found that addition of an auxiliary was necessary to allow for the observation of the effect. Stoichiometric amounts

of either HCl or DCl, HNO_3, $HClO_4$, or NaCl were added to the prepared samples. The effect observed was similar in all of the cases. It was concluded therefore, that the enantioselective effect of $[M^{III}(S,S\text{-EDDS})]^-$ does not depend on the pH of the solution (similar results were observed in the case of HCl and NaCl) and that the presence of an additional small anion ($r_i \sim 2$ Å) is necessary for the diastereoselection. This is in excellent agreement with the conclusions drawn from the analysis of the crystal structure of the $\{\Lambda\text{-}[Ru^{II}(bpy)_3]\}\{\Lambda\text{-}[Fe^{II}(S,S\text{-EDDS})]\}Cl\cdot H_2O$ adduct, which shows a chiral interaction between the complex ions and the chloride in the solid state. Results of the ^1H NMR studies demonstrate that an interaction of a similar nature is responsible for the diastereoselectivity in the solution as well.

The comparison of the ^1H NMR spectra of (±)-, Λ- and Δ-$[Co^{III}(en)_3]^{3+}$ in the presence of **33** and HCl are presented in figure 5.7. The splitting of one of the amine peaks at ~5.10 ppm allows for integration and thus the determination the enantiomeric composition of the complex.

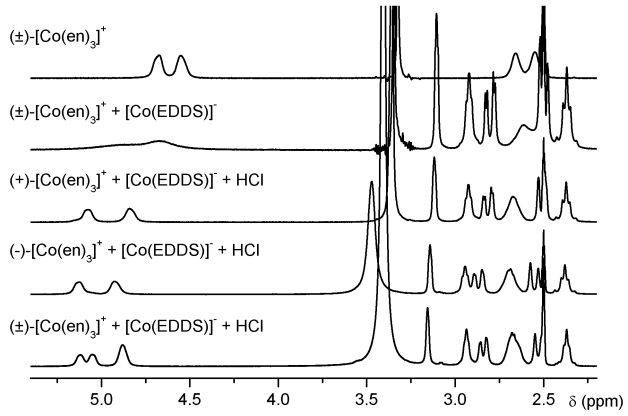

Figure 5.7. Comparison of the ^1H NMR spectra of (±)-, Λ- and Δ-$[Co^{III}(en)_3]I_3$ in the presence of **33** and HCl (1:4:1 mol ratio) with the spectrum of (±)-$[Co^{III}(en)_3]I_3$ in the presence of **33** (1:4 mol ratio) and $[Co^{III}(en)_3]I_3$. All spectra recorded in d^6-DMSO.

Interestingly the residual water peak (~3.30 ppm) seems to also shift strongly depending on the enantiomeric composition of the sample. This confirms previous observations (see Chapter 4) suggesting that the first solvation sphere of EDDS complexes is anisotropic and interacts with its environment in a chiral way.

$[M^{II}(phen)_3]^{2+}$

Several tests were conducted with $[M^{II}(phen)_3](ClO_4)_2$ (M = Co, Fe, Cr), and $[Ru^{II}(phen)_3](PF_6)_2$. It was found that addition of **33** to dilute solutions of these salts in d^4-methanol and d^6-dimethyl sulfoxide significantly affects their ^{1}H NMR spectra. The effect however was found to be the same for optically pure and racemic samples. There was also no further changes after addition of stoichiometric amounts or excess of HCl or DCl.

Chiral amines

To assess the possibility of application of **33** as a ^{1}H NMR shift agent for simple, chiral organic molecules, a series of experiments with *R*-, *S*- and (±)-phenylglycinol was conducted. Due to the large difference in the molecular weights of the phenylglycinol (137.18 g·mol^{-1}) and **33** (722.56 g·mol^{-1}), and the limited solubility of **33** in methanol, it was unfeasible to keep the 1:4 reagent ratio previously determined. A saturated solution of **33** was therefore used instead. The samples were prepared by dissolution of **33** (approx. 12.5 mg) in hot d^4-methanol (0.6 ml), the solution was then allowed to cool and the remaining solid was removed by filtration. Each sample of phenylglycinol (1 mg) was dissolved in thus prepared solution and the ^{1}H NMR spectrum was recorded. It was found that addition of **33** causes seemingly no difference to the

spectrum of phenylglycinol. It was however noted that after heating the ^{1}H NMR spectrum of the sample changes. Weak splitting was observed for all of the signals, with the most significant effect for the chiral proton peaks at 3.94 ppm, (Fig. 5.8).

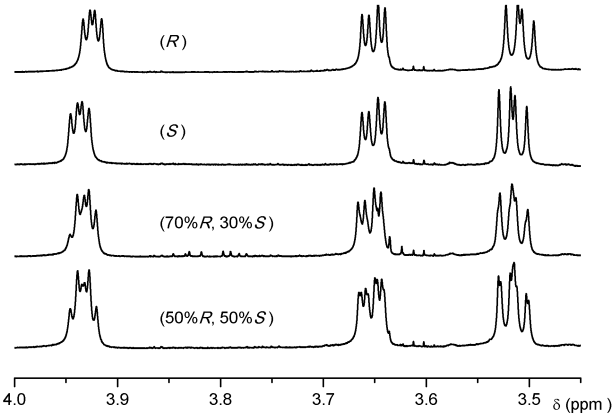

Figure 5.8. The ^{1}H NMR spectra of (*R*)-, (*S*)-, (70%*R*, 30%*S*)- and (±)-phenylglycinol in the presence of **33** recorded in *d*^{4}-methanol after 48 h.

The weak splitting of the peaks and necessity for heating of the sample, which might cause racemisation of some more sensitive materials, limits the usability of **33** as a chiral shift reagent for this type of compound. It was however noted that an addition of HCl might improve the results the presence of Cl^- anion might improve the diastereoselection analogous to the case of $[Co^{III}(en)_3]I_3$. Also the introduction of the additional charge from the protonation of the amine group might improve the association between phenylglycinol and $[Co^{III}(S,S\text{-EDDS})]^-$ ions in the solution.

Phenylglycinol hydrochloride was prepared by a dissolution of phenylglycinol in ethanol and an addition of concentrated HCl, followed by removal of all the solvent and excess HCl *in vacuo*. ^{1}H NMR samples of

phenylglycinol hydrochloride were prepared in a similar manner to the samples of phenylglycinol. The ^{1}H NMR spectra recorded demonstrate much stronger interactions between the aminoalcohol and the shift agent (Fig. 5.9). All of the phenylglycinol hydrochloride peaks show significant splitting compared with the sample without **33** (Fig. 5.9 top). The effect is most pronounced for the stereogenic C*H* signal at 4.4 ppm allowing for an easy integration. The integrations obtained from samples of (70%*R*, 30%*S*)- and (50%*R*, 50%*S*)-phenylglycinol hydrochloride show an excellent agreement with the known enantiomeric compositions.

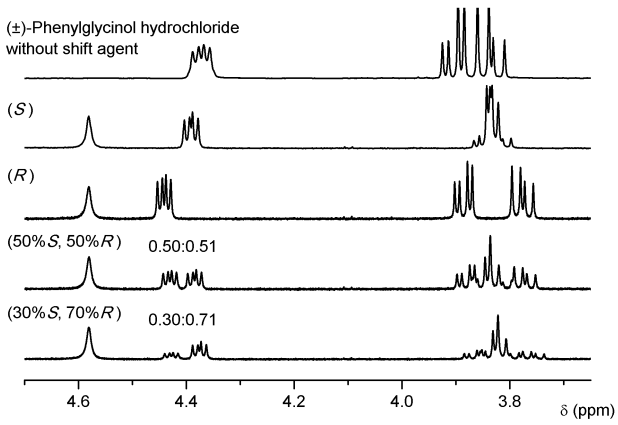

Figure 5.9. The ^{1}H NMR spectra of (*R*)-, (*S*)-, (70%*R*, 30%*S*)- and (±)-phenylglycinol hydrochloride recorded in saturated solution of **33** in d^4-methanol.

Additional tests were conducted to find if it is possible to simplify the procedure by the exclusion of the phenylglycinol hydrochloride preparation step. A sample was prepared by dissolution of phenylglycinol in the saturated solution of **33** and an addition of the stoichiometric amount of conc. HCl (~0.5 µl). It was found that the quality of the ^{1}H NMR spectrum of the sample strongly depends on the amount of acid added which is difficult to control on such a small scale. The overall spectrum quality is also worse compared to the

spectrum of phenylglycinol hydrochloride (Fig. 5.10). The method however allows for a quick qualitative assessment of optical purity of this class of compounds.

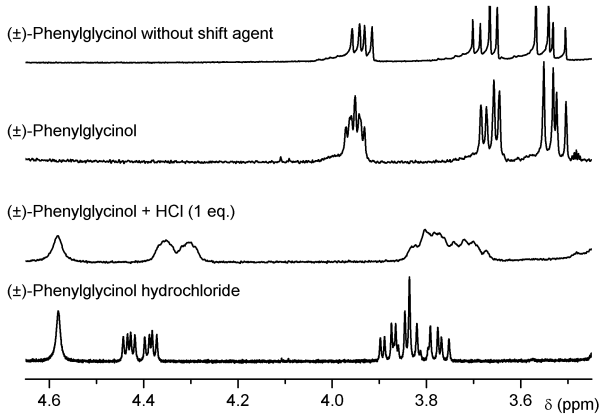

Figure 5.10. Comparison of ^{1}H NMR spectrum of phenylyglycinol in d^4-methanol (top) with spectra of phenylglycinol, phenylglycinol and HCl (1:1) and phenylglycinol hydrochloride in saturated solution of $PPh_4[Co^{III}(S,S\text{-EDDS})]$ (**33**) in d^4-methanol.

Conclusions

The family of $PPh_4[M^{III}(S,S\text{-EDDS})]\cdot 2H_2O$ complexes has proven to be a potentially useful tool in the optical resolution and the determination of enantiomeric purity. The initial results obtained from the resolution of $[Ru^{II}(bpy)_3]Cl_2$ are promising, more work is however required to optimise the results in order to obtain better yields and ee.

$PPh_4[M^{III}(S,S\text{-EDDS})]\cdot 2H_2O$ (**33**) demonstrates a potential as a chiral shift agent for various families of compounds: *i.e*. small organic molecules and cationic metal complexes. The tests conducted with phenylglycinol hydrochloride show an excellent diastereoselectivity of **33** towards this class of

compounds; large peak separations in the ^{1}H NMR allow for an easy assessment of their optical purity and determination of ee.

Experiments conducted with the racemic and optically pure chiral-at-metal transition metal complexes show that **33** exhibits a good diastereoselectivity towards this class of compounds. The results however are strongly dependent on the type of compound. The importance of an auxiliary counterion in the recognition process has also been noted. The results suggest that the presence of a small (~2 Å) anion facilitates the recognition process, with only the size and not the type of the ion playing an important role.

Overall, the $PPh_4[M^{III}(S,S\text{-EDDS})]$ family shows similar properties to the recently popular TRISPHAT anion, without the necessity for complicated synthetic procedure and optical resolution.

References

1. J. Lacour, C. Ginglinger, C. Grivet and G. Bernardinelli, *Angew. Chem. Int. Ed.*, 1997, **36**, 608-610.
2. J. Lacour, C. Ginglinger and F. Favarger, *Tetrahedron Lett.*, 1998, **39**, 4825-4828.
3. J. Lacour, C. Ginglinger, F. Favarger and S. TorcheHaldimann, *Chem Commun*, 1997, 2285-2286.
4. C. Ginglinger, D. Jeannerat, J. Lacour, S. Jugé and J. Uziel, *Tetrahedron Lett.*, 1998, **39**, 7495-7498.
5. D. Monchaud, J. Lacour, C. Coudret and S. Fraysse, *J. Organomet. Chem.*, 2001, **624**, 388-391.
6. G. Bruylants, C. Bresson, A. Boisdenghien, F. Pierard, A. K.-D. Mesmaeker, J. Lacour and K. Bartik, *New J. Chem.*, 2003, **27**, 748-751.
7. J. Lacour, J. J. Jodry, C. Ginglinger and S. Torche-Haldimann, *Angew. Chem. Int. Ed.*, 1998, **37**, 2379-2380.
8. H. Ratni, J. J. Jodry, J. Lacour and E. P. Kundig, *Organometallics*, 2000, **19**, 3997-3999.
9. H. Amouri, R. Thouvenot, M. Gruselle, B. Malezieux and J. Vaissermann, *Organometallics*, 2001, **20**, 1904-1906.
10. S. D. Bergman, R. Frantz, D. Gut, M. Kol and J. Lacour, *Chem Commun*, 2006, 850-852.
11. L. Mimassi, C. Guyard-Duhayon, M. N. Rager and H. Amouri, *Inorg. Chem.*, 2004, **43**, 6644-6649.
12. J. J. Jodry, R. Frantz and J. Lacour, *Inorg. Chem.*, 2004, **43**, 3329-3331.
13. F. Favarger, C. Goujon-Ginglinger, D. Monchaud and J. Lacour, *J. Org. Chem.*, 2004, **69**, 8521-8524.
14. F. P. Dwyer and A. M. Sargeson, *J. Phys. Chem.*, 2002, **60**, 1331-1332.
15. S. Bremer and O. Trapp, *Electrophoresis*, 2009, **30**, 329-336.
16. C. H. Langford and V. S. Sastri, *J. Phys. Chem.*, 2002, **74**, 3945-3949.
17. R. H. Fenn, A. J. Graham and R. D. Gillard, *Nature*, 1967, **213**, 1012-1013.
18. A. Damianoglou, E. J. Crust, M. R. Hicks, S. E. Howson, A. E. Knight, J. Ravi, P. Scott and A. Rodger, *Chirality*, 2008, **20**, 1029-1038.
19. P. Belser, C. Daul and A. Von Zelewsky, *Chem. Phys. Lett.*, 1981, **79**, 596-598.
20. J. Ferguson, F. Herren and G. M. McLaughlin, *Chem. Phys. Lett.*, 1982, **89**, 376-380.
21. J. A. Broomhead and C. G. Young, *Inorg. Synth.*, 1990, **28**, 338-340.
22. V. Joshi and P. K. Ghosh, *J. Am. Chem. Soc.*, 1989, **111**, 5604-5612.

Chapter 6

Synthesis of conductive salts of $[M^{III}(S,S\text{-EDDS})]^-$ complex anions

Introduction

In Chapter 1 the advances in the field of charge transfer organic conductors and different approaches towards the construction of chiral conductive materials were reviewed. The use of achiral donor molecules and chiral counterions was singled out as a promising method and therefore was chosen as the main approach in this work. The synthesis of several achiral donor molecules was described in Chapter 2. Different families of anionic metal complexes were explored in Chapters 3 and 4, in order to find viable counterions for the synthesis of conductive materials. This chapter focuses on the synthesis of such materials using our selection of donor molecules and the $[M^{III}(S,S\text{-EDDS})]^-$ family of complex anions.

Charge transfer salts of the $PPh_4[M^{III}(S,S\text{-EDDS})]\cdot 2H_2O$ (M = Co, Fe, Cr) salts were prepared electrochemically, as previously described (see Chapter 3). Four different donor molecules were used: tetrathiafulvalene (TTF), tetraselenafulvalene (TSF), bis(ethylenedithio)tetrathiafulvalene (ET) and bis(ethylenedithio)-tetraselenafulvalene (BETS). Where possible the solids

obtained were characterised using single crystal X-ray diffraction, as well as by conductivity measurements, IR spectroscopy and elemental microanalysis.

Results and Discussion

Synthesis of charge transfer salts

All of the compounds in this chapter were obtained by electrocrystallisation. The solid donor molecule (TTF, TSF, ET or BETS) was placed in the anode chamber of an electrocrystallisation cell filled with a solution of one of the complex anions salts: $PPh_4[Co^{III}(S,S\text{-EDDS})]\cdot 2H_2O$ (**33**), $PPh_4[Fe^{III}(S,S\text{-EDDS})]\cdot 2H_2O$ (**35**) or $PPh_4[Cr^{III}(S,S\text{-EDDS})]\cdot 2H_2O$ (**37**). Several different solvents and solvent mixtures were tested initially in order to find optimal conditions for the crystal growth. The solvents used were: methanol, acetonitrile, benzonitrile, tetrahydrofuran and dichloromethane, as well as their mixtures with water. It was found that acetonitrile/water (20:1) mixture produced crystalline materials of highest quality for the systems tested. This combination was therefore used in all of the subsequent experiments. The electrocrystallisation cells were kept at ambient temperature under constant current conditions (1 μA) for a period of a few weeks to a few months depending on the rate of the crystal growth.

TTF and TSF salts

Salts of TTF and TSF were obtained following the described procedure, the resulting salts, $(TTF)_3[Co^{III}(S,S\text{-EDDS})]_2\cdot 6H_2O$ (**38**), $(TTF)_3[Fe^{III}(S,S\text{-EDDS})]2\cdot 5H_2O$ (**39**), $(TTF)_x[Cr^{III}(S,S\text{-EDDS})]_2\cdot 4.5H_2O$ (**40**), $(TSF)_3[Co^{III}(S,S\text{-EDDS})]_2\cdot 6H_2O$ (**41**), $(TSF)_3[Fe^{III}(S,S\text{-EDDS})]_2\cdot 6H_2O$ (**42**) and $(TSF)_3[Cr^{III}(S,S\text{-}$

EDDS)]$_2$·6H$_2$O (**43**) were harvested after a period of two to three weeks and were characterised by single crystal X-ray diffraction and single crystal conductivity measurements.

ET and BETS salts

Pale purple crystals of (ET)$_x$[Co^{III}(*S*,*S*-EDDS)]$_2$·5H$_2$O (**44**) and (ET)$_x$[Cr^{III}(*S*,*S*-EDDS)]$_2$·6H$_2$O (**46**) were obtained by the same method and characterised by single crystal X-ray diffraction and conductivity measurements. No product was obtained from the cell containing ET and PPh$_4$[Fe^{III}(*S*,*S*-EDDS)]·2H$_2$O (**35**). Additionally in the case of **45** a small amount of dark needle like crystals were also observed. Unfortunately no crystals of this phase of quality suitable for single crystal X-ray diffraction measurements were found.

Due to the low solubility of BETS in polar solvents, electrocrystallisation experiments with this donor molecule were left for a period of few months. Microcrystalline solids were collected from cells containing cobalt(III) and chromium(III) salts. Again no product was obtained from the cell containing the iron(III) complex. The solids were characterised using IR spectroscopy and powder pellet conductivity measurements. No crystals of quality suitable for single crystal X-ray diffraction were found.

Both ET and BETS compounds exhibit light colours [pale purple for cobalt(III), pink for chromium(III) salts], which suggests a non-charge transfer character of these materials. This is consistent with their non-conductive properties (*vide infra*), low sulphur content (microelemental analysis) and lack of bands characteristic for TTF type salts in IR spectrum.

Single crystal X-ray structures

(TTF)$_3$[Co^{III}(S,S-EDDS)]$_2$·6H$_2$O (38)

To varying extents, all of the investigated crystals of this compound were found to be twinned. Solution and refinement of the crystal structure was however possible using a twin refinement. The compound **38** crystallises in a chiral monoclinic space group $P2_1$ with two complex anions, three TTF units and six molecules of water in the asymmetric part of the unit cell. Hydrogen atoms of the water molecules could not be located most likely due to the formation of a disordered H-bonding network, they were however included for formula completeness. Details of the crystal solution and refinement can be found in Table A.5 in Appendix A. Selected bond lengths and angles are in Table B.8 in Appendix B.

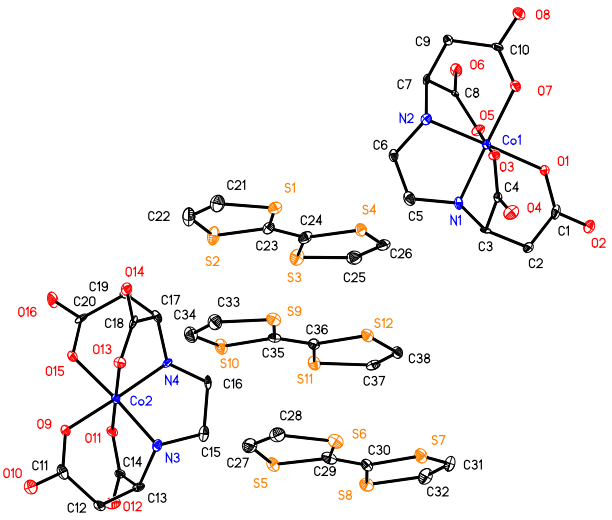

Figure 6.1. Solid state structure of (TTF)$_3$[Co^{III}(*S*,*S*-EDDS)]$_2$·6H$_2$O (**38**) with thermal parameters drawn at 50% probability. Water molecules and hydrogen atoms removed for clarity.

The three TTF molecules are not crystallographically identical, with one of the molecules exhibiting a significant bend. Analysis of the bond lengths of these

TTF units (see Chapter 3) shows different oxidation states for each of the units (Fig. 6.2). Distances between the TTF units in the π-stacks ranges between 3.2 to 3.7 Å. The molecules in the stack are parallel, with the angles between mean planes of the molecules below 2.3°

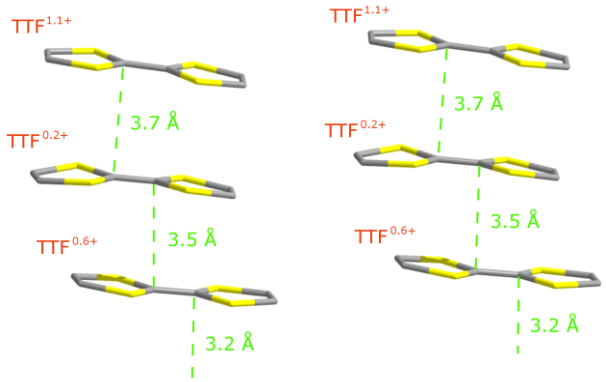

Figure 6.2. Distances between the TTF molecules in the stacks and the average charges.

The extended packing of the compound is typical, with the TTF units forming infinite stacks running between the columns of the complex anions along the [100] direction. These stacks and columns form infinite layers along [110] direction.

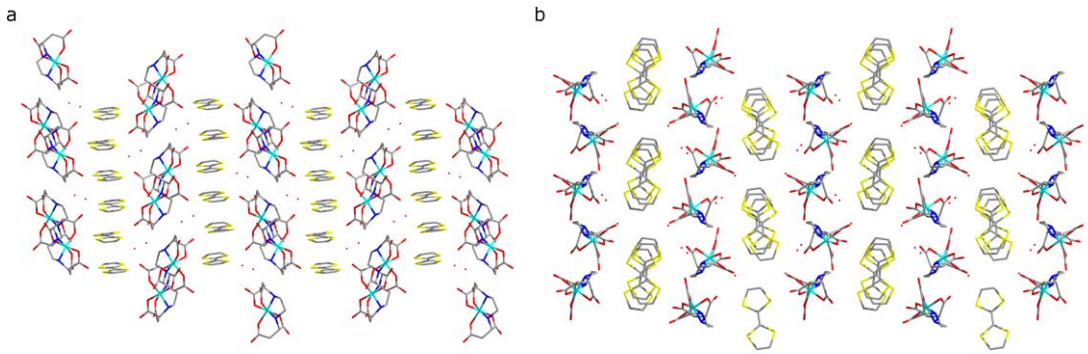

Figure 6.3. Solid state packing of $(TTF)_3[Co^{III}(S,S\text{-EDDS})]_2 \cdot 6H_2O$ (**38**), (a) view from [010] and (b) [100] direction.

(TTF)$_3$[Fe^{III}(S,S-EDDS)]$_2$·5H$_2$O (39)

Similar to its cobalt(III) analogue all of the crystals of this compound were twinned, the twin components were identified using Platon TwinRotMat.[1] The structure was solved in a triclinic P1 unit cell and was refined using SHELX twin refinement.[2] Due to a large amount of disorder in the structure further reduction of symmetry was not possible. Attempts to solve the structure in the apparent orthorhombic system resulted in meaningless solutions.

The asymmetric part of the cell contains four complex anions, ten molecules of water and two stacks of three TTF molecules each, with all of the TTFs disordered between two positions with occupation factor of a half. No hydrogen atoms on water molecules were located, most likely due to overall disorder in the structure. Details of the structure solution and refinement are summarised in Table A.5 in Appendix A and the selected bond lengths and angles are listed in Table B.9 in Appendix B.

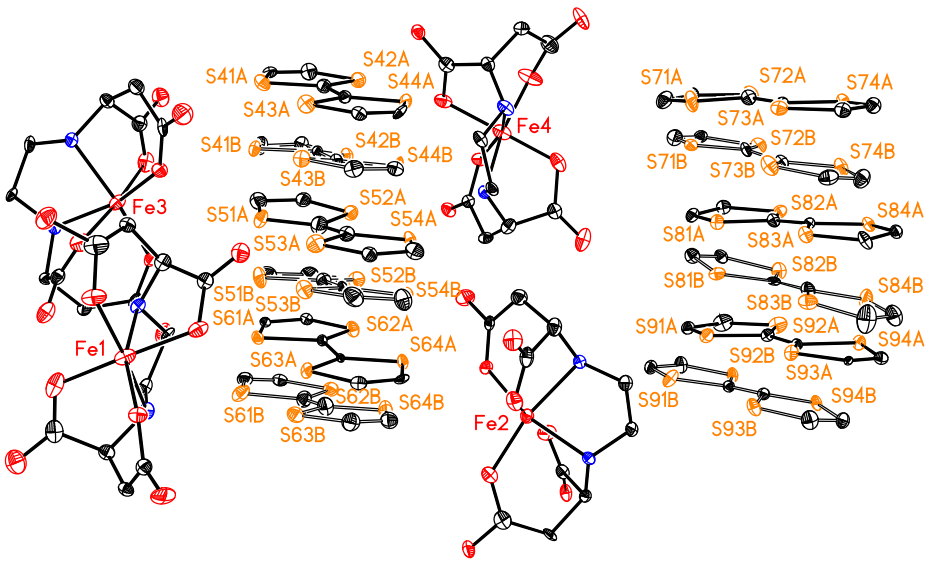

Figure 6.4. Solid state structure of (TTF)$_3$[Fe^{III}(*S*,*S*-EDDS)]$_2$·5H$_2$O (**39**) with thermal parameters drawn at 50% probability. Water molecules and hydrogen atoms were removed for clarity.

Similar as in the case of the cobalt(III) analogue, the TTF molecules in the stacks are not identical. The analysis of the bond lengths shows different oxidation state for each of the moieties, with the charges varying between 0 and 1.2+.

The extended packing in the solid state is analogous to that of the cobalt(III) compound.

$(TTF)_x[Cr^{III}(S,S\text{-}EDDS)]_2 \cdot 4.5H_2O$ (40)

Solution of the single crystal diffraction data collected for this compound was possible for only the anionic sub-lattice of the assembly. This suggests that the compound might have an incommensurate (misfit) structure, relatively common for this type of compound.[3] Unfortunately the structure of the cationic part of the assembly was not obtained. The presence of the organic donor cationic sub-lattice is however demonstrated by the IR spectrum (presence of peaks characteristic for oxidised TTF)[4] and the results of the conductivity measurements (*vide infra*). Incidentally all of the obtained crystals of the compound were dark brown/black, a colour characteristic for TTF charge transfer compounds.

The anionic sub-lattice crystallises in monoclinic $P2_1$ space group. The asymmetric part of the unit cell contains four complex anions and nine water molecules. One of the complex anions and the water molecules were modelled as disordered. Details of the crystal solution and refinement can be found in Table A.5 in Appendix A. The selected bond lengths and angles are listed in Table B.10 in Appendix B.

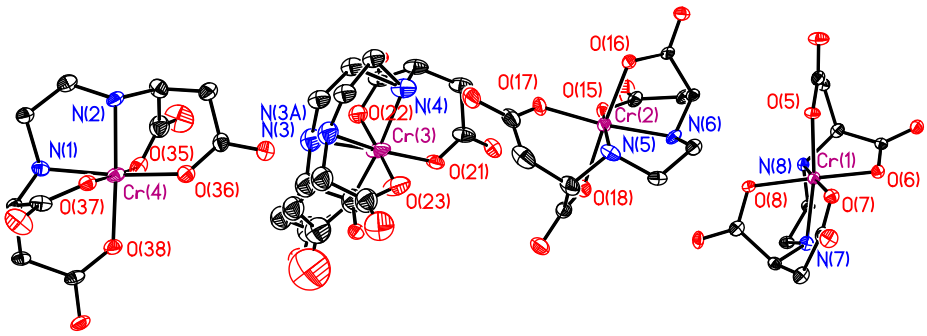

Figure 6.5 Solid state structure of the anionic sub-lattice of $(TTF)_x[Cr^{III}(S,S\text{-EDDS})]_2 \cdot 4.5H_2O$ (**40**), hydrogen atoms and solvent molecules were removed for clarity.

Due to lack of the structure of the cationic moieties, the stoichiometry of the compound was not established. It is however expected to be similar to the cobalt(III) and iron(III) analogues, considering the similarities the IR spectra and electrical conductivity of all three compounds. The proposed formula is therefore $(TTF)_3[Cr^{III}(S,S\text{-EDDS})]_2 \cdot 4.5H_2O$.

$(TSF)_3[M^{III}(S,S\text{-EDDS})]_2 \cdot 6H_2O$

All of the obtained TSF salts were found to have very similar solid state structures, analogous with that obtained for $(TTF)_3[Co^{III}(S,S\text{-EDDS})]_2 \cdot 6H_2O$. The compounds crystallise in a monoclinic $P2_1$ space group. The asymmetric unit comprises of three TSF molecules, two complex anions and six water molecules. Hydrogen atoms on water molecules were not located, most likely due to a disordered network of hydrogen bonding in the structure. Details of structure solution and refinement can be found in Table A.5 in Appendix A. The selected bond lengths and angles for cobalt(III), ironIII) and chromium (III) structures can be found in Tables B.13, B14 and B.15 respectively in Appendix B.

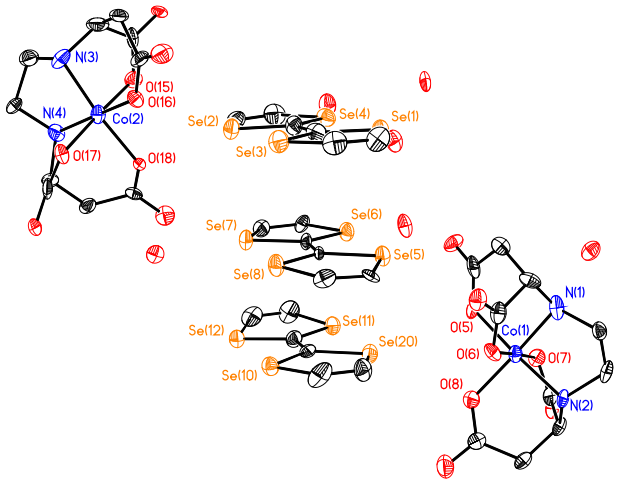

Figure 6.6. Solid state structure of the anionic sub-lattice of $(TSF)_3[Co^{III}(S,S\text{-EDDS})]_2 \cdot 6H_2O$ (**41**), hydrogen atoms were removed for clarity.

The average Se-C bond lengths in the TSF molecules vary between 1.86 to 1.91 Å. This suggests that, similar to the TTF case, each of the TSF unit has a different oxidation state.

The extended packing of the compound is directly comparable with that of $(TTF)_3[Co^{III}(S,S\text{-EDDS})]_2 \cdot 6H_2O$. The TSF stacks form infinite layers which alternate in the structure with layers of the complex anions.

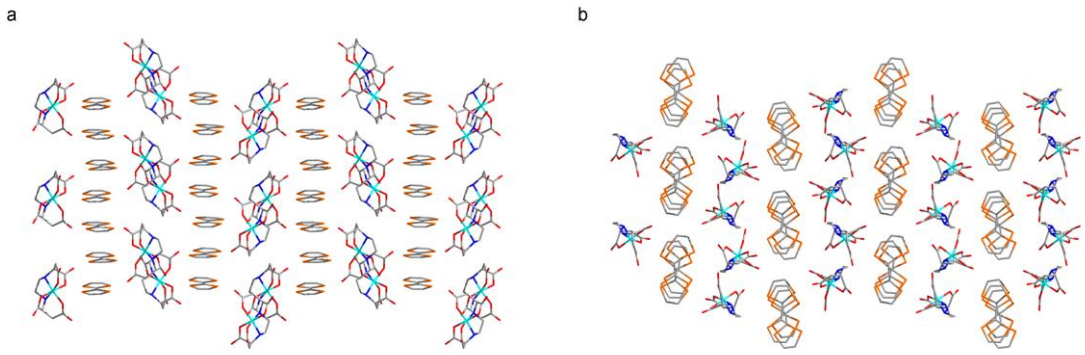

Figure 6.7. Solid state packing of $(TSF)_3[Co^{III}(S,S\text{-EDDS})]_2 \cdot 6H_2O$ (**41**), (a) view from [100] and (b) [001] direction.

(ET)$_x$[M^{III}(S,S-EDDS)]$_y$·zH$_2$O

The obtained solids of ET salts with [Co^{III}(*S*,*S*-EDDS)]$^-$ and [Cr^{III}(*S*,*S*-EDDS)]$^-$ were found to be of incommensurate type. In both cases, only the structure of the anionic sub-lattices were solved. Both salts crystallise in an orthorhombic $P2_12_12_1$ space group with two complex anions and five (Co^{III}) or six water (Cr^{III}) molecules in the asymmetric part of the unit cell. Several of the water molecules in both structures were modelled as disordered, hydrogen atoms on these were not located, they were however included for formula completeness.

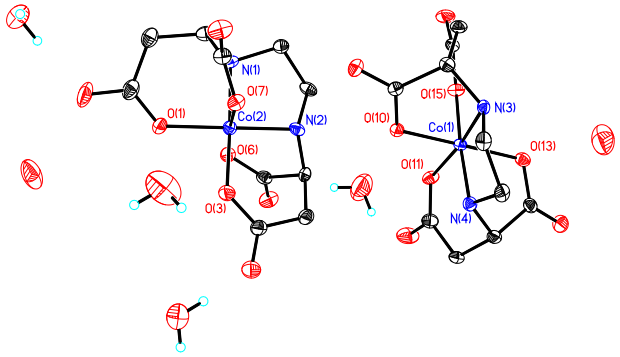

Figure 6.8. Solid state structure of the anionic sub-lattice of (ET)$_x$[Co^{III}(*S*,*S*-EDDS)]$_2$·5H$_2$O (**44**), hydrogen atoms on the complex anions were removed for clarity.

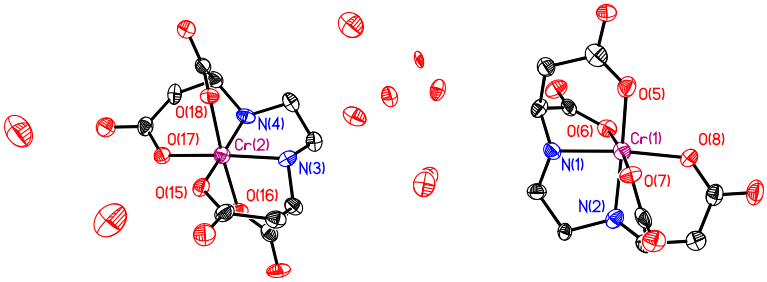

Figure 6.9. Solid state structure of the anionic sub-lattice of (ET)$_x$[Cr^{III}(*S*,*S*-EDDS)]$_2$·5H$_2$O (**46**), hydrogen atoms were removed for clarity.

Details of the crystal solution and refinement for both structures can be found in Table A.5 in Appendix A. Selected bond lengths and angles are listed in Tables B.11 and B.12 for cobalt(III) and chromium(III) structures respectively.

No formulae were established due to the misfit nature of the solid state structures. Elemental analysis however, suggests only a small amount of ET present in the solid state (2-3% sulphur). This is consistent with the lack of dark brown/black colour characteristic for charge transfer compounds, and their non-conductive properties (*vide infra*).

Conductivity measurements

Conductivity measurements of all of the obtained compounds at ambient and variable temperatures were performed using standard 2- and 4- probe setups (see Chapter 3).

$(TTF)_3[M^{III}(S,S\text{-}EDDS)]_2 \cdot xH_2O$

All of the TTF salts exhibit similar, relatively low average ambient temperature conductivities: $\sigma_{RT}^{Cr} = 1.1 \cdot 10^{-5}$ S·cm^{-1}, $\sigma_{RT}^{Fe} = 1.3 \cdot 10^{-5}$ S·cm^{-1}, $\sigma_{RT}^{Cr} = 6.9 \cdot 10^{-6}$ S·cm^{-1}.

Table 6.1. Results of conductivity measurements of $(TTF)_3[M^{III}(S,S\text{-EDDS})]_2 \cdot xH_2O$.

Sample	Resistance	Distance (mm)	Width (mm)	Thickness (mm)	Conductivity (S·cm^{-1})
$(TTF)_3[Co^{III}(S,S\text{-EDDS})]_2 \cdot 6H_2O$ (**38**)					
1	$4.50 \cdot 10^6$	1.20	1.71	0.14	$1.09 \cdot 10^{-5}$
2	$3.15 \cdot 10^6$	0.77	1.71	0.14	$1.00 \cdot 10^{-5}$
3	$5.20 \cdot 10^6$	0.63	1.06	0.17	$6.67 \cdot 10^{-6}$
4	$6.20 \cdot 10^6$	1.26	1.03	0.17	$1.15 \cdot 10^{-5}$
5	$7.75 \cdot 10^6$	0.57	0.66	0.09	$1.31 \cdot 10^{-5}$
6	$4.15 \cdot 10^6$	0.51	0.46	0.20	$1.36 \cdot 10^{-5}$
$(TTF)_3[Fe^{III}(S,S\text{-EDDS})]_2 \cdot 6H_2O$ (**39**)					
1	$3.06 \cdot 10^7$	0.66	0.57	0.09	$4.38 \cdot 10^{-6}$
2	$4.31 \cdot 10^7$	0.74	0.94	0.09	$2.13 \cdot 10^{-6}$

Sample	Resistance	Distance (mm)	Width (mm)	Thickness (mm)	Conductivity ($S \cdot cm^{-1}$)
$(TTF)_3[Fe^{III}(S,S\text{-EDDS})]_2 \cdot 6H_2O$ (**39**)					
3	$1.62 \cdot 10^7$	0.63	0.51	0.06	$1.32 \cdot 10^{-5}$
4	$2.09 \cdot 10^7$	1.71	1.23	0.14	$4.68 \cdot 10^{-6}$
5	$1.22 \cdot 10^7$	0.51	0.51	0.06	$1.43 \cdot 10^{-5}$
6	$2.45 \cdot 10^7$	2.29	0.51	0.06	$3.18 \cdot 10^{-5}$
7	$9.70 \cdot 10^6$	0.51	0.51	0.06	$1.80 \cdot 10^{-5}$
$(TTF)_x[Cr^{III}(S,S\text{-EDDS})]_2 \cdot 4.5H_2O$ (**40**)					
1	$2.40 \cdot 10^8$	0.43	0.17	0.34	$3.04 \cdot 10^{-7}$
2	$9.15 \cdot 10^7$	1.06	0.40	0.31	$9.19 \cdot 10^{-7}$
3	$3.60 \cdot 10^7$	0.69	0.69	0.06	$4.86 \cdot 10^{-6}$
4	$1.40 \cdot 10^7$	0.63	0.49	0.04	$2.12 \cdot 10^{-5}$

The discrepancies between the results of individual measurements, especially evident in the case of chromium(III) analogue, are a result of strong twinning of the crystals, which made finding a single conductive crystal surface challenging. The results of the individual measurements are summarised in Table 6.1.

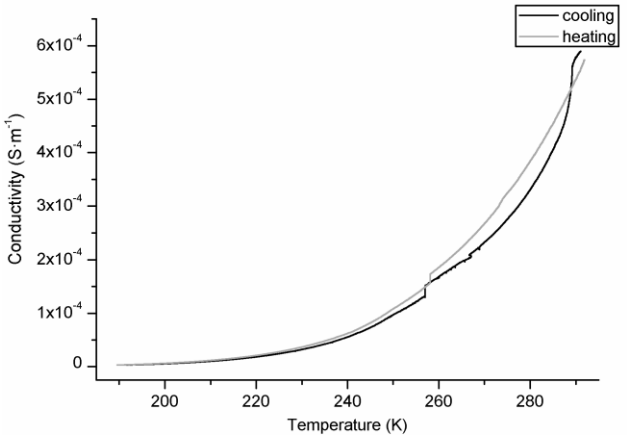

Figure 6.10. Temperature dependence of the conductivity of $(TTF)_3[Co^{III}(S,S\text{-EDDS})]_2 \cdot 6H_2O$ (**38**)

The temperature dependence of the conductivity for all of the compounds follows an exponential curve, typical for semiconductive materials. $(TTF)_3[Co^{III}(S,S\text{-EDDS})]_2 \cdot 6H_2O$ additionally exhibits a small reversible change of conductivity at 260 K, which is most likely due to a phase change (Fig. 6.10).

Graphs of the temperature dependence of the conductivity for **39** and **40** can be found in Appendix C.

The temperature dependence of the electrical conductivity follows the Arrhenius law, which allows for the calculation of the activation energy (Fig. 6.4 for Co^{III}, Appendix C for Fe^{III} and Cr^{III}).

$$\sigma = \sigma_0 e^{-\frac{\Delta E_a}{kT}} \quad \Longrightarrow \quad \ln\sigma = -\frac{E_a}{k}\cdot\frac{1}{T} + \ln\sigma_0$$

The calculated activation energies, E_a^{Co} = 0.244 eV, E_a^{Fe} = 0.357 eV and E_a^{Cr} = 0.252 eV, are all in the range typical for these types of compounds. It is worth noticing that the value calculated for the iron(III) analogue is much higher than those obtained for cobal(III) and chromium(III).

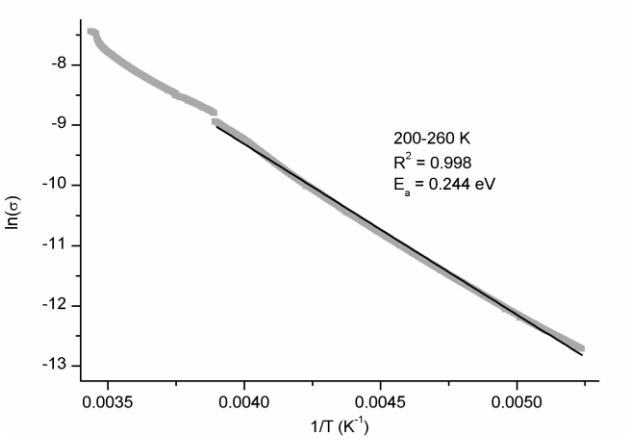

Figure 6.11. Dependence of natural logarithm of conductivity of **38** on reciprocal of temperature and the linear fit of the data.

$TSF_3[M^{III}(S,S\text{-}EDDS)]_2\cdot 6H_2O$

In order to explore the possibility of obtaining $[M^{III}(S,S\text{-EDDS})]^-$ charge transfer salts with better conductive properties, tetraselenafulvalenium (TSF) analogues of the obtained TTF salts were synthesised. The results of the

ambient temperature conductivity measurements of these compounds are summarised in Table 6.2. As was anticipated, the obtained average ambient temperature conductivities, $\sigma_{RT}^{Co} = 5.7 \cdot 10^{-4}$ S·cm^{-1} $\sigma_{RT}^{Fe} = 2.8 \cdot 10^{-5}$ S·cm^{-1} $\sigma_{RT}^{Cr} = 2.8 \cdot 10^{-4}$ S·cm^{-1}, are between one to two orders of magnitude higher compared to their TTF analogues

Table 6.2. Representative selection of results of conductivity measurements of $(TSF)_3[M^{III}(S,S\text{-}EDDS)]_2 \cdot 6H_2O$ (M = Co, Fe, Cr).

Sample	Resistance (Ω)	Distance (mm)	Width (mm)	Thickness (mm)	Conductivity (S·cm^{-1})
$(TSF)_3[Co^{III}(S,S\text{-}EDDS)]_2 \cdot 6H_2O$ (**41**)					
1	$1.71 \cdot 10^6$	0.34	0.23	0.06	$1.54 \cdot 10^{-4}$
2	$1.98 \cdot 10^5$	0.57	0.17	0.14	$1.18 \cdot 10^{-3}$
3	$2.08 \cdot 10^5$	0.23	0.14	0.11	$6.75 \cdot 10^{-4}$
4	$4.00 \cdot 10^5$	0.20	0.23	0.09	$2.55 \cdot 10^{-4}$
$(TSF)_3[Fe^{III}(S,S\text{-}EDDS)]_2 \cdot 6H_2O$ (**42**)					
1	$1.73 \cdot 10^7$	0.43	0.11	0.06	$3.79 \cdot 10^{-5}$
2	$2.58 \cdot 10^7$	0.43	0.29	0.06	$1.02 \cdot 10^{-5}$
3	$2.14 \cdot 10^7$	0.37	0.17	0.03	$3.55 \cdot 10^{-5}$
$(TSF)_3[Cr^{III}(S,S\text{-}EDDS)]_2 \cdot 6H_2O$ (**43**)					
1	$4.35 \cdot 10^5$	0.34	0.20	0.14	$2.76 \cdot 10^{-4}$
2	$2.31 \cdot 10^5$	0.51	0.23	0.14	$6.82 \cdot 10^{-4}$
3	$4.85 \cdot 10^6$	0.43	0.20	0.14	$3.09 \cdot 10^{-5}$
4	$2.55 \cdot 10^6$	0.43	0.14	0.09	$1.37 \cdot 10^{-4}$

Unfortunately, similar to their TTF analogues, all of the TSF salts exhibit semiconducting behaviour upon cooling. Additionally small reversible changes of conductivity, most likely caused by phase changes, were observed for $(TSF)_3[Co^{III}(S,S\text{-}EDDS)]_2 \cdot 6H_2O$ (**41**) and $(TSF)_3[Cr^{III}(S,S\text{-}EDDS)]_2 \cdot 6H_2O$ (**43**). Activation energies for all of the compounds and all of the phases were calculated, the results are summarised in Table 6.3. The calculated values are much lower than those obtained for the TTF analogues, what was to be expected. It is worth noting that the value obtained for the iron(III) analogue is

significantly higher than those obtained for the other compounds, the same trend was observed previously for the TTF salts.

Table 6.3. The calculated activation energies of $(TSF)_3[M^{III}(S,S\text{-EDDS})]_2 \cdot 6H_2O$ (M = Co, Fe, Cr).

Compound	Temperature range (K)	Ea (eV)
$(TSF)_3[Co^{III}(S,S\text{-EDDS})]_2 \cdot 6H_2O$ (**41**)	200-250	0.106
	170-200	0.135
$(TSF)_3[Fe^{III}(S,S\text{-EDDS})]_2 \cdot 6H_2O$ (**42**)	210-300	0.200
$(TSF)_3[Cr^{III}(S,S\text{-EDDS})]_2 \cdot 6H_2O$ (**43**)	250-285	0.107
	190-250	0.125
	125-150	0.093

ET and BETS salts

In order to investigate the possibility of obtaining charge transfer salts of $[M^{III}(S,S\text{-EDDS})]^-$ anions with metallic conductivity, an attempt was made to synthesise analogues of the obtained TTF and TSF salts with bis(ethylenedithio)tetrathiafulvalene (ET) and bis(ethylenedithio)tetraselena-fulvalene, as salts of these donor molecules are known to often exhibit metallic conductivity and even superconductivity. [5-8]

The obtained compounds crystallised as clusters of microcrystalline solids. No single crystals big enough for conductivity measurements were found. Thus, the compounds were ground up and powder pellets were prepared. In all cases thus prepared samples were found to be insulating ($R > 10^9\ \Omega$).

A small amount of black needle like crystalline solid was found in the sample of $(ET)_x[Cr^{III}(S,S\text{-EDDS})]_2 \cdot 6H_2O$. This apparent second phase was found

to exhibit high room temperature conductivity and metallic properties upon cooling. Unfortunately these crystals were found to be very fragile and were destroyed during the measurements. The collected variable temperature data are plotted in Figure 6.12.

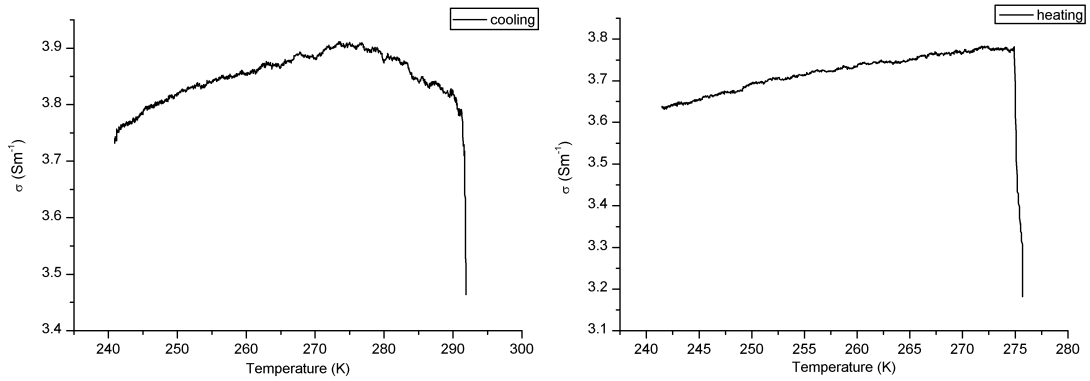

Figure 6.12. Temperature dependence of the conductivity of a single crystal of $(ET)_x[Cr^{III}(S,S\text{-EDDS})]_y \cdot zH_2O$.

The compound exhibits metallic behaviour down to 275K with the conductivity rising sharply with decreasing temperature. Below 275 K a metal-semiconductor transition occurs. The semiconductive phase is characterised by a very low value of activation energy E_a = 0.07 eV.

DFT calculations

In order to investigate the relatively low conductivity of the TTF based compounds, simple DFT calculations using the solid state structure of $(TTF)_3[Co^{III}(S,S\text{-EDDS})]_2 \cdot 6H_2O$ were performed in collaboration with Jack Sleigh (A. Troisi group).[9] The calculation only considers a one dimensional chain of TTF molecules, with three TTF moieties per cell unit, and assumes that the highest occupied and the lowest unoccupied bands can be expressed as linear combination of the TTF's HOMO and LUMO orbitals. The one dimensional band

structure is determined by the electronic coupling V between the HOMO and LUMO orbitals, which is more rigorously defined as the integral $\langle \phi_i | F | \phi_j \rangle$ where ϕ_i and ϕ_j are the orbitals and F is the Fock operator. The calculation was performed using the ZINDO and B3LYP/6-31G* methods.[10-12]

Table 6.4. Absolute coupling values in cm^{-1}. See Fig. 6.13 for the coupling directions.

	ZINDO		*B3LYP/6-31G**	
Coupling	HOMO-HOMO	LUMO-LUMO	HOMO-HOMO	LUMO-LUMO
aa	4314.2	869.9	5874.8	1850.2
ab	1568.6	292.5	2440.8	368.5
ab'	1912.0	588.9	4110.1	912.1

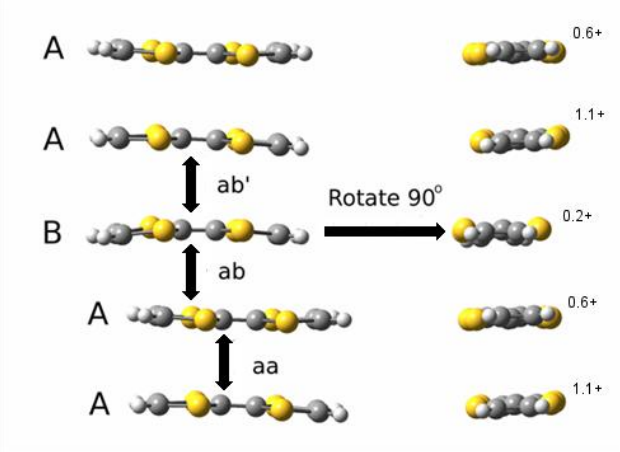

Figure 6.13. Inequivalent couplings in the $(TTF)_3[Co^{III}(S,S\text{-EDDS})]_2 \cdot 6H_2O$ (**38**) structure. Charges calculated from the crystal structure.

From the inter-orbital couplings given in Table 6.4, it is apparent that two different types of TTF molecules are present in the structure. Two of the TTF molecules are of the same type (A) whereas the third one is significantly different (B). This is consistent with the findings from the solid state structure suggesting that the charge on one of the TTF molecules is close to zero (molecule B). It is worth noting that whilst the two charged molecules

(molecules A) are quite similar, they are not equivalent. As a result of these differences, the coupling between molecule types A and B is significantly smaller than coupling between two molecules of type A.

In order to additionally explain the conductive properties of the compound, a one dimensional band structure along the largest coupling direction was computed. The closest neighbour approximation was assumed, meaning that unit cell only 'sees' the next and previous unit. For the current purpose, the unit cell is just the AAB unit of TTF molecules (counterions and solvent molecules were discarded). The single dimension of the band is the axis through the TTF molecules. Additionally for a comparison, the band structure for a hypothetical AAA unit was also calculated.

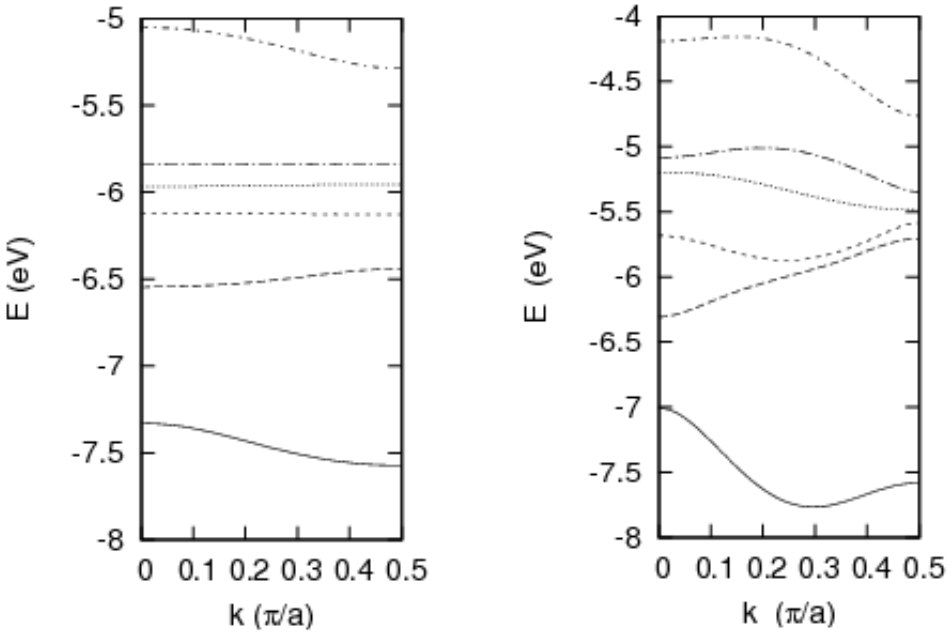

Figure 6.14. Band diagrams for (left) the 'AAB' unit and (right) the 'AAA' unit. The bands shown are valence-2 to conduction+2. The valence band (3rd band from the bottom) is 2/3 filled (due to the charge stoichiometry of the crystal). Computed at B3LYP/6-31G* level of theory.

Interestingly, in the 'AAB' case, the valence band is very flat (Fig. 6.14). Consequently the material is a semiconductor (the gap between valence and conduction band is 0.15 eV at the smallest separation), which compares reasonably well with the activation energy calculated from the Arrhenius plot (*vide supra*). However in the hypothetical 'AAA' case, the valence band is considerably more dispersed (the difference between minimum and maximum values is 0.29 eV), and since this band would be only partially occupied, the system would behave as a metal.

Conclusions

Several novel conductive and non-conductive salts of optically pure $[M^{III}(S,S\text{-EDDS})]^-$ anions (M = Co, Fe, Cr) with TTF, TSF, ET and BETS were synthesised and characterised.

The EDDS complexes were found to form semiconductive materials with tetrathiafulvalene. The stoichiometry of all of the compounds was found to be 3:2 (donor:counterion), all of the structures also contained several water molecules (2-3 per complex anion). The average ambient temperature conductivities σ_{RT} were found to be between 10^{-5} to 10^{-6} S·cm^{-1}. The activation energies of these compounds, E_a^{Co} = 0.24 eV, E_a^{Fe} = 0.36 eV, E_a^{Cr} = 0.25 eV, are in the range typical for TTF charge transfer salts. The E_a of the iron(III) compound was found to be significantly higher that those of the cobalt and chromium analogues.

In order to further investigate the properties of these compounds simple DFT calculations were performed on $(TTF)_3[Co^{III}(S,S\text{-}EDDS)]_2 \cdot 6H_2O$. It was found that this compound consists principally of two types of TTF molecules with the coupling interactions between these being significantly different. This is consistent with conclusions drawn from the analysis of the bond lengths in the solid state, suggesting the presence of non-oxidised TTF molecules in the structure, disrupting the stacking interactions. The calculated band structure points to the compound being a semiconductor, which is consistent with the results of the conductivity measurements.

To improve the conductive properties, tetraselenafulvalene (TSF) analogues of the obtained materials were synthesised. The obtained compounds, $(TSF)_3[M^{III}(S,S\text{-}EDDS)]_2 \cdot 6H_2O$ (M = Co, Fe, Cr), were found to have very similar stoichiometry and solid state structure to those of the TTF salts. The compounds exhibit semiconductive properties with generally higher ambient temperature conductivities (10^{-4} to 10^{-5} $S \cdot cm^{-1}$) and lower activation energies (0.09 to 0.20 eV). Similar to the TTF case, the iron(III) salt exhibits much higher activation energy and lower conductivity than the cobalt and chromium analogues.

To examine the possibility of the synthesis of EDDS complexes' salts with metallic properties, an attempt was made to obtain materials of this type with bis(ethylenedithio)tetrathiafulvalene (ET) and bis(ethylenedithio)tetraselena-fulvalene (BETS). In all of the cases, the main product was found to be a non-conductive material with low sulphur content. In the case of $ET_x[Co^{III}(S,S\text{-}EDDS)]_y$ a second minor product was also collected. No crystal structure was

obtained for this material. The conductivity measurements however show high ambient temperature conductivity of σ_{RT} = $3.2 \cdot 10^{-2}$ $S \cdot cm^{-1}$ and metallic behaviour down to 275 K, where metal-to-semiconductor transition occurs.

It was demonstrated that it is possible to obtain conductive chiral materials using optically pure anionic metal complexes. The TTF and TSF salts of $[M^{III}(S,S\text{-EDDS})]^-$ (M = Co, Fe, Cr) however, show irregular AAB stacking which, as supported by calculations, reduces their potential as conductors. We are not able to discern a correlation between the properties of the anion (size, optical purity, magnetism *etc*.) and the stacking and conductive properties of its charge transfer salt, which would allow us to improve the properties of the future systems.

Interestingly we have encountered difficulties in synthesising ET and BETS analogues of the obtained TTF compounds. We believe that this might be due to the high hydrophilicity of the anions, which causes crystallisation with sulphur-rich hydrophobic donors to be unfavourable. The successful separation of the minor product in the case of $(ET)_x[Co^{III}(S,S\text{-EDDS})]_y$ has however shown that in principle it is not unfeasible to obtain these types of salts, and that these may be highly conductive.

References

1. A. Spek, *J. Appl. Cryst.*, 2003, **36**, 7-13.
2. G. M. Sheldrick, *Acta Crystallogr., Sect. A*, 2008, **64**, 112-122.
3. E. Makovicky and B. Hyde, in *Inorganic Chemistry*, Springer Berlin / Heidelberg, 1981, vol. 46, pp. 101-170.
4. S. Matsuzaki, N. Koga, I. Moriyama and K. Toyoda, *Bull. Chem. Soc. Jpn.*, 1983, **56**, 2090-2092.
5. A. E. Underhill, *J. Mater. Chem.*, 1992, **2**, 1-11.
6. G. Saito and Y. Yoshida, *Bull. Chem. Soc. Jpn.*, 2007, **80**, 1-137.
7. K. Bechgaard and D. Jérome, *Physica Scripta*, 1991, **1991**, 37.
8. H. Kobayashi, H. Cui and A. Kobayashi, *Chem. Rev.*, 2004, **104**, 5265-5288.
9. J. Sleigh, *Intermolecular Orbital Coupling in TTF (tetrathiafulvalene) derivatives*, University of Warwick, 2009.
10. A. D. Bacon and M. C. Zerner, *Theoret. Chim. Acta*, 1979, **53**, 21-54.
11. A. D. Becke, *J. Chem. Phys.*, 1993, **98**, 5648-5652.
12. C. Lee, W. Yang and R. G. Parr, *Phys. Rev. B*, 1988, **37**, 785.

Chapter 7

Experimental details

General considerations

S,*S*-EDDS was obtained from Innospec Inc. and used without further purification. Most other solvents and chemicals were purchased from Sigma-Aldrich, Acros or Alfa Aesar and used without further purification. Sodium and potassium hydride dispersions in mineral oil were placed in a Schlenk vessel under an inert atmosphere and washed three times with diethyl ether to remove the oil. Solids were dried and stored in the glove box.

Where necessary reactions were carried out under argon using a dual manifold argon/vacuum line and standard Schlenk techniques or MBraun dry box. Solvents (Fisher Scientific, Sigma-Aldrich) were dried by heating to reflux for 3 d under dinitrogen over the appropriate drying agents (sodium for toluene, potassium for THF, sodium/potassium alloy for diethyl ether and pentane, calcium hydride for acetonitrile, dichloromethane and triethylamine) and degassed before use. THF and diethyl ether were additionally pre-dried over Na wire. Dried solvents were stored in glass ampoules under argon. All glassware and cannulae were stored in an oven at > 375 K.

Deuterated solvents were purchased from Cambridge Isotope Laboratories and where necessary were freeze-thaw degassed and dried by

heating to their boiling points *in vacuo* over an appropriate drying agent (potassium for d^6-benzene, d^8-toluene and d^8-THF, calcium hydride for d^2-dichloromethane, d^3-acetonitrile and d^5-pyridine) for 3 d. The solvents were then vacuum distilled (trap-to-trap) to a clean, dry Young's tap ampoule and stored in a dry box.

Unless stated otherwise column chromatography was performed using Flashmaster Personal II on silica cartridges, using 5% loading ratio.

Electrocrystallisations were performed in custom made glass H-tubes with anode and cathode compartments separated by a glass frit. Tubes were prepared under dinitrogen atmosphere in a dry box using dry solvents and sealed using rubber septum (Suba Seal). Electrodes were made of platinum wire (Ø = 1 mm, Goodfellow Cambridge Ltd.).

NMR spectra were recorded on Bruker Spectrospin 300/400/500 spectrometers. The spectra were internally referenced using the residual protio solvent ($CDCl_3$, CD_3CN etc.) resonance relative to tetramethylsilane (δ = 0 ppm). ESI mass spectra were recorded on a Bruker Esquire 2000 spectrometer. Infra-Red spectra were measured using a Perkin-Elmer FTIR spectrometer. Elemental analyses were performed by Warwick Analytical Services and Medac Ltd.

UV-Vis spectra were recorded in 1 cm and 1 mm path length quartz cuvettes using Jasco J-610 spectrometer. Sample concentrations were chosen to keep the absorbance value below 1. The standard parameters used were: bandwidth 1 nm; response time 1 sec; wavelength scan range 200–800 nm; data pitch 0.2 nm; and scanning speed 100 nm/min, accumulation 2. CD spectra were recorded in 1 cm path length quartz cuvettes using Jasco J-810 (calibrated

using 0.060% ACS for intensity and a holmium filter for wavelength). Sample concentrations were chosen to keep the high tension voltage below 600 V. The standard parameters used were: bandwidth 1 nm; response time 1 sec; wavelength scan range 200–800 nm; data pitch 0.2 nm; and scanning speed 100 nm/min, accumulation 4.

The crystal data was collected using an Oxford Diffraction Gemini R and Siemens SMART CCD single crystal diffractometers using MoK_α (λ = 0.71073 Å) or CuK_α (λ = 1.54178 Å) radiation source. Structures in Chapters 2 – 5 were solved by Dr. Guy Clarkson using direct methods: SHELX (TREF)[1,2] with additional light atoms found by Fourier methods. Crystal refinement was performed using SHELX97.[2] Publication data were prepared using SHELXTL. Structures in Chapter 6 were solved (direct methods) and refined by author using using SHELX97.[2] Publication data were prepared using WINGX.[3]

Powder diffraction data were recorded using a Siemens D500 diffractometer with the CuKα (λ = 1.54218 Å) radiation source, step 0.02° and step interval 1 s.

Magnetization measurements were performed on a Quantum Design MPMS 5S SQuID magnetometer, using an external field of 1000G in the temperature range 2 – 300 K. Where necessary samples were placed in air-tight Teflon holder under argon and additional background data ware recorded for the empty holder, otherwise samples were placed in gelatine capsules. Diamagnetic corrections were calculated using Pascal's constants.[4]

Electrical conductivity measurements were performed with a Keithley 2001 Multimeter using typical two and four probe setups at ambient temperature. Contacts to the crystal were made by gold wires (25 μm, Goodfellow Cambridge Ltd.) and attached with carbon cement (Agar Scientific).

Experimental Details for Chapter 2

Dimethyl 1,3-dithiole-2-thione-4,5-dicarboxylate (*1*)[5]

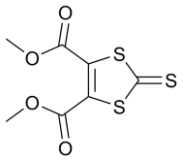

Dimethyl acetylenedicarboxylate (10.4 g, 0.073 mol) and ethylene tricarbonate (10 g, 0.073 mol) were dissolved in toluene (25 ml) and were heated to reflux overnight at 150°C. The product precipitated upon cooling and was collected by filtration and dried *in vacuo*. Concentration of the filtrate gave the second crop. The compound was used in subsequent step without further purification. Overall yield 16.3 g (89%).

^{1}H NMR (400 MHz, 298 K, acetone-*d*^{6}) δ_H 3.91 (s, CH_3)

1,3-Dithiole-2-thione-4,5-dicarboxylic acid (2)[5]

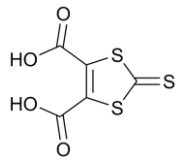

A mixture of dimethyl 1,3-dithiole-2-thione-4,5-dicarboxylate (0.079 mol, 20 g), concentrated HCl (36%, 86 ml) and glacial acetic acid (40 ml) in water (120 ml) was heated to reflux (~170°C) until all the material dissolved (approx. 2 h). The product precipitated upon cooling (water/ice bath) and was collected by filtration without washing and dried *in vacuo*. The filtrate was evaporated to dryness, the residue was investigated using ^{1}H NMR and was found to contain

mainly pure product The compound was used in subsequent step without further purification. Combined yield 17.6 g (100%).

^{1}H NMR (400 MHz, 298 K, acetone-d_6) δ 8.32 (s, COOH)

1,3-Dithiole-2-thione (3)[5]

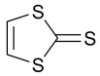

1,3-Dithiole-2-thione-4,5-dicarboxylic acid (15.2 g, 0.067 mol) was heated to reflux in pyridine (70 ml) for 3 h and then was stirred overnight at ambient temperature. The mixture was concentrated under reduced pressure with gentle heating to obtain a thick black oil (yellow film starts showing on the neck of the flask). The resulting oil was heated to reflux with hexanes (200 ml) for 0.5 h at 95°C. The hot solution was decanted and cooled in an acetone/dry ice bath. The yellow precipitate was collected by filtration without washing and dried *in vacuo*. The extraction procedure was repeated at least four times. Overall yield 7.4 g (82%).

Elemental analysis found (calculated for $C_3H_2S_3$) %: C 28.12 (26.84), H 1.75 (1.50), S 69.56 (71.66).

^{1}H NMR (400 MHz, 298 K, acetone-d^6) δ_H 7.52 (s, CH)

^{13}C NMR (100 MHz, 298 K, acetone-d^6) δ_C 132.28 (very weak), 207.11

1,3-Dithiolium hydrogen sulphate (4)[5]

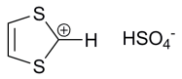

1,3-Dithiole-2-thione (10 g, 0.075 mol) was dissolved in acetone (200 ml) and cooled to -50°C. Peracetic acid (50 ml of 40% solution, 0.3 mol) in acetone (120 ml) was added dropwise, keeping the temperature below -40°C. The cooling bath was then removed and the mixture was allowed to warm to 10-15°C (after a few min the mixture starts to warm rapidly). The cooling bath was then replaced and the mixture was cooled again to -50°C. The bath was removed and the mixture was allowed to warm up slowly to 5-10°C. The solids were collected by filtration and dried by suction a under constant stream of dinitrogen. The product was found to be air sensitive and was used immediately in the subsequent reaction, without purification. Yield 13.5 g (90%).

1,3-Dithiolium hexafluorophosphate (5)[5]

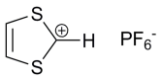

Sodium hexafluorophosphate (12.5g, 0.074 mol) was dissolved in deaerated water (30 ml) and filtered. 1,3-Dithiolium hydrogen sulphate (13.5 g, 0.068 mol) was dissolved in deaerated water (60 ml), activated charcoal was added and the mixture was filtered into the solution of hexafluorophosphate. The mixture was then stirred gently, flushed with dinitrogen, capped and refrigerated overnight. The product was collected by filtration, washed with

cold water and dried by suction under a stream of dinitrogen. Yield 13.4 g (73%).

Elemental analysis found (calculated for $C_3H_3F_6PS_2$) %: C 16.49 (14.52), H (1.291.22), S 25.89 (25.84), F 43.11 (45.94), P 12.48 (12.48).

^{1}H NMR (400 MHz, 298 K, CD_3CN) δ_H 9.19 (2H, d, $^4J_{HH}$=2Hz, CH) 11.15 (1H, t, $^4J_{HH}$=2Hz, C^+-H)

^{13}C NMR (100 MHz, 298 K, CD_3CN) δ_C 132.28 (very weak), 207.11

MS (ESI^+) m/z 103.0 ($C_3H_3S_2^+$); (ESI^-) m/z 144.8 (PF_6^-)

IR (cm^{-1}) ν 3084, 1450, 1290, 944, 881, 813, 790, 729

Tetrathiafulvalene (6)[5]

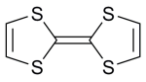

1,3-Dithiolium hexafluorophosphate (10 g, 0.040 mol) was dissolved in dry MeCN (200 ml) under argon and filtered into a 1 l round bottom flask with an argon inlet. Dry TEA was then added dropwise (approx. 10 min) and the solution was stirred for 15 min. Deaerated water (800 ml) was added slowly *via* cannula and the resulting mixture was stirred for another 15 min. Fine orange crystalline needles of product were collected by filtration and dried by suction under a stream of dinitrogen. The product was stored in the glove box. Yield 3.95 g (97%).

Elemental analysis found (calculated for $C_6H_4S_4$) %: C 35.35 (35.27), H 1.97 (1.97), S 62.89 (62.76).

^{1}H NMR (400 MHz, 298 K, CD_3CN) δ_H 6.45 (s, CH)

^{13}C NMR (100 MHz, 298 K, CD_3CN) δ_C 110.40, 120.46

MS (ESI^+) m/z 203.92 ($[M]^+$)

IR (cm^{-1}) ν 3063, 1861, 1699, 1658, 1597, 1525, 1497, 1474, 1298, 1252, 1087, 1075, 1036, 868, 793, 779, 734.

2-Methylene-1,3-diselenole (7)[6]

Sodium acetylide (2.4 g, 0.05 mol) was suspended in dry THF (50 ml) and cooled to -78°C. Selenium powder (3.8 g, 0.048 mol) was added and the mixture was allowed to warm to 0°C with stirring for 1 h. The mixture was cooled to -78°C and MeOH was added dropwise (30 ml). After 15 min the mixture was allowed to warm to 0°C and was stirred for another 2.5 h.

From this point on all of the operations were performed in the dark. All of the solutions used were kept at 0°C at all times.

The mixture was quenched with water (60 ml) and extracted with pentane (5 ×30 ml). The combined organic extracts were washed with water (2 × 30 ml) and dried over Na_2SO_4. The solvents were removed *in vacuo* without heating. The obtained red solid was immediately used in the following reaction or stored overnight under dinitrogen, in the dark at -30°C. Yield 2.4 g (24%).

^{1}H NMR (400 MHz, 298 K, CD_2Cl_2) δ_H 6.97 (dd, $^{2}J_{HH}$ = 1.1 Hz, C*H*=C*H*), 5.65 (dd, 2H, $^{2}J_{HH}$ = 1.1 Hz, C=CH_2).

^{13}C NMR (100 MHz, 298 K, CD_2Cl_2) δ_C 120.5 (*C*H=*C*H), 108.2 (C=*C*H$_2$), (*C*=CH$_2$ peak missing)

Tetraselenafulvalene (8)[6]

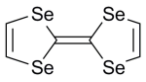

All of the operations were performed in the dark. Iodine (2.5 g, 9.8 mmol) was dissolved in the solution of dry morpholine (2.7 g, 31 mmol) in dry DMF (40 ml) under argon and cooled in a water bath. 2-Methylene-1,3-diselenole (1.0 g, 4.8 mmol) in dry DMF (25 ml) was added and the mixture was stirred for 1 h at ambient temperature. The reaction was then quenched with water (20 ml) and extracted with DCM (4 × 15 ml). The combined organic extracts were washed with aqueous $Na_2S_2O_3$ (2 × 50 ml) and water (3 × 20 ml), and dried over anhydrous Na_2SO_4. The solvents were removed *in vacuo* (without heating). The residue was purified on silica using DCM:hexane (1:2) mixture as eluent. The obtained product was additionaly recrystallised from hexane. Yield 80 mg (8.5%).

This reaction was performed several times with similar yields (literature yield >35%).

Elemental analysis found (calculated for $C_6H_4Se_4$) %: C 18.21 (18.39), H 1.13 (1.03), N >0.1 (0.0)

^{1}H NMR (400 MHz, 298 K, $CDCl_3$) δ_H 7.21 (s, 4H, C*H*=C*H*)

^{13}C NMR (100 MHz, 298 K, CD_2Cl_2) δ_C 123.0 (*C*H=*C*H), 107.0 (*C*=*C*)

MS (ESI^+) m/z 393.2 ($[M]^+$)

IR (cm^{-1}) ν 3039, 1535, 1527, 1471, 1453, 1231, 1222, 1093, 1071, 857, 829, 716, 669

2,3-Dihydro-1,4-dithiin (9)[7]

Toluene (330 ml) and *p*-toluenesulfonic acid monohydrate (0.33 g, 1.7 mmol) were heated to reflux in Dean-Stark apparatus under dinitrogen for 24 h. The collected water was removed and the Dean-Stark apparatus was replaced with a reflux condenser. 1,2-ethanedithiol (14 ml, 0.167 mol) and 2-bromo-1,1-diethoxyethane (24.5 ml, 0.163 mol) were added and the mixture was heated to reflux for 24 h. The cooled mixture was then washed with water (300 ml). The water layer was back extracted with diethyl ether (3 × 100 ml) and the combined organic extracts were washed with brine (3 × 100 ml) and dried over anhydrous Na_2SO_4. The solvents were removed *in vacuo* and the residue was distilled under vacuum (50°C, $4 \cdot 10^{-3}$ mbar). Yield 6.46 g (34%).

^1H NMR (400 MHz, 298K, $CDCl_3$) δ_H 6.04 (s, 2H, C*H*), 3.14 (s, 4H, CH_2)

^{13}C NMR (101 MHz, 298K, CDCl3) δ_C 114.39 (*C*H), 26.30 (*C*H_2)

MS (ESI^-) m/z 118.0 ($[M]^-$)

IR (cm^{-1}) ν 2903, 1690, 1577, 1550, 1408, 1318, 1276, 1254, 1227, 1200, 1149, 1125, 1087, 998, 937, 920, 884, 848, 811, 753, 720, 682

Bis(η^5-cyclopentadienyl)(5,6-dihydro-1,4-dithiine-2,3-diselenolato-κ^2*Se,Se'*)titanium(IV) (10)[7,8]

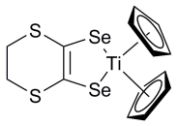

A solution of LDA was prepared *in situ* as follows.[9] Diisopropylamine (1.54 ml, 0.011 mol) was dissolved in dry THF (5 ml) under argon, and cooled to -78°C (dry ice/acetone bath). 2.5 M solution of ^{n}BuLi in hexanes (4.4 ml, 0.011 mol) was added dropwise. The mixture was allowed to warm to ambient temperature and was stirred for additional 2 h.

2,3-dihydro-1,4-dithiin (2.0 g, 16.9 mmol) was dissolved in dry THF (100 ml) under argon and cooled to -78°C. The solution of LDA was added dropwise and the mixture was stirred for 0.5 h at -78°C. Selenium powder (2.94 g, 37.2 mmol) was suspended in dry THF (100 ml) and cooled to -40°C (dry ice/acetonitrile bath). The solution of lithiated thiin was then added dropwise and the mixture was stirred for 4 h at -40°C before cooling to -78°C. Solid titanocene dichloride (4.63 g, 18.6 mmol) was added and the mixture was stirred for 1 h at -78°C. The dry ice/acetone cooling bath was replaced with a dry ice/acetonitrile bath and the mixture was allowed to warm slowly overnight. The solvents were removed under reduced pressure and the residue was redissolved in DCM and filtered through celite. The product was purified on silica using DCM:hexane (1:1) as eluent. The green solid obtained was used in the subsequent step without further purifcation. Yield 3.01 g (39%).

^{1}H NMR (400 MHz, 298K, $CDCl_3$) δ_H 6.14 (s, 5H, Cp), 5.93 (s, 5H, Cp), 3.33 (d, $^{3}J_{HH}$ = 15.6 Hz, 4H, CH_2)

^{13}C NMR (101 MHz, 298K, CDCl3) δ_C 111.4 (Cp), 109.4 (Cp), 31.6 (CH$_2$)

MS (ESI$^+$/ESI$^-$) only fragmentation products detected

4,5-Ethylenedithio-1,3-diselenol-2-on (11)[7,8]

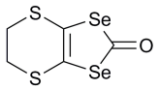

10 (3.0 g, 6.66 mmol) and bis(trichloromethyl)carbonate (1.98 g, 6.66 mmol) were dissolved in dry THF (200 ml) under dinitrogen. The mixture was heated to reflux for 1 h. The cooled mixture was quenched then with methanol (10 ml) and stirred for further 15 min. The solids were removed by filtration and the filtrate was evaporated dry under reduced pressure. The residue was purified on silica using DCM:hexane (1:1) as eluent. The solvents were removed under reduced pressure and the residue was re-dissolved in acetonitrile (100 ml) and heated to reflux with activated carbon for 0.5 h. The hot solution was filtered and the filtrate was concentrated to approximately half volume. The solution was left at -30°C overnight for crystallisation. A pale yellow solid was collected by filtration and washed with small amount of cold acetone. Yield 0.33 g (16%).

^{1}H NMR (400 MHz, 298K, $CDCl_3$) δ_H 3.44 (s, 4H, CH_2)

^{13}C NMR (125 MHz, 298K, CDCl3) δ_C 185.49 (C=O), 116.92 (C=C), 33.12 (CH$_2$)

MS (ESI+/ESI-) no identifiable fragments detected

IR (cm^{-1}) ν 2909, 1651, 1586, 1499, 1475, 1411, 1280, 1174, 1127, 948, 919, 883, 802, 757, 694

Bis(etylenedithio)tetraselenafulvalene (BETS) (12)[10]

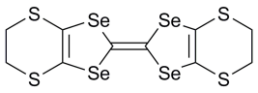

Triethyl phosphite (10 ml) was added dropwise over 15 min to a solution of 4,5-ethylenedithio-1,3-diselenol-2-one (0.3 g, 0.99 mmol) in dry toluene (30 ml) under argon. The mixture was heated to reflux for 2 h and then allowed to cool. The product was collected by filtration and recrystallised from carbon disulfide. Yield 0.15 g (52%).

Elemental analysis found (calculated for $C_{10}H_8S_4Se_4$) %: C 21.10 (20.99), H 1.20 (1.41)

^{1}H NMR (400 MHz, 298K, $CDCl_3$) δ_H 1.56 (s, 8H, CH_2)

^{13}C NMR, MS – no data obtained due to very low solubility

IR (cm^{-1}) ν 2960, 2919, 1505, 1406, 1281, 1258, 1171, 1124, 1037, 1017, 999, 939, 918, 896, 877, 839, 807, 740, 710, 683, 651

4-Formyltetrathiafulvalene (13)[11]

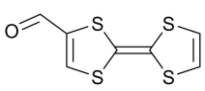

A solution of LDA was prepared *in situ*.[9] Diisopropylamine (1.54 ml, 0.011 mol) was dissolved in dry THF (5 ml) under argon, and cooled to -78°C (dry ice/acetone bath). 2.5 M solution of ^{n}BuLi in hexanes (4.4 ml, 0.011 mol) was

added dropwise. The mixture was allowed to warm to ambient temperature and was stirred for 2 h.

TTF (2.0 g, 0.01 mol) was dissolved in dry Et_2O (120 ml) under argon and cooled to -78°C. The solution of LDA was added dropwise over a period of 5 min and the mixture was stirred for 1.5 h at -78°C. *N*-methyl-*N*-phenylformamide (2.4 ml, 0.02 mol) was added dropwise and the stirring was continued for another 3 h. The dry ice/acetone bath was replaced with a dry ice/acetonitrile bath (-40°C) and the mixture was allowed to warm overnight. The mixture was then quenched with water (60 ml) and 2M HCl (20 ml). The product was extracted with DCM (3×40 ml) and dried over $MgSO_4$. The product was purified by flash chromatography: the unreacted TTF was washed off initially with toluene:hexane (1:1), continued elution with DCM yielded the product as a deep red solid. Traces of *N*-methyl-*N*-phenylformamide were washed off with Et_2O. Yield 1.62 g (70%).

Elemental analysis found (calculated for $C_6H_4S_4$) %: C 36.42 (36.19), H 1.81 (1.74), S 55.14 (55.20).

^{1}H NMR (400 MHz, 298 K, $CDCl_3$) δ_H 6.34 (2×d, 2×1H, $^3J_{HH}$=6Hz, $^3J_{HH}$=6Hz, CH), 7.42 (s, 1H, CH), 9.47 (s, 1H, CHO)

^{13}C NMR (100 MHz, 298 K, $CDCl_3$) δ_C 105.49, 115.95, 118.69, 119.36, 139.82, 141.54, 179.63

MS (ESI^+) m/z 231.91 ($[M]^+$)

IR (cm^{-1}) ν 3063, 2954, 1713, 1646, 1591, 1552, 1532, 1506, 1462, 1431, 1403, 1356, 1332, 1236, 1197, 1144, 1089, 1069, 1028, 1007, 921, 894, 862, 830, 796, 775, 743, 696, 667

4-(Hydroxymethyl)tetrathiafulvalene (14)[11]

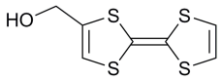

4-Formyltetrathiafulvalene (1.0 g, 4.3 mmol) was dissolved in methanol (40 ml). $NaBH_4$ (0.18 g, 4.75 mmol) was added in small portions and the mixture was stirred for 30 min DCM (50 ml) was added and the resulting mixture was washed with brine (2 × 25 ml) and water (2 × 25 ml), and dried over anhydrous Na_2SO_4. The solvents were removed under reduced pressure and the resulting thick brown oil was dried in vacuum oven overnight. The product was stored in the glove box. Yield 0.83 g (83%)

Elemental Analysis found (Calculated for $C_7H_6OS_4$) %: C 35.87 (35.82), H 2.58 (2.75), S 54.72 (56.52)

^1H NMR (400 MHz, 298 K, $CDCl_3$) δ_H 2.25 (s, 1H, OH), 4.38 (s, 2H, CH_2), 6.21 (s, 1H, CH), 6.30 (s, 2H, CH)

^{13}C NMR (100 MHz, 298 K, $CDCl_3$) δ_C 60.6 (CH_2), 109.5, 111.5 (C=C), 115.4, 119.0, 119.1 (CH), 136.6

MS (ESI^+) m/z 233.8 ($[M]^+$)

IR (cm^{-1}) ν 3284, 3058, 2963, 2922, 2907, 2856, 1540, 1455, 1332, 1260, 1185, 1109, 1092, 1017, 972, 865, 793, 769, 733, 713

(*R*)-2-Amino-2-phenylethan-1-ol, (*R*)-2-phenylglycinol[12]

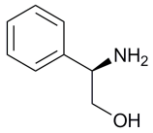

Sodium borohydride (31.21 g, 0.825 mol) and (*R*)-2-phenylglycine (50 g, 0.33 mol) were dissolved in dry THF (400 ml) under argon. Iodine (92.1 g, 0.36 mol) in dry THF (~100 ml) was added dropwise while cooling in an ice/water bath. The mixture was heated to reflux for 48 h and then was cooled in an ice/water bath. Methanol (~250 ml) was added slowly until the solution cleared and the mixture was stirred for additional 15 min. The solvents were removed under reduced pressure and the obtained residue was suspended in 20% KOH (600 ml) and was stirred overnight. The product was extracted with DCM (3×150 mol) and dried over $MgSO_4$. The solvents were removed under reduced pressure and the residue was recrystallised from hot toluene. Yield 22.6 g (50%).

Elemental Analysis found (Calculated for $C_8H_{11}NO$) %: C 69.79 (70.04), H 8.08 (8.08), N 10.18 (10.21).

^{1}H NMR (400 MHz, 298 K, $CDCl_3$) δ_H 2.05 (s, 2H, NH_2), 3.48 (dd, 1H, $^2J_{HH}$=8Hz, $^3J_{HH}$=11Hz, CH_2), 3.66 (dd, 1H, $^2J_{HH}$=4Hz, $^3J_{HH}$=11Hz, CH_2), 3.97 (dd, 1H, $^3J_{HH}$=4Hz, $^3J_{HH}$=8Hz, CH), 7.18-7.30 (m, 5H, Ph-H)

^{13}C NMR (100 MHz, 298 K, $CDCl_3$) δ_C 57.39 (CH), 68.02 (CH_2), 126.51, 127.52, 128.65, 142.67 (Ph)

MS (ESI^+)m/z 138 ($[M+H]^+$), 121 ($[M-NH_2]^+$)

IR (cm^{-1}) ν 3330, 3275, 3058, 3035, 2909, 2835, 2656, 1604, 1557, 1524, 1496, 1453, 1394, 1360, 1306, 1197, 1077, 1047, 978, 914, 883, 855, 819, 756, 699

Optical rotation (589 nm, 293K, MeOH) *n* -25.99° (6.60 g/100 ml), lit. -25.8°.[13]

For optical purity determination by ^{1}H NMR see Chapter 5.

(*R*)-2-(*Tert*-butoxycarbonylamino)-2-phenylethyl methanesulfonate (16)[14]

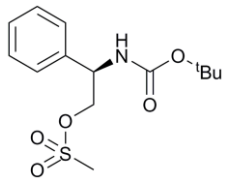

BOC anhydride (1.68 g, 7.7 mmol) in THF (5 ml) was added dropwise to a solution of (*R*)-phenylglycinol (1.0 g, 7.3 mmol) and was stirred for 30 min. TMEDA (0.90 g, 7.7 mmol) was added and the mixture was cooled in an ice/water bath. Methanesulfonyl chloride (0.89 g, 7.7 mmol) was added and the mixture was stirred for 1.5 h. The solids were removed by filtration and washed with THF. Hexanes were added to the combined filtrates to initiate the crystallisation. The product was collected by filtration, washed with hexanes and dried in air. Yield 2.0 g (87%).

^{1}H NMR (400 MHz, 298 K, $CDCl_3$) δ_H 7.42 – 7.28 (m, 5H, Ph), 5.25 – 5.09 (m, 1H, N*H*), 5.08 – 4.94 (m, 1H, C*H*), 4.55 – 4.33 (m, 2H, CH_2), 2.88 (s, 3H, SO_3CH_3), 1.43 (s, 9H, ^{t}Bu).

^{13}C NMR (100 MHz, 298 K, $CDCl_3$) δ_C 137.8, 129.09, 128.47, 126.82 (Ph), 71.38 (CH_2), 53.7 (CH), 37.61 (SO_3CH_3), 28.44 ($C(CH_3)_3$)

MS (ESI$^+$) m/z 338.0 ([M+Na]$^+$)

IR (cm^{-1}) ν 3357, 2982, 2939, 1693, 1522, 1497, 1456, 1391, 1356, 1329, 1277, 1252, 1163, 1099, 1079, 1053, 1028, 1002, 959, 923, 886, 851, 815, 758, 702, 653.

(*R*)-2-Amino-2-phenylethyl methanesulfonate (15)[15]

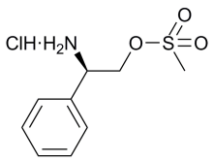

A solution of HCl (10 ml, 4 M) was added to a solution of (*R*)-2-(tert-butoxycarbonylamino)-2-phenylethyl methanesulfonate (**16**) (2.5 g, 7.9 mmol) in dioxane (10 ml) and was stirred for 1 h. The volatiles were removed under reduced pressure and the residue was recrystallised from acetonitrile/diethyl ehter. Yield 1.28 g (65%).

^{1}H NMR (400 MHz, 298 K, CD_3CN) δ_H 7.63 (2H, dd, $^3J_{HH}$ = 7.5 Hz, $^4J_{HH}$ = 1.7 Hz, Ph), 7.52 – 7.42 (3H, m, Ph), 4.80 – 4.68 (2H, m, CH_2), 4.58 (1H, dd, $^3J_{HH}$ = 9.8 Hz, $^3J_{HH}$ = 3.5 Hz, CH), 3.20 (3H, s, SO_3CH_3).

^{13}C NMR (100 MHz, 298 K, CD_3CN) δ_C 130.65, 130.07, 128.99 (Ph), 70.05 (CH), 55.26 (CH_2), 38.22 (SO_3CH_3),

MS (ESI$^+$) m/z 198.9 ([M-NH_2·HCl]$^+$), 215.9 ([M-Cl]$^+$)

MS (ESI^-) m/z 248.9 ($[M-H]^-$)

IR (cm^{-1}) ν 2962, 2804, 2658, 2578, 2494, 2037, 1595, 1518, 1456, 1410, 1380, 1347, 1268, 1205, 1180, 1126, 1068, 1033, 992, 950, 919, 860, 831, 787, 759, 739, 695.

(*R*)-2-(2-Hydroxy-1-phenylethyl)isoindoline-1,3-dione[16]

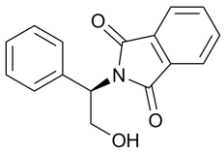

Solid (*R*)-phenylglycinol (2.0 g, 14.5 mmol) and phtalic anhydride (2.16 g, 14.5 mmol) were heated with stirring to 145°C for 4 h. The obtained yellow oil was dissolved in DCM (50 ml) and dried over anhydrous sodium sulphate. The solvent was then removed under reduced pressure and the obtained product was used in the subsequent step without further purification. Yield 3.7 g (95%).

^1H NMR (400 MHz, 298 K, $CDCl_3$) δ_H 7.83 – 7.74 (2H, m, Pht), 7.70 – 7.60 (2H, m, Pht), 7.49 (2H, d, $^3J_{HH}$ = 7.4 Hz, Ph), 7.41 – 7.23 (3H, m, Ph), 5.51 (1H, dd, $^3J_{HH}$ = 8.9 Hz, $^3J_{HH}$ = 5.0 Hz, C*H*), 4.76 – 4.66 (1H, m, CH_2), 4.24 (1H, dd, $^3J_{HH}$ = 11.4 Hz, $^4J_{HH}$ = 4.9 Hz, CH_2), 3.47 (1H, s, O*H*).

^{13}C NMR (100 MHz, 298 K, $CDCl_3$) δ_C 168.89 (*C*=O), 136.88, 134.08 (Pht), 131.72, 128.70, 128.13, 127.97 (Ph), 123.31 (Pht), 61.98 (CH_2), 57.46 (*C*H).

MS (ESI^+) m/z 290.1 ($[M+Na]^+$)

IR (cm^{-1}) ν 3457, 1772, 1700, 1611, 1585, 1495, 1467, 1388, 1358, 1332, 1288, 1266, 1185, 1172, 1120, 1065, 1040, 1013, 999, 962, 919, 877, 838, 793, 765, 719, 698.

(*R*)-2-(1,3-Dioxoisoindolin-2-yl)-2-phenylethyl methanesulfonate (17)

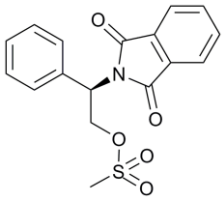

Methanesulfonyl chloride (0.32 ml, 4.12 mmol) and TEA (0.57 ml, 4.12 mmol) were added to a solution of (*R*)-2-(2-hydroxy-1-phenylethyl)isoindoline-1,3-dione (1.0 g, 3.7 mmol) in DCM (20 ml) and were stirred overnight. The resulting solution was washed with water (3 × 20 ml) and dried over anhydrous sodium sulphate. The solvents were removed under reduced pressure and the residue was used in the subsequent reaction without further purification. Yield 1.22 g (94%).

^{1}H NMR (400 MHz, 298 K, $CDCl_3$) δ_H 7. 84 (2H, dd, $^{3}J_{HH}$ = 5.4 Hz J_{HH} = 3.1 Hz, Pht), 7.72 (2H, dd, $^{3}J_{HH}$ = 5.5 Hz, $^{3}J_{HH}$ = 3.0 Hz, Pht), 7.55 – 7.48 (2H, m, Ph), 7.40 – 7.31 (3H, m, Ph), 5.68 (1H, dd, $^{3}J_{HH}$ = 10.5 Hz, $^{2}J_{HH}$ = 5.4 Hz, C*H*), 5.41 (1H, t, $^{3}J_{HH}$ = 10.4 Hz, CH_2), 4.78 (1H, dd, $^{3}J_{HH}$ = 10.4 Hz, $^{2}J_{HH}$ = 5.4 Hz, CH_2), 2.98 (3H, s, SO_3CH_3).

^{13}C NMR (100 MHz, 298 K, $CDCl_3$) δ_C 168.22 (C=O), 135.19, 134.44 (Pht), 131.77, 129.19, 128.20 (Ph), 123.66 (Pht), 67.23 (CH_2), 54.25 (CH), 37.67 (SO_3CH_3).

MS (ESI$^+$) m/z 368.0 ([M+Na]$^+$), 250.1 ([M-SO_3CH_3]$^+$)

IR (cm^{-1}) ν 1774, 1708, 1611, 1544, 1496, 1468, 1386, 1355, 1335, 1290, 1266, 1205, 1174, 1136, 1110, 1087, 987, 961, 918, 902, 878, 809, 767, 720, 698

(*R*)-*Tert*-butyl 2-hydroxy-1-phenylethylcarbamate[17]

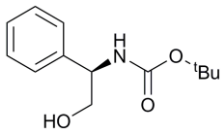

(*R*)-phenylglycinol (1.0 g, 7.3 mmol) was dissolved in THF (10 ml) and cooled in an ice/water bath. A solution of di-tert-butyldicarbonate (1.08 g, 7.7 mmol) in THF (10 ml) and TEA (2.14 ml, 15.4 mmol) were added and the reaction mixture was stirred for 2 h at ambient temperature. The resulting solution was concentrated under reduced pressure to approximately half volume and hexanes were added to initialise crystallisation. The obtained solid was collected by suction filtration and washed with hexane. Yield 1.72 g (99%).

^{1}H NMR (400 MHz, 298 K, $CDCl_3$) δ_H 7.36 – 7.21 (5H, m, Ph), 5.30 (1H, s br, NH), 4.74 (1H, s br, CH), 3.78 (2H, s br, CH_2), 2.62 (1H, s, OH), 1.40 (9H, s, ^{t}Bu).

^{13}C NMR (100 MHz, 298 K, $CDCl_3$) δ_C 156.29 (C=O), 139.65, 128.85, 127.79, 126.69 (Ph), 80.10 (*C*(CH_3)$_3$), 66.90 (CH_2), 56.95 (CH), 28.46 (C(*C*H_3)$_3$).

MS (ESI$^+$) m/z 260.1 ([M+Na]$^+$)

IR (cm^{-1}) ν 3237, 1670, 1605, 1584, 1547, 1493, 1469, 1454, 1431, 1392, 1367, 1343, 1314, 1283, 1255, 1232, 1159, 1103, 1054, 1027, 918, 866, 842, 760, 701, 663.

(*R*)-*Tert*-butyl 2-iodo-1-phenylethylcarbamate (18)[18,19]

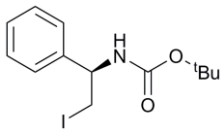

(*R*)-tert-butyl 2-hydroxy-1-phenylethylcarbamate (1.0 g, 4.2 mmol) was dissolved in dry THF (50 ml) under argon and cooled in an ice/water bath. Imidazole (1.06 g, 15.6 mmol), triphenylphosphine (2.91 g, 11.1 mmol) and iodine (2.72 g, 10.7 mmol) were added in that order. The resulting mixure was stirred for 1 h at 0°C and then at ambient temperature for 2 d. The reaction was quenched with a saturated solution of sodium thiosulphate (40 ml) and brine (40 ml). The aqueous layer was extracted with DCM (30 ml) and the combined organic layers were dried over anhydrous magnesium suphate. The solvents were removed under reduced pressure and the residue was purified on silica using DCM as eluent. Yield 0.85 g (58%).

Elemental analysis found (calculated for $C_{13}H_{18}NO_2$) %: 45.50 (44.97), H 5.35 (5.23), N 4.01 (4.03).

^{1}H NMR (400 MHz, 298 K, $CDCl_3$) δ_H 7.40 – 7.21 (5H, m, Ph), 5.04 (1H, s, N*H*), 4.78 (1H, s br, C*H*), 3.59 – 3.40 (2H, m, CH_2), 1.43 (9H, s, ^{t}Bu).

^{13}C NMR (100 MHz, 298 K, $CDCl_3$) δ_C 128.90, 128.17, 126.38 (Ph), 55.46 (CH), 28.48 (CH_3), 12.33 (CH_2).

MS (ESI^+) m/z 370.0 ($[M+Na]^+$)

IR (cm^{-1}) ν 3354, 3009, 2981, 1688, 1521, 1453, 1417, 1392, 1368, 1351, 1333, 1316, 1279, 1247, 1155, 1123, 1079, 1044, 1020, 914, 877, 842, 758, 742, 698, 658.

(*R*)-2-(2-Iodo-1-phenylethyl)isoindoline-1,3-dione (19)[18]

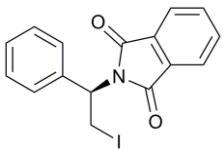

(*R*)-2-(2-hydroxy-1-phenylethyl)isoindoline-1,3-dione (1.0 g, 3.7 mmol) was dissolved in dry THF (50 ml) under argon and cooled in an ice/water bath. Imidazole (0.97 g, 14.1 mmol), triphenylphosphine (2.62 g, 10.0 mmol) and iodine (2.44 g, 9.6 mmol) were added in that order. The resulting mixure was stirred for 1 h at 0°C and then at ambient temperature for 2 d. The reaction was quenched with a saturated solution of sodium thiosulphate (40 ml) and brine (40 ml). The aqueous layer was extracted with DCM (30 ml) and the combined organic layers were dried over anhydrous magnesium sulphate. The solvents were removed under reduced pressure and the residue was purified on silica using DCM as eluent. After two purifications on column contamination with triphenylphosphine oxide was still detectable by ^1H NMR. The product was used without further purification. Yield 0.5 g (<37%).

^{1}H NMR (400 MHz, 298 K, $CDCl_3$) δ_H 7.89 – 7.81 (2H, m, Pht), 7.78 – 7.68 (2H+, m, Pht+P(O)Ph_3), 7.57 – 7.48 (2H+, m, Ph+ P(O)Ph_3), 7.48 – 7.40 (3H, m, Ph), 7.39 – 7.28 (3H, m), 5.56 (1H, dd, $^{3}J_{HH}$ = 11.5 Hz, $^{2}J_{HH}$ = 5.3 Hz, C*H*$_2$), 4.53 (1H, dd, $^{3}J_{HH}$ = 11.4 Hz, $^{3}J_{HH}$ = 10.4 Hz, C*H*), 3.84 (1H, dd, $^{3}J_{HH}$ = 10.3 Hz, $^{2}J_{HH}$ = 5.3 Hz, C*H*$_2$).

MS (ESI$^+$) m/z 250.1 ([M-I]$^+$)

IR (cm^{-1}) ν 3457, 1772, 1700, 1611, 1495, 1467, 1388, 1358, 1266, 1185, 1172, 1120, 1065, 1040, 1013, 999, 877, 838, 793, 765, 719, 698

(*S*)-2-Aminopropan-1-ol, L-alaninol[20]

Lithium aluminium hydride (17 g, 0.43 mol) was suspended in dry THF (600 ml) under argon at 273 K. Solid L-alanine (20 g, 0.22 mol) was added in small portions. The mixture was heated to reflux overnight. A saturated potassium carbonate solution (~100 ml) was added very slowly to the mixture cooled in an ice/water bath. The mixture was then filtered and the solvents were removed under reduced pressure. The residue was distilled under vacuum (~100°C, 4×10^{-3} mbar). Yield 12.7 g (77%).

Elemental analysis found (calculated for $C_3H_9NO{\cdot}¼H_2O$) %: 45.21 (45.24), H 12.48 (12.05), N 17.34 (17.59).

^{1}H NMR (400 MHz, 298 K, $CDCl_3$) δ_H 0.96 (dd, 3H, $^{2}J_{HH}$=6Hz, $^{3}J_{HH}$=1Hz, CH_3), 2.58 (br s, ~3H, NH_2+OH), 2.87-2.97 (m, 1H, CH), 3.15 (overlapping dd, 1H, $^{2}J_{HH}$=8Hz, $^{3}J_{HH}$=1Hz, CH_2), 3.44 (ddd, 1H, $^{2}J_{HH}$=11Hz, $^{3}J_{HH}$=4Hz, $^{3}J_{HH}$=1Hz, CH_2)

^{13}C NMR (100 MHz, 298 K, $CDCl_3$) δ_C 19.4 (CH_3), 48.2 (CH), 67.8 (CH_2)

MS (ESI^+) m/z 76.1 ($[M+H]^+$), 98.1 ($[M+Na]^+$)

IR (cm^{-1}) ν 3347, 3280, 3167, 2961, 2897, 2870, 1592, 1457, 1376, 1353, 1310, 1268, 1214, 1146, 1119, 1055, 988, 969, 917, 833, 797

Optical rotation (589 nm, 293K, EtOH) *n* +20.49° (2.10 g/100 ml), lit. +21.4° (2.00g/100 ml).[21]

(*S*)-*Tert*-butyl 1-hydroxypropan-2-ylcarbamate[22]

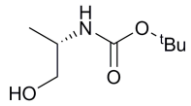

(*S*)-Alaninol (2.0 g, 26.6 mmol) was dissolved in aqueous NaOH solution (50 ml, 1 M) and was cooled in an ice/water bath. A solution of di-tert-butyldicarbonate (6.5 g, 30.0 mmol) in dioxane (30 ml) was added and the mixture was stirred for 3 h. The mixture was then allowed to separate. The aqueous layer was acidified to pH ≈ 8 using a saturated NH_4Cl solution and extracted with ethyl acetate (4 × 30 ml). The organic layer and ethyl acetate extracts were combined and the solvents were removed under reduced pressure. The obtained residue was extracted with ethyl acetate/hexane (1:2) mixture, filtered and the solvents were removed under reduced pressure. The obtained product was used in the subsequent step without further purification. Yield 3.3 g (71%).

^{1}H NMR (400 MHz, 298 K, $CDCl_3$) δ_H 4.78 (1H, s, N*H*), 3.73 (1H, s, C*H*), 3.59 (1H, dd, $^{3}J_{HH}$ = 10.8 Hz, $^{2}J_{HH}$ = 3.5 Hz, CH_2), 3.47 (1H, dd, $^{3}J_{HH}$ = 10.8 Hz, $^{2}J_{HH}$ = 6.0 Hz, CH_2), 3.06 (1H, s, O*H*), 1.42 (9H, s, ^{t}Bu), 1.12 (3H, d, $^{3}J_{HH}$ = 6.8 Hz, CHCH_3).

^{13}C NMR (100 MHz, 298 K, $CDCl_3$) δ_C 156.31 (C=O), 79.50 (*C*$(CH_3)_3$), 66.54 (CH_2), 48.38 (CH), 28.40 (C(*C*$H_3)_3$), 17.33 (CH*C*H_3).

MS (ESI^+) m/z 198.2 ($[M+Na]^+$)

MS (ESI^-) m/z 174.8 ($[M]^-$)

IR (cm^{-1}) ν 3445, 3340, 2977, 2938, 2878, 1675, 1650, 1531, 1456, 1393, 1363, 1344, 1313, 1277, 1251, 1160, 1102, 1060, 1025, 934, 915, 880, 843, 781, 754.

(*S*)-2-(*Tert*-butoxycarbonylamino)propyl methanesulfonate (21)[15]

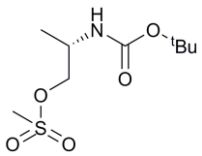

A solution of methanesulfonyl chloride (0.93 ml, 12 mmol) in DCM (20 ml) was added dropwise over 30 min to a solution of (*S*)-tert-butyl 1-hydroxypropan-2-ylcarbamate (2.0 g, 11 mmol) and TEA (1.8 ml, 12.5 mmol) in DCM (40 ml). The volatiles were then removed under reduced pressure and the residue was redissolved in ethyl acetate (30 ml) and water (30 ml). The organic layer was washed with an aqueous solution of $NaHCO_3$ (30 ml, 5%), brine (30 ml) and dried over anhydrous Na_2SO_4. The product was obtained upon removal of the solvent under reduced pressure and used without further purfication. Yield 2.1 g (75%).

^{1}H NMR (400 MHz, 298 K, $CDCl_3$) δ_H 4.65 (1H, s, NH), 4.27 – 4.17 (1H, m, CH_2), 4.14 (1H, dd, $^{3}J_{HH}$ = 10.0 Hz, $^{2}J_{HH}$ = 4.3 Hz, CH_2), 4.02 – 3.90 (1H, m, CH), 3.02 (3H, s, SO_3CH_3), 1.43 (9H, s, ^{t}Bu), 1.22 (3H, d, $^{3}J_{HH}$ = 6.9 Hz, CHCH_3).

^{13}C NMR (100 MHz, 298 K, $CDCl_3$) δ_C 155.22 (C=O), 72.17 (CH_2), 45.65 (CH), 37.45 (SO_3CH_3), 28.45 ($C(CH_3)_3$), 17.30 ($CHCH_3$), no quaternary carbon peak found

MS (ESI^+) m/z 276.1 ($[M+Na]^+$)

IR (cm^{-1}) ν 3358, 2978, 2937, 1687, 1527, 1463, 1430, 1394, 1368, 1347, 1331, 1301, 1279, 1242, 1159, 1109, 1061, 1031, 996, 972, 941, 927, 900, 850, 812, 779, 743.

(*S*)-2-Aminopropyl methanesulfonate hydrochloride (20)[15]

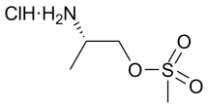

A solution of (*S*)-2-(tert-butoxycarbonylamino)propyl methanesulfonate (2.0 g, 7.9 mmol) in dioxane (10 ml) was acidified with an aqueous solution of HCl (10 ml, 4 M) and was stirred for 1 h. The volatiles were removed under reduced pressure and the residue was washed with acetonitrile. Yield 0.84 g (56%).

^{1}H NMR (400 MHz, 298 K, MeOD) δ_H 4.44 (1H, dd, $^{3}J_{HH}$ = 11.2 Hz, $^{2}J_{HH}$ = 3.4 Hz, CH_2), 4.27 (1H, dd, $^{3}J_{HH}$ = 11.2 Hz, $^{2}J_{HH}$ = 6.8 Hz, CH_2), 3.73 – 3.62 (1H, m, CH), 3.19 (3H, s, SO_3CH_3), 1.37 (3H, d, $^{3}J_{HH}$ = 6.8 Hz, CHCH_3).

^{13}C NMR (100 MHz, 298 K, MeOD) δ_C 70.65 (CH_2), 47.93 (CH), 37.40 ($SO_3\mathit{C}H_3$), 15.06 (CH_3).

MS (ESI^+) m/z 154.2 ($[M\text{-}Cl]^+$)

IR (cm^{-1}) ν 2865, 2779, 2713, 2693, 2604, 2525, 2022, 1609, 1508, 1460, 1403, 1387, 1324, 1282, 1211, 1170, 1134, 1022, 998, 967, 947, 928, 852, 819, 769.

(*R*)-N-(Tetrathiafulvalene-4-ylmethylene)-1-phenylethylamine

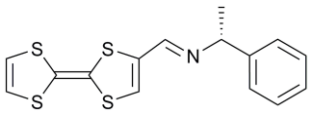

4-Formyltetrathiafulvalene (**13**) (0.100 g, 0.43 mmol) and (*R*)-α-methylbenzylamine (0.081 ml, 0.63 mmol) were dissolved in dry DCM (~10 ml) under argon and were heated to reflux over molecular sieves (4Å) under partial vacuum for 48 h. The reaction mixture was then allowed to cool and the solids were filtered off. The solvents were removed *in vacuo* and the residue was stored under argon.

Attempts to purify the product using column chromatography (silica), distillation/sublimation under high vacuum (10^{-6} mbar) resulted in decomposition.

^{1}H NMR (400 MHz, 298 K, CD_2Cl_2) δ_H 8.03 (1H, s, *H*C=N), 7.34 – 7.30 (5H, m, Ph), 6.76 (1H, s, TTF), 6.34 (2 H, q, $^7J_{HH}$ = 6.5 Hz, TTF), 4.45 (1H, q, $^3J_{HH}$ = 6.6 Hz, C*H*CH_3), 1.50 (3H, d, $^3J_{HH}$ = 6.6 Hz, CH_3).

(*R*)-2-(Tetrathiafulvalen-2-ylmethyleneamino)-2-phenylethanol

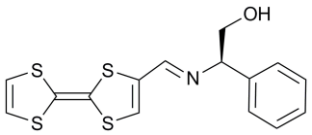

4-Formyltetrathiafulvalene (**13**) (0.100 g, 0.43 mmol) and (*R*)-phenylglycinol (0.065 g, 0.47 mmol) were dissolved in dry DCM (~10 ml) under argon and were heated to reflux over molecular sieves (4Å) under partial vacuum for 48 h. The reaction mixture was then allowed to cool and the solids were filtered off. The solvents were removed in vacuo and the residue was stored under argon.

Attempts to purify the product using column chromatography (silica), distillation/sublimation under high vacuum (10^{-6} mbar) resulted in decomposition.

^{1}H NMR (400 MHz, 298 K, CD_2Cl_2) δ_H 8.08 (1H, s, *H*C=N), 7.41 – 7.31 (5H, m, Ph), 6.83 (1H, s, TTF), 6.36 (2H, q, $^{7}J_{HH}$ = 6.6 Hz, TTF), 4.39 (1H, dd, $^{3}J_{HH}$ = 12.2 Hz, $^{3}J_{HH}$ = 5.7 Hz, C*H*CH_2), 3.87 – 3.77 (2H, m, CH_2).

(±)-6,6'-Dimethyl-N^2,$N^{2'}$-bis(tetrathiafulvalen-2-ylmethylene)biphenyl-2,2'-diamine ((±)-biphTTF)

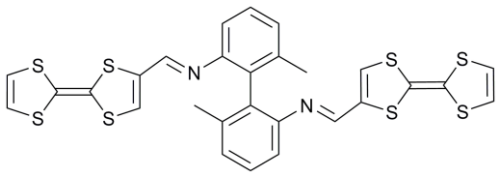

(±)-6,6'-Dimethyl-2,2'-biphenyldiamine (0.046 g, 0.215 mmol) was dissolved in dry THF (10 ml) in a Rotaflo ampoule under argon. Dry TEA (0.36 ml, 2.58

mmol) was added dropwise and the solution was cooled in a water/ice bath. $TiCl_4(THF)_2$ (0.113 g, 0.34 mmol) was dissolved in dry THF (10 ml) and added dropwise. The reaction mixture was stirred vigorously for 10 min and 4-formyltetrathiafulvalene (0.100 g, 0.43 mmol) in dry THF (10 ml) was added in one portion. The cooling bath was removed and the mixture was heated to reflux (~65°C) under static vacuum for 2 h. The mixture was diluted with DCM (20 ml), washed with water (3 × 20 ml) and dried over Na_2SO_4. The solvents were removed under reduced pressure and the residue was dried *in vacuo*. Yield 0.110 g (80%).

The product can be additionally purified by flash chromatography using DCM as eluent. Low yields are however obtained, due to decomposition of the compound on silica. Yield 0.070 g (51%).

Elemental analysis found (calculated for $C_{28}H_{20}N_2S_8 \cdot ½CH_2Cl_2$) %: C 50.46 (50.08), H 2.60 (3.10), N 4.02 (4.10)

^{1}H NMR (400 MHz, 298 K, CD_3Cl) δ_H 7.92 (2H, s, C*H*=N), 7.22 (2H, t, $^3J_{HH}$ = 7.2 Hz, Ph), 7.10 (2H, d, $^3J_{HH}$ = 6.8 Hz, Ph), 6.75 (2H, d, $^3J_{HH}$ = 8.7 Hz, Ph), 6.73 (2H, s, C*H*=C), 6.35 – 6.21 (4H, m, C*H*=C*H*), 1.99 (6H, s, CH_3).

^{1}H NMR (400 MHz, 298 K, CD_2Cl_2) δ_H, 7.98 (2H, s, C*H*=N) 7.28 (2H, t, $^3J_{HH}$ = 7.7 Hz, Ph), 7.17 (2H, d, $^3J_{HH}$ = 7.5 Hz, Ph), 6.84 (2H, s, C*H*=C), 6.80 (2H, d, $^3J_{HH}$ = 7.7 Hz, Ph), 6.40 – 6.30 (4H, m, C*H*=C*H*), 2.01 (6H, s, CH_3)

^{13}C NMR (100 MHz, 298 K, CD_2Cl_2) δ_C 19.7 (CH_3), 115.6, 119.1, 119.4 (TTF), 127.5, 128.1, 128.2 (Ph), 132.1, 137.3, 139.1 (Ph), 150.0 (TTF), 150.5 (CH=N)

MS (ESI^+) m/z 641.0 ($[M]^+$)

IR (cm^{-1}) ν 1611, 1563, 1534, 1463, 1376, 1284, 1218, 1149, 1106, 1090, 1033, 939, 859, 826, 775, 737, 693

(*R*)-6,6'-Dimethyl-N^2,$N^{2'}$-bis(tetrathiafulvalen-2-ylmethylene)biphenyl-2,2'-diamine ((*R*)-biphTTF)

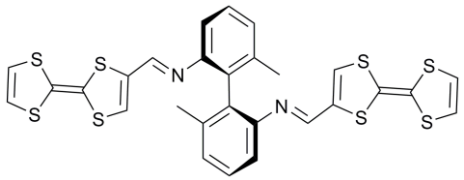

(*R*)-BiphTTF was prepared analogously to (±)-biphTTF using (*R*)-6,6'-Dimethyl-2,2'-biphenyldiamine (0.046 g, 0.215 mmol). Yield 55 mg (40 %, after column).

^{1}H NMR (400 MHz, 298 K, CD_2Cl_2) δ_H 7.92 (2H, s, C*H*=N), 7.22 (2H, t, $^3J_{HH}$ = 7.7 Hz, Ph), 7.10 (2H, d, $^3J_{HH}$ = 7.5 Hz, Ph), 6.75 (2H, d, $^3J_{HH}$ = 7.8 Hz, Ph), 6.73 (2H, s, TTF), 6.30 – 6.24 (4 H, m, TTF), 1.99 (6H, s, CH_3).

The data was found to be in excellent agreement with these obtained for (±)-biphTTF.

$[Cu^{I}_2((\pm)\text{-biphTTF})_2](BF_4)_2 \cdot 0.5H_2O \cdot 1.5CH_2Cl_2$

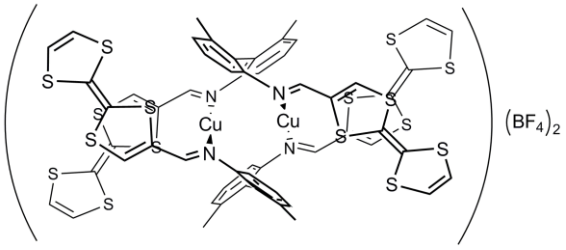

Tetrakis(acetonitrile)copper(I) tetrafluoroborate (9.8 mg, 31.2 μmol) and (±)-biphTTF (20 mg, 31.2 μmol) were dissolved in a minimal amount of dry DCM

under argon and stirred for 30 min. The product was collected by filtration. Yield 18 mg (57 %).

Single crystals suitable for X-ray diffraction were obtained from the filtrate after 30 days at -30°C.

Elemental analysis found (calculated for $C_{57.5}H_{44}B_2Cl_3Cu_2F_8N_4OS_{16}$) %: 40.05 (40.17), H 2.18 (2.58), N 3.75 (3.26).

MS (ESI^+) m/z 1407.8 ($[M]^+$), 702.7 ($[M]^{2+}$), 662.9 ($[L+Na]^+$)

Experimental Details for Chapter 3

Pyridine-2,6-dicarbonyl dichloride[23]

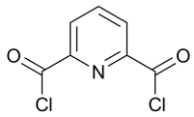

Pyridine-2,6-dicarboxylic acid (18.3 g, 0.11 mol) and thionyl chloride (19 ml) were dissolved in dioxane (50 ml) and heated to reflux for 3 h at 105°C. The solvent and excess thionyl chloride were removed under reduced pressure. The residue was distilled under vacuum (180-190°C, $4 \cdot 10^{-3}$ mbar). Yield 15.9 g (71%).

Elemental Analysis found (Calculated for $C_6H_4S_4$) % C 41.38 (41.21), H 1.65 (1.48), N 6.90 (6.86), Cl 31.18 (34.75).

^{1}H NMR (400 MHz, 298 K, $CDCl_3$) δ_H 8.16 (t, 1H, $_3J_{HH}$=8Hz, Ph-H), 8.36 (d, 2H, $_3J_{HH}$=8Hz, Ph-H)

^{13}C NMR (100 MHz, 298 K, CDCl3) δC 129.0, 139.4, 149.2, 169.4

MS (ESI^+) m/z 167.9 ($[M-Cl]^-$)

IR (cm^{-1}) ν 2744, 2599, 2555, 2453, 1747, 1608, 1576, 1405, 1242, 1199, 1157, 995, 954, 864, 828, 733, 706, 667

(*R*)-2-Methoxy-1-phenylethan-1-amine [(*R*)-2-phenylglycinol methyl ether][24]

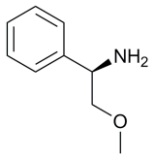

A solution of (*R*)-2-phenylglycinol (1.0 g, 7.3 mmol) in dry THF (10 ml) was transferred under argon into a suspension of sodium hydride (0.36 g, 15 mmol) in dry THF (5 ml) and was stirred for 1 h under static vacuum. Iodomethane (0.48 ml, 7.7 mmol) was added dropwise, and the mixture was stirred for further 1 h before heating to reflux under static vacuum for 2 h. The cooled mixture was diluted with a saturated sodium chloride solution and extracted with diethyl ether (3×20 ml). The extracts were dried over $MgSO_4$ and the solvents were removed under reduced pressure. The residue was distilled under vacuum (70°C, $4 \cdot 10^{-3}$ mbar) . Yield 0.63 g (57%).

Elemental analysis found (calculated for $C_9H_{13}NO$) %: 71.01 (71.49), H 8.65 (8.67), N 8.92 (9.26).

^{1}H NMR (400 MHz, 298 K, $CDCl_3$) δ_H 7.18-7.35 (m, 5H, Ph-H), 4.14 (dd, 1H, $^3J_{HH}$=9Hz, $^3J_{HH}$=4Hz, CH), 3.45 (dd, 1H, $^2J_{HH}$=9Hz, $^3J_{HH}$=4Hz, CH_2), 3.29-3.34 (m, 4H, CH_2, CH_3), 1.65 (s, 2H, NH_2)

^{13}C NMR (100 MHz, 298 K, $CDCl_3$) δ_C 142.4, 128.4, 127.3, 126.7 (Ph), 78.9 (CH_2), 58.9 (OCH_3), 55.3 (CH)

MS (ESI^+) m/z 135.0 ($[M\text{-}NH_2]^+$)

IR (cm^{-1}) ν 3028 w, 2888 m, 1603 w, 1493 m, 1453 m, 1355 w, 1194 m, 1111 s, 968 m, 844 m, 758/700 s

(*S*)-1-Methoxypropan-2-amine (L-alaninol methyl ether)[24]

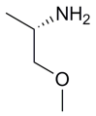

Sodium hydride (1.27 g, 53.0 mmol) was suspended in dry THF and was stirred for 1h under argon. L-alaninol (2.07 ml, 26.6 mmol) was added and the mixture was stirred for further 1h under static vacuum. Iodomethane (1.68 ml, 27 mmol) was added dropwise and the mixture was heated to reflux under static vacuum overnight. The mixture was then quenched with brine (50 ml) and extracted with diethyl ether (3 × 40 ml). The combined organic extracts were dried over sodium sulfate and the solvent was removed under reduced pressure. The residue was distilled under atmospheric pressure (~95°C) to obtain clear oil. Yield 1.15 g (49%).

^{1}H NMR (400 MHz, 298 K, $CDCl_3$) δ_H 3.15 – 3.08 (m, 3H, OC*H*$_3$), 3.08 – 3.00 (m, 1H, C*H*), 2.92 – 2.80 (m, 2H, C*H*$_2$), 1.12 (s, 2H, N*H*$_2$), 0.83 – 0.75 (m, 3H, CHC*H*$_3$).

^{13}C NMR (100 MHz, 298 K, $CDCl_3$) δ_C 79.45 (*C*H$_2$), 58.47 (O*C*H$_3$), 46.04 (*C*H), 19.52 (CH$_2$*C*H$_3$).

MS (ESI^+) m/z 90.2 ($[M+H]^+$)

IR (cm^{-1}) ν 2962, 2925, 2877, 1590, 1452, 1377, 1350, 1196, 1155, 1106, 966, 877, 833

N^2,N^6-Bis((*R*)-α-methylbenzyl)pyridine-2,6-dicarboxamide (H_2L^3)

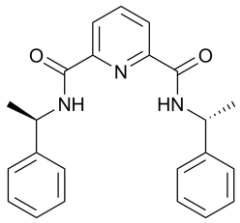

Pyridine-2,6-dicarbonyl dichloride (2.04 g, 10 mmol) was dissolved in dry DCM (50 ml). (*R*)-(+)-α-methylbenzylamine (2.42g, 2.54 ml, 20mmol) and dry triethylamine (2.02g, 2.8 ml, 20mmol) were added dropwise and the solution was stirred for 2 h. The reaction mixture was then washed with water (3×50 ml) and dried over $MgSO_4$. The solvent was removed under reduced pressure and the obtained solid was recrystallised from DCM/pentane. Yield 2.7 g (72%).

Elemental Analysis found (Calculated for $C_{23}H_{23}N_3O_2$) %: C 73.63 (73.97), H 6.50 (6.21), N 10.99 (11.25).

^{1}H NMR (300 MHz, 298 K, $CDCl_3$) δ_H 1.62 (6H, d, $^3J_{HH}$=7Hz, CH_3), 5.31 (2H, pent, $^3J_{HH}$=7Hz, C-H), 7.35 (11H, m, Ar-H), 8.03 (1H, t, $^3J_{HH}$=7Hz, Ar-H), 8.35 (2H, d, $^3J_{HH}$=8Hz, Ar-H)

^{13}C NMR (100 MHz, 298 K, $CDCl_3$) δ_C 21.9 (CH_3), 49.1 (C-H), 125.1 (ph), 126.1, 127.6, 128.9, 139.1 (pyr), 143.0, 148.8, 162.6 (C=O)

MS (ESI^+)m/z 396.17 ($[M+Na]^+$)

IR (cm^{-1}) ν 3610, 3395 (N-H), 1713, 1663 (C=O), 1508 (N-H), 1445 (C-C ar.),1256, 1183, 1100, 1073 (C-H ar.), 1000, 840, 698 (C-H ar)

N^2,N^6-Bis((*S*)-1-methoxypropan-2-yl)pyridine-2,6-dicarboxyamide (H_2L^4)

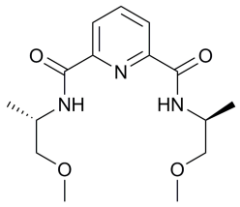

Pyridine-2,6-dicarbonyl dichloride (1.0 g, 4.8 mmol) was dissolved in dry DCM (20 ml) under argon. *S*-(+)-1-methoxy-2-propylamine (1.08 ml, 10.2 mmol) was added dropwise and the mixture was stirred for 15 min. Dry TEA (~6 ml) was added and the mixture was stirred at ambient temperature overnight. The mixture was then washed with water (3 × 20 ml) and dried over sodium sulphate. The solvent was removed under reduced pressure and the residue was recrystallised from DCM/pentane. Yield 1.2 g (78%).

Elemental Analysis found (Calculated for $C_{15}H_{23}N_3O_4$) %: C 58.45 (58.24), H 7.60 (7.49), N 13.64 (13.58)

^{1}H NMR (400 MHz, 298 K, $CDCl_3$) δ_H 1.33 (6H, d, $^3J_{HH}$ = 6.8 Hz, -CH_3), 3.42 (6H, s, -OCH_3), 3.46-3.56 (4H, m, CH_2), 4.29-4.42 (2H, m, CH), 7.92-8.05 (3H, m (s+t), NH, py), 8.32 (2H, d, $^3J_{HH}$ = 7.8 Hz, pyr)

^{13}C NMR (100 MHz, 298 K, $CDCl_3$) δ_C 17.7 (-*C*H_3), 45.0 (CH), 59.1 (-O*C*H_3), 75.4 (*C*H_2), 124.8, 138.9, 148.8 (py), 162.8 (C=O)

MS (ESI^+) m/z 332.1 ($[M+Na]^+$); (ESI^-) m/z 308.1 ($[M-H]^-$)

IR (cm^{-1}) ν 3327, 2974, 2930, 2879, 2831, 1651, 1519, 1440, 1393, 1365, 1353, 1325, 1303, 1255, 1230, 1203, 1173, 1150, 1108, 1080, 1062, 997, 978, 925, 847, 758, 726

N^2,N^6-Bis((*R*)-carboxy(phenyl)methyl)pyridine-2,6-dicarboxamide (H_2L^5)[25]

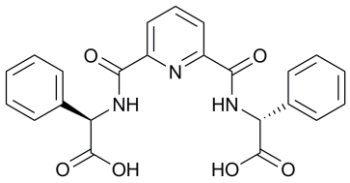

(*R*)-2-phenylglycine (1.53 g, 10.2 mmol) was suspended in water (25 ml) and solid KOH was added until the solution cleared. The mixture was chilled in an ice/water bath and pyridine-2,6-dicarbonyl chloride (1.04 g, 5.1 mmol) in DCM (25 ml) was added. The mixture was stirred for 0.5 h in an ice/water bath, then for another 0.5 h at ambient temperature. The DCM layer was discarded. The aqueous layer was diluted with a further 100 ml of water and was acidified with formic acid (6 ml of conc. HCOOH in 30 ml of water) until turbidity developed. The solution was left to crystallise overnight. The product was filtered, washed successively with water, ethanol and diethyl ether and dried *in vacuo*. The filtrate was concentrated to obtain the second crop. The combined product was recrystallised from methanol/water. Yield 0.55 g (25%).

Elemental analysis found (calculated for $C_{23}H_{19}N_3O_6 \cdot 3H_2O$) %: C 56.91 (56.67), H 5.17 (5.17), N 8.55 (8.62).

^{1}H NMR (400 MHz, 298 K, $CDCl_3$) δ_H 5.71 (s, 2H, CH), 7.31-7.43 (m, 6H, Ph-H), 7.54 (d, 4H, $^{3}J_{HH}$=8Hz, Ph-H), 8.13 (t, 1H, $^{3}J_{HH}$=8Hz, pyr), 8.26 (d, 2H, $^{3}J_{HH}$=8Hz)

^{13}C NMR (100 MHz, 298 K, $CDCl_3$) δ_C 58.2 (CH), 126.4, 128.7, 129.5, 130.0 (Ph), 138.0, 140.7, 150.0 (pyr), 165.3 (C=O), 153.6 (COOH)

MS (ESI^+) m/z 456.12 [$(M+Na)^+$), 889.24 ([$2M+Na]^+$)

IR (cm^{-1}) ν 3391, 3036, 1725, 1669, 1513, 1442, 1389, 1319, 1253, 1182, 1095, 1074, 1030, 1001, 967, 843, 749, 724, 695, 663

N^2,N^6-Bis((*S*)-carboxy(isopropyl)methyl)pyridine-2,6-dicarboxamide (H_2L^6)

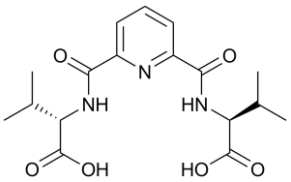

Prepared analogously to H_2L^5 using L-Valine (1.2 g, 10.2 mmol). The product was collected without recrystallisation. Yield 0.73 g (39%).

Elemental analysis found (calculated for $C_{17}H_{23}N_3O_6 \cdot 0.5H_2O$) %: C 54.26 (54.54), H 6.42 (6.46), N 11.09 (11.22).

^{1}H NMR (400 MHz, 298 K, $CDCl_3$) δ^H 1.08 (dd, 12H, $^{3}J_{HH}$=7Hz, $^{4}J_{HH}$=2Hz, CH_3), 2.37 (overlapping d sept, 2H, $^{3}J_{HH}$=6Hz, $^{3}J_{HH}$=7Hz, CH), 4.55-4.60 (m, 2H, CH), 8.20 (dd, 1H, $^{3}J_{HH}$=7Hz, $^{3}J_{HH}$=8Hz, pyr), 8.30 (d, 2H, $^{3}J_{HH}$=8Hz, pyr), 8.90 (d, 2H, $^{3}J_{HH}$=9Hz, NH)

^{13}C NMR (100 MHz, 298 K $CDCl_3$) δ_C 18.4, 19.7 (CH_3), 32.2 (CH), 59.3 (CH), 126.3, 140.9, 150.0 (pyr), 165.6 (C=O), 174.5 (COOH)

MS (ESI^+)m/z 388.15 ($[M+Na]^+$), 753.31 ($[2M+Na]^+$)

IR (cm^{-1}) ν 3373, 2964, 1734, 1670, 1648, 1569, 1520, 1448, 1402, 1373, 1347, 1311, 1289, 1260, 1227, 1202, 1185, 1129, 1089, 1074, 1038, 1004, 957, 840, 745, 719, 655

N^2,N^6-Bis((*R*)-(2-methoxy-2-oxoethyl)(phenyl)methyl)pyridine-2,6-dicarboxamide (H_2L^7)

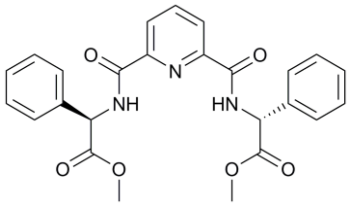

(*R*)-2-Phenylglycine methyl ester hydrochloride (4.03 g, 20 mmol) was dissolved in dry DCM (40 ml) under argon. Dry TEA (8.4 ml, 60 mmol) was added, and the resulting mixture was filtered into a solution of pyridine-2,6-dicarbonyl chloride (2.04 g, 10 mmol) in dry DCM (40 ml). The reaction was stirred overnight. The resulting mixture was washed with water (3 × 40 ml) and dried over sodium sulphate. The solvents were removed under reduced pressure to obtain a yellow oil. Recrystallisation from DCM/pentane yielded white crystalline solid. Yield 2.3 g (49%).

Elemental analysis found (calculated for $C_{25}H_{23}N_3O_6 \cdot CH_2Cl_2$) %: C 60.51 (60.78), H 4.77 (4.80), N 8.43 (8.34)

^{1}H NMR (400 MHz, 298K, $CDCl_3$) δ_H 8.81 (d, 2H, $^{3}J_{HH}$ = 6.6 Hz, NH_2), 8.31 (d, 2H, $^{3}J_{HH}$ = 7.7 Hz, pyr), 8.02 (t, 1H, $^{3}J_{HH}$ = 7.7 Hz, pyr), 7.52 (d, 4H $^{3}J_{HH}$ = 6.8 Hz, Ph), 7.46 – 7.30 (m, 6H, Ph), 5.75 (d, 2H, $^{3}J_{HH}$ = 7.0 Hz, CH), 5.29 (s, >1H, DCM), 3.79 (s, 6H, OCH_3).

^{13}C NMR (100 MHz, 298K, CDCl3) δ_C 171.02 (*C*ONH), 162.78 (*C*OO), 148.40 (Ph), 139.27, 136.36 (pyr), 129.25, 128.81, 127.38 (Ph), 125.45 (pyr), 56.87 (*C*H), 53.10 (O*C*H$_3$).

MS (ESI$^+$) m/z 462.1 ([M+H]$^+$), 484.1 9[M+Na]$^+$); (ESI$^-$) m/z 460.1 ([M-H]$^-$)

IR (cm^{-1}) ν 3379, 2957, 1735, 1677, 1587, 1569, 1505, 1437, 1355, 1326, 1257, 1215, 1195, 1173, 1100, 1072, 998, 945, 926, 859, 842, 788, 781, 754, 732, 695, 671

N^2,N^6-Bis((*R*)-2-hydroxy-1-phenylethyl) pyridine-2,6-dicarboxamide (H_2L^8)

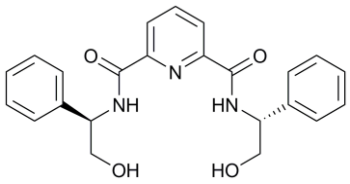

Pyridine-2,6-dicarbonyl chloride (2.24 g, 11 mmol) was dissolved in dry DCM (40 ml) under argon. A solution of (*R*)-2-phenylglycinol (2.98 g, 22 mmol) in dry DCM (40 ml) and TEA were added and the mixture was left stirred overnight. The solids were filtered off and the filtrate was washed with water (3 × 40 ml) and dried over sodium sulphate. The product was obtained upon slow addition of diethyl ether. Yield 2.6 g (59%).

Elemental analysis found (calculated for $C_{23}H_{23}N_3O_4 \cdot H_2O$) %: C 65.30 (65.24), H 5.72 (5.95), N 9.95 (9.92).

^{1}H NMR (400 MHz, 298 K, $CDCl_3$) δ_H 3.95 (d, 4H, $^3J_{HH}$=5Hz, CH_2), 5.18-5.26 (m, 2H, CH), 7.20-7.38 (m, 12H (incl. $CDCl_3$), Ph-H), 7.88 (t, 1H, $^3J_{HH}$=8Hz, pyr), 8.20 (d, 2H, $^3J_{HH}$=8Hz, pyr), 8.76 (d, 2H, $^3J_{HH}$ = 7Hz, NH)

^{13}C NMR (100 MHz, 298 K, $CDCl_3$) δ_C 55.9 (CH), 66.2 (CH_2), 125.1, 126.7, 127.8, 128.8 (Ph), 139.0, 139.0, 146.7 (pyr), 163.7 (C=O)

MS (ESI$^-$) m/z 404.1 ([M-H]$^-$)

IR (cm^{-1}) ν 3282, 1651, 1524, 1451, 1377, 1317, 1242, 1165, 1072, 1029, 999, 842, 750, 698

N^2,N^6-Bis((*R*)-2-methoxy-1-phenylethyl)pyridine-2,6-dicarboxamide (H_2L^9)

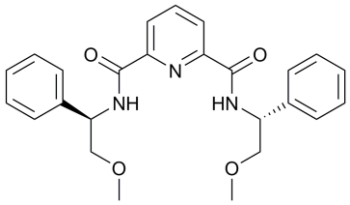

Prepared analogously to H_2L^8 using (*R*)-2-phenylglycinol methyl ether (3.02 g, 20 mmol). Yield 2.6 g (60%).

Elemental analysis found (calculated for $C_{25}H_{27}N_3O_4 \cdot ¼H_2O$) %: C 68.88 (68.54), H 6.64 (6.23), N 9.46 (9.59).

^{1}H NMR (400 MHz, 298 K, $CDCl_3$) δ_H 3.35, (s, 6H, CH_3), 3.76 (d, 4H, $^3J_{HH}$=5Hz, CH_2), 5.35-5.40 (m, 2H, CH), 7.20-7.45 (m, 12H (incl. $CDCl_3$), Ph-H), 7.96 (t, 1H, $^3J_{HH}$=8Hz, pyr), 8.29 (d, 2H, $^3J_{HH}$=8Hz, pyr), 8.52 (d, 2H, $^3J_{HH}$ = 9Hz, NH)

^{13}C NMR (100 MHz, 298 K, $CDCl_3$) δ_C 52.7 (CH), 59.1 (CH_3), 75.1 (CH_2), 125.0 (pyr), 126.8, 127.6, 128.6 (Ph), 139.0, 139.7 (pyr), 148.7 (Ph) 162.8 (C=O)

MS (ESI^+) m/z 434.1 ($[M+H]^+$); (ESI^-) m/z 432.1 ($[M-H]^-$)

IR (cm^{-1}) ν 3315, 3065, 2928, 2894, 2812, 1675, 1652, 1524, 1452, 1414, 1383, 1360, 1309, 1253, 1198, 1121, 1030, 1000, 973, 846, 753, 698, 663

(18-Crown-6)K[$Co^{III}(L^3)_2$] (24)

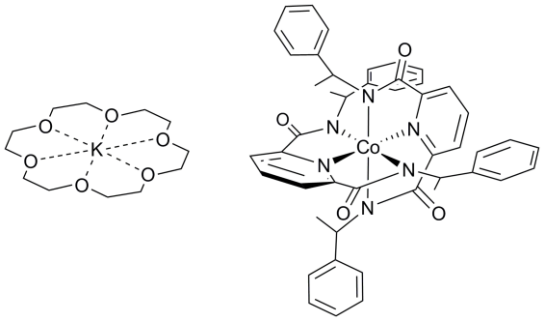

KH (0.08 g, 1.34 mmol) and *N*^{2},*N*^{6}-bis((R)-α-methylbenzyl)pyridine-2,6-dicarboxamide (H_2L^3) (0.250 g, 0.67 mmol) were dissolved in dry THF (15 ml) under argon and stirred for 1 h. A solution of $CoCl_2$ (0.045 g, 0.34 mmol) in dry MeCN (15 ml) was added and stirred under argon overnight. The solution was left for oxidation in air and then filtered. The precipitate was redissolved in MeCN, solid 18-crown-6 (0.09g, 0.34mmol) was added and the solution was stirred overnight. The reaction mixture was concentrated, and crystallised upon slow addition of Et_2O. Yield 0.122g, 0.14 g (38%).

Elemental analysis found (calculated for $C_{58}H_{66}CoKN_6O_{10}$) %: C 62.57 (63.03), H 6.11 (6.02), N 7.79 (7.60).

^{1}H NMR (300 MHz, 298K, CD_3CN) δ^{H} 8.26 (2H, t, $^{3}J_{HH}$=8Hz, Ar-H), 7.90 (4H, d, $^{3}J_{HH}$=8Hz, Ar-H), 6.87 (20H, m, Ar-H), 3.57 (24H, s, C-H, crown), 2.68 (4H, q, $^{3}J_{HH}$=7Hz, C-H), 1.02 (12H, d, $^{3}J_{HH}$=7Hz, CH_3)

^{13}C NMR (100 MHz, 298 K, MeOD) δ_C 169.0 (C=O), 160.0, 144.4, 141.8 (pyr), 129.5, 128.6, 127.1, 125.2 (ph), 71.3 (crown) 57.4 (C-H), 20.8 (CH_3)

MS (ESI^+) m/z 303.0 ([(18-crown-6)K]$^+$); (ESI^-) m/z 801.4 ([M(L^3)$_2^-$])

IR (cm^{-1}) ν 2888, 1571, 1492, 1452, 1102, 956, 835, 775, 698, 685.

(18-Crown-6)K[Fe^{III}(L^3)$_2$]·2H_2O (25)

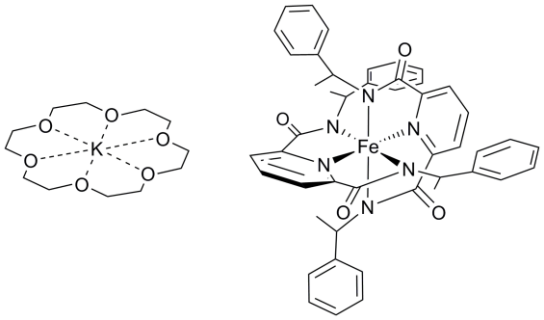

Compound was prepared analogously to **24** using $FeCl_2$ (0.043 g, 0.34 mmol). Yield 0.11 g (29%).

Elemental analysis found (calculated for $C_{58}H_{70}FeKN_6O_{12}$) %: C 61.20 (61.20), H 5.83 (6.20), N 7.34 (7.38).

MS (ESI^+) m/z 303.0 ([(18-crown-6)K]$^+$); (ESI^-) m/z 798.5 ([M(L^3)$_2^-$])

IR (cm^{-1}) ν 3059, 2901, 1565, 1492, 1452, 1386, 1352, 1324, 1287, 1251, 1216 1197, 1101, 1034, 1013, 953, 923, 864, 838, 773, 746, 735, 699, 690

$K[Co^{III}(L^4)]\cdot 3H_2O$ (26)

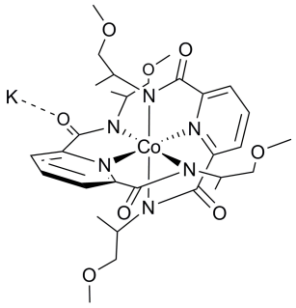

Sodium hydride (0.038 g, 0.96 mmol) and H_2L^4 (0.100 g, 0.32 mmol) were suspended in dry THF (10 ml) under argon and stirred under partial vacuum for 15 min. Cobalt(II) chloride (0.021 g, 0.16 mmol) in dry MeCN (10 ml) was then added dropwise and the mixture was stirred overnight under argon. The mixture was opened to air and stirred for 24 h. The solids were removed by filtration and a few drops of water were added to the filtrate. The crystalline product was obtained upon a slow addition of Et_2O. Yield 0.077 g (62.8%).

Elemental Analysis found (Calculated for $C_{30}H_{48}CoKN_6O_{11}$) %: C 47.06 (46.99), H 6.18 (6.31), N 10.80 (10.96)

^{1}H NMR (400 MHz, 298 K, CD_3CN) δ_H 0.89 (6H, d, $^2J_{HH}$ = 6.7 Hz, -CH_3), 1.49 (2H, s br, CH), 2.98 (6H, s, -OCH_3), 3.11 (2H, dd, $^3J_{HH}$ = 9.2 Hz, $^2J_{HH}$ = 3.5 Hz, CH_2), 3.67 (2H, t, $^3J_{HH}$ = 9.1 Hz, CH_2), 7.93 (2H, d, $^3J_{HH}$ = 7.7 Hz, pyr), 8.28 (1H, t, $^3J_{HH}$ = 7.7 Hz, pyr)

^{13}C NMR (100 MHz, 298 K, CD_3CN) δ_C 17.6 (-CH_3), 52.5 (CH), 58.3 (-OCH_3), 77.3 (CH_2), 123.6, 140.7, 159.1 (pyr), 167.8 (C=O)

MS (ESI^-) m/z 673.3 ($[M-K]^-$); MS (ESI^+) m/z 751.1 ($[M+K]^+$), 713.1 ($[M+H]^+$)

IR (cm^{-1}) ν 3510, 3039, 2974, 2936, 2824, 1571, 1449, 1425, 1397, 1387, 1357, 1336, 1317, 1227, 1198, 1146, 1086, 976, 943, 929, 893, 866, 847, 778, 685

(TTF)[$Co^{III}(L^3)_2$] (27)

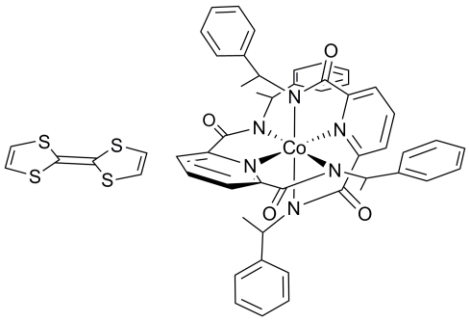

(18-crown-6)K[$Co^{III}(L^3)_2$] (**24**) (20 mg) was dissolved in dry THF (25 ml). Solid TTF (5 mg) was placed in the anode chamber of an electrocrystallisation cell, then the cell was carefully filled with the solution of the counterion. The cell was fitted with platinum electrodes and sealed. Constant current of 1μA was applied. After two weeks dark crystals suitable for X-ray diffraction and conductivity measurement were harvested.

IR (cm^{-1}) ν 1577, 1475, 1451, 1362, 1330, 1291, 1226, 1093, 1077, 1063, 822, 756,697, 682

(TTF)[$Fe^{III}(L^3)_2$]

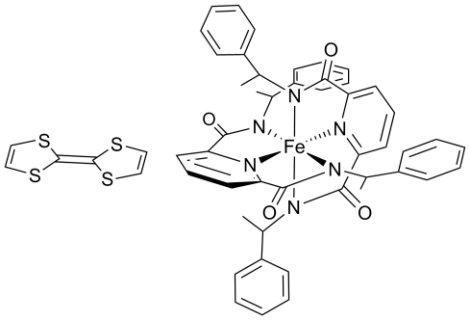

Obtained analogously to **27** using (18-crown-6)K[$Fe^{III}(L^3)_2$] (25) (20 mg). Dark microcrystalline solid collected. No crystals of quality suitable for X-ray diffraction or conductivity measurements were found.

IR (cm^{-1}) ν 1564, 1491, 1473, 1451, 1383, 1361, 1324, 1288, 1274, 1211, 1195, 1151, 1077, 1054, 1032, 1010, 947, 911, 868, 842, 824, 772, 756, 741.9, 786

$TTF_3(BF_4)_2$ [26]

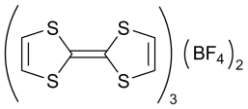

This procedure was performed by C.Hart and was included here for completeness.

Tetrathiafulvalene (0.80 g, 3.9 mmol) was dissolved in acetonitrile (30 ml). Hydrogen peroxide (30%, 0.13 ml, 1.3 mmol) was added to an ice cold fluoroboric acid solution (48%, 0.35 ml, 2.7 mmol). The solutions were mixed and left for crystallisation at 4°C for 2h. The product was collected by filtration without washing. The second crop was obtained after concentration of the filtrate. Yield 0.76 g (73%).

Elemental analysis found (calculated for $C_{18}H_{12}B_2F_8S_{12}$) %: C 27.47 (27.48), H 1.74 (1.54), S 48.65 (48.91).

MS (ESI^+) m/z 203.9 ($[TTF]^+$); MS (ESI^-) m/z 87.0 ($[BF_4]^-$)

IR (cm^{-1}) ν 1507, 1471, 1341 (C=C), 1290, 1274, 1254 1117 (B-F), 1023, 872, 836, 824, 798, 742, 731, 698, 668.

$(TTF)[Co^{III}(L^4)_2]\cdot EtOAc$

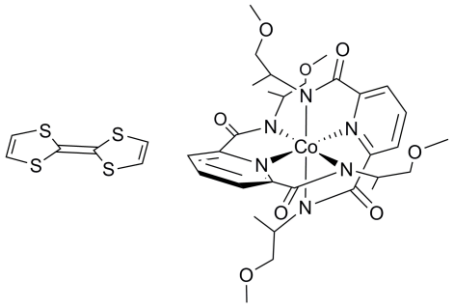

$TTF_3(BF_4)_2$ (10 mg, 12.9 μmol) was dissolved in a minimal amount of acetonitrile (~1 ml). $K[Co^{III}(L^4)_2]\cdot 3H_2O$ (19.5 mg, 25.4 μmol) was dissolved in a minimal amount of acetonitrile (~1 ml). The solutions were mixed slowly and filtered through a cotton wool plug. Dark crystalline solid was obtained by a slow diffusion of ethyl acetate into the solution. Single crystals suitable for X-ray diffraction and conductivity measurement were harvested.

MS (ESI^+) m/z 203.9 ($[TTF]^+$); MS (ESI^-) m/z 673.3 ($[Co^{III}(L^4)_2]^-$)

IR (cm^{-1}) ν 1716, 1571, 1506, 1574, 1452, 1394, 1374, 1357, 1347, 1312, 1294, 1272, 1231, 1193 1143, 1102, 1087, 1071, 1039, 965, 930, 900, 866, 845, 823.8, 778, 732, 682

Experimental Details for Chapter 4

$Na[Co^{III}(S,S\text{-}EDDS)]\cdot 2H_2O$ (29)[27]

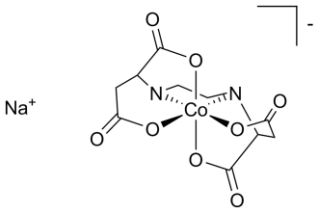

Cobalt(II) acetate tetrahydrate (7.45 g, 35.0 mmol), *S*,*S*-H_4EDDS (10.2 g, 35.0 mmol) and NaOH (1.4 g, 35.0 mmol) were dissolved in distilled water (30 ml). H_2O_2 (30%, 2 ml) was added dropwise and the mixture was stirred overnight. The mixture was concentrated to approximately half of the volume and the product was precipitated by the addition of ethanol. The solid was filtered, washed with ethanol and dried in air. The product was recrystallised by dissolution in a minimal amount of water followed by precipitation by the slow addition of ethanol. Yield 7.8 g (56%)

Elemental Analysis found (Calculated for $C_{10}H_{16}O_{10}CoN_2Na$) % C 29.66 (29.57), H 3.92 (3.97), N 6.86 (6.90).

^{1}H NMR (400 MHz, 298 K, D_2O) δ_H 2.81 (2H, m, CH_2NH), 2.98 (2H, d, $^3J_{HH}$ = 18 Hz, CHCH_2), 3.17-3.34 (4H, m, CH_2NH, CHCH_2), 3.56-3.63 (2H, m, CH).

^{13}C NMR (100 MHz, 298 K, D_2O) δ_C 37.0 (CH*C*H_2), 52.7 (*C*H_2NH), 65.4 (CH), 177.6 (C=O), 182.8 (C=O).

MS (ESI$^-$) m/z 346.9 ([M]$^-$), 302.9 ([M]$^-$ - COO), 259.0 ([M]$^-$ - 2×COO).

IR (cm^{-1}): 1563 s (ν_{as} COO), 1383 s (ν_s COO), 1209 m, 1134 w, 1040 m, 925 w, 879 m.

UV-Vis (λ_{max}/nm, ε/dm^{3}mol^{-1}cm^{-1}): 222 (17,200), 380 (130), 513 (290).

$NBu_4[Co^{III}(S,S\text{-}EDDS)]\cdot xH_2O$ (31)

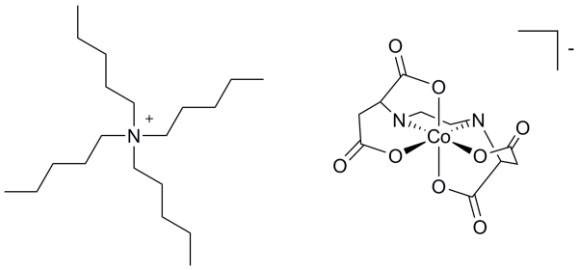

Cobalt(II) acetate tetrahydrate (0.74 g, 3.5 mmol), *S*,*S*-H_4EDDS (1.02 g, 3.5 mmol) and $NBu_4OH\cdot 30H_2O$ (2.8 g, 3.5 mmol) were dissolved in distilled water (5 ml). Additional $NBu_4OH\cdot 30H_2O$ was added until pH 10 and the mixture was stirred for 4 h. H_2O_2 (30%, 1 ml) was added dropwise and the mixture was stirred overnight. The solvent was removed under reduced pressure and the residue was redissolved in MeCN. The product separated as a thick highly hygroscopic purple oil upon the addition of Et_2O. The product was washed with Et_2O, dried and stored *in vacuo*. Yield 1.8 g.

^{1}H NMR (400 MHz, 298 K, D_2O) δ_H 6.07 (~1.4H, s, NH), 3.27 – 3.14 (2H, m, CH), 3.14 – 3.03 (8 H, m, $N(CH_2CH_2CH_2CH_3)_4$), 3.04 – 2.94 (2H, m, CH_2NH/CH_2CH), 2.94 – 2.78 (2 H, m, CH_2NH/CH_2CH), 2.75 – 2.52 (4H, m CH_2NH/CH_2CH), 1.65 – 1.54 (8H, m, $N(CH_2CH_2CH_2CH_3)_4$), 1.35 (8H, tq, $^3J_{HH}$ = 7.4 Hz, $N(CH_2CH_2CH_2CH_3)_4$), 0.97 (12 H, t, $^3J_{HH}$ = 7.3 Hz, $N(CH_2CH_2CH_2CH_3)_4$).

MS (ESI$^-$) m/z 346.9 ($[Co(S,S\text{-}EDDS)]^-$)

MS (ESI$^+$) m/z 242.2 ($[NBu_4]^+$)

$PPh_4[Co^{III}(S,S\text{-}EDDS)]\cdot 2H_2O$ (33)

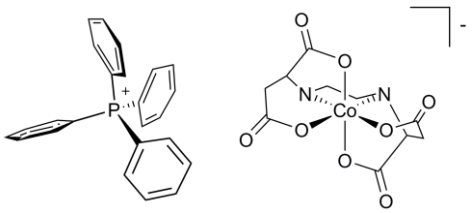

$Na[Co(S,S\text{-}EDDS)]\cdot 2H_2O$ (3.0 g, 8.1 mmol) was dissolved in a minimal amount of water (*ca* 10 ml). A solution of silver nitrate (4.19 g, 24.3 mmol) in water (10 ml) was added. The initial precipitate was removed by filtration and methanol was added slowly to the filtrate to induce precipitation. The product was filtered and washed with methanol. The $Ag[Co^{III}(S,S\text{-}EDDS)]\cdot xH_2O$ thus obtained (2.0 g, *ca* 4.4 mmol) was dissolved in water (10 ml). A solution of PPh_4Br (1.8 g, 4.4 mmol) in hot water (20 ml) was added. The precipitate (AgBr) was removed by filtration and the filtrate was evaporated to dryness under reduced pressure. The residue was dissolved in a minimal amount of hot acetonitrile, filtered and left to cool. A few drops of water were added and the crystallisation was initiated by the slow addition of ethyl acetate. Yield 0.53 g (10%).

Elemental Analysis found (Calculated for $C_{34}H_{36}O_{10}CoN_2P$) % C 56.15 (56.52), H 5.29 (5.02), N 3.92 (3.88).

^1H NMR (300 MHz, 298 K, CD_3CN) δ_H 2.54 (2H, dd, $^2J_{HH}$ = 17.8 Hz, $^3J_{HH}$ = 2.1 Hz), 2.64-2.82 (2H, m, CH_2NH), 2.82-3.04 (4H, m, CHCH_2/CH_2NH), 3.14-3.23 (2H, m, CH), 6.37 (2H, s, NH), 7.63-7.80 (16H, m, Ph), 7.87-7.97 (4H, m, Ph).

^{13}C NMR (100 MHz, 298 K, CD_3CN) δ_C 38.9, 53.5 (CH_2), 66.7 (CH), 131.2, 131.3, 135.6, 135.7, 136.3, 136.3 (Ph).

MS (ESI-) m/z 346.9 ([Co(S,S-EDDS)]-), 290.9 (H3EDDS-), 259.0

MS (ESI^+) m/z: 339.1 (PPh_4^+).

IR (cm^{-1}) ν 3527, 3411, 3232, 1650, 1597, 1484, 1438, 1376, 1354, 1311, 1276, 1211, 1195, 1162, 1110, 1060, 1032, 1000, 919, 893, 872, 821, 754, 723, 685.

UV-Vis (λ_{max}/nm, ε/$dm^3mol^{-1}cm^{-1}$): 256 sh (16100), 376 (320), 513 (480).

$NH_4[Fe^{III}(S,S\text{-}EDDS)]$ (34)[28]

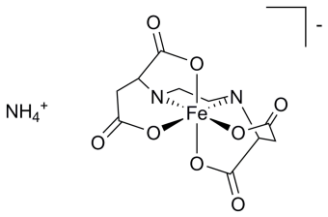

Anhydrous iron(III) chloride (4.00 g, 24.7 mmol) was dissolved in warm deionised water (6 ml). Ammonium hydroxide (9 ml, excess) was added dropwise with constant stirring. The mixture was heated to 150°C for 20 min and allowed to cool to ambient temperature. The red/brown solid (iron(III) hydroxide) was collected by filtration and washed with deionised water (2 × 100 ml) to remove chloride. Thus obtained iron(III) hydroxide and iron powder (0.07 g) were suspended in deionised water (14 ml). The mixture was heated to 75°C while *S*,*S*-H_4EDDS (7.21 g, 24.7 mmol) was added in portions, maintaining pH 6 throughout by the addition of NH_4OH. The resulting mixture was heated to 85°C for 45 min and allowed to cool to ambient temperature. The solids were removed by filtration and the filtrate was concentrated under reduced pressure. Methanol was added slowly to induce precipitation. The product, $NH_4[Fe^{III}$(*S*,*S*-EDDS)], was filtered, washed with methanol (2 × 50 ml) and dried *in vacuo*. The

product was recrystallised by dissolution in a minimal amount of water followed by precipitation by the slow addition of methanol. Yield 4.02 g (47%).

Elemental Analysis found (Calculated for $C_{10}H_{16}O_8FeN_3$) %: C 33.23 (33.17), H 4.58 (4.45), N 11.49 (11.60).

MS (ESI^-) m/z 343.9.

IR (cm^{-1}): 3158 m (NH_4), 1589 s (ν_{as} COO), 1358 s (ν_s COO), 1216, 1103 m, 1064 m, 1023 w, 996 m, 957 w, 913 m, 894 m, 859 m.

UV-Vis (λ_{max}/nm, ε/$dm^3mol^{-1}cm^{-1}$): 209 (9700), 240 (8500) br, ~285 sh (5200).

$PPh_4[Fe^{III}$(S,S-EDDS)]·$2H_2O$ (35)

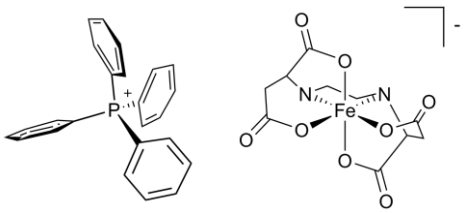

$NH_4[Fe^{III}$(*S*,*S*-EDDS)] (2.93 g, 8.1 mmol) was dissolved in the minimal amount of water (*ca* 10 ml). A solution of silver nitrate (4.19 g, 24.3 mmol) in water (10 ml) was added. The initial precipitate was removed by filtration and methanol was added slowly to the filtrate to induce precipitation. The product was filtered and washed with methanol. The $Ag[Fe^{III}$(*S*,*S*-EDDS)]·xH_2O thus obtained was dissolved in water (10 ml). A solution of PPh_4Br (1.8 g, 4.4 mmol) in hot water (20 ml) was added. The precipitate (AgBr) was filtered and the filtrate was evaporated to dryness under reduced pressure. The residue was dissolved in a minimal amount of hot acetonitrile, filtered and left to cool. A few drops of

water were added and the crystallisation was initiated by the slow addition of ethyl acetate. Yield 0.50 g (10%).

Elemental Analysis found (Calculated for $C_{34}H_{36}O_{10}FeN_2P$) % C 56.29 (56.76), H 5.29 (5.04), N 4.31 (3.89).

IR (cm^{-1}): 1614 s (ν_{as} COO), 1484 w, 1437 m, 1348 s, 1306 s (ν_{s} COO), 1199 m, 1108 s, 996 m, 910 m, 855 m, 805 m, 752 m, 722 s, 686 s.

MS (ESI^-) m/z 346.9 ($[Fe(S,S\text{-}EDDS)]^-$), 300.0, 256.0.

MS (ESI^+) m/z: 339.1 (PPh_4^+).

UV-Vis (λ_{max}/nm, ε/$dm^3mol^{-1}cm^{-1}$): 262 (9400), 268 (9800), 275 (8700), ~290 sh (4570).

$Ag[Cr^{III}(S,S\text{-}EDDS)]\cdot 1.5\ H_2O$ (36)

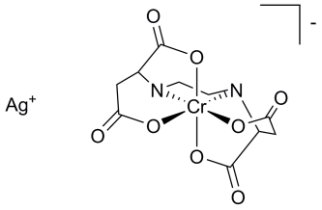

Barium hydroxide octahydrate (10.8 g, 34.0 mmol) and *S*,*S*-H_4EDDS (10.0 g, 34.0 mmol) were suspended in water (300 ml) and stirred at 70°C for 1 h. Solid chromium(III) sulphate (6.7 g, 17.0 mmol) was added and the mixture was stirred overnight at 70°C. The mixture was filtered and the barium sulfate precipitate was washed with water. The combined filtrates were concentrated to half volume and solid silver nitrate (5.8 g, 34.0 mmol) was added. The mixture was stirred for 1 h. A small amount of solid was removed by filtration

and methanol was added slowly to the filtrate to induce precipitation. The product was filtered off, washed with methanol and dried *in vacuo*. Yield 5.8 g (36 %).

Elemental Analysis found (Calculated for $C_{10}H_{15}AgCrN_2O_{9.5}$) %: C 25.34 (25.28), H 3.23 (3.18), N 5.80 (5.90).

MS (ESI^-) m/z: 339.9 ($[Cr(S,S\text{-}EDDS)]^-$).

IR (cm^{-1}): 1655 s, 1571 s (ν_{as} COO), 1380 s, 1352 s (ν_s COO), 1288 m, 1217 s, 1104 m, 1048 m, 1007 m, 921 m, 896 m, 867 s, 815 m, 712 m.

UV-Vis (λ_{max}/nm, ε/$dm^3mol^{-1}cm^{-1}$): 382 (230), 513 (320), ~700 sh (110).

$PPh_4[Cr^{III}(S,S\text{-}EDDS)]\cdot 2H_2O$ (37)

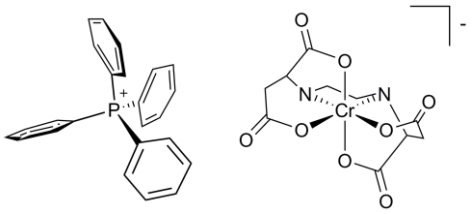

$Ag[Cr^{III}(S,S\text{-}EDDS)]\cdot 1.5H_2O$ (2.0 g, 4.5 mmol) was dissolved in a minimal amount of water. A solution of PPh_4Br (1.89 g, 4.4 mmol) in hot water was added. The mixture was stirred for 15 min. The precipitate was filtered and the filtrate was evaporated to dryness under reduced pressure. The residue was dissolved in a minimal amount of hot methanol, filtered and left to cool. A few drops of water were added and the crystallisation was initiated by the slow addition of ethyl acetate. Yield 0.8 g (25%).

Elemental Analysis found (Calculated for $C_{34}H_{36}O_{10}CrN_2P$) % C 57.37 (57.06), H 5.44 (5.07), N 3.69 (3.91).

IR (cm^{-1}): 1652 s, 1603 s (ν_{as} COO), 1484 w, 1438 m, 1369 m, 1354 m (ν_s COO), 1311m, 1214 m, 1198 m, 1161 w, 1107 s, 1030 m, 997 m, 954 w, 914 w, 890 m, 866 m, 812 m 755 m, 724 s, 683 s.

MS (ESI^-) m/z 339.9 ($[Cr(S,S\text{-}EDDS)]^-$).

MS (ESI^+) m/z: 339.1 (PPh_4^+).

UV-Vis (λ_{max}/nm, ε/$dm^3mol^{-1}cm^{-1}$): ~223 sh (40400), 262 (2700), 268 (4700), 275 (4000), 383 (280), 511 (360), ~700 sh (110).

^1H NMR (400 MHz, 298 K, CD_3CN) δ_C 0.96 (12H, t, $^3J_{HH}$ = 7.3 Hz), 1.35 (8H, sx, $^3J_{HH}$ = 7.4 Hz), 1.54-1.65 (8H, m), 2.53-2.75 (4H, m), 2.78-2.93 (2H, m), 2.95-3.05 (2H, m), 3.05-3.14 (8H, m), 3.15-3.25 (2H, m), 5.98-6.15 (~2H, s, br).

MS (ESI^+) m/z: 242.2 (NBu_4^+), (ESI^-)m/z: 346.9 ($[Co(S,S\text{-}EDDS)]^-$).

Experimental Details for Chapter 5

Synthesis of $[Ru^{II}(bpy)_3]Cl_2 \cdot 6H_2O$[29]

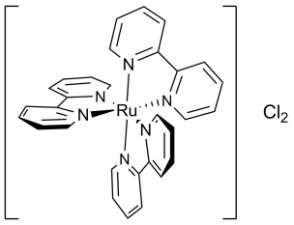

Ruthenium(III) chloride n-hydrate was dried over P_2O_5 *in vacuo* overnight. Fresh solution of sodium hypophosphite was prepared by dissolution of solid NaOH in 50% H_2PO_2 (10 ml) until a white precipitate appeared. The solution of 50% H_2PO_2 was then added dropwise until all of the precipitate dissolved. The prepared solution (7.5 ml), 2,2'-bipyridyl (4.5 g – 29 mmol) and dry $RuCl_3$ (2.0 g – 9.6 mmol) were suspended in distilled water (200 ml) and heated to reflux for 0.5 h. KCl (63 g) was added to the filtered solution and heated until all solids dissolved (small amount of water was added if necessary). The resulting mixture was filtered hot and left for crystallisation. Red/orange crystals of $Ru^{II}(bpy)_3]Cl_2 \cdot 6H_2O$ separated upon cooling. Yield 3.82 g (53%). The product was recrystallised from hot water.

Elemental Analysis found (Calculated for $C_{30}H_{36}O_6Cl_2N_6Ru$) % C 48.72 (48.13), H 4.38 (4.85), N 11.23 (11.23).

^{1}H NMR (400 MHz, 298 K, MeOD) δ_H 8.74 (3H, d, $^3J_{HH}$ = 8.1 Hz), 8.15 (3H, d, $^3J_{HH}$ 15.8 Hz), 7.84 (3H, d, $^3J_{HH}$ = 5.5 Hz), 7.52 (3H, t, $^3J_{HH}$ = 7.5 Hz).

^{13}C NMR (100 MHz, 298 K, MeOD) δ_C 158.52, 152.61, 139.27, 128.96, 125.68.

MS (ESI$^+$) m/z 285.05 ($[M\text{-}Cl_2]^{2+}$)

Resolution of $[Ru^{III}(bpy)_3]Cl_2 \cdot 6H_2O$[30]

Potassium iodide (0.17 g – 1.05 mmol) and potassium antimonyl tartrate 0.67 g – 2.07 mmmol) were co-dissolved in distilled water (20 ml) and added to a solution of $[Ru^{III}(bpy)_3]Cl_2 \cdot 6H_2O$ (1.0 g – 1.56 mmol) in distilled water (20 ml) and the resulting solution was left standing for 0.5 h. The mixture was then filtered and both filtrate and precipitate were collected.

Saturated KBr solution (2 ml) was added to the filtrate to initiate the crystallisation and the solution was left standing for 0.5 h. Separated solids were collected by filtration without washing and recrystallised twice from hot water to obtain Λ-$[Ru^{II}(bpy)_3]Br_2 \cdot 6H_2O$ (45 mg). (30% ee. HPLC)

The precipitate was washed with distilled water and dried in air. The solid was dissolved in hot (~80°C) 0.05 M NaOH solution (10 ml) and filtered immediately. Saturated KBr solution was added (2ml) to initiate the crystallisation. The separated solid was collected by filtration without washing and recrystallised twice from hot water, to obtain Δ-$[Ru^{II}(bpy)_3]Br_2 \cdot 6H_2O$ (53 mg). (60% ee. HPLC)

Resolution of $[Ru^{II}(bpy)_3]Cl_2 \cdot 6H_2O$ with $PPh_4[Fe^{III}(S,S\text{-}EDDS)] \cdot 2H_2O$

$PPh_4[Fe^{III}(S,S\text{-}EDDS)] \cdot 2H_2O$ (100 mg, 0.14 mmol) was dissolved in hot acetonitrile (10 ml), allowed to cool and filtered. $[Ru^{II}(bpy)_3]Cl_2 \cdot 6H_2O$ (178 mg, 0.28 mmol) was dissolved in acetonitrile (15 ml) and filtered. The prepared $PPh_4[Co^{III}(S,S\text{-}EDDS)]$ solution was added dropwise with stirring. The stirring was continued for further 5-10 min. The resulting mixture was filtered and both filtrate and precipitate were collected.

The precipitate was washed with acetonitrile (5 ml) and redissolved in methanol (10 ml). An excess of solid silver nitrate (71 mg, 0.42 mmol) was added and the mixture was stirred vigorously for 5 min. Precipitated solids were filtered off and the solvent was removed under reduced pressure. The residue was recrystallised from acetonitrile/diethyl ether to obtain Λ-$[Ru^{II}(bpy)_3](NO_3)_2$. (16 % ee., HPLC)

The filtrate was evaporated to dryness under reduced pressure, redissolved in methanol (10 ml) and underwent the same treatment as the precipitate to obtain Δ-$[Ru^{II}(bpy)_3](NO_3)_2$. (33 % ee., HPLC)

^{1}H NMR and CD spectra of the obtained compounds are consistent with the literature examples.[31,32]

General procedure for preparation of ^{1}H NMR samples of metal complexes for *ee* determination

$PPh_4[Co^{III}$(S,S-EDDS)]·$2H_2O$ (14.4 mg, 20.0 μmol) was dissolved in deuterated solvent (d^4-methanol or d^6-DMSO) (~0.6 ml) with heating. A sample of the appropriate complex (5.0 μmol) was dissolved in thus prepared solution and the auxiliary compound was added if necessary (5.0 μmol). The solution was filtered through a plug of cotton wool. The exact amounts and solvent combinations are listed below.

Compound (+,- and ±)-	Mass	Solvent	Auxiliary	Aux. Mass/vol.
$[Ru^{II}(bpy)_3]Cl_2$	3.2 mg	d^4-methanol	-	-
$[Ru^{II}(phen)_3](PF_6)_2$	4.7 mg	d^4-methanol/d^6-DMSO	HCl (conc.)	0.5 μl
$[Ru^{II}(phen)_3](PF_6)_2$	4.7 mg	d^4-methanol/d^6-DMSO	DCl in D_2O ($35\%_{wt}$)	0.5 μl

Compound (+,- and ±)-	Mass	Solvent	Auxiliary	Aux. Mass/vol.
$[Co^{II}(phen)_3](ClO_4)_2$	4.0 mg	d^4-methanol/d^6-DMSO	-	-
$[Fe^{II}(phen)_3](ClO_4)_2$	4.0 mg	d^4-methanol/d^6-DMSO	-	-
$[Co^{III}(en)_3]I_3$	3.1 mg	d^6-DMSO	HCl (conc.)	0.5 µl
$[Co^{III}(en)_3]I_3$	3.1 mg	d^6-DMSO	DCl in D_2O ($35\%_{wt}$)	0.5 µl
$[Co^{III}(en)_3]I_3$	3.1 mg	d^6-DMSO	HNO_3 (conc.)	0.3 µl
$[Co^{III}(en)_3]I_3$	3.1 mg	d^6-DMSO	$HClO_4$ (60%)	0.6 µl
$[Co^{III}(en)_3]I_3$	3.1 mg	d^6-DMSO	NaCl	~0.5 mg

General procedure for preparation of ^{1}H NMR samples of organic compounds for *ee* determination

A saturated stock solution of $PPh_4[Co^{III}(S,S\text{-EDDS})]\cdot 2H_2O$ was prepared by dissolution of the complex (0.14 g, 2.0 mmol) in d^4-methanol (10 ml) with heating. The solution was allowed to cool and the excess complex crystallised out. A sample of the appropriate compound (1.0 mg) was dissolved in thus prepared solution (0.6 ml) and filtered through a plug of cotton wool if necessary.

Experimental Details for Chapter 6

Electrocrystallisation – general procedure

Tetraphenylphosphonium salt of the chiral counterion was dissolved in dry MeCN (20 ml) under dinitrogen in a dry-box. The appropriate donor was placed in the anode chamber of an electrocrystallisation cell in the solid form. The cell was carefully filled with the solution of the counterion, fitted with platinum electrodes and sealed. The cell was then removed from the dry-box and water (1 ml) was injected into the sealed cell. Constant current of 1μA was applied. After two to four weeks dark crystals were harvested.

$(TTF)_3[Co^{III}(S,S\text{-}EDDS)]_2 \cdot 6H_2O$

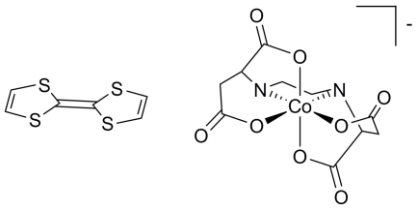

Obtained following the general procedure, using $PPh_4[Co^{III}(S,S\text{-}EDDS)] \cdot 2H_2O$ (25 mg) and TTF (5 mg).

IR (cm^{-1}) ν 3198, 1655, 1438, 1396, 1339, 1283, 1213, 1199, 1113, 1091, 1044, 1017, 871, 731, 700

$(TTF)_3[Fe^{III}(S,S\text{-}EDDS)]_2 \cdot 5H_2O$

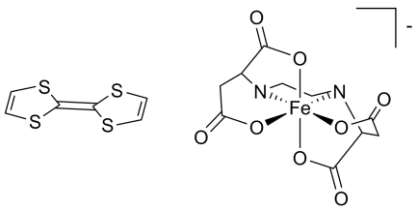

Obtained following the general procedure, using $PPh_4[Fe^{III}(S,S\text{-}EDDS)] \cdot 2H_2O$ (25 mg) and TTF (5 mg).

IR (cm^{-1}) ν 3188, 1603, 1439, 1350, 1314, 1272, 1207, 1100, 1045, 1020, 974, 912, 875, 807, 788, 656

$(TTF)_x[Cr^{III}(S,S\text{-}EDDS)]_2 \cdot 4.5H_2O$

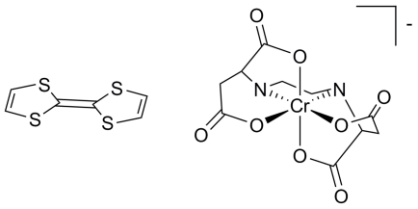

Obtained following the general procedure, using $PPh_4[Cr^{III}(S,S\text{-}EDDS)] \cdot 2H_2O$ (25 mg) and TTF (5 mg).

IR (cm^{-1}) ν 3580, 3176, 3048, 2917, 1661, 1629, 1592, 1472, 1445, 1392, 1366, 1348, 1326, 1256, 1221, 1205, 1094, 1050, 1019, 1003, 914, 869, 813, 800, 724, 699, 678

Elemental analysis found (calculated for $C_{38}H_{45}N_4O_{20.5}S_{12}Cr_2$) %: C 33.16 (33.20), H 3.38 (3.30), N 4.45 (4.08).

$(TSF)_3[Co^{III}(S,S\text{-}EDDS)]_2 \cdot 6H_2O$

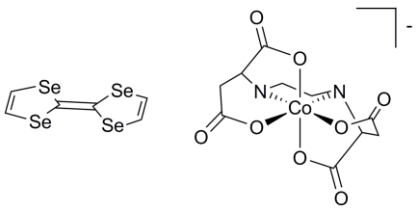

Obtained following the general procedure, using $PPh_4[Co^{III}(S,S\text{-}EDDS)] \cdot 2H_2O$ (25 mg) and TSF (10 mg).

IR (cm^{-1}) ν 3189, 3032, 1655, 1619, 1596, 1571, 1455, 1376, 1342, 1275, 1236, 1214, 1199, 1078, 1058, 1043, 1017, 918, 874, 667

Elemental analysis found (calculated for $C_{38}H_{48}N_4O_{22}Se_{12}Co_2$) %: C 23.22 (23.07), H 2.53 (2.45), N 2.80 (2.83).

$(TSF)_3[Fe^{III}(S,S\text{-}EDDS)]_2 \cdot 6H_2O$

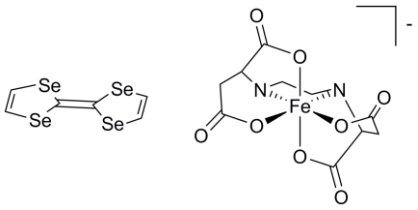

Obtained following the general procedure, using $PPh_4[Fe^{III}(S,S\text{-}EDDS)] \cdot 2H_2O$ (25 mg) and TSF (10 mg).

IR (cm^{-1}) ν 3209, 3031, 2931, 1592, 1447, 1355, 1311, 1232, 1204, 1101, 1058, 1018, 973, 956, 910, 864, 812, 713

Elemental analysis found (calculated for $C_{38}H_{48}N_4O_{22}Se_{12}Fe_2$) %: C 22.82 (23.14), H 2.66 (2.45), N 2.90 (2.84).

$(TSF)_3[Cr^{III}(S,S\text{-}EDDS)]_2 \cdot 6H_2O$

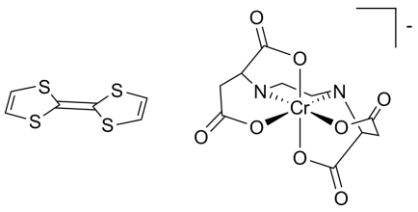

Obtained following the general procedure, using $PPh_4[Cr^{III}(S,S\text{-}EDDS)] \cdot 2H_2O$ (25 mg) and TSF (10 mg).

IR (cm^{-1}) ν 3575, 3174, 2917, 1660, 1624, 1588, 1444, 1389, 1372, 1315, 1270, 1216, 1201, 1098, 1078, 1047, 994, 946, 913, 865, 806, 720, 699

Elemental analysis found (calculated for $C_{38}H_{48}N_4O_{22}Se_{12}Cr_2$) %: C 23.66 (23.24), H 2.58 (2.46), N 2.96 (2.85).

$(ET)_x[Co^{III}(S,S\text{-}EDDS)]_2 \cdot 5H_2O$

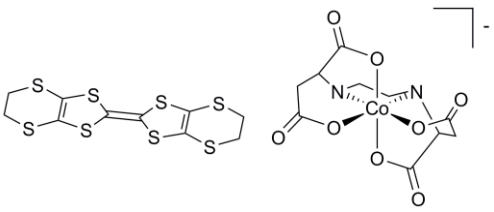

Obtained following the general procedure, using $PPh_4[Co^{III}(S,S\text{-}EDDS)] \cdot 2H_2O$ (25 mg) and ET (10 mg).

Elemental Analysis found % C 33.15, H 4.27, N 8.35, S 2.26.

IR (cm^{-1}) ν 3194, 2964, 2925, 1648, 1437, 1393, 1338, 1274, 1213, 1198, 1114, 1091, 1043, 1017, 971, 943, 921, 895, 870, 771, 734, 702.

$(ET)_x[Cr^{III}(S,S\text{-}EDDS)]_2 \cdot 6H_2O$

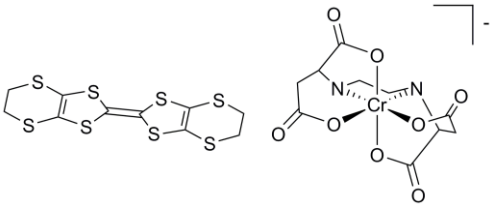

Obtained following the general procedure, using $PPh_4[Cr^{III}(S,S\text{-}EDDS)] \cdot 2H_2O$ (25 mg) and ET (10 mg).

Elemental Analysis found % C 32.82, H 3.69, N 7.61, S 1.77.

IR (cm^{-1}) ν 3211, 2959, 2920, 1648, 1594, 1392, 1336, 1271, 1215, 1199, 1097, 1043, 1015, 991, 944, 916, 890, 861, 796, 721, 687, 651.

$(BETS)_x[Co^{III}(S,S\text{-}EDDS)]_y \cdot zH_2O$

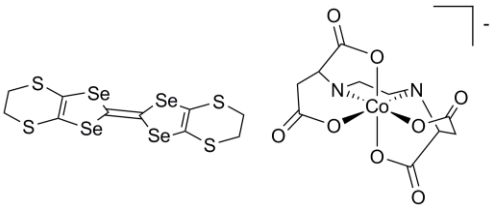

Obtained following the general procedure, using $PPh_4[Co^{III}(S,S\text{-}EDDS)] \cdot 2H_2O$ (25 mg) and BETS (8 mg).

Elemental Analysis found % C 33.04, H 4.12, N 8.85.

IR (cm^{-1}) ν 3190, 1655, 1594, 1438, 1395, 1341, 1283, 1214, 1200, 1114, 1092, 1044, 1018, 921, 896, 872, 733, 701.

$(BETS)_x[Cr^{III}(S,S\text{-}EDDS)]_y \cdot zH_2O$

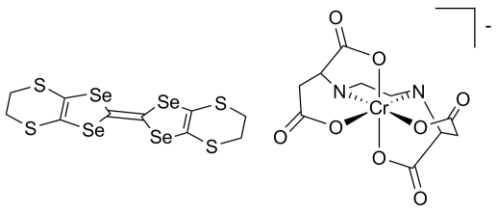

Obtained following the general procedure, using $PPh_4[Cr^{III}(S,S\text{-}EDDS)]\cdot 2H_2O$ (25 mg) and BETS (8 mg).

Elemental Analysis found % C 3.39, H 3.86, N 8.523, S 2.66.

IR (cm^{-1}) ν 3215, 1658, 1441, 1394, 1336, 1272, 1215, 1200, 1097, 1043, 1015, 991, 940, 917, 862, 790, 723, 688.

References

1. G. M. Sheldrick, *Acta Crystallogr., Sect. A*, 1990, **46**, 467-473.
2. G. M. Sheldrick, *Acta Crystallogr., Sect. A*, 2008, **64**, 112-122.
3. L. Farrugia, *J. Appl. Cryst.*, 1999, **32**, 837-838.
4. G. A. Bain and J. F. Berry, *J. Chem. Educ.*, 2008, **85**, 532-536.
5. L. R. Melby, H. D. Hartzler and W. A. Sheppard, *J. Org. Chem.*, 1974, **39**, 2456-2458.
6. K. Takimiya, H. J. Jeon and T. Otsubo, *Synthesis*, 2005, **2005**, 2810-2813.
7. T. Courcet, I. Malfant, K. Pokhodnia and P. Cassoux, *New J. Chem.*, 1998, **22**, 585-589.
8. R. Kato, H. Kobayashi and A. Kobayashi, *Synth. Met.*, 1991, **42**, 2093-2096.
9. S. R. Coles, PhD, University of Warwick, 2006.
10. T. Imakubo, M. Kibune, H. Yoshino, T. Shirahata and K. Yoza, *J. Mater. Chem.*, 2006, **16**, 4110-4116.
11. J. Garin, J. Orduna, S. Uriel, A. J. Moore, M. R. Bryce, S. Wegener, D. S. Yufit and J. A. K. Howard, *Synthesis*, 1994, 489-493.
12. M. J. McKennon, A. I. Meyers, K. Drauz and M. Schwarm, *J. Org. Chem.*, 1993, **58**, 3568-3571.
13. K. Sutowardoyo, M. Emziane and D. Sinou, *Tetrahedron Lett.*, 1989, **30**, 4673-4676.
14. D. B. Damon, R. W. Dugger, S. E. Hubbs, J. M. Scott and R. W. Scott, *Org. Process Res. Dev.*, 2006, **10**, 472-480.
15. K. Higashiura, H. Morino, H. Matsuura, Y. Toyomaki and K. Ienaga, *J. Chem. Soc., Perkin Trans. 1*, 1989, 1479-1481.
16. M.-D. Chen, M.-Z. He, X. Zhou, L.-Q. Huang, Y.-P. Ruan and P.-Q. Huang, *Tetrahedron*, 2005, **61**, 1335-1344.
17. M. Tiecco, L. Testaferri, F. Marini, S. Sternativo, C. Santi, L. Bagnoli and A. Temperini, *Tetrahedron: Asymmetry*, 2003, **14**, 2651-2657.
18. D. L. J. Clive, J. Peng, S. P. Fletcher, V. E. Ziffle and D. Wingert, *J. Org. Chem.*, 2008, **73**, 2330-2344.
19. R. Caputo, E. Cassano, L. Longobardo and G. Palumbo, *Tetrahedron Lett.*, 1995, **36**, 167-168.
20. Y. Hsiao and L. S. Hegedus, *J. Org. Chem.*, 1997, **62**, 3586-3591.
21. J. Danklmaier and H. Hönig, *Liebigs Ann. Chem.*, 1988, **1988**, 851-854.
22. A. Benalil, B. Carboni and M. Vaultier, *Tetrahedron*, 1991, **47**, 8177-8194.
23. J. P. Leonard, P. Jensen, T. McCabe, J. E. O'Brien, R. D. Peacock, P. E. Kruger and T. Gunnlaugsson, *J. Am. Chem. Soc.*, 2007, **129**, 10986-10987.
24. R. N. Bream, S. V. Ley, B. McDermott and P. A. Procopiou, *J. Chem. Soc., Perkin Trans. 1*, 2002, 2237-2242.
25. A. G. Talma, P. Jouin, J. G. De Vries, C. B. Troostwijk, G. H. W. Buning, J. K. Waninge, J. Visscher and R. M. Kellogg, *J. Am. Chem. Soc.*, 1985, **107**, 3981-3997.
26. F. Wudl, *J. Am. Chem. Soc.*, 1975, **97**, 1962-1963.
27. S. Howson, MChem, University of Warwick, 2007.
28. J. Barker, C. Blundell and N. W. Alcock, *Unpublished results*.
29. J. A. Broomhead and C. G. Young, *Inorg. Synth.*, 1990, **28**, 338-340.

30. V. Joshi and P. K. Ghosh, *J. Am. Chem. Soc.*, 1989, **111**, 5604-5612.
31. P. Belser, C. Daul and A. Von Zelewsky, *Chem. Phys. Lett.*, 1981, **79**, 596-598.
32. J. Ferguson, F. Herren and G. M. McLaughlin, *Chem. Phys. Lett.*, 1982, **89**, 376-380.

Appendix A

Details of the crystal solutions and refinement

Table A.1. Details of the crystal solution and refinement of structures included in Chapter 2.

Complex	$[Cu_2(biphTTF)_2](BF4)_2 \cdot CH_2Cl_2 \cdot H_2O$
Formula	$C_{56.75}H_{42}B_2Cl_{1.50}Cu_2F_8N_4O_{0.25}S_{16}$
Formula mass	1650.78
Crystal dimensions [mm]	0.22×0.10×0.02
Crystal system	Triclinic
Space group	$P\bar{1}$
Z	2
a (Å)	12.6465(2)
b (Å)	13.6162(3)
c (Å)	22.9997(7)
α (°)	79.284(2)
β (°)	88.4382(19)
γ (°)	69.413(2)
Volume (Å)	3639.79(16)
D_c ($g \cdot cm^{-3}$)	1.506
T (K)	296(2)
Radiation (Å)	Mo-Kα (λ = 0.71073)
2θ max (°)	29.36
F(000)	1668
μ (mm^{-1})	1.158
Total no. of reflections	64684
No. of unique reflections	17671
R_{int}	0.0780
Goodness-of-fit	0.797
R1 [I > 2σ(I)]	0.0651
wR2 [I > 2σ(I)]	0.1887

Table A.2. Details of the crystal solution and refinement of structures included in Chapter 3.

Compound	(18-C-6)K[Co(*R*,*R*-L^1)$_2$]·H2O·MeCN (**24**)	K[Co(*R*,*R*-L^1)$_2$]·MeOH	K[Co(*R*,*R*-L^2)$_2$]·3H_2O (**26**)	(TTF)[Co(*R*,*R*-L^1)$_2$] (**27**)	(TTF)[Co^{III}(*S*,*S*-L^2)$_2$]·EtOAc (**28**)
Formula	$C_{60}H_{71}CoKN_7O_{11}$	$C_{47}H_{46}CoKN_6O_5$	$C_{30}H_{48}CoKN_6O_{11}$	$C_{52}H_{46}CoN_6O_4S_4$	$C_{40}H_{54}CoN_6O_{10}S_4$
Fw	1164.27	872.93	766.77	1006.12	966.06
Crystal size	0.40×0.18×0.08	0.40×0.40×0.04	0.30×0.10×0.10	0.17×0.12×0.03	0.14×0.08×0.06
Crystal system	Monoclinic	Monoclinic	Monoclinic	Monoclinic	Monoclinic
Space group	$P2_1$	$P2_1$	$P2_1$	C2	$P2_1$
a (Å)	9.3421(2)	9.8734(2)	10.5953(2)	15.8680(8)	9.58540(10)
b (Å)	23.3274(5)	17.1654(3)	16.0147(2)	10.5601(4)	25.4527(3)
c (Å)	13.6888(4)	12.4840(2)	11.11937(18)	15.6312(7)	9.74480(10)
α (deg)	90	90	90	90	90
β (deg)	104.304(2)	95.238(2)	106.5681(19)	109.222(5)	113.302(2)
γ (deg)	90	90	90	90	90
V (Å^3)	2890.66(12)	2106.96(7)	1808.41(5)	2473.26(19)	2183.55(4)
d_{calcd} (mg/cm^3)	1.338	1.376	1.408	1.351	1.469
Temp (K)	95(2)	293(3)	120(2)	173(2)	100(2)
Radiation (Å)	0.71073	0.71073	0.71073	0.71073	1.54178
2θ max	29.38	29.22	29.41	27.49	61.94
μ (mm^{-1})	0.435	0.561	0.654	0.567	5.403
F_{000}	1228	912	808	1046	1014
Total no. of reflections	28920	22326	17987	10074	13998
No. of independent reflections	13656	9979	8485	5410	6707
R_{int}	0.0459	0.0282	0.0223	0.0352	0.0198
R1, [I>2σ(I)]	0.0460	0.0350	0.0336	0.0405	0.0304
wR2	0.0932	0.0748	0.0803	0.0695	0.0808
GooF	0.976	0.942	1.006	0.888	1.093

Table A.3. Details of the crystal solution and refinement of structures included in Chapter 4.

Complex	$Ag[Co^{III}(S,S\text{-}EDDS)]\cdot 2H_2O\cdot 2AgNO_3$	$PPh_4[Co^{III}(S,S\text{-}EDDS)]\cdot 2H_2O$ (**33**)	$PPh_4[Fe^{III}(S,S\text{-}EDDS)]\cdot 2H_2O$ (**35**)	$PPh_4[Cr^{III}(S,S\text{-}EDDS)]\cdot 2H_2O$ (**37**)
Formula	C10 H16 Ag3 Co N4 O16	$C_{34}H_{36}CoN_2O_{10}P$	$C_{34}H_{36}FeN_2O_{10}P$	$C_{34}H_{36}CrN_2O_{10}P$
Formula mass	830.81	722.55	719.47	715.62
Crystal dimensions (mm)	0.35 x 0.30 x 0.26	0.35×0.2×0.08	0.4×0.3×0.3	0.28×0.15×0.1
Crystal system	Orthorhombic	Orthorhombic	Orthorhombic	Orthorhombic
Space group	$P2_12_12_1$	$P2_12_12$	$P2_12_12$	$P2_12_12$
Z	8	2	2	2
a (Å)	10.54436(4)	16.9107(6)	12.8761(3)	12.7168(3)
b (Å)	17.47746(7)	12.8825(4)	17.2456(4)	16.9853(3)
c (Å)	20.93177(8)	7.3322(2)	7.4186(2)	7.3700(2)
Volume (Å)	3857.49(3)	1597.34	1647.35	1591.91
D_c ($g\cdot cm^{-3}$)	2.861	1.502	1.450	1.493
T (K)	100(2)	293(2)	293(2)	100(2)
Radiation (Å)		Mo-Kα (λ = 0.71073)	Mo-Kα (λ = 0.71073)	Mo-Kα (λ = 0.71073)
2θ max (°)	29.46	32.83	29.21	29.36
F(000)	3200	752	750	746
μ (mm^{-1})	3.943	0.651	0.568	0.473
Total no. of reflections	264984	50153	9632	6946
No. of unique reflections	10446	5741	3843	3713
R_{int}	0.0387	0.0374	0.0293	0.0255
Goodness-of-fit	1.131	1.045	0.924	0.991
R1 [I > 2σ(I)]	0.0154	0.0303	0.0331	0.0309
wR2 [I > 2σ(I)]	0.0349	0.0759	0.0679	0.0688

Table A.4. Details of the crystal solution and refinement of structures included in Chapter 5.

Complex	[Λ-{$Ru^{II}(bpy)_3$)][Λ-{Fe^{III}(*S*,*S*-EDDS)]}86Cl
Formula	$C_{40}H_{38}ClFeN_8O_9Ru$
Formula mass	967.15
Crystal dimensions [mm]	0.40×0.30×0.15
Crystal system	Orthorhombic
Space group	$P2_12_12_1$
Z	2
a (Å)	13.24468(18)
b (Å)	17.0831(2)
c (Å)	17.1928(2)
Volume (Å)	3890.05
D_c ($g \cdot cm^{-3}$)	1.651
T (K)	100(2)
Radiation (Å)	Mo-Kα (λ = 0.71073)
2θ max (°)	32.74
F(000)	1972
μ (mm^{-1})	0.899
Total no. of reflections	25049
No. of unique reflections	12924
R_{int}	0.0219
Goodness-of-fit	0.981
R1 [I > 2σ(I)]	0.0252
wR2 [I > 2σ(I)]	0.0557

Table A.5. Details of the crystal solution and refinement of structures included in Chapter 6.

Compound	$(TTF)_3[Co(S,S\text{-}EDDS)]_2 \cdot 6H_2O$	$(TTF)_3[Fe(S,S\text{-}EDDS)]_2 \cdot 5H_2O$	$(TTF)_x[Cr(S,S\text{-}EDDS)]_2 \cdot 6.5H_2O$	$(ET)_x[Co(S,S\text{-}EDDS)]_2 \cdot 5H_2O$
Formula	$C_{19}H_{24}CoN_2O_{11}S_6$	$C_{19}H_{22}FeN_2O_{10}S_6$	$C_{40}H_{74}Cr_4N_8O_{45}$	$C_{20}H_{34}Co_2N_4O_{21}$
Fw	707.69	686.60	1595.07	784.37
Crystal size	0.24×0.10×0.02	0.24×0.08×0.08	0.18×0.18×0.07	0.20×0.11×0.07
Crystal system	Monoclinic	Triclinic	Monoclinic	Orthorhombic
Space group	$P2_1$	P1	$P2_1$	$P2_12_12_1$
a (Å)	10.5591(2)	10.4392(2)	16.4999(8)	9.5754(3)
b (Å)	10.3507(2)	10.5270(2)	10.7581(4)	10.7418(3)
c (Å)	24.2916(5)	23.9133(3)	18.9837(9)	30.4018(8)
α (deg)	90	90	90	90
β (deg)	93.3972(19)	90	102.388(2)	90
γ (deg)	90	90	90	90
V (Å^3)	2650.26(9)	2627.92(8)	3291.3(3)	2127.04(15)
d_{calcd} (mg/cm^3)	1.774	1.735	1.610	1.662
Temp (K)	100(2)	100(2)	120(2)	120(2)
Radiation (Å)	Mo-Kα (λ = 0.71073)	Mo-Kα (λ = 0.71073)	Mo-Kα (λ = 0.71073)	Mo-Kα (λ = 0.71073)
2θ max	32.61	27.49	27.50	27.49
μ (mm^{-1})	1.182	1.108	0.756	1.155
F_{000}	1452	1408	1652	1608
Total no. of reflections	35590	39836	42041	25260
No. of independent reflections	35590	39836	15069	7054
R_{int}	0.0000	0.0000	0.1025	0.0473
R1, [I>2σ(I)]	0.0511	0.0391	0.0778	0.0550
wR2	0.1158	0.0910	0.1767	0.1485
GooF	0.984	0.991	1.040	1.057

Table A.5. continued.

Compound	$(ET)_x[Fe(S,S\text{-}EDDS)]_2{\cdot}6H_2O$	$(TSF)_3[Co(S,S\text{-}EDDS)]_2{\cdot}6H_2O$	$(TSF)_3[Fe(S,S\text{-}EDDS)]_2{\cdot}6H_2O$	$(TSF)_3[Cr(S,S\text{-}EDDS)]_2{\cdot}6H_2O$
Formula	$C_{20}H_{36}Co_2N_4O_{22}$	$C_{38}H_{48}Co_2N_4O_{22}Se_{12}$	$C_{38}H_{48}Fe_2N_4O_{22}Se_{12}$	$C_{38}H_{48}Cr_2N_4O_{22}Se_{12}$
Fw	788.53	1978.18	1972.02	1964.32
Crystal size	0.17×0.10×0.01	0.20×0.17×0.14	0.30×0.04×0.03	0.17×0.08×0.01
Crystal system	Orthorhombic	Monoclinic	Monoclinic	Monoclinic
Space group	$P2_12_12_1$	$P2_1$	$P2_1$	$P2_1$
a (Å)	9.7647(3)	10.3219(5)	10.9413(5)	10.8846(5)
b (Å)	10.8437(5)	24.9435(11)	10.4374(4)	10.3773(5)
c (Å)	30.5475(13)	10.7594(5)	25.0015(11)	25.0263(10)
α (deg)	90	90	90	90
β (deg)	90	90.399(3)	94.188(2)	94.094(3)
γ (deg)	90	90	90	90
V (Å^3)	3234.5(2)	2770.1(2)	2847.5(2)	2819.6(2)
d_{calcd} (mg/cm^3)	1.619	2.372	2.300	2.314
Temp (K)	120(2)	120(2)	120(2)	120(2)
Radiation (Å)	Mo-Kα (λ = 0.71073)	Mo-Kα (λ = 0.71073)	Mo-Kα (λ = 0.71073)	Mo-Kα (λ = 0.71073)
2θ max	27.48	27.50	27.48	27.48
μ (mm^{-1})	0.767	8.562	8.257	8.210
F_{000}	1632	1884.0	1880	1872
Total no. of reflections	24551	55875	41116	28563
No. of independent reflections	7371	12654	41116	28563
R_{int}	0.1550	0.1095	0.0000	0.0000
R1, [I>2σ(I)]	0.0834	0.0721	0.0876	0.0950
wR2	0.1771	0.1648	0.1619	0.1884
GooF	1.019	1.040	1.043	1.081

Appendix B

Selected bond lengths and angles

Table B.1. Selected bond lengths and angles in the solid state structure of $[Cu^{I}_2(biphTTF)_2]\cdot CH_2Cl_2\cdot H_2O$ (**23**)

Bond/Angle	(Å/°)	Bond/Angle	(Å/°)
Cu(1)-N(3)	1.899(4)	C(29)-S(9)	1.720(9)
Cu(1)-N(1)	1.906(4)	C(30)-S(10)	1.738(8)
Cu(2)-N(2)	1.882(4)	S(10)-C(31)	1.740(6)
Cu(2)-N(4)	1.890(4)	S(9)-C(31)	1.750(6)
S(1)-C(1)	1.703(8)	C(31)-C(32)	1.328(7)
S(1)-C(3)	1.735(7)	C(32)-S(11)	1.733(6)
C(2)-S(2)	1.681(9)	C(32)-S(12)	1.765(5)
S(2)-C(3)	1.744(7)	S(11)-C(33)	1.712(6)
C(3)-C(4)	1.346(8)	C(34)-S(12)	1.753(5)
C(4)-S(3)	1.748(6)	C(51)-S(13)	1.761(5)
C(4)-S(4)	1.764(6)	S(13)-C(53)	1.763(5)
S(3)-C(5)	1.708(6)	C(52)-S(14)	1.713(5)
C(6)-S(4)	1.761(5)	S(14)-C(53)	1.759(5)
C(23)-S(5)	1.765(6)	C(53)-C(54)	1.343(7)
S(5)-C(25)	1.782(5)	C(54)-S(15)	1.752(6)
C(24)-S(6)	1.709(6)	C(54)-S(16)	1.759(6)
S(6)-C(25)	1.730(6)	S(15)-C(55)	1.734(8)
C(25)-C(26)	1.320(8)	C(55)-C(56)	1.307(10)
C(26)-S(8)	1.750(6)	C(56)-S(16)	1.708(8)
C(26)-S(7)	1.771(6)		
S(7)-C(27)	1.695(9)	N(3)-Cu(1)-N(1)	174.82(17)
C(28)-S(8)	1.731(9)	N(2)-Cu(2)-N(4)	177.30(17)

Table B.2. Selected bond lengths and angles in the solid state structure of $K[Co^{III}(L^3)_2]\cdot CH_3OH$

Bond/Angle	(Å/°)	Bond/Angle	(Å/°)
Co(1)-N(5)	1.8556(15)	N(4)-Co(1)-N(6)	163.76(7)
Co(1)-N(2)	1.8568(15)	N(5)-Co(1)-N(3)	92.53(8)
Co(1)-N(4)	1.978(2)	N(2)-Co(1)-N(3)	81.41(8)
Co(1)-N(6)	1.9838(19)	N(4)-Co(1)-N(3)	89.76(8)
Co(1)-N(3)	1.999(2)	N(6)-Co(1)-N(3)	93.22(9)
Co(1)-N(1)	2.0002(19)	N(5)-Co(1)-N(1)	104.52(8)
K(1)-O(4)	2.5000(19)	N(2)-Co(1)-N(1)	81.55(8)
K(1)-O(3')	2.5885(18)	N(4)-Co(1)-N(1)	91.85(8)
K(1)-O(1")	2.6123(18)	N(6)-Co(1)-N(1)	89.98(8)
K(1)-O(5)	2.635(3)	N(3)-Co(1)-N(1)	162.93(7)
		O(4)-K(1)-O(3')	125.30(7)
N(5)-Co(1)-N(2)	173.92(9)	O(4)-K(1)-O(1")	106.13(6)
N(5)-Co(1)-N(4)	81.79(8)	O(3')-K(1)-O(1")	88.62(6)
N(2)-Co(1)-N(4)	98.58(8)	O(4)-K(1)-O(5)	121.48(9)
N(5)-Co(1)-N(6)	82.12(8)	O(3')-K(1)-O(5)	106.77(9)
N(2)-Co(1)-N(6)	97.66(8)	O(1")-K(1)-O(5)	99.29(8)

Table B.3. Selected bond lengths and angles in the solid state structure of (18-crown-6)$K[Co^{III}(L^3)_2]\cdot H_2O\cdot CH_3CN$ (**24**)

Bond	(Å)	Angle	(°)
Co(1)-N(5)	1.853(2)	N(5)-Co(1)-N(2)	176.25(10)
Co(1)-N(2)	1.862(2)	N(5)-Co(1)-N(6)	81.94(9)
Co(1)-N(6)	1.960(2)	N(2)-Co(1)-N(6)	97.11(9)
Co(1)-N(4)	1.972(2)	N(5)-Co(1)-N(4)	81.90(9)
Co(1)-N(3)	1.994(2)	N(2)-Co(1)-N(4)	99.09(9)
Co(1)-N(1)	2.017(2)	N(6)-Co(1)-N(4)	163.80(8)
K(1)-O(1)	2.6906(19)	N(5)-Co(1)-N(3)	94.55(9)
K(1)-O(10)	2.769(2)	N(2)-Co(1)-N(3)	81.80(9)
K(1)-O(6)	2.786(2)	N(6)-Co(1)-N(3)	89.69(9)
K(1)-O(5)	2.807(2)	N(4)-Co(1)-N(3)	92.73(9)
K(1)-O(9)	2.870(2)	N(5)-Co(1)-N(1)	101.87(9)
K(1)-O(11)	2.882(2)	N(2)-Co(1)-N(1)	81.74(9)
K(1)-O(8)	2.900(2)	N(6)-Co(1)-N(1)	90.49(9)
K(1)-O(7)	2.900(2)	N(4)-Co(1)-N(1)	91.71(9)
		N(3)-Co(1)-N(1)	163.43(8)
		O(1)-K(1)-O(11)	164.07(6)

Table B.4. Selected bond lengths and angles in the solid state structure of $K[Co^{III}(L^4)_2]\cdot 3H_2O$ (**26**)

Bond/Angle	(Å/°)	Bond/Angle	(Å/°)
Co(1)-N(2)	1.856(2)	N(5)-Co(1)-N(6)	81.57(7)
Co(1)-N(5)	1.860(2)	N(1)-Co(1)-N(6)	90.07(8)
Co(1)-N(1)	1.961(2)	N(3)-Co(1)-N(6)	92.13(8)
Co(1)-N(3)	1.9631(19)	N(2)-Co(1)-N(4)	98.47(7)
Co(1)-N(6)	1.9740(17)	N(5)-Co(1)-N(4)	81.61(7)
Co(1)-N(4)	1.9741(18)	N(1)-Co(1)-N(4)	92.00(8)
O(2)-K(1)	2.6498(17)	N(3)-Co(1)-N(4)	90.71(8)
K(1)-O(11)	2.648(2)	N(6)-Co(1)-N(4)	163.17(7)
K(1)-O(10)	2.651(2)	O(11)-K(1)-O(2)	150.23(7)
K(1)-O(9)	2.7003(19)	O(11)-K(1)-O(10)	98.32(7)
K(1)-O(6)#2	2.8123(16)	O(2)-K(1)-O(10)	110.21(7)
N(2)-Co(1)-N(5)	179.76(9)	O(11)-K(1)-O(9)	87.19(7)
N(2)-Co(1)-N(1)	81.70(8)	O(2)-K(1)-O(9)	91.95(6)
N(5)-Co(1)-N(1)	98.53(8)	O(10)-K(1)-O(9)	75.08(7)
N(2)-Co(1)-N(3)	81.49(8)	O(11)-K(1)-O(6)#2	78.71(6)
N(5)-Co(1)-N(3)	98.28(8)	O(2)-K(1)-O(6)#2	86.96(5)
N(1)-Co(1)-N(3)	163.19(7)	O(10)-K(1)-O(6)#2	134.41(6)
N(2)-Co(1)-N(6)	98.36(7)	O(9)-K(1)-O(6)#2	148.55(6)

Table B.5. Selected bond lengths and angles in the solid state structure of $(TTF)[Co^{III}(L^3)_2]$ (**27**)

Bond/Angle	(Å/°)	Bond/Angle	(Å/°)
Co(1)-N(3)	1.848(2)	N(3)-Co(1)-N(2)	82.23(11)
Co(1)-N(1)	1.958(2)	N(3')-Co(1)-N(2)	95.07(10)
Co(1)-N(2)	1.976(3)	N(1)-Co(1)-N(2)	164.72(9)
S(1)-C(24)	1.719(3)	N(1')-Co(1)-N(2)	91.62(9)
S(1)-C(26)	1.722(3)	N(3)-Co(1)-N(2')	95.07(10)
S(2)-C(25)	1.725(3)	N(2)-Co(1)-N(2')	92.05(15)
S(2)-C(24)	1.728(3)	C(24)-S(1)-C(26)	94.95(15)
C(24)-C(24")	1.379(6)	C(25)-S(2)-C(24)	95.08(15)
		C(24")-C(24)-S(1)	122.7(3)
N(3)-Co(1)-N(3')	176.13(19)	C(24")-C(24)-S(2)	122.2(3)
N(3)-Co(1)-N(1)	82.67(11)	S(1)-C(24)-S(2)	115.05(18)
N(3')-Co(1)-N(1)	100.12(10)	C(26)-C(25)-S(2)	117.0(3)
N(1)-Co(1)-N(1')	88.71(15)	C(25)-C(26)-S(1)	117.9(3)

Table B.6. Selected bond lengths and angles in the solid state structure of (TTF)[$Co^{III}(L^4)_2$]·EtOAc (**27**)

Bond/Angle	(Å/°)	Bond/Angle	(Å/°)
Co(1)-N(5)	1.848(2)	N(2)-Co(1)-N(6)	96.49(9)
Co(1)-N(2)	1.856(2)	N(4)-Co(1)-N(6)	163.06(9)
Co(1)-N(4)	1.963(2)	N(1)-Co(1)-N(6)	92.66(10)
Co(1)-N(1)	1.964(2)	N(5)-Co(1)-N(3)	95.62(9)
Co(1)-N(6)	1.978(2)	N(2)-Co(1)-N(3)	81.48(9)
Co(1)-N(3)	1.980(2)	N(4)-Co(1)-N(3)	91.97(9)
S(1)-C(33)	1.723(3)	N(1)-Co(1)-N(3)	162.87(9)
S(1)-C(31)	1.723(3)	N(6)-Co(1)-N(3)	92.51(9)
S(2)-C(33)	1.716(3)	C(33)-S(1)-C(31)	95.20(14)
S(2)-C(32)	1.718(3)	C(33)-S(2)-C(32)	95.65(14)
S(3)-C(35)	1.722(3)	C(35)-S(3)-C(34)	95.35(14)
S(3)-C(34)	1.723(3)	C(36)-S(4)-C(34)	95.10(14)
S(4)-C(36)	1.721(3)	C(32)-C(31)-S(1)	117.1(2)
S(4)-C(34)	1.722(3)	C(31)-C(32)-S(2)	116.9(2)
C(33)-C(34)	1.395(4)	C(34)-C(33)-S(2)	122.1(2)
N(5)-Co(1)-N(2)	176.49(9)	C(34)-C(33)-S(1)	122.8(2)
N(5)-Co(1)-N(4)	81.70(9)	S(2)-C(33)-S(1)	115.15(16)
N(2)-Co(1)-N(4)	100.33(9)	C(33)-C(34)-S(4)	122.0(2)
N(5)-Co(1)-N(1)	101.29(9)	C(33)-C(34)-S(3)	122.7(2)
N(2)-Co(1)-N(1)	81.71(9)	S(4)-C(34)-S(3)	115.25(16)
N(4)-Co(1)-N(1)	87.79(9)	C(36)-C(35)-S(3)	116.9(2)
N(5)-Co(1)-N(6)	81.61(9)	C(35)-C(36)-S(4)	117.4(2)

Table B.7. Selected bond lengths and angles in the solid state structure of {Λ-[$Ru^{II}(bpy)_3$]}{Λ-[Fe^{III}(*S*,*S*-EDDS)]}Cl·H_2O

Bond/Angle	(Å/°)	Bond/Angle	(Å/°)
Fe(1)-O(7)	1.9248(13)	O(5)-Fe(1)-N(2)	78.56(5)
Fe(1)-O(1)	1.9591(11)	O(7)-Fe(1)-N(1)	164.92(6)
Fe(1)-O(3)	2.0065(12)	O(1)-Fe(1)-N(1)	89.09(5)
Fe(1)-O(5)	2.0250(12)	O(3)-Fe(1)-N(1)	78.49(6)
Fe(1)-N(2)	2.1463(14)	O(5)-Fe(1)-N(1)	95.29(6)
Fe(1)-N(1)	2.1578(15)	N(2)-Fe(1)-N(1)	80.63(6)
N(3)-Ru(1)	2.0581(13)	N(6)-Ru(1)-N(5)	79.25(5)
Ru(1)-N(6)	2.0563(14)	N(6)-Ru(1)-N(3)	92.09(5)
Ru(1)-N(5)	2.0579(13)	N(5)-Ru(1)-N(3)	96.06(5)
Ru(1)-N(7)	2.0582(13)	N(6)-Ru(1)-N(7)	170.62(6)
Ru(1)-N(8)	2.0622(14)	N(5)-Ru(1)-N(7)	94.21(5)
Ru(1)-N(4)	2.0636(13)	N(3)-Ru(1)-N(7)	95.31(5)
O(7)-Fe(1)-O(1)	103.58(5)	N(6)-Ru(1)-N(8)	93.81(5)
O(7)-Fe(1)-O(3)	92.48(5)	N(5)-Ru(1)-N(8)	88.20(5)
O(1)-Fe(1)-O(3)	93.13(5)	N(3)-Ru(1)-N(8)	173.28(6)
O(7)-Fe(1)-O(5)	92.92(5)	N(7)-Ru(1)-N(8)	79.16(5)
O(1)-Fe(1)-O(5)	89.89(5)	N(6)-Ru(1)-N(4)	97.58(5)
O(3)-Fe(1)-O(5)	173.02(6)	N(5)-Ru(1)-N(4)	173.78(5)
O(7)-Fe(1)-N(2)	88.65(6)	N(3)-Ru(1)-N(4)	78.62(5)
O(1)-Fe(1)-N(2)	163.67(6)	N(7)-Ru(1)-N(4)	89.54(5)
O(3)-Fe(1)-N(2)	97.16(5)	N(8)-Ru(1)-N(4)	97.39(5)

Table B.8. Selected bond lengths and angles in the solid state structure of $(TTF)_3[Co^{III}(S,S\text{-}EDDS)]_2 \cdot 6H_2O$ (**38**)

Bond	(Å)	Angle	(°)
Co(1)-O(3)	1.890(3)	O(3)-Co(1)-O(5)	177.17(12)
Co(1)-O(5)	1.899(3)	O(3)-Co(1)-N(1)	84.34(13)
Co(1)-N(1)	1.911(3)	O(5)-Co(1)-N(1)	98.08(13)
Co(1)-N(2)	1.921(3)	O(3)-Co(1)-N(2)	96.08(13)
Co(1)-O(1)	1.924(3)	O(5)-Co(1)-N(2)	82.60(13)
Co(1)-O(7)	1.937(3)	N(1)-Co(1)-N(2)	87.55(14)
O(1)-C(1)	1.272(4)	O(3)-Co(1)-O(1)	92.93(11)
O(2)-C(1)	1.243(5)	O(5)-Co(1)-O(1)	88.50(11)
C(1)-C(2)	1.525(6)	N(1)-Co(1)-O(1)	91.18(12)
C(2)-C(3)	1.506(5)	N(2)-Co(1)-O(1)	170.73(13)
Co(2)-O(11)	1.891(3)	O(3)-Co(1)-O(7)	87.82(11)
Co(2)-O(13)	1.899(3)	O(5)-Co(1)-O(7)	89.75(12)
Co(2)-N(4)	1.915(3)	N(1)-Co(1)-O(7)	172.16(13)
Co(2)-N(3)	1.916(3)	N(2)-Co(1)-O(7)	93.06(13)
Co(2)-O(9)	1.917(3)	O(1)-Co(1)-O(7)	89.45(11)
Co(2)-O(15)	1.938(3)	O(11)-Co(2)-O(13)	176.85(12)
S(1)-C(23)	1.714(4)	O(11)-Co(2)-N(4)	94.99(13)
S(2)-C(23)	1.719(4)	O(13)-Co(2)-N(4)	82.66(13)
S(3)-C(24)	1.715(4)	O(11)-Co(2)-N(3)	84.54(13)
S(4)-C(24)	1.711(4)	O(13)-Co(2)-N(3)	97.45(13)
C(23)-C(24)	1.401(5)	N(4)-Co(2)-N(3)	87.98(14)
S(5)-C(29)	1.748(4)	O(11)-Co(2)-O(9)	93.71(12)
S(6)-C(29)	1.755(4)	O(13)-Co(2)-O(9)	88.70(12)
S(7)-C(30)	1.744(4)	N(4)-Co(2)-O(9)	171.16(14)
S(8)-C(30)	1.756(4)	N(3)-Co(2)-O(9)	91.29(12)
C(29)-C(30)	1.365(6)	O(11)-Co(2)-O(15)	87.35(12)
S(9)-C(35)	1.735(4)	O(13)-Co(2)-O(15)	90.69(12)
S(10)-C(35)	1.733(4)	N(4)-Co(2)-O(15)	93.34(12)
S(11)-C(36)	1.736(4)	N(3)-Co(2)-O(15)	171.86(14)
S(12)-C(36)	1.734(4)	O(9)-Co(2)-O(15)	88.62(11)
C(35)-C(36)	1.371(5)		

Table B.9. Selected bond lengths and angles in the solid state structure of $(TTF)_3[Fe^{III}(S,S\text{-}EDDS)]_2 \cdot 5H_2O$ (**39**).

Bond	(Å)	Bond	(Å)
Fe(1)-N(1)	2.173(16)	S(64A)-C(64A)	1.72(4)
Fe(1)-N(2)	2.14(2)	S(71A)-C(73A)	1.79(5)
Fe(1)-O(5)	1.944(16)	S(71B)-C(73B)	1.68(4)
Fe(1)-O(6)	1.994(17)	S(72A)-C(73A)	1.79(5)
Fe(1)-O(7)	1.966(13)	S(72B)-C(73B)	1.74(5)
Fe(1)-O(8)	2.010(18)	S(73A)-C(74A)	1.71(4)
Fe(2)-N(3)	2.13(2)	S(73B)-C(74B)	1.78(4)
Fe(2)-N(4)	2.119(17)	S(74A)-C(74A)	1.76(5)
Fe(2)-O(15)	1.935(12)	S(74B)-C(74B)	1.70(4)
Fe(2)-O(16)	1.987(17)	S(81A)-C(83A)	1.79(4)
Fe(2)-O(17)	1.966(16)	S(82A)-C(83A)	1.69(4)
Fe(2)-O(18)	2.047(17)	S(83A)-C(84A)	1.70(4)
Fe(3)-N(5)	2.138(17)	S(83B)-C(84B)	1.76(5)
Fe(3)-N(6)	2.14(2)	S(84A)-C(84A)	1.80(4)
Fe(3)-O(25)	1.970(17)	S(84B)-C(84B)	1.81(4)
Fe(3)-O(26)	2.080(15)	S(91A)-C(93A)	1.83(4)
Fe(3)-O(27)	2.022(16)	S(91B)-C(93B)	1.81(4)
Fe(3)-O(28)	1.972(16)	S(92A)-C(93A)	1.74(4)
Fe(4)-N(7)	2.122(18)	S(92B)-C(93B)	1.73(4)
Fe(4)-N(8)	2.135(19)	S(93A)-C(94A)	1.72(4)
Fe(4)-O(35)	1.929(16)	S(93B)-C(94B)	1.65(4)
Fe(4)-O(36)	1.897(15)	S(94A)-C(94A)	1.84(4)
Fe(4)-O(38)	2.015(17)	C(43B)-C(44B)	1.54(6)
O(37)-Fe(4)	1.944(16)	C(43B)-S(41B)	1.76(4)
S(41A)-C(43A)	1.78(5)	C(43B)-S(42B)	1.62(4)
S(42A)-C(43A)	1.70(4)	C(44A)-C(43A)	1.47(6)
S(43A)-C(44A)	1.72(4)	C(51A)-C(52A)	1.48(6)
S(43B)-C(44B)	1.65(4)	C(53B)-C(54B)	1.29(7)
S(44A)-C(44A)	1.69(4)	C(54A)-C(53A)	1.38(7)
S(44B)-C(44B)	1.75(4)	C(64A)-C(63A)	1.42(5)
S(51A)-C(53A)	1.62(5)	C(64B)-C(63B)	1.56(7)
S(51B)-C(53B)	1.83(5)	C(64B)-S(63B)	1.65(5)
S(52A)-C(53A)	1.77(5)	C(64B)-S(64B)	1.69(5)
S(52B)-C(53B)	1.76(5)	C(73A)-C(74A)	1.33(7)
S(53A)-C(54A)	1.77(5)	C(73B)-C(74B)	1.43(6)
S(53B)-C(54B)	1.76(4)	C(83A)-C(84A)	1.31(6)
S(54A)-C(54A)	1.72(5)	C(84B)-C(83B)	1.20(7)
S(54B)-C(54B)	1.73(5)	C(93B)-C(94B)	1.40(6)
S(61A)-C(63A)	1.82(4)	C(94A)-C(93A)	1.21(6)
S(62A)-C(63A)	1.73(4)	C(94B)-S(94B)	1.69(4)
S(63A)-C(64A)	1.64(4)		

Table B.9. continued

Angle	(°)	Angle	(°)
O(5)-Fe(1)-O(7)	108.1(6)	O(15)-Fe(2)-O(17)	108.3(7)
O(5)-Fe(1)-O(6)	93.4(7)	O(15)-Fe(2)-O(16)	95.7(6)
O(7)-Fe(1)-O(6)	90.3(6)	O(17)-Fe(2)-O(16)	90.8(7)
O(5)-Fe(1)-O(8)	90.7(7)	O(15)-Fe(2)-O(18)	90.7(6)
O(7)-Fe(1)-O(8)	92.5(6)	O(17)-Fe(2)-O(18)	90.8(7)
O(6)-Fe(1)-O(8)	174.1(7)	O(16)-Fe(2)-O(18)	172.5(6)
O(5)-Fe(1)-N(2)	162.6(8)	O(15)-Fe(2)-N(4)	159.6(6)
O(7)-Fe(1)-N(2)	86.4(7)	O(17)-Fe(2)-N(4)	87.8(7)
O(6)-Fe(1)-N(2)	96.1(7)	O(16)-Fe(2)-N(4)	96.6(7)
O(8)-Fe(1)-N(2)	78.9(7)	O(18)-Fe(2)-N(4)	76.2(7)
O(5)-Fe(1)-N(1)	87.9(6)	O(15)-Fe(2)-N(3)	86.6(6)
O(7)-Fe(1)-N(1)	160.3(7)	O(17)-Fe(2)-N(3)	163.5(7)
O(6)-Fe(1)-N(1)	77.2(7)	O(16)-Fe(2)-N(3)	80.6(7)
O(8)-Fe(1)-N(1)	98.7(7)	O(18)-Fe(2)-N(3)	96.0(7)
N(2)-Fe(1)-N(1)	80.0(7)	N(4)-Fe(2)-N(3)	79.4(7)
O(25)-Fe(3)-O(28)	108.7(7)	O(36)-Fe(4)-O(35)	97.1(7)
O(25)-Fe(3)-O(27)	92.5(7)	O(36)-Fe(4)-O(37)	92.0(7)
O(28)-Fe(3)-O(27)	92.8(7)	O(35)-Fe(4)-O(37)	107.4(7)
O(25)-Fe(3)-O(26)	91.6(6)	O(36)-Fe(4)-O(38)	172.3(7)
O(28)-Fe(3)-O(26)	89.7(7)	O(35)-Fe(4)-O(38)	89.1(7)
O(27)-Fe(3)-O(26)	174.3(7)	O(37)-Fe(4)-O(38)	90.4(7)
O(25)-Fe(3)-N(5)	86.5(7)	O(36)-Fe(4)-N(7)	79.2(7)
O(28)-Fe(3)-N(5)	162.3(8)	O(35)-Fe(4)-N(7)	86.8(7)
O(27)-Fe(3)-N(5)	95.6(6)	O(37)-Fe(4)-N(7)	164.3(8)
O(26)-Fe(3)-N(5)	80.6(6)	O(38)-Fe(4)-N(7)	96.7(7)
O(25)-Fe(3)-N(6)	160.4(7)	O(36)-Fe(4)-N(8)	96.0(7)
O(28)-Fe(3)-N(6)	88.3(7)	O(35)-Fe(4)-N(8)	159.8(7)
O(27)-Fe(3)-N(6)	76.5(7)	O(37)-Fe(4)-N(8)	87.3(7)
O(26)-Fe(3)-N(6)	98.5(6)	O(38)-Fe(4)-N(8)	76.8(7)
N(5)-Fe(3)-N(6)	78.6(7)	N(7)-Fe(4)-N(8)	80.7(7)

Table B.10. Selected bond lengths and angles in the solid state structure of $(TTF)_x[Cr^{III}(S,S\text{-}EDDS)]_2 \cdot 4.5H_2O$ (**40**).

Bond/Angle	(Å/°)	Angle	(°)	Angle	(°)
O(6)-Cr(1)	1.986(4)	O(8)-Cr(1)-O(6)	175.87(19)	O(23)-Cr(3)-N(3A)	77.9(5)
O(5)-Cr(1)	1.958(4)	O(7)-Cr(1)-N(8)	173.3(2)	O(24)-Cr(3)-N(3A)	97.2(5)
O(8)-Cr(1)	1.969(5)	O(5)-Cr(1)-N(8)	91.6(2)	O(21)-Cr(3)-N(3A)	165.2(6)
N(7)-Cr(1)	2.034(6)	O(8)-Cr(1)-N(8)	96.2(2)	O(22)-Cr(3)-N(3A)	98.9(5)
N(8)-Cr(1)	2.018(6)	O(6)-Cr(1)-N(8)	80.4(2)	O(23)-Cr(3)-N(4)	97.2(3)
O(7)-Cr(1)	1.957(4)	O(7)-Cr(1)-N(7)	92.0(2)	O(24)-Cr(3)-N(4)	172.8(4)
O(16)-Cr(2)	1.981(5)	O(5)-Cr(1)-N(7)	172.0(2)	O(21)-Cr(3)-N(4)	89.4(3)
O(15)-Cr(2)	1.958(5)	O(8)-Cr(1)-N(7)	81.0(2)	O(22)-Cr(3)-N(4)	81.9(3)
N(6)-Cr(2)	2.034(6)	O(6)-Cr(1)-N(7)	96.3(2)	N(3A)-Cr(3)-N(4)	80.6(5)
O(17)-Cr(2)	1.963(5)	N(8)-Cr(1)-N(7)	84.7(2)	O(23)-Cr(3)-N(3)	89.6(6)
O(18)-Cr(2)	1.970(5)	O(15)-Cr(2)-O(17)	97.0(2)	O(24)-Cr(3)-N(3)	81.9(5)
N(5)-Cr(2)	2.042(6)	O(15)-Cr(2)-O(18)	91.8(2)	O(21)-Cr(3)-N(3)	175.3(6)
Cr(3)-O(23)	1.925(8)	O(17)-Cr(2)-O(18)	89.9(2)	O(22)-Cr(3)-N(3)	87.3(5)
Cr(3)-O(24)	1.950(7)	O(15)-Cr(2)-O(16)	91.1(2)	N(3A)-Cr(3)-N(3)	19.5(5)
Cr(3)-O(21)	1.951(5)	O(17)-Cr(2)-O(16)	92.7(2)	N(4)-Cr(3)-N(3)	94.3(5)
Cr(3)-O(22)	1.960(7)	O(18)-Cr(2)-O(16)	175.9(2)	O(38)-Cr(4)-O(36)	94.9(2)
Cr(3)-N(3A)	2.030(14)	O(15)-Cr(2)-N(6)	89.7(2)	O(38)-Cr(4)-O(35)	91.2(2)
Cr(3)-N(4)	2.051(8)	O(17)-Cr(2)-N(6)	169.8(2)	O(36)-Cr(4)-O(35)	90.4(2)
Cr(3)-N(3)	2.149(18)	O(18)-Cr(2)-N(6)	97.7(2)	O(38)-Cr(4)-O(37)	89.1(2)
O(35)-Cr(4)	1.964(6)	O(16)-Cr(2)-N(6)	79.4(2)	O(36)-Cr(4)-O(37)	92.3(2)
N(1)-Cr(4)	2.035(6)	O(15)-Cr(2)-N(5)	169.3(2)	O(35)-Cr(4)-O(37)	177.2(2)
O(36)-Cr(4)	1.956(5)	O(17)-Cr(2)-N(5)	90.0(3)	O(38)-Cr(4)-N(1)	91.6(2)
O(37)-Cr(4)	1.983(5)	O(18)-Cr(2)-N(5)	80.1(2)	O(36)-Cr(4)-N(1)	169.9(2)
O(38)-Cr(4)	1.950(5)	O(16)-Cr(2)-N(5)	96.7(2)	O(35)-Cr(4)-N(1)	97.1(2)
N(2)-Cr(4)	2.045(6)	N(6)-Cr(2)-N(5)	84.6(3)	O(37)-Cr(4)-N(1)	80.1(2)
		O(23)-Cr(3)-O(24)	89.0(4)	O(38)-Cr(4)-N(2)	170.5(2)
O(7)-Cr(1)-O(5)	92.37(19)	O(23)-Cr(3)-O(21)	92.7(3)	O(36)-Cr(4)-N(2)	90.5(2)
O(7)-Cr(1)-O(8)	89.1(2)	O(24)-Cr(3)-O(21)	94.1(2)	O(35)-Cr(4)-N(2)	80.9(2)
O(5)-Cr(1)-O(8)	92.40(19)	O(23)-Cr(3)-O(22)	176.7(3)	O(37)-Cr(4)-N(2)	98.5(2)
O(7)-Cr(1)-O(6)	94.17(18)	O(24)-Cr(3)-O(22)	91.7(3)	N(1)-Cr(4)-N(2)	84.1(2)
O(5)-Cr(1)-O(6)	90.03(19)	O(21)-Cr(3)-O(22)	90.4(2)		

Table B.11. Selected bond lengths and angles in the solid state structure of $(ET)_x[Co^{III}(S,S\text{-}EDDS)]_2 \cdot 5H_2O$ (**44**).

Bond/Angle	(Å/°)	Angle	(°)
N(3)-Co(1)	1.922(4)	N(3)-Co(1)-O(15)	94.47(16)
Co(1)-O(10)	1.891(3)	O(10)-Co(1)-O(11)	89.43(15)
Co(1)-O(13)	1.907(3)	O(13)-Co(1)-O(11)	91.03(15)
Co(1)-N(4)	1.917(4)	N(4)-Co(1)-O(11)	93.26(16)
Co(1)-O(15)	1.928(3)	N(3)-Co(1)-O(11)	172.87(16)
Co(1)-O(11)	1.931(3)	O(15)-Co(1)-O(11)	85.36(15)
Co(2)-O(7)	1.895(3)	O(7)-Co(2)-N(2)	94.14(17)
Co(2)-N(2)	1.905(4)	O(7)-Co(2)-N(1)	85.57(17)
Co(2)-N(1)	1.918(4)	N(2)-Co(2)-N(1)	87.95(19)
Co(2)-O(3)	1.924(4)	O(7)-Co(2)-O(3)	88.57(16)
Co(2)-O(1)	1.932(4)	N(2)-Co(2)-O(3)	94.90(17)
Co(2)-O(6)	1.933(4)	N(1)-Co(2)-O(3)	173.65(18)
O(10)-Co(1)-O(13)	179.12(16)	O(7)-Co(2)-O(1)	91.00(16)
O(10)-Co(1)-N(4)	95.83(17)	N(2)-Co(2)-O(1)	174.43(17)
O(13)-Co(1)-N(4)	83.40(16)	N(1)-Co(2)-O(1)	90.31(17)
O(10)-Co(1)-N(3)	83.43(15)	O(3)-Co(2)-O(1)	87.37(16)
O(13)-Co(1)-N(3)	96.10(16)	O(7)-Co(2)-O(6)	175.34(15)
N(4)-Co(1)-N(3)	87.57(18)	N(2)-Co(2)-O(6)	82.45(16)
O(10)-Co(1)-O(15)	89.58(16)	N(1)-Co(2)-O(6)	97.45(17)
O(13)-Co(1)-O(15)	91.20(15)	O(3)-Co(2)-O(6)	88.56(16)
N(4)-Co(1)-O(15)	174.41(17)	O(1)-Co(2)-O(6)	92.54(16)

Table B.12. Selected bond lengths and angles in the solid state structure of $(ET)_3[Cr^{III}(S,S\text{-}EDDS)]_2 \cdot 6H_2O$ (**46**).

Bond/Angle	(Å/°)	Angle	(°)
Cr(1)-O(7)	1.968(5)	O(6)-Cr(1)-N(1)	79.8(3)
Cr(1)-O(5)	1.971(6)	O(7)-Cr(1)-N(2)	82.0(3)
Cr(1)-O(8)	1.984(6)	O(5)-Cr(1)-N(2)	171.7(3)
Cr(1)-O(6)	1.998(6)	O(8)-Cr(1)-N(2)	88.4(3)
Cr(1)-N(1)	2.024(7)	O(6)-Cr(1)-N(2)	98.1(3)
Cr(1)-N(2)	2.040(8)	N(1)-Cr(1)-N(2)	84.7(3)
Cr(2)-O(16)	1.963(6)	O(16)-Cr(2)-O(15)	90.9(2)
Cr(2)-O(15)	1.968(5)	O(16)-Cr(2)-O(18)	175.6(2)
Cr(2)-O(18)	1.969(5)	O(15)-Cr(2)-O(18)	92.0(2)
Cr(2)-O(17)	1.981(5)	O(16)-Cr(2)-O(17)	93.6(2)
Cr(2)-N(4)	2.047(7)	O(15)-Cr(2)-O(17)	92.2(2)
Cr(2)-N(3)	2.051(7)	O(18)-Cr(2)-O(17)	89.6(2)
		O(16)-Cr(2)-N(4)	96.5(3)
O(7)-Cr(1)-O(5)	90.3(2)	O(15)-Cr(2)-N(4)	170.8(3)
O(7)-Cr(1)-O(8)	90.3(2)	O(18)-Cr(2)-N(4)	80.3(2)
O(5)-Cr(1)-O(8)	94.7(2)	O(17)-Cr(2)-N(4)	92.8(3)
O(7)-Cr(1)-O(6)	174.3(2)	O(16)-Cr(2)-N(3)	81.0(2)
O(5)-Cr(1)-O(6)	89.3(2)	O(15)-Cr(2)-N(3)	90.9(3)
O(8)-Cr(1)-O(6)	95.4(2)	O(18)-Cr(2)-N(3)	95.7(3)
O(7)-Cr(1)-N(1)	94.6(3)	O(17)-Cr(2)-N(3)	173.8(3)
O(5)-Cr(1)-N(1)	92.9(3)	N(4)-Cr(2)-N(3)	84.9(3)
O(8)-Cr(1)-N(1)	171.0(3)		

Table B.13. Selected bond lengths and angles in the solid state structure of $(TSF)_3[Co^{III}(S,S\text{-}EDDS)]_2 \cdot 6H_2O$ (**41**).

Bond/Angle	(Å/°)	Bond/Angle	(Å/°)
Co(1)-O(6)	1.911(13)	O(6)-Co(1)-N(1)	84.0(6)
Co(1)-O(7)	1.920(13)	O(7)-Co(1)-N(1)	97.3(6)
Co(1)-N(1)	1.929(17)	O(6)-Co(1)-N(2)	95.9(6)
Co(1)-N(2)	1.935(15)	O(7)-Co(1)-N(2)	82.7(6)
Co(1)-O(8)	1.948(13)	N(1)-Co(1)-N(2)	88.5(7)
Co(1)-O(5)	1.960(14)	O(6)-Co(1)-O(8)	88.5(6)
Co(2)-O(15)	1.891(13)	O(7)-Co(1)-O(8)	90.1(6)
Co(2)-O(17)	1.914(12)	N(1)-Co(1)-O(8)	172.5(7)
Co(2)-N(4)	1.933(15)	N(2)-Co(1)-O(8)	92.4(6)
Co(2)-O(16)	1.936(12)	O(6)-Co(1)-O(5)	92.5(6)
Co(2)-N(3)	1.947(16)	O(7)-Co(1)-O(5)	88.9(6)
Co(2)-O(18)	1.951(12)	N(1)-Co(1)-O(5)	90.6(7)
Se(10)-C(34)	1.91(2)	N(2)-Co(1)-O(5)	171.4(6)
Se(11)-C(33)	1.89(2)	O(8)-Co(1)-O(5)	89.6(6)
Se(12)-C(33)	1.89(2)	O(15)-Co(2)-O(17)	177.3(6)
C(34)-C(33)	1.32(3)	O(15)-Co(2)-N(4)	96.0(6)
C(34)-Se(20)	1.92(2)	O(17)-Co(2)-N(4)	83.4(6)
Se(1)-C(44)	1.84(2)	O(15)-Co(2)-O(16)	92.7(5)
Se(2)-C(43)	1.85(2)	O(17)-Co(2)-O(16)	88.0(5)
Se(3)-C(44)	1.89(2)	N(4)-Co(2)-O(16)	171.1(6)
Se(4)-C(43)	1.876(19)	O(15)-Co(2)-N(3)	84.6(6)
C(43)-C(44)	1.39(3)	O(17)-Co(2)-N(3)	97.9(6)
Se(5)-C(54)	1.894(16)	N(4)-Co(2)-N(3)	87.0(7)
Se(6)-C(53)	1.896(17)	O(16)-Co(2)-N(3)	91.9(6)
Se(7)-C(53)	1.889(17)	O(15)-Co(2)-O(18)	87.6(6)
Se(8)-C(54)	1.877(18)	O(17)-Co(2)-O(18)	89.8(5)
C(54)-C(53)	1.35(2)	N(4)-Co(2)-O(18)	93.2(6)
		O(16)-Co(2)-O(18)	89.2(5)
O(6)-Co(1)-O(7)	178.0(6)	N(3)-Co(2)-O(18)	172.2(6)

Table B.14. Selected bond lengths and angles in the solid state structure of $(TSF)_3[Fe^{III}(S,S\text{-}EDDS)]_2 \cdot 6H_2O$ (**42**).

Bond/Angle	(Å/°)	Bond/Angle	(Å/°)
Fe(1)-O(8)	1.949(7)	O(8)-Fe(1)-O(7)	94.6(3)
Fe(1)-O(5)	1.954(7)	O(5)-Fe(1)-O(7)	89.8(3)
Fe(1)-O(7)	2.012(8)	O(8)-Fe(1)-O(6)	91.6(3)
Fe(1)-O(6)	2.019(7)	O(5)-Fe(1)-O(6)	90.6(3)
Fe(1)-N(1)	2.146(9)	O(7)-Fe(1)-O(6)	173.2(3)
Fe(1)-N(2)	2.148(8)	O(8)-Fe(1)-N(1)	160.4(3)
Fe(2)-O(17)	1.951(7)	O(5)-Fe(1)-N(1)	88.3(3)
Fe(2)-O(18)	1.957(7)	O(7)-Fe(1)-N(1)	96.3(3)
Fe(2)-O(15)	1.995(7)	O(6)-Fe(1)-N(1)	77.0(3)
Fe(2)-O(16)	2.002(7)	O(8)-Fe(1)-N(2)	86.4(3)
Fe(2)-N(3)	2.141(9)	O(5)-Fe(1)-N(2)	162.9(3)
Fe(2)-N(4)	2.149(8)	O(7)-Fe(1)-N(2)	79.6(3)
Se(1)-C(23)	1.875(12)	O(6)-Fe(1)-N(2)	98.4(3)
Se(2)-C(23)	1.880(13)	N(1)-Fe(1)-N(2)	79.7(3)
Se(3)-C(24)	1.894(13)	O(17)-Fe(2)-O(18)	105.1(3)
Se(4)-C(24)	1.859(12)	O(17)-Fe(2)-O(15)	88.7(3)
Se(5)-C(33)	1.898(12)	O(18)-Fe(2)-O(15)	95.1(3)
Se(6)-C(33)	1.889(12)	O(17)-Fe(2)-O(16)	91.3(3)
Se(7)-C(34)	1.909(14)	O(18)-Fe(2)-O(16)	93.0(3)
Se(8)-C(34)	1.877(13)	O(15)-Fe(2)-O(16)	171.7(3)
Se(9)-C(43)	1.908(12)	O(17)-Fe(2)-N(3)	163.2(3)
Se(10)-C(43)	1.875(11)	O(18)-Fe(2)-N(3)	87.9(3)
Se(11)-C(44)	1.880(11)	O(15)-Fe(2)-N(3)	79.3(3)
Se(12)-C(44)	1.928(11)	O(16)-Fe(2)-N(3)	98.9(3)
C(33)-C(34)	1.342(17)	O(17)-Fe(2)-N(4)	88.1(3)
C(44)-C(43)	1.331(16)	O(18)-Fe(2)-N(4)	164.1(3)
C(23)-C(24)	1.332(14)	O(15)-Fe(2)-N(4)	94.1(3)
		O(16)-Fe(2)-N(4)	77.6(3)
O(8)-Fe(1)-O(5)	108.0(3)	N(3)-Fe(2)-N(4)	81.0(3)

Table B.15. Selected bond lengths and angles in the solid state structure of $(TSF)_3[Cr^{III}(S,S\text{-}EDDS)]_2 \cdot 6H_2O$ (**43**).

Bond/Angle	(Å/°)	Bond/Angle	(Å/°)
C(23)-C(24)	1.40(2)	O(6)-Cr(1)-O(8)	96.9(4)
C(23)-Se(1)	1.901(17)	O(5)-Cr(1)-O(8)	88.4(4)
C(23)-Se(2)	1.914(15)	O(6)-Cr(1)-O(7)	92.5(4)
C(24)-Se(4)	1.828(14)	O(5)-Cr(1)-O(7)	174.1(4)
C(24)-Se(3)	1.864(14)	O(8)-Cr(1)-O(7)	90.3(4)
C(43)-C(54)	1.37(2)	O(6)-Cr(1)-N(1)	88.7(4)
C(43)-Se(9)	1.883(15)	O(5)-Cr(1)-N(1)	81.5(4)
C(43)-Se(10)	1.892(14)	O(8)-Cr(1)-N(1)	168.7(5)
C(54)-Se(12)	1.841(17)	O(7)-Cr(1)-N(1)	99.3(4)
C(54)-Se(11)	1.852(17)	O(6)-Cr(1)-N(2)	168.0(4)
C(33)-C(34)	1.33(2)	O(5)-Cr(1)-N(2)	95.1(4)
C(33)-Se(6)	1.890(14)	O(8)-Cr(1)-N(2)	91.9(5)
C(33)-Se(5)	1.923(14)	O(7)-Cr(1)-N(2)	79.2(5)
C(34)-Se(7)	1.861(16)	N(1)-Cr(1)-N(2)	84.1(5)
C(34)-Se(8)	1.898(15)	O(15)-Cr(2)-O(16)	93.4(4)
Cr(1)-O(6)	1.922(10)	O(15)-Cr(2)-O(17)	97.7(4)
Cr(1)-O(5)	1.949(10)	O(16)-Cr(2)-O(17)	91.2(4)
Cr(1)-O(8)	1.972(9)	O(15)-Cr(2)-O(18)	89.8(4)
Cr(1)-O(7)	1.997(10)	O(16)-Cr(2)-O(18)	176.7(4)
Cr(1)-N(1)	2.040(13)	O(17)-Cr(2)-O(18)	89.1(4)
Cr(1)-N(2)	2.059(12)	O(15)-Cr(2)-N(3)	90.6(4)
Cr(2)-O(15)	1.952(10)	O(16)-Cr(2)-N(3)	81.7(5)
Cr(2)-O(16)	1.970(10)	O(17)-Cr(2)-N(3)	169.4(5)
Cr(2)-O(17)	1.994(11)	O(18)-Cr(2)-N(3)	97.6(4)
Cr(2)-O(18)	2.005(9)	O(15)-Cr(2)-N(4)	166.8(5)
Cr(2)-N(3)	2.028(13)	O(16)-Cr(2)-N(4)	97.5(5)
Cr(2)-N(4)	2.032(13)	O(17)-Cr(2)-N(4)	89.4(5)
		O(18)-Cr(2)-N(4)	79.2(5)
O(6)-Cr(1)-O(5)	93.4(4)	N(3)-Cr(2)-N(4)	83.8(5)

Appendix C

Results of the conductivity measurements

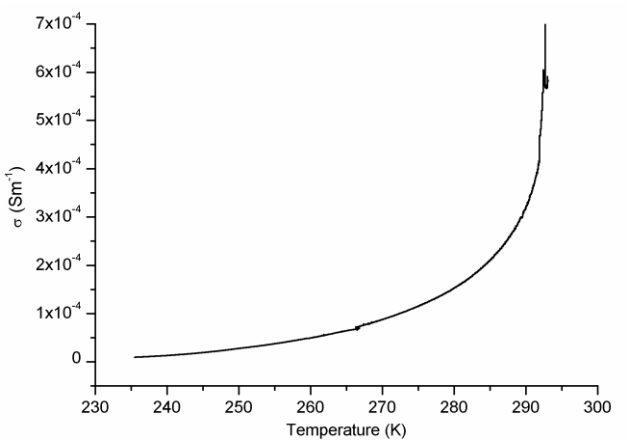

Figure C.1. Temperature dependence of the conductivity of $(TTF)_3[Fe^{III}(S,S\text{-EDDS})]_2 \cdot 5H_2O$ (**39**)

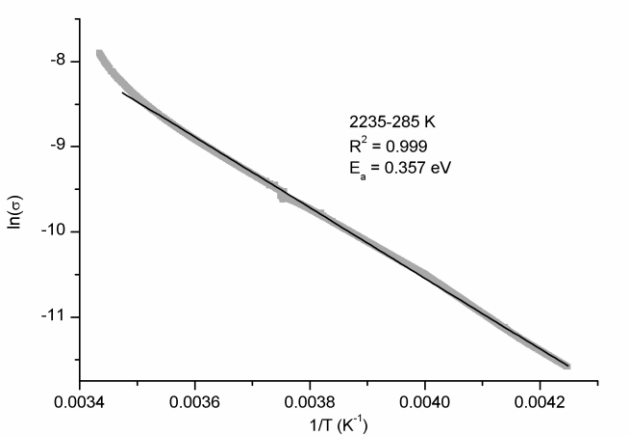

Figure C.2. Dependence of natural logarithm of conductivity of **39** on reciprocal of temperature and the linear fit of the data.

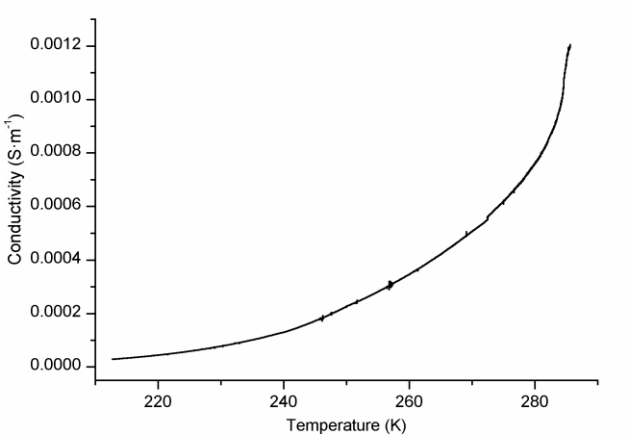

Figure C.3. Temperature dependence of the conductivity of $(TTF)_3[Cr^{III}(S,S\text{-EDDS})]_2 \cdot 4.5H_2O$ (**40**)

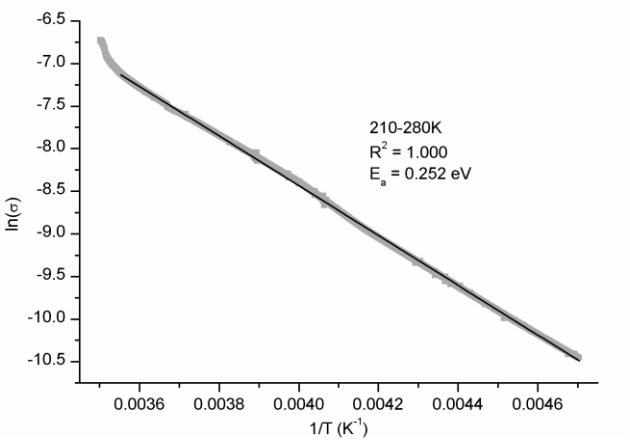

Figure C.4. Dependence of natural logarithm of conductivity of **39** on reciprocal of temperature and the linear fit of the data.

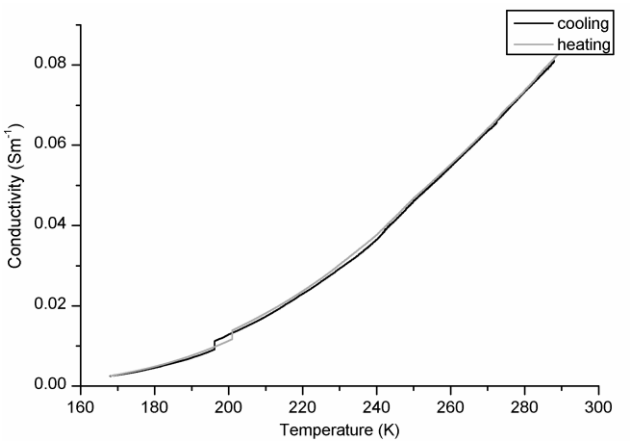

Figure C.5. Temperature dependence of the conductivity of $(TSF)_3[Co^{III}(S,S\text{-EDDS})]_2 \cdot 6H_2O$ (**41**)

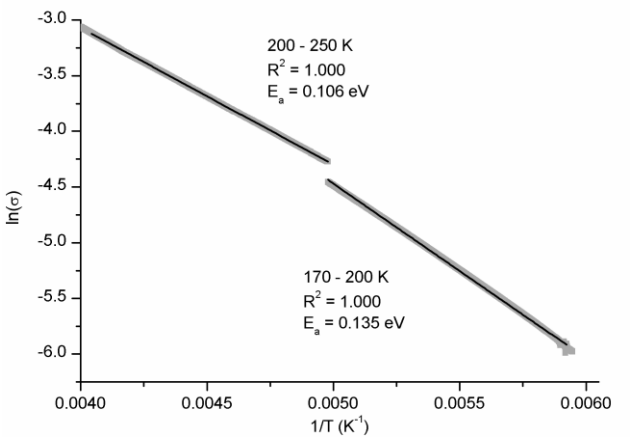

Figure C.6. Dependence of natural logarithm of conductivity of **41** on reciprocal of temperature and linear fits of the data.

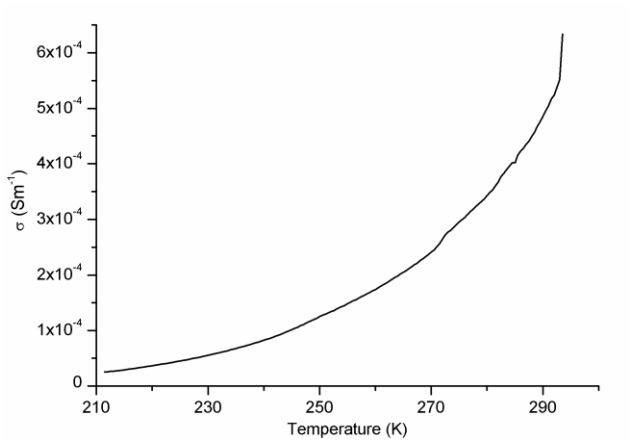

Figure C.7. Temperature dependence of the conductivity of $(TSF)_3[Fe^{III}(S,S\text{-EDDS})]_2 \cdot 6H_2O$ (**42**)

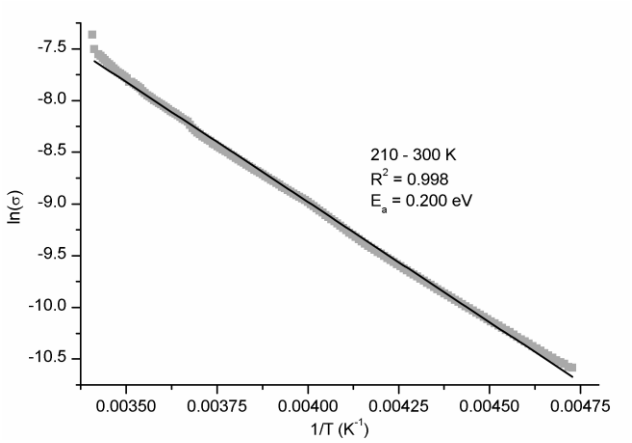

Figure C.8. Dependence of natural logarithm of conductivity of **42** on reciprocal of temperature and the linear fit of the data.

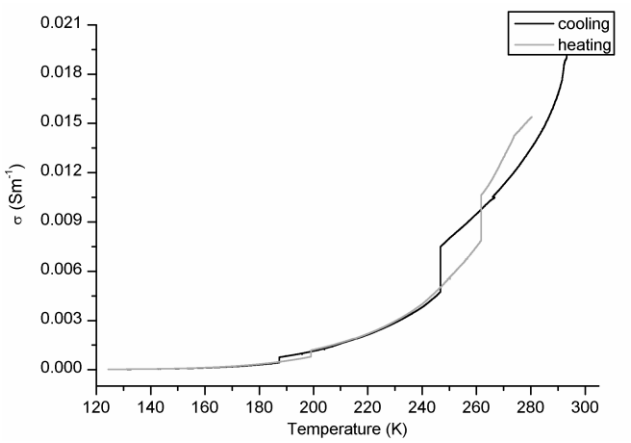

Figure C.9. Temperature dependence of the conductivity of $(TSF)_3[Cr^{III}(S,S\text{-EDDS})]_2 \cdot 6H_2O$ (**43**)

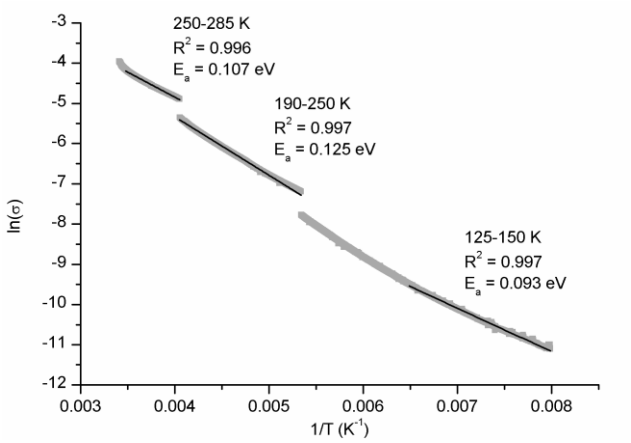

Figure C.10. Dependence of natural logarithm of conductivity of **43** on reciprocal of temperature and the linear fit of the data.